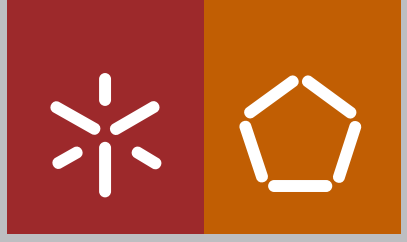

Universidade do Minho
Escola de Engenharia

Óscar Samuel Novais de Carvalho

Mechanical, fatigue and wear properties of sintered Carbon Nanotube-based functionally graded materials

julho de 2015

Universidade do Minho
Escola de Engenharia

Óscar Samuel Novais de Carvalho

Mechanical, fatigue and wear properties of sintered Carbon Nanotube-based functionally graded materials

Tese de Doutoramento
Engenharia Mecânica

Trabalho efectuado sob a orientação de
Professor Doutor Filipe Samuel Pereira Correia da Silva
Professor Doutor Delfim Fernandes Soares

julho de 2015

DECLARAÇÃO DE INTEGRIDADE

Declaro ter atuado com integridade na elaboração da presente tese. Confirmo que em todo o trabalho conducente à sua elaboração não recorri à prática de plágio ou a qualquer forma de falsificação de resultados.

Mais declaro que tomei conhecimento integral do Código de Conduta Ética da Universidade do Minho.

Universidade do Minho, ___ de _____ de _____

Nome completo: Óscar Samuel Novais de Carvalho

Assinatura: _____

"Intellectual growth should commence at birth and cease only at death."

Albert Einstein

ACKNOWLEDGMENTS

I would like to express my gratitude to my supervisors Professor FilipeSamuel Silva and Professor Delfim Soares. I wanted to give special thanks to Professor Filipe Samuel who always gave me strength and motivation to carry out the work.

I would like to express my gratitude to Mihaela Buciumeanu and Georgina Miranda for their help and friendship during this journey.

I want also to thank to all my colleagues in laboratory Sara Madeira, José Pires, Bruno Henriques, Paulo Pinto and Paulo Silva.

I would like to thanks my family and specially my wife, Stephanie, who always gave me support in this journey.

Finally, I also thank the University of Minho, because without it, this project would never have been possible.

Finally, I gratefully acknowledge Portuguese Foundation of Science and Technology through the project references PTDC/EME-PME/68664/2006, EXCL/EMS-TEC/0460/2012 and through the PhD grant with the reference SFRH/BD/44077/2008.

ABSTRACT

Mechanical, fatigue and wear properties of sintered Carbon Nanotube-based functionally graded materials

This PhD thesis is concerned with the development of nickel coated carbon nanotubes (CNTs) functionally graded metal matrix composites, based on an aluminium-silicon alloy matrix, obtained by powder metallurgy. Besides their development and production, this thesis focus on these composites characterization when regarding metallurgical, mechanical, fatigue and wear behaviour.

The experimental and theoretical work undertaken on this thesis was performed through the following steps: Assessment of several mixing processes for mixing aluminium powders and the reinforcement; Assessment of the optimum reinforcement fraction for these composites; Study and explanation of the effective reinforcing mechanisms on these composites (tensile, fatigue and wear) and Development of an equipment to obtain components with selected graded composition and design of a graded composition (reinforcement distribution) for piston rings production.

CNTs dispersion is a common issue, to which great efforts are being placed by the scientific community. This work also faced this topic, with CNT agglomerates being found in these composites produced with several mixing procedures. This thesis allowed to conclude that higher improvements on CNTs dispersion is possible by using a combination of different mixing processes.

Several CNT-reinforced composites were produced, aiming to assess the optimum reinforcement fraction for several properties. The 2 wt.% CNT-reinforced composite revealed the highest tensile strength, showing that, for CNT's reinforcement wt.% higher than 2%, the detrimental effect of agglomerates is higher that the beneficial effect of well dispersed CNTs. In spite of the reduction on mechanical properties for higher CNT content, a wear resistance increase was verified. This work also showed that the fatigue behaviour was found to increase by adding CNTs until a certain percentage. Regarding wear behaviour the agglomerates may also contribute to improved wear performance.

In this thesis, hybrid composites reinforced by CNTs and SiCp were also produced and characterized. It was possible to conclude that the addition of a second reinforcement brought a beneficial effect on tribological and mechanical behaviours, unachievable by using solely one of the reinforcements.

The final outcome of this thesis was the development of an equipment to produce components with selected graded composition (functionally graded material - FGM) by powder metallurgy. This development also included the design of a graded composition (CNT distribution). This equipment was found adequate for the production of these graded composites.

This study is very appealing for components design once it allows to develop controlled materials gradients suited for particular requirements. This work developed a possible solution for a piston ring, but a similar analysis/process can be applied to other components, where there is differential mechanical and wear requirements along a component.

This study also showed, that the use of commercial aluminium alloys (at least Al-Si alloys) reinforced with Ni coated CNTs seems to be adequate for industrial applications.

RESUMO

Propriedades Mecânicas, Fadiga e de Desgaste de compósitos sinterizados com nanotubos de carbono e com gradiente de propriedades

Esta tese de doutoramento está relacionada com o desenvolvimento de compósitos de nanotubos de carbono com gradiente de composição, por via da metalurgia dos pós. Além do seu desenvolvimento e produção, esta tese foca-se na caracterização metalúrgica, mecânica, fadiga e desgaste dos compósitos produzidos.

O trabalho experimental e teórico realizado nesta tese seguiu as seguintes etapas: avaliação de vários processos de mistura para misturar o pó da matriz e reforço; avaliação da fracção óptima de reforço nos compósitos; estudo e explicação dos mecanismos de reforço nos compósitos (tração, fadiga e desgaste) e desenvolvimento de um equipamento de obtenção de componentes com gradiente de composição e design de um gradiente de composição (distribuição do reforço) para a produção de segmento de motor de combustão.

A dispersão dos nanotubos de carbono é um problema comum, para o qual grandes esforços têm sido levados a cabo pela comunidade científica. Este trabalho também enfrentou o mesmo problema, visto que os aglomerados de nanotubos de carbono foram encontrados nos compósitos produzidos através de vários procedimentos de mistura. Esta tese permitiu concluir que as melhorias no processo de dispersão de nanotubos de carbono são possíveis, usando uma combinação de diferentes processos de mistura.

Vários compósitos reforçados com nanotubos de carbono foram produzidos com o objectivo de avaliar a fração ideal de reforço para várias propriedades. O compósito com 2 % em massa de nanotubos de carbono foi o compósito que revelou a mais elevada resistência à tração, e para maiores percentagens de reforço, o efeito prejudicial dos aglomerados é maior que o efeito benéfico de nanotubos de carbono bem dispersos. Apesar da redução nas propriedades mecânicas para maior fração de nanotubos de carbono, foi verificado um aumento de resistência ao desgaste. Este trabalho também mostrou que o comportamento de fadiga melhora com adição

de nanotubos de carbono até uma determinada percentagem. Em relação ao comportamento de desgaste, os aglomerados também podem contribuir para um melhor desempenho.

Nesta tese, compósitos híbridos reforçados por nanotubos de carbono e carboneto de silício também foram produzidos e caracterizados. Foi possível concluir que a adição de um segundo reforço tem um efeito benéfico sobre o desempenho tribológico e mecânico, inatingível utilizando unicamente um dos reforços.

O resultado final desta tese foi o desenvolvimento de um equipamento para produzir componentes com gradiente específico de composição por metalurgia dos pós. Este desenvolvimento também incluiu a concepção de um gradiente de composição (distribuição do reforço). Este equipamento mostrou-se adequado para a produção de compósitos com gradiente de composição.

Este estudo é muito atrativo para o projeto de componentes mecânicos, uma vez que permite desenvolver materiais com gradiente de composição adequados para necessidades específicas. Este trabalho desenvolveu uma possível solução para segmentos de motor de combustão, mas uma análise semelhante pode ser aplicada em outros componentes mecânicos, onde há diferencial de requisitos mecânicos e de desgaste ao longo de um componente.

Este estudo também demonstrou que a utilização de ligas de alumínio comerciais (pelo menos ligas de Al-Si) reforçadas com nanotubos de carbono revestido a Ni parece ser adequada para aplicações industriais.

TABLE OF CONTENTS

ACKNOWLEDGMENTS v
ABSTRACT vii
RESUMO ix
LIST OF SYMBOLS, ABBREVIATIONS AND NOTATION xvii
LIST OF FIGURES xix
LIST OF TABLES xxvii
1 Scope of the thesis 1
1.1 Motivation and objectives 1
1.2 Work development strategy 3
1.3 Thesis structure 3
2 State of the art 6
2.1 Aluminium Silicon Alloys 8
2.2 Powder metallurgy 8
2.3 Carbon nanotube aluminium composites 14
2.3.1 Aluminium matrix composites 14
2.3.2 Carbon nanotubes 15
2.3.3 Carbon nanotube aluminium composites by powder metallurgy 17
2.4 Functionally Graded Materials obtained by powder metallurgy 21
2.4.1 Gradient of porosity and pore size 23
2.4.2 Chemical and metallurgical composition gradients 26
2.5 Piston rings 33
2.6 Strengthening mechanisms 37
2.7 Fatigue in Metal Matrix composites 41
2.8 Wear 47
2.8.1 Abrasive wear 51
2.8.2 Adhesive wear 58
2.9 References 60
3 Evaluation of CNT dispersion methodology effect on mechanical properties of an Al-Si composite 75
3.1 Abstract 75
3.2 Introduction 75

3.3 Experimental procedure....77
3.3.1 Materials....77
3.3.2 Methods....77
3.4 Results and discussion....79
3.4.1 Microstructural characterization....79
3.4.2 Effect of the CNT mixing processing route on mechanical properties....82
3.4.3 Reactivity between CNTs and Matrix....91
3.5 Conclusions....94
3.6 Acknowledgements....94
3.7 References....94
4 Carbon nanotube dispersion in aluminum matrix composites – quantification and influence on strength....99
4.1 Abstract....99
4.2 Introduction....99
4.3 Experimental procedure....101
4.3.1 Fabrication of CNT-reinforced Al-Si composites....101
4.3.2 Characterization techniques and image analysis....102
4.3.3 Mechanical testing....104
4.4 Results and discussion....104
4.4.1 Tensile Strength....104
4.4.2 CNT distribution....107
4.4.3 Proposed empirical model....110
4.5 Conclusions....113
4.6 Acknowledgements....113
4.7 References....113
5 Improvement on sliding wear behaviour of Al/cast iron tribopair by CNTs reinforcement of an Al alloy....115
5.1 Abstract....115
5.2 Introdution....115
5.3 Experimental Procedure....117
5.3.1 Fabrication of AlSi-CNTs composites....117
5.3.2 Chemical characterization....119
5.3.3 Hardness measurements....119
5.3.4 Details of the reciprocating wear test....119
5.4 Results and Discussion....121

5.4.1 Coefficient of friction as a function of the CNT content 121
5.4.2 Hardness values as a function of the CNT content 123
5.4.3 Wear loss as a function of the CNT content 124
5.4.4 Analysis of wear track (SEM and EDS analysis) 126
5.5 Conclusions 135
5.6 Acknowledgments 135
5.7 References 135
6 Mechanisms Governing the Tensile, Fatigue and Wear Behaviour of Carbon Nanotube reinforced Aluminum Alloy 139
6.1 Abstract 139
6.2 Introduction 139
6.3 Experimental procedure 141
6.3.1 Materials 141
6.3.2 Methods 142
6.4 Results and discussion 144
6.4.1 Mechanical properties (Tensile tests) 144
6.4.2 Fatigue properties 149
6.4.3 Wear properties 151
6.5 Conclusions 154
6.6 Acknowledgements 155
6.7 References 155
7 Dry sliding wear behaviour of AlSi-CNTs-SiCp hybrid composites 159
7.1 Abstract 159
7.2 Introduction 159
7.3 Experimental procedure 161
7.3.1 Fabrication of AlSi composites 161
7.3.2 Microstructural and chemical characterization 162
7.3.3 Hardness tests 162
7.3.4 Details of the reciprocating wear tests 162
7.4 Results and discussion 163
7.4.1 Microstructural characterization 163
7.4.2 Hardness values 165
7.4.3 Wear loss 166
7.4.4 Coefficient of friction 168
7.4.5 Wear mechanism - SEM and EDS analysis 170

7.5 Conclusions 177
7.6 Acknowledgements 177
7.7 References 178
8 Mechanical, wear and fatigue behaviour of an AlSi-CNTs-SiCp hybrid composite 181
8.1 Abstract 181
8.2 Introduction 181
8.3 Experimental procedure 183
8.3.1 Fabrication of AlSi composites 183
8.3.2 Methods 184
8.4 Results and discussion 185
8.4.1 Microstructural characterization 185
8.4.2 Mechanical properties (Tensile tests) 187
8.4.3 Fatigue properties 192
8.4.4 Wear properties 197
8.5 Conclusions 200
8.6 Acknowledgements 201
8.7 References 201
9 Optimization of AlSi-CNTs functionally graded material composites for engine piston rings 205
9.1 Abstract 205
9.2 Introduction 205
9.3 Experimental procedure 208
9.3.1 Materials 208
9.3.2 Sintering process 209
9.3.3 Mechanical characterization 209
9.4 Results and discussion 211
9.4.1 Effect of CNT content over the mechanical behaviour of AlSi-CNT composites 211
9.4.2 Developed equipment and the feasibility of the proposed process 221
9.4.3 Mechanical properties of theAlSi -CNT functionally graded composite 226
9.5 Conclusions 230
9.6 Acknowledgements 231
9.7 References 231
10 Interface analysis on an eutectic AlSi alloy reinforced with Ni coated MWCNT 235
10.1 Abstract 235
10.2 Introduction 235

10.3 Experimental procedure 237
10.3.1 Fabrication of CNT-reinforced Al-Si composites 237
10.3.2 Metallurgical evaluation 238
10.4 Results and discussion 238
10.4.1 SEM with EDS analysis 238
10.4.2 Differential Scanning Calorimetry analyses 241
10.4.3 X-ray diffraction analysis 242
10.4.4 Transmission electron microscopy 242
10.5 Conclusions 245
10.6 Acknowledgements 246
10.7 References 246
11 General discussion 249
11.1 Suggestions for future works 260

LIST OF SYMBOLS, ABBREVIATIONS AND NOTATION

Al_4C_3	Aluminium carbide
AMC	Aluminium matrix composite
AlSi-CNT	Carbon nanotube reinforced aluminium silicon composite
At. %	Atomic percentage
BSE	Backscattered electron imaging
CNT	Carbon nanotube
CTE	Coefficient of thermal expansion
COF	Coefficient of friction
CVD	Chemical vapour deposition
d	Alternated displacement amplitude
DSC	Differential Scanning Calorimetry
EDS	Energy dispersive spectroscopy
FGM	Functionally graded material
Fn	Normal load
GCI	Gray cast iron
H	Hardness of the material being worn
HIP	Hot isostatic pressing
HP	Hot pressing
K	Wear coefficient (Archard coefficient)
K_{abr}	Abrasive wear coefficient
K_{ad}	Adhesion wear coefficient
MMC	Metal matrix composite

PM	Powder metallurgy
Q	Worn volume by unit sliding (Archard equation)
SEM	Scanning electron microscopy
SiC_p	Silicon carbide particle
TEM	Transmission electron microscopy
UTS	Ultimate tensile strength
Wt. %	Weight percentage
XRD	X-ray diffraction
ε_r	Tensile strain
σ_r	Tensile strength,
σ_y	Yield strength

LIST OF FIGURES

Figure 2. 1 - a) Al-12%Si alloy powder obtained by inert gas atomization (from TLS Technik) and b) Al-12%Si alloy powder obtained by a hybrid atomizer developed by O. Carvalho..... 10

Figure 2. 2 - Schematic phase diagram with indication of various sintering processes [18]..... 11

Figure 2.3 - Schematic model representing the sintering process by surface and bulk transport [19]..... 12

Figure 2. 4 - Disintegrated oxide films, into particles of 50–150 nm on pure aluminium powder [26]..... 14

Figure 2. 5 - Carbon nanotube functionalized with magnesium (arroys indicate the Mg layer) [64]. 17

Figure 2. 6 - Schematic representation of the sintering-dissolution process for manufacturing foams by powder metallurgy [139] 24

Figure 2. 7 - Schematic representation of the space-holder burning method by powder metallurgy [145]..... 24

Figure 2. 8 - Prodution method of hollow spheres by injection of metal through a coaxial nozzle [152]..... 25

Figure 2. 9 - Schematic representation of the combustion reaction for synthesizing porous materials [154]..... 26

Figure 2. 10 - FGM with a).discrete and b).continuous composition variation..... 26

Figure 2. 11 - FGM part obtained by powder stacking [156]..... 27

Figure 2. 12 - Schematic representation of powder rolling system [158]. 28

Figure 2. 13 - Schematic flow diagram of wet powder spraying process [159]. 29

Figure 2. 14 - Schematic representation of slip casting steps [160]. 29

Figure 2. 15 - Schematic representation of centrifugal system powder forming equipment [122] 30

Figure 2. 16 - Schematic representation of gravity sedimentation process [162]. 31

Figure 2. 17 - Schematic representation of the experimental set up for electrophoretic deposition[171] 31

Figure 2. 18 - Schematic representation of computer controled slip casting process [175]. 32

Figure 2. 19 - Schematic representation of rapid prototyping by direct DLF [179]..... 33

Figure 2. 20 - Power cylinder system a) general view; b) detail view [185]..... 34

Figure 2. 21 - Internal combustion engine piston ring. 35

Figure 2. 22 - Schematic representation of Orowan model. 39

Figure 2. 23 - Calculated dislocation density (ρ) vs. reinforcement aspect ratio (R) [208]..... 40

Figure 2. 24 - Schematic representation of a fatigue fracture surface showing..... 43

Figure 2. 25 - Schematic illustration of the sequence of events during failure of MMCs reinfroced by a) fibres and b) particles [233]. 44

Figure 2. 26 - Schematic representation of crack bowing mechanism [243]. 45

Figure 2. 27 - Crack deflection by cracking of the particlein an MoSI2/Nb composite [246]..... 46

Figure 2. 28 - Schematic representation of crack deflection by delamination [247]. 46

Figure 2. 29 - Schematic representation showing elastic, frictional and pullout bridging [250]. . 46

Figure 2. 30 - Schematic representation of a) contacts between surfaces asperities [260] and b) roughness profile [257]. 48

Figure 2. 31 - Aparent and real contact area [259]. 49

Figure 2. 32 - a) Friction coefficient vs sliding distance on a pin-on-disc test for a metal–metal contact under dry conditions b) Stick-slip effect [257]. 49

Figure 2. 33 - Factors affecting friction force [266]. 50

Figure 2. 34 - Schematic representation of a main types of wear [271] 51

Figure 2. 35 - Abrasive wear by two and three bodies modes [272]. 52

Figure 2.36 - Abrasive wear by a) two and b)three bodies [273]. 52

Figure 2.37 - Mechanisms of abrasive wear: microcutting, fracture, fatigue and grain pull-out [272]. 53

Figure 2.38 - Abrasive wear of a) ductile and b) fragile materials [271]. 54

Figure 2. 39 - Abrasive wear as a function of the ratio between hardness of abrasive and hardness of the worn material (steel) for for homogeneos material and non-homogeneous [259]. 55

Figure 2.40 - Ratio of microcutting to microploughing as a function of the ratio of the attack angle to the critical attack angle [259]. 56

Figure 2.41 - Abrasive wear resistance vs material hardness[259]. 56

Figure 2. 42 - Schematic representation of reinforcement orientation, size, modulus of elasticity, hardness and brittleness effect on the abrasive wear of composites [259]. 58

Figure 2. 43 - Schematic representation of adhesive wear [272]. 59

Figure 3. 1 - SEM images showing: a. CNTs (); 80
Figure 3. 2 - EDS spectrum of the CNT agglomerates corresponding to zone Z1 (white zone) identified in Figure 3. 1 a 80
Figure 3. 3 - SEM images of unreinforced AlSi alloy and AlSi - CNT composites microstructure. 82
Figure 3. 4 - Stress–strain curves for all studied mixing processes. 83
Figure 3. 5 - Mechanical properties as obtained on the composites with different mixing processes (A to E on Table 3.2): a. rupture shear strength; b. yield shear strength; c. rupture shear strain. 84
Figure 3. 6 - SEM micrographs of the fracture surface of the composites obtained by different mixing processes (a,d,g,j,n – backscattered images with 150x magnification and c,f,i,l,o – 2000x magnification; and b,e,h,k ,m– secondary electron images with 150x magnification). 88
Figure 3. 7 - SEM micrograph of the fracture surface of the composite obtained by 89

Figure 3. 8 - Schematic representation of the proposed physical model for the shear tests. 90
Figure 3. 9 - DSC curves obtained for samples with and without CNTs. 93

Figure 4. 1 - Hot pressing (a) schematic representation and (b) vacuum chamber detail. 102

Figure 4. 2 - SEM image in backscattered view of an Al-Si/2%CNT composite sample. 103

Figure 4. 3 - Figure 1.SEM image in backscattered view: (a) Al-Si/CNT composite with 2 wt. % MWCNT and (b) same SEM image, with threshold filter, enhancing the carbon nanotubes distribution and presence of agglomerates. 103

Figure 4. 4 -Implemented procedure for SEM images analysis, for CNT agglomerates quantification. 104

Figure 4. 5 -Tensile strength for different Al-Si/CNT composites, with 0; 2; 4 and 6 wt. % CNT,produced and tested in the present work. 106

Figure 4. 6 - Tensile strength of different Al/CNT composites, with 0; 1.5; 3.5; 5 and 6.5 wt. % CNT,produced and tested by C. N. He et al. Data extracted from [27]. 106

Figure 4. 7 - CNTs agglomerates distribution, determined in pictures with 5000 times magnification - percentage of agglomerates by size classes (y-axis withlogarithmic scale). 108

Figure 4. 8 - Type A agglomerates ([0, 1]μm^2) counts for Al-Si/CNT composites with 2, 4 and 6 wt.% CNT. 108

Figure 4. 9 - CNTs agglomerates distribution, determined in pictures with 123 times magnification - percentage of agglomerates by size classes (y-axis withlogarithmic scale). 109

Figure 4. 10 - Type B agglomerates ( ]50, 550]μm^2) counts for Al-Si/CNT composites with 2, 4 and 6 wt.% CNT. 110

Figure 4. 11 - Type A and type B agglomerates area fraction (in percentage) for Al-Si/CNT composites with 2, 4 and 6 wt. % CNT. 110

Figure 4. 12 - Tensile strength (C.N. He et. al. results and present work) and agglomerate area fraction for produced Al-Si/CNT composites. 111

Figure 4. 13 - Tensile strength (without and with agglomerates) and agglomerate area fraction (for types A and B) in Al-Si/CNT composites. 112

Figure 5. 1 - SEM images of unreinforced AlSi alloy and AlSi - CNT composites microstructure 118

Figure 5. 2 - SEM images of CNTs 119

Figure 5. 3 - SEM image of cast iron microstructure 120

Figure 5. 4 - Schematic test configuration: Fn – Normal applied load; d – alternated displacement amplitude 121

Figure 5. 5- Evolution of coefficient of friction with sliding distance for unreinforced AlSi alloy and all AlSi- CNT composites (AlSi - CNT against GCI 123

Figure 5. 6 - COF as a function of the CNT content 123

Figure 5. 7 - Hardness as a function of the CNT content 124

Figure 5. 8 - Wear loss as a function of the CNT content 125

Figure 5. 9 - SEM images of the worn surface of GCI plates after sliding against AlSi-based pins with different CNT content: (a) unreinforced AlSi alloy; (b) AlSi - 2 wt. % CNT; (c) AlSi – 4 wt. % CNT and (d) AlSi – 6 wt. % CNT 127

Figure 5. 10 - a. Backscattered SEM image of GCI plate worn surface after sliding against AlSi -2 wt. % CNT pin; b. and EDS spectrum representative of the dark zones in the micrograph 128

Figure 5. 11 - SEM images of the worn surface of unreinforced AlSi alloy (a), (b) and (c); AlSi -2 wt. % CNT (d), (e) and (f); AlSi – 4 wt. % CNT (g), (h) and (i) and AlSi – 6 wt. % CNT (j), (k) and (l). Global (130x) view (a), (d), (g) and (j); close-up (1000x) backscattered view (b), (e), (h) and (k); high magnification (5000x) view (c), (f), (i) and (l). 129

Figure 5. 12 - EDS spectra of the pin worn surface with AlSi – 2 wt. % CNT content corresponding to three zones, Z1, Z2 and Z3, identified in Figure 5. 11-e: (a) spectrum from the analysis in Z1 (white zone); (b) spectrum representative of Z2 and Z3 131

Figure 5. 13 - SEM image of the AlSi-based pins with 2 wt. % CNT (1000×) backscattered view 133

Figure 5. 14 - EDS spectra of an AlSi surface with 2 wt. % CNT content corresponding to three zones, Z1 and Z3, identified in Figure 5. 13: (a) spectrum from the analysis in Z3; (b) spectrum from the analysis in Z1 (white zone)(this is equal to zone Z2) 133

Figure 6. 1 - SEM images showing: (a) microstructure of CNT (magnification 190x) and (b) microstructure of AlSi-2 wt.% CNTs composite (magnification 5000x) 142

Figure 6. 2 - Geometry of the specimen for tensile and fatigue tests 143

Figure 6. 3 - Schematic test configuration: F_n – Normal applied load; d – alternated displacement amplitude. All tests have been stopped after a sliding distance of 148 m. During the tests compressed air was flown to the contact zone in order to remove loose. 144

Figure 6. 4 - Stress–strain curves from tensile testing of unreinforced AlSi alloy and AlSi – 2 wt.% CNT's composite 145

Figure 6. 5 - SEM images of the fracture surface after tensile test of: (a) unreinforced AlSi alloy and (b) AlSi-2 wt. % CNT's composite (with different magnifications) 146

Figure 6. 6 - SEM images of the fracture surface after tensile test showing the presence of CNTs agglomerates (AlSi-2 wt. % CNT's composite –with magnification 1000x) 147

Figure 6. 7 - Schematic representation of the proposed physical model for the tensile tests: a. unreinforced AlSi alloy (intragranular crack) b. AlSi -2 wt. % CNT's composite (intragranular and intergranular crack) 148

Figure 6. 8 - Maximum stresses (σ_{max}) vs. number of cycles to failure for unreinforced AlSi alloy and AlSi-2 wt. % CNT's composite 149

Figure 6. 9 - SEM images of the fracture surface after fatigue test of: (a) unreinforced AlSi alloy and (b) AlSi-2 wt. % CNT's composite(with different magnifications) 150

Figure 6. 10 - Schematic representation of the proposed physical model for fatigue tests for AlSi-2 wt. % CNT's composite 151

Figure 6. 11 - Wear loss as a function of the CNT content..... 151

Figure 6. 12 - SEM images of the worn surface of unreinforced AlSi alloy (a), (b) and (c); and AlSi-2 wt.% CNT's composite (d), (e) and (f); b) and e) is a backscattered view..... 153

Figure 6. 13 - Schematic representation of the proposed physical model for the wear test: AlSi grains are bonded with an improved strength due to CNT's interface reinforcement effect. Friction force (pin) cause pull-out of the grains..... 154

Figure 7. 1 - Schematic test configuration: Fn – Normal applied load; d – alternated displacement amplitude..... 163

Figure 7. 2 - SEM images of the composites microstructures: a. unreinforced AlSi alloy; b. AlSi-2%wt.CNTs; c. AlSi-5wt.%SiCp and d. AlSi-2%wt.CNTs-5% wt.SiCp..... 164

Figure 7. 3 - Hardness of the unreinforced AlSi alloy and all AlSi composites..... 166

Figure 7. 4 - Variation on volume loss for unreinforced AlSi and AlSi - composites..... 167

Figure 7. 5 - Evolution of COF with sliding distance of AlSi-2wt.%CNTs-5wt.%SiC_p hybrid composite..... 168

Figure 7. 6 - Average COF of the unreinforced AlSi alloy and of the Al-Si composites..... 169

Figure 7. 7 - SEM images of the worn surfaces of GCI plates after sliding against AlSi-based pins: a. unreinforced AlSi alloy; b. AlSi-2wt.%CNT; c. AlSi-5wt.%SiC and d. AlSi-2wt.%CNT-5wt.%SiC. 170

Figure 7. 8 - Backscattered SEM image of GCI plate worn surface and EDS spectrum after sliding against (representative of the dark/grey zones in the micrograph) AlSi-2wt.%CNTs-5wt.%SiCp hybrid composite..... 171

Figure 7. 9 - SEM images of the worn surface of AlSi-based pins (130x magnification) and mating GCI plates (backscattered): a1/a2 - unreinforced AlSi alloy/GCI plate; b1/b2 - AlSi-2wt.%CNTs/GCI plate; c1/c2 - AlSi-5wt.%SiCp/GCI plate and d1/d2 AlSi-2wt.%CNTs-5wt.%SiCp/GCI plate..... 173

Figure 7. 10 - SEM images of the worn surface of AlSi-2wt.%CNTs-5wt.%SiCp hybrid composite..... 175

Figure 7. 11 - SEM image (backscattered view) and EDS spectra (corresponding to Z1) of 2wt.%CNTs-5wt.%SiCp hybrid composite..... 175

Figure 8. 1 - SEM images showing: a. CNTs and b. SiCp..... 184

Figure 8. 2 - SEM images of: a. unreinforced AlSi alloy; b. AlSi-2wt.%CNT; c. AlSi- 5wt.%SiCp and d. AlSi-2wt.%CNT-5wt.%SiCp composites..... 186

Figure 8. 3 - SEM images of AlSi-2%wt.CNTs-5%wt.SiCp hybrid composites..... 187

Figure 8. 4 - Stress–strain curves from tensile testing of unreinforced AlSi alloy and of the AlSi composites..... 187

Figure 8. 5 - SEM images of the fracture surface after tensile test: a unreinforced AlSi alloy; b. AlSi - 2wt.%CNTs; c. AlSi - 5wt.%SiCp and d. Al-2wt.%CNTs-5wt.%SiCp..... 189

Figure 8. 6 - SEM images of the fracture surface after tensile test of: a. AlSi - 5wt.%SiCp and b. Al-2wt.%CNTs-5wt.%SiCp 190

Figure 8. 7 - Maximum stresses (σ_{max}) vs. number of cycles to failure for unreinforced AlSi alloy and for the AlSi composites 193

Figure 8. 8 - SEM images of the fracture surface after fatigue test: a. unreinforced AlSi alloy; b. AlSi-2wt. %CNT; c. AlSi-5wt.%SiCp and, d. Al-2wt.%CNT-5wt.%SiCp 195

Figure 8. 9 - Variation on volume loss for unreinforced AlSi alloy and AlSi - composites 197

Figure 8. 10 - SEM images of the worn surface of: a and b. unreinforced AlSi-based pins, c and d 2wt.% CNTs; e and f. 5wt.%SiCp (g), g and h. 2%CNTs -5wt.%SiCp 198

Figure 9. 1 - Schematic test configuration: Fn – Normal applied load; d – alternated displacement amplitude 210

Figure 9. 2 - Results of tensile testing of unreinforced AlSi alloy and of the AlSi composites: a. tensile strength, b. yield strength, and c. tensile strain 213

Figure 9. 3 - SEM images of the fracture surface after tensile test (with different magnifications) of: a. unreinforced AlSi alloy; b. AlSi - 2wt.%CNT 214

Figure 9. 4 - SEM images of the fracture surface after tensile test showing the presence of CNTs agglomerates (AlSi-2 wt. % CNT composite –with magnification 1000x) 214

Figure 9. 5 - SEM micrographs of the composites with different amounts of CNTs to highlight the CNTs agglomerates: a. 2wt.% CNTs; b. 4 wt.% CNTs and c. 6 wt.% CNTs 216

Figure 9. 6 - SEM micrographs of the composites with 2 wt% CNTs showing the crack formation on an CNT agglomerate 217

Figure 9. 7 - Hardness as a function of the CNT content 217

Figure 9. 8 - Wear loss as a function of the CNT content 218

Figure 9. 9 - SEM images of the worn surface of unreinforced AlSi alloy and all AlSi-CNT composites and of the GCI plates: (a/b) unreinforced AlSi alloy/GCI plate; (c/d) AlSi - 2wt.%CNT/GCI plate; (e/f) AlSi – 4 wt. % CNT/GCI plate and (g/h) AlSi – 6 wt. % CNT/GCI plate 219

Figure 9. 10 - Schematic representation of the equipment developed to produce FGMs by powders deposition; b. improved device to produce piston rings from FGM: c. centrifugal system 223

Figure 9. 11 - The variation of chemical composition of AlSi-2 wt. % CNTs FGM composite. a. Cross section of sample where the chemical composition was evaluated; b. Variation of the CNTs (wt.%) vs. position 225

Figure 9. 12- Stress–strain curves from tensile testing of unreinforced AlSi alloy and AlSi – 2 wt.% CNT's composite 226

Figure 9. 13 - Maximum alternating stresses (σ_{max}) vs. number of cycles to failure for unreinforced AlSi alloy , AlSi-2 wt. % CNTs and AlSi-2 wt. % CNTs FGM composite 227

Figure 9. 14 - SEM images of the fracture surface after fatigue test of: 228

Figure 9. 15 - Hardness values of the AlSi-2 wt. % CNT's FGM composite: a. Position on the sample where the hardness was measured and CNTs wt% as a function of the position; c. Hardness as a function of the position 229

Figure 10. 1 - Hot pressing (a) schematic representation and (b) vacuum chamber detail. 238

Figure 10. 2 - SEM images showing: (a) CNTs (magnification 190x);..... 239

Figure 10. 3- EDS spectrum of a CNT agglomerate, corresponding to zone Z1 (white zone) identified in Figure 10. 2 a)..... 240

Figure 10. 4 - SEM image in backscattered view of an Al-Si/2%CNT composite sample. 240

Figure 10. 5 - DSC curves obtained for AlSi alloy and AlSi-CNT composite powders. 241

Figure 10. 6 - XRD analyses for AlSi alloy and AlSi-CNT composite powders and Al-Si/2%CNT composite. 242

Figure 10.7 - EDS spectrum of several identified zones. 244

Figure 10.8 - TEM images of CNT-AlSi composite regions, showing a) CNT next to agglomerate; b)-d) well dispersed CNT. 245

LIST OF TABLES

Table2.1 - Adhesion of some metals in contact with iron under vacuum system [293]..... 60

Table 4. 1 - Chemical composition of zones Z2 and Z4 presented in Figure 4. 2. 103
Table 4. 2 - Agglomerates area fraction of: type A (*y*) and type B (*z*) agglomerates, as a function of CNT content (wt. %) (*x*) inan Al-Si/CNT composite. 112

Table 5. 1 - Chemical composition of AlSi alloy (wt%)..... 117
Table 5. 2 - Chemical Composition of GCI 120

Table 6. 1 - Chemical composition of AlSi alloy (wt%)..... 141
Table 6. 2 – Chemical Composition of GCI..... 142
Table 6. 3 - Results of tensile testing of unreinforced AlSi alloy and AlSi-2 wt. % CNT's composite 145

Table 7. 1 - Chemical composition of AlSi alloy (wt.%)..... 162
Table 7. 2 - Chemical Composition of GCI 163

Table 8. 1 - Chemical composition of AlSi alloy (wt.%)..... 183
Table 8. 2 - Chemical composition of GCI..... 183
Table 8. 3 - Results of tensile testing of unreinforced AlSi alloy and of the AlSi composites 188

Table 9. 1 - Chemical composition of AlSi alloy (wt.%)..... 209
Table 9. 2 - Characteristics of equipment developed to produce FGMs..... 223
Table 9. 3 - Results of tensile testing of unreinforced AlSi alloy and AlSi-2 wt. % CNT's composite 226

Table 10. 1 - Chemical composition of Z2 and Z4 zones, presented in Figure 10. 4. 241

1 Scope of the thesis

1.1 Motivation and objectives

This thesis main focus is the development and characterization of new and improved functionally graded materials (FGMs), based on aluminium-silicon alloys reinforced by nickel coated carbon nanotubes (CNTs) and obtained by a powder metallurgy technique.

Although the outputs of the studies included on this thesis can be applied in a wide range of industrial applications such as cutting tools, moulds industry, automotive components, this work final phase focuses on the development of a piston ring, which will act as demonstrator of the proposed concept validity. This type of component has several requirements as mechanical, wear and fatigue behaviour at different zones that can be achieved with a FGM type of material.

Compression piston rings are found inserted in internal combustion engine pistons, having the function of sealing the gap between the piston and the cylinder. It is submitted to high temperatures, corrosive gases and friction against the cylinder walls. Their function is to maintain the combustion pressure, prevent gas escaping, and avoid oil entrance in the combustion chamber. Therefore, piston rings must have high wear resistance on outer surface, high fatigue and mechanical resistance in a range of temperatures allied to a high thermal conductivity.

Thus, the solution to overcome the previously mentioned problems would be the development of a piston ring with different properties/materials/structure along their section, suited to different local solicitations.

Piston rings damage can be substantially mitigated by creating a FGM-Functionally Graded Material that promotes a smooth transition between different materials, unlike traditional manufactured materials where sharp transitions occur (leading for example to detrimental sharp local stress concentrations). The great advantage of using FGMs is the ability to control composition and/or structure and thereby obtain transitions with designed properties (mechanical, tribological, thermal properties among others) between different locations of a component. A piston ring design that allocates mechanically resistant material in the inner region and a wear and fatigue resistant material at outer regions can benefit greatly from using the FGM concept – upgrading the existing

commercial solutions (where outer surfaces are mainly coated by, for example, PVD or electrocoating).

Powder metallurgy (PM) processes start with powdered metals (or non-metals) until the component final consolidation (below the melting points of main constituents). These processes generally occur with high pressures and simultaneously or subsequently heat. The ease of processing FGMs via powder metallurgy and other inherent advantages like being near-net shape processes; the reduced waist of material and among others, make this process suited for the production of these composites.

Components on aluminium based alloys, obtained by powder metallurgy, can exhibit high mechanical, wear and fatigue properties. They allow, also, the production of low weight components which contributes to energy consumption reduction. When regarding aluminium matrix composites, the ease of introducing different types of reinforcements, by the powder metallurgy technology, is an additional significant advantage. Therefore, PM processes are competitive solutions for the production of aluminium-based components.

Carbon nanotubes (CNTs) outstanding properties seem to fit very well the design of high performance functionally graded materials composites due to their high specific tensile strength and elastic modulus, high wear resistance and also excellent thermal conductivity.

CNTs nickel coated not only contributes to load transfer to CNTs but also maintaining CNT integrity. The Ni coating allows the introduction of CNTs on commercial alloys, an advance in current CNT-reinforced metal matrix composites.

This thesis is concerned with the development of carbon nanotubes functionally graded metal matrix composites, obtained by powder metallurgy. Inspired by piston rings, AlSi-CNTs functionally graded material (FGM) here presented were designed in order to fulfill their requirements.

Additionally, hybrid composites were also produced in order to verifiy the component properties. Combinations of CNTs and SiC particles additions were tested. Hybrid composites present as strategic advantage the ability to take benefit of different reinforcements for the final overall composite performance (regarding mechanical and wear).

Following this rational, a comprehensive characterization of the produced materials, regarding metallurgical, mechanical, fatigue properties and also wear behaviour was conducted.

1.2 Work development strategy

The main goal of this work is to develop and design new materials based on aluminium composites reinforced by CNTs towards more efficient components that respond differently in different locations, where suited materials are allocated (using smooth transitions) by a powder metallurgy route – hot pressing technology.

To achieve this goal, a strategy was formulated, comprising the following steps:

- Review (Include chapter 2);

- Assessment of several mixing processes for mixing aluminium powders and the reinforcement (Include chapter 3 and 10);

- Assessment of the optimum reinforcement fraction for these composites (Include chapter 4);

- Study and explanation of the effective reinforcing mechanisms on these composites (tensile, fatigue and wear) (Includes chapter 5, 6, 7, 8);

- Development of an equipment to obtain components with selected graded composition and design of a graded composition (reinforcement distribution) for piston rings production (Include chapter 9).

1.3 Thesis structure

This thesis is organized as a compilation of eight research papers (6 published and 2 submitted for publication in ISI journals). Preceding the research papers presentation, two chapters are included – chapter 1 and 2.

Chapter 1 (current one) presents the motivation and objectives of the thesis, the implemented strategy of the work developed in the context of the thesis and its structure. Chapter 2 presents a literature review (state of the art) on several theoretical concepts that are central to this work, namely, Aluminium Silicon Alloy (2.1), Powder Metallurgy (2.2), Carbon nanotube aluminium composites (2.3), Carbon nanotubes (2.3.2), Carbon nanotube aluminium composites

(2.3.3), Functionally Graded Materials obtained by powder metallurgy(2.4), Piston rings (2.5), Strengthening mechanisms (2.6), Fatigue in Metal Matrix composites(2.7) and Wear (2.8).

These topics selection was based on the general objective of this thesis: production of piston rings with improved performance by using a powder metallurgy technique.

Subchapter 2.1, besides a bibliographical research on aluminium silicon alloys, presents the criteria used for the selection of eutectic aluminium-silicon alloy for the composites developed in this work. Since a powder metallurgy technique was used for producing these composites, a general overview regarding these techniques (starting from powders production until the final sintered part) is presented on subchapter 2.2.

Metal matrix composites (MMCs) are shortly addressed in subchapter 2.3, followed by a comprehensive review regarding Carbon nanotubes (CNTs), the reinforcement used for the production of these composites. Following this topic, subchapter2.3.3 presents a review on Carbon nanotube aluminium composites obtained by powder metallurgy techniques.

Functionally graded materials (FGMs) production by power metallurgy, relevant topic for the final model of controlled deposition powders equipment (Chapter 9) and on this work general concept and approach, is presented in subchapter 2.4.

Starting from piston rings requirements and aiming to their performance improvement, subchapter 2.5 brings a brief outline on Piston rings: their role in an internal combustion engine and manufacturing processes by power metallurgy. This subchapter is important for the understanding of the final model of controlled deposition powders equipment.

Composites mechanical properties relation with several strengthening mechanisms is addressed in subchapter 2.6. Subchapter 2.7, on fatigue, presents some concepts on this area once high fatigue resistance is desirable for piston rings. Additionally reinforcement's roles on composites fatigue resistance are also addressed. Once wear is an important issue regarding piston rings performance, subchapter 2.8 focuses on this subject, mainly abrasive and adhesive wear, the main wear mechanisms identified in the produced composites.

Chapters 3 to 10 gather the research papers, which comprise the following sections: Introduction, Experimental procedures; Results and discussion and Conclusions.

Chapter 3 (Evaluation of CNT dispersion methodology effect on mechanical properties of an Al-Si composite) presents an assessment on different dispersion methodologies influence on

mechanical properties of an Al-Si alloy reinforced with multi-wall carbon nanotubes (MWCNT), functionalized with Ni.

In chapter 4 (Carbon nanotube dispersion in aluminium matrix composites – quantification and influence on strength) the influence of different volume fractions of carbon nanotubes in the metallurgical and mechanical properties of CNT-reinforced Al-Si composites are studied. Additionally CNT's agglomerates were quantified and their content influence on these composites mechanical properties is assessed.

Chapter 5 (Improvement on sliding wear behaviour of Al/cast iron tribopair by CNTs reinforcement of an Al alloy) is focused on the influence of different CNTs volume fractions on the tribological behaviour of these composites – under dry reciprocating sliding conditions against a grey cast iron (GCI).

In chapter 6 (Mechanisms Governing the Tensile, Fatigue and Wear Behaviour of Carbon Nanotube reinforced Aluminium Alloy) the influence of several acting mechanisms in AlSi-CNTs mechanical, wear and fatigue behaviour are presented, through tensile tests (yield strength, ultimate tensile strength and strain and fracture morphology), wear and fatigue tests.

Chapter 7(Dry sliding wear behaviour of AlSi-CNTs-SiCp hybrid composites) and chapter 8 (Mechanical, wear and fatigue behaviour of an AlSi-CNTs-SiCp hybrid composite) concern the same hybrid composite: AlSi-2wt. %CNTs-5wt. %SiC. These two chapters fully characterize this hybrid composite when regarding mechanical, wear and fatigue behaviours and determine the combined effects of both reinforcing constituents (CNTs and SiC).

In chapter 9 (Optimization of AlSi-CNTs functionally graded material composites for engine piston rings) an FGM piston ring design proposal is presented, encompassing the conclusions obtained from the previous studies (chapters).

In chapter10 (Interface analysis on an eutectic AlSi alloy reinforced with Ni coated MWCNT) is performed a performed a detailed study about chemical reactivity between Ni coated MWCNT and AlSi matrix.

Finally, in chapter11 (General discussion), a global analysis and discussion of all the performed work, the main conclusions and also an outlook for future works are presented.

2 State of the art

This chapter presents a comprehensive review on theoretical concepts and technological aspects on several topics related with the main subject of this thesis: development of new and improved functionally graded materials (FGMs), based on aluminium-silicon alloys reinforced by Ni Coated CNTs, obtained by a powder metallurgy route.

This review focuses on aluminium silicon alloys; powder metallurgy; metal matrix composites; Ni coated carbon nanotubes; Carbon nanotube aluminium composites; Functionally Graded Materials obtained by powder metallurgy and piston rings. Afterwards, a brief review concerning strengthening mechanisms, fatigue and wear are included.

Starting with aluminium silicon alloys, a brief comment on aluminium alloys and particularly aluminium-silicon alloys is made, presenting the rational for the matrix alloy selection for developing these composites. In order to introduce powder metallurgy techniques and to contextualize their selection for the studies here presented, an overview on several aspects regarding these processing routes is included.

Metal matrix composites, CNTs and CNTs aluminium composites are subsequently addressed, in order to contextualize readers with different backgrounds to several issues but especially to CNTs and their use as reinforcement.

As the final aim of this work is FGMs development and production, an overview on FGMs, mainly regarding their productive process by powder metallurgy is included. This overview was conducted to understand different processes aiming to the final FGM production system.

With the selected demonstrative component in mind, a review on piston rings is included, mainly focused on powder metallurgy for these components production.

A review on strengthening mechanisms, fatigue and wear are included, in order to understand the role of reinforcements on mechanical, fatigue and wear behaviour.

2.1 Aluminium Silicon Alloys

Aluminium and its alloys are widely used in a large number of applications due to their low density (Al density of 2.71 g/cm^3, approximately one third of that of steel (7.83 g/cm^3)), high specific strength, high thermal and electrical conductivity, a relatively low melting temperature, corrosion resistance and the fact of being a 100% recyclable material without degrading mechanical and metallurgical properties [1]. Aluminium alloys are found in vehicles, due to the enormous advantage of reducing the vehicle weight and power consumption, increasing the load capacity.

Aluminium alloys have the additional advantage of being processed using various techniques (cast, rolled, extruded, forged). The mechanical strength of aluminium alloys can be improved by modifying the alloy composition and also performing a variety of thermal and mechanical treatments. The addition of alloying elements and also reinforcements have, not only the intention of increasing mechanical properties, but, for instance, improve machinability, castability or sinterability (for powder metallurgy).

Among aluminium alloys, near eutectic aluminium silicon (Al-12%Si) alloys present a superior wear resistance. These alloys are widely used as piston materials for petrol engines due to their low thermal expansion coefficient and also high wear resistance [2]. Al-12%Si alloy is a widely used commercial one, highly available, regarding which there are few works, opening an opportunity to explore new CNT-reinforced composites based on this alloy.

2.2 Powder metallurgy

Powder metallurgy can be defined as a set of techniques and processes for producing powdered materials, and their subsequent processing into consolidated products with powder coherent mass (metallic or non-metallic) through simultaneous or subsequent application of high pressures and heat, generally below the melting temperature of the main constituent [3].

Powder metallurgy is used due to its multiple advantages, like being a near-net shape technology with great dimensional control and tight tolerances; the low material waste; the ability to process certain high melting temperatures metals or alloys (e.g. Tungsten) and

the fact of these processes can be more easily automated, making them a competitive process for certain materials [4]. However these techniques have some disadvantages, namely the high cost of tools, equipment and powders and the difficulty in storing and handling powders (oxidation, reaction, etc.) [4].

The manufacture of components by powdered techniques start with the production of powders, and their ensuing mixture (in the desired quantities, for alloy production; composites production; binder and/or lubricant addition), followed by the compaction step (being obtained a green compact in the case of press and sinter). After these steps, the sintering is carried out by heating. If necessary, a forging/cold work step can be performed to the sintered component, in order to obtain final desired properties (densification; reinforcement orientation; work hardening) [4]. There are processes where the compaction and heating are simultaneously performed and the forging/cold work step can be neglected (hot pressing and hot isostatic pressing).

Powders production is mainly mechanical atomization. There are different kinds of mechanical atomization: by gas; by water; centrifugal atomization and ultrasonic atomization [5]. There are also combinations of different atomization systems - hybrid systems [6]. All of these processes act by breaking liquid into droplets [5].

In gas atomization, one or many stream of inert gas are projected towards a jet of molten metal [7]. This process was used to produce the Al-12%Si alloy powders used to produce the composites developed in the scope of this thesis (Figure 2.1).

The process that is used to obtain metal powders influences the shape and size of the powders. Depending on the metal/alloy and also on liquid metal temperature, smaller surface tension leads to smaller and irregular powder particles [8]. For instance, in gas atomization, the cooling produced in the molten metal (process with low cooling rates) gives enough time to liquid metal particles to become spherical, due to surface tension. By water atomization, due to higher cooling rates, more irregular and harder particles are obtained [3]. Figure 2. 1 shows powders obtained by two different processes, evidencing the influence of the process on the final powders shape.

The atomization process can also influence other aspects such as purity of the powders, particle size distribution, chemical composition and microstructure that can have

an effect on properties like flowability, compressibility and compaction of powders; green compact strength; sinterability and hardness [3].

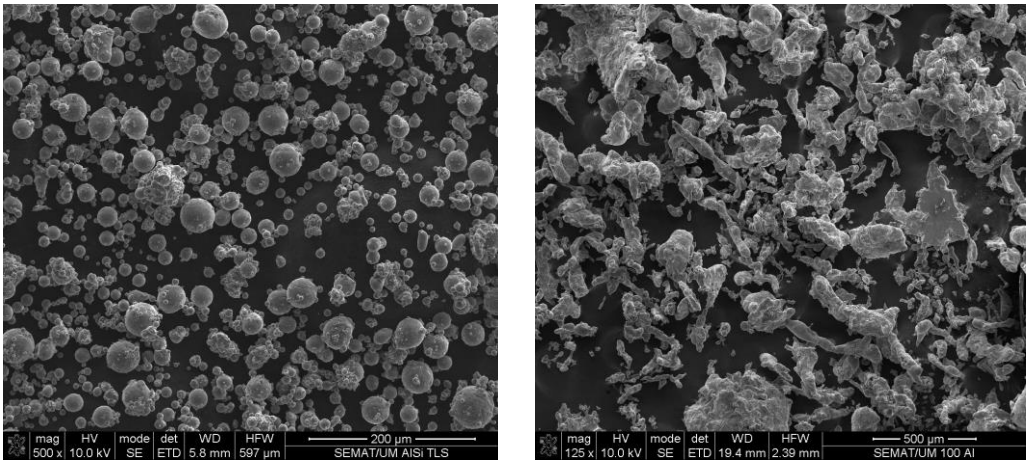

a) b)

Figure 2. 1 - a) Al-12%Si alloy powder obtained by inert gas atomization (from TLS Technik) and b) Al-12%Si alloy powder obtained by a hybrid atomizer developed by O. Carvalho.

The obtained powders mixing and homogenization is then performed, in order to proceed to compaction and sintering. Sintering can be defined as a thermal treatment for bonding particles into a coherent, predominantly solid structure via mass transport events that often occur on the atomic scale. The bonding leads to improved strength and lower system energy [9].

Sintering processes can be divided into two major groups: solid state sintering and liquid phase sintering. Liquid phase sintering occurs when one of the constituents of the powder mixture melts (the one with lower melting temperature), promoting consolidation [4]. For example, to Al powders are often added Zn, Sn or Cu, such that at the aluminium sintering temperature, these metals melts, helping to consolidate the material [10-17]. Solid state sintering occurs when the powder compact is consolidated with all the constituents in the solid state (at the sintering temperature) [18].

Others types of sintering include transient liquid phase sintering and viscous flow sintering [18]. Phase diagrams help to identify where these different processes can occur (Figure 2. 2).

A special attention will be given to solid state sintering once this was the process used in this work.

During solid state sintering there is a surface energy reduction. By the influence of heat there is a reduction of surface area, when comparing with the green compact (set of grains with a large surface area). This happens through growth and formation of bonds between particles. Macroscopic driving force for sintering is related with the reduction of excess free energy associated with surfaces.

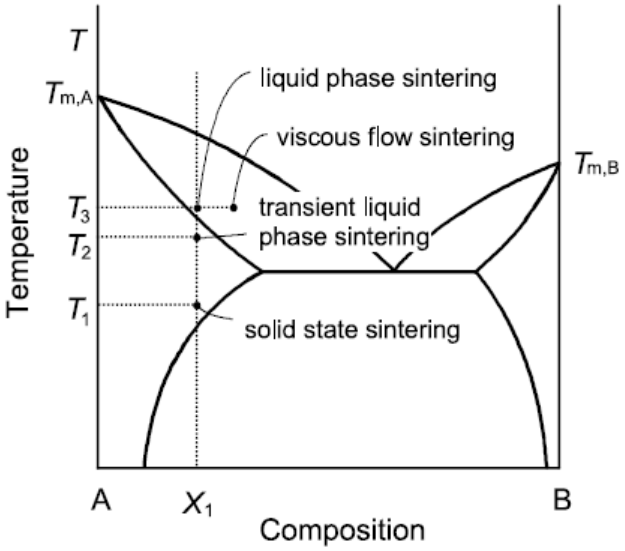

Figure 2. 2 - Schematic phase diagram with indication of various sintering processes [18].

This phenomenon can occur in two ways: by reducing the total surface area with increasing average particle size, leading to "coarsening" (particle growth) or by elimination of a solid/vapour interfaces and creating the contour area grain, followed by grain growth [18].

Figure 2.3 shows a schematic model of two spherical particles, representing the contact of two adjacent particles, typically used to explain the mechanisms involved in sintering.

The sintering microstructure consists of a mixture of convex and concave surfaces and during sintering the curvature gradient gives a thermodynamic impulse that drives mass flow along this process[20]. As seen in Figure 2.3, the sinter neck is concave (curved inward) and the particle surface is convex (curved outward). The atomic motion takes place from regions of higher tension (convex region) to zones of lower tension (concave region). Thus, the atoms moves from convex region to concave zones (necks) which is responsible for neck

grow. Atom motion is faster at higher temperatures and small particles have large gradients in curvature, thus it is expected a higher sintering rate for smaller powders and higher temperatures [20].

Vapour transport (evaporation/condensation), surface diffusion, lattice (volume) diffusion, grain boundary diffusion, and plastic flow (in amorphous material) are the main mass transport mechanisms during sintering and determine how mass flows in response to the driving force for sintering [21].

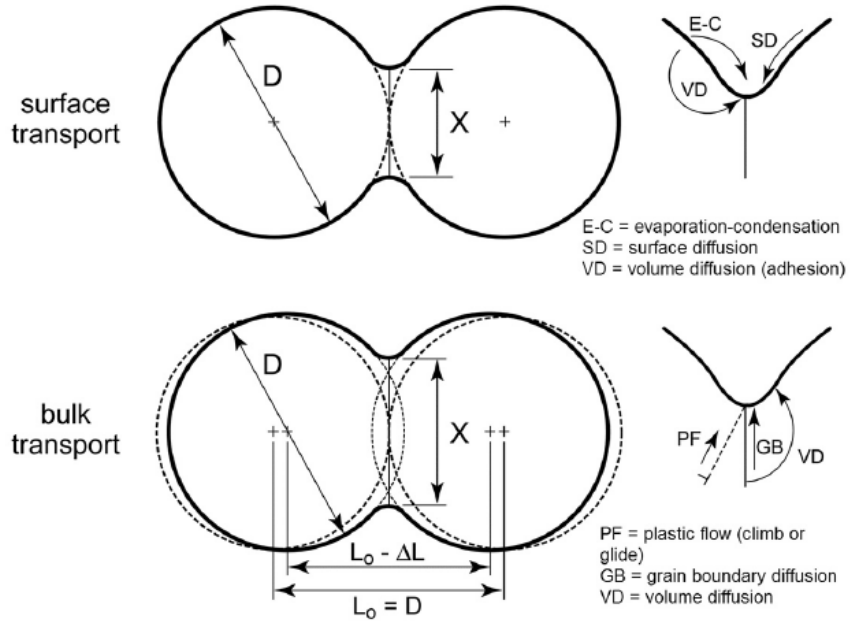

Figure 2.3 - Schematic model representing the sintering process by surface and bulk transport [19].

Evaporation/condensation occurs preferably on flat or convex surfaces of the particles, while the deposition occurs on the necks (concave). This is usually a dominant process mainly when fine powders (with high specific surface area and high vapour pressure) are used. Transport by surface diffusion occurs by movement along the surfaces of the particles boosted by roughness and defects such as vacancies or edges. Volume diffusion involves movement of vacancies through the crystal structure, and the diffusion rate is a function of temperature and composition of the particles. In the mechanism of diffusion through grain boundaries, the material is removed along the contours, and placed at the intersection of the neck's surface contours. Transport by plastic occurs via generation of

dislocations in the material, which interact with vacancies during sintering leading to atoms movement [9].

Vapour transport, surface diffusion, and lattice diffusion from the particle surfaces to the neck lead to neck growth and coarsening of the particles [20] but since they are surface transport mechanisms they do not provide densification to the compacts [19]. Grain boundary diffusion, lattice (volume) diffusion from the grain boundary to the neck and plastic flow cause neck growth and densification (shrinkage) [20]. Figure 2.3 shows two different mass transport mechanisms.

Higher sintering rate is expected when pressure and temperature are applied simultaneously. Hot pressing is an example of these processes. With application of external pressure, lattice and grain boundary diffusion, plastic deformation and creep mechanisms are the major mechanisms, unimportant in pressureless sintering [18]. However, the overall densification rate of a compact is the sum of the densification rates for all the above-mentioned mechanisms and additionally vapour transport (evaporation/condensation) and surface diffusion.

An important aspect that influences the sinterability of metals and aluminium alloys in particular is the powders surface condition. For instance, during atomization and subsequent handling aluminium powders can oxidize and the oxide film can have different thickness and can be amorphous or crystalline [22]. Aluminium powder produced by air-atomizing process have oxygen contents ranging from 0.3 to 0.6 wt.% [23].

Thermodynamically stable alumina (aluminium oxide) film on each aluminium particle tend to hamper the sintering process because this film works as a barrier to inter-particle diffusion of aluminium atoms and to the diffusion of solute atoms into the aluminium particles [24]. Oxide films need to be chemically reduced or mechanically disrupted to enable effective sintering both in solid state sintering and liquid phase sintering.

In pressure assisted processes (e.g. hot pressing), the powder compaction using pressure presents the advantage of disrupting these oxide films due to the considerable distortion of the ductile aluminium powders. Oxide films rupture at the points where particles touch are local areas of contact free from oxides [25].The rupture of oxide films can originate nanoscale oxide particles (Figure 2. 4) mainly when severe plastic deformation is higher than that required for sintering [26; 27].

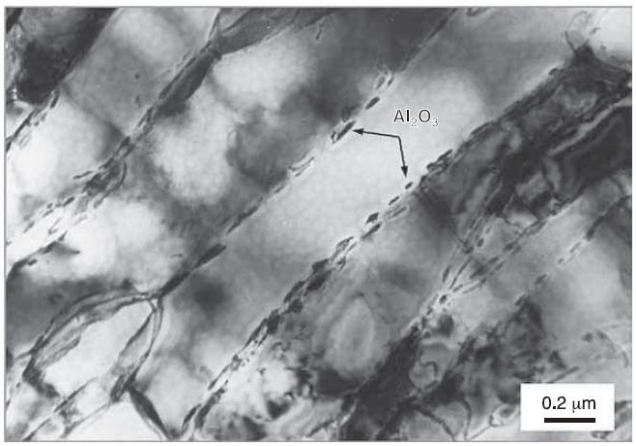

Figure 2. 4 - Disintegrated oxide films, into particles of 50–150 nmon pure aluminium powder [26].

2.3 Carbon nanotube aluminium composites

2.3.1 Aluminium matrix composites

Metal matrix composites (MMCs) first emerged in advanced military systems [28] and were extended to other fields like high technology aerospace [29,30], automotive industry [30, 31], sports, biomedical, electrical and electronic components and also machining tools.

Generally speaking, composite materials can be defined as a matrix with one or more physically distinct, distributed phases, known as reinforcements. The reinforcement is added to the matrix to meet the desired properties improvement like strength, stiffness, toughness, thermal conductivity, electrical conductivity, coefficient of thermal expansion, electromagnetic shielding, damping and wear resistance [32].

Aluminium matrix composites (AMCs) are MMCs in which aluminium or aluminium alloys are the matrix material. According to literature, AMCs have some advantages when compared to unreinforced materials: greater strength; improved stiffness; reduced density (weight); improved high temperature properties; controlled thermal expansion coefficient; thermal/heat management; enhanced and tailored electrical performance; improved abrasion and wear resistance; control of mass (especially in reciprocating applications); improved damping capabilities [33].

According to the type of reinforcement used, AMCs can be divided into four main groups: Particle-reinforced AMCs (PAMCs); Whisker-or short fibre-reinforced AMCs

(SFAMCs); Continuous fibre-reinforced AMCs (CFAMCs); Mono filament-reinforced AMCs (MFAMCs) [4].

There is a wide variety of MMCs fabrication techniques, including powder metallurgy [34,35],molten metal methods [36,37],semi-solid casting, pressure infiltration [38] and spray deposition [39,40]. However, there are other techniques that have emerged making this division outdated. For example, in the production of metal matrix composites reinforced with carbon nanotubes, Bakshi et al. [41] and Agarwal [32] classified the production processes of CNTs metal matrix composites (CNT-MMC) in five major groups: Powder metallurgy, Melting and solidification, Thermal spray, Electrochemical deposition and other novel techniques (that include a mixing by chemical processes combined with powder metallurgy processes). Thermal spray, and Electrochemical deposition are difficult to include in any of the groups proposed by Srivatsan et al. [42].

2.3.2 Carbon nanotubes

In 1991, a Japanese researcher Sumio Ijima discovered carbon nanotubes, i.e. cylindrical structures whose walls are formed by carbon atoms tri-coordinated in their sp2-hybridized orbital's [43]. The bonds between carbon atoms confers to carbon nanotubes exceptional structural, mechanical and electrical properties, making these materials very appealing for research on several areas like physics, chemistry, materials science and biology pharmacology [43].

CNTs can be described as a graphite sheet rolled up into a nanoscale-tube [44]. If this tube has just one sheet, these are designated as single-layer nanotubes, called single-wall carbon nanotube (SWNT). The double-walled nanotube is named double-wall carbon nanotube (DWNTs), a special kind of Multi-wall carbon nanotube (MWNTs), that have more than two layers [44,45].

CNTs diameter ranges between fractions of nanometres and tens of nanometres, while their length can go up to several micrometres, with tips normally closed. The bonding between CNTs layers are made by Van der Walls forces [45-47] conferring different mechanical properties to SWCNT and MWCNT reinforced composites, as shown by George et al. for aluminium composites [48]. Van der Walls forces between layers of MWCNT,

confers them a good self-lubricating properties, once the layers can slip or rotate, leading to a low coefficient of friction [49-51]. Due to the good tribological properties, CNTs can also be used in other applications such as additives in oils [52-54].

Some theoretical and experimental measurements have shown that CNTs have both excellent mechanical properties (e.g. elastic modulus of more than 1TPa [55,56] and tensile strength of 10 to 100 times higher than steel [45]) and exceptional physical properties (high thermal conductivity, of about twice that of diamond and electrical properties 1000 times higher than copper [57]).

In addition, CNTs exhibit low density, with SWCNT having a density of 0.6 g/cm^3 and MWNT density ranging between 1 and 2 g/cm^3. This makes CNTs a high specific strength material, making them ideal reinforcements for composites [58].

CNTs stability under temperatures as high as 2700 K, in an argon atmosphere or under vacuum [59], can favour their application without degradation. Due to their electrical, optical and mechanical properties they have been used for the production of different types of devices, such as electron emitters, gas sensors and biological sensors, tips for atomic force microscope (AFM), and when combined with other materials such as polymers, ceramics and metals serve as reinforcing constituent, forming composites with improved properties [43].

The functionalization of CNTs walls is a promising trend for exploring these materials potential, by suiting the functionalization to specific requirements (e.g. favour chemical bonding). This process consists in promoting bonding between other molecules/elements and CNTs. When thinking on composites, functionalization has specific functions like improving bonding between CNTs and a matrix. This process is widely used in the production of polymer composites [60-62]. In the case of metal matrix composites, CNTs can be metal coated or used other inorganic coating, in order to improve interfacial adhesion between CNTs and the metal matrix [62-66]. Figure 2. 5 shows an example of CNT metal coated. Functionalized CNTs can present electrical and mechanical properties that are substantially different from non-functionalized CNTs [67].

SWCNT and MWCNT can be produced by several techniques like arc-discharge [68,69], laser ablation [70], gas-phase catalytic growth from carbon monoxide [71], and chemical vapour deposition (CVD) from hydrocarbons [72-74]. The process used for

producing CNTs influences their mechanical properties: CNTs produced by catalytic process exhibit worst mechanical properties when compared with those obtained by arc-discharge [46].

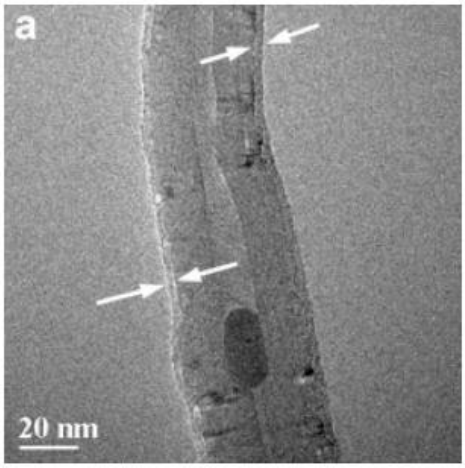

Figure 2. 5 - Carbon nanotube functionalized with magnesium (arroys indicate the Mg layer) [64].

2.3.3 Carbon nanotube aluminium composites by powder metallurgy

Due to CNTs excellent properties, these have been used as reinforcement in different kinds of composites, whether metal, ceramic or polymeric matrix composites [75]. In recent years much work has been done with regard to metal matrix composites reinforced with CNTs [75,76]. With the introduction of CNTs, it is expected to overcome some of the shortcomings presented by some materials, such as electrical conductivity of polymers and toughness of ceramics.

When analysing several research studies related with aluminium matrix composites reinforced with CNTs, a common issue arises: dispersion of CNTs, regarded as the dominating factor when considering these composites mechanical properties.

Different approaches have been used to disperse CNTs in a metallic matrix. These processes can be divided in five main groups: powder metallurgy techniques, electrochemical processes, thermal spraying processes, welding processes and some innovative techniques [41, 77]. This work will mainly address power metallurgy processes, once they were used in the studies presented in this thesis.

Powder metallurgy processes usually start by mixing CNTs with the metallic matrix powder, both being introduced into a metallic cup with steel balls (the movement of the power mixture and the balls friction and shocks between balls and the mixture promotes CNTs deagglomeration). This process can also be designated as mechanical alloying. In this type of technique, different agitation speeds can be used, so that these processes can be divided into low and high energy milling [78], both leading to CNTs dispersion. Regarding these processes it is essential to control time and energy, once damage CNTs with excessive mixing times and velocities can occur. These processes can also lead to powder growth [79] as a result of the welding between particles, which hinders the composite sintering.

Esawi et al. [80] used high energy milling to make the mixture of aluminium and 2 wt% of CNTs, obtaining a tensile strength increase of about 21%. In this work the composites were extruded after sintering, which means that the mechanical proprieties could be lower if no extrusion had been performed.

Carbon nanotube aluminium composites production by powder metallurgy process can be performed using cold pressing and sintering [48], hot pressing [81] and spark plasma sintering [82], with subsequent plastic deformation processes [48, 80, 83-86] or not.

By cold pressing and sintering the mixture is cold pressed and then sintered[48]. On the other hand, by hot pressing [8,81] the mixture is compressed while it is sintered. In spark plasma sintering process [82] the mixture is sintered by pressing with electrical discharges. Final plastic deformation can be performed after sintering the composites (consolidation step) [48, 80, 83-86], by forcing the material to pass through a channel with a certain angle. This step contributes to the fragmentation of CNTs agglomerates, improving final mechanical properties.

George et. al. [48] produced SWCNT and MWCNT reinforced aluminium composites (with 0-2 wt.%) by cold pressing and sintering with final hot extrusion. By this process, CNTs dispersion was improved (when compared to non-extruded) and an increases in yield strength (8% for composites with 0.5wt % CNTs and 24% for composites with 2 wt.% CNTs) as well as in elastic modulus (12 and 23% for 0.5 and 2 wt.%CNTs respectively).

Hot pressing process [81] main advantage, when compared to cold press and sintering, is the possibility of achieving higher densification in a lower time interval. Spark

plasma sintering is even a faster process and can be carried out at lower temperatures, thus avoiding grain growth and undesirable reactivity [87].

Esawi et. al. [83] used hot pressing followed by a plastic deformation process (lamination).The mixture of aluminium and CNTs is placed in a copper package that is then hot laminated. Al-0.5wt.% CNTs samples presented the higher mechanical properties, with improvements of 43% and 20 % in yield stress and elastic modulus, respectively and a 19% reduction in strain to failure. This study, showed that higher CNT content's lead to poorer CNTs dispersion and consequent lowering of mechanical properties.

Esawi et. al. have conducted a further study [80], which showed the effect of cold working on the composites final properties. In this study, there was a 21% improvement in tensile strength, for 2wt.% CNT composites. This improvement was attributed to cold working and hot extrusion (that dispersed and aligned the CNTs in the direction of load application during extrusion and compression process).The limitation of this technique is that it cannot be applied to all geometries, being especially suited to cylindrical samples, making difficult its industrial implementation.

Deng et. al. [84, 88] used a similar processing route than Esawi et. al. [83], where the powders mixture (Al and CNTs) was placed in a rubber package that was then isostatically pressed. This compact was afterwards hot extruded. Deng et. al. [84 ,88] found that the higher properties were obtained for composites with 1wt.% CNTs, with 41, 34, and 33% increase in elastic modulus, tensile strength and hardness respectively, accompanied by 4% reduction strain to rupture.

Perez et. al. [85, 89] tried different mixing times and different volume fractions of CNTs (in an Al matrix), making the mixture by ball milling and using cold pressing and sintering, followed by hot extrusion. Effective dispersion was achieved and improvements of80, 53 and 48% in yield stress, tensile strength and hardness, respectively, were observed (for composites with 1.75 wt.% CNTs).

Sridhar et. al. [86] used a similar process to Perez et al. [85, 89] obtaining improvements of 93, 88, 9 and 12% in yield strength, tensile strength, elastic modulus and strain to failure correspondingly.

The major challenge in the manufacture CNT-reinforced metal matrix composites is the CNTs dispersion on the matrix. The second major challenge is to establish a favourable bonding at metal matrix/CNT interface.

Regarding aluminium matrices some studies use CNTs as reinforcement for commercial alloys by means of powder metallurgy. However, most of the studies use pure aluminium, once it allows a higher control over the reactivity between CNTs and the matrix.

It has been reported that CNTs are very stable when regarding chemical reactions. Nevertheless, some of the defects on CNTs (open tips in CNTs [90]) might lead to reaction with aluminium [91]. According to the majority of the studies, the reaction product between aluminium and CNTs is aluminium carbide (Al_4C_3) [91-93]. In this reaction it is assumed that the free surface of CNT remains intact, due to the reduced processing time and temperature. Otherwise, CNTs would be fully transformed into Al_4C_3 [94].

This reaction product was mainly identified in liquid phase processes, like in plasma sintering [91]. However Al_4C_3 was also identified in processes like the one used in this work (hot pressing [95]), where aluminium melting temperature is not achieved.

According to Kwon et. al. [92, 96] the formation of Al_4C_3 has a beneficial effect on enhancing mechanical strength. Additionally, this compound is responsible for an efficient stress transfer effect from matrix to reinforcement [97].For aluminium alloys, the formation of Al_4C_3 was also observed due to the presence of carbon, as in aluminium silicon matrix composites reinforced with carbon fibres, produced by metal liquid infiltration [98]. Vidal-Setif et. al. [99] showed that in this case there was a strength reduction due to Al_4C_3 formation. Therefore, Al_4C_3 formation and extent should be carefully controlled because of its brittleness [100,101].

Furthermore, in CNT-reinforced aluminium silicon composites, besides Al_4C_3, also SiC was formed [102,103]. Different carbides (formed in interfacial zones) distinctly influence these composites mechanical properties. The carbides strength determines the stress transfer ability from matrix to reinforcement.

The reinforcement/matrix interface should guarantee the chemical stability of CNTs, by avoiding its complete reaction. Additionally, the interface should also assure the formation of reaction that allow the effective stress transfer from matrix to interface.

A possible approach to control reactivity between a reinforcement and matrix is the use of coatings on reinforcements [104, 105]. Similar to carbon fibres coating [104, 105], CNTs coating could be a solution towards reactivity control. Few works used this solution: Li et. al. [106] work added 0.67 wt.% nickel coated CNTs to a magnesium matrix, and achieved an increase of more than 150% on ultimate tensile strength besides a 30% ductility improvement. No studies were found concerning nickel coated CNTs as reinforcement for commercial aluminium alloys.

Nickel is the most widely used metal for coating particles and ceramic fibres for use on aluminium composites [107-111]. The majority of the coatings are made by electroless plating, process also used for coating CNTs [112-114]. Coating the reinforcement influences the physical, mechanical and chemical properties of the composites.

Aluminium reaction with Nickel can lead to the formation of stable intermetallic compounds like $NiAl_3$ and Ni_2Al_3 [115].

In this work, Ni coated MWCNT were used to reinforce an AlSi alloy. As already mentioned, according to Kwon et. al. [92, 96] the formation of Al_4C_3can be beneficial to improve the stress transfer ability. Related with aspect, no studies were found regarding $NiAl_3$ andNi_2Al_3CNT/AlSi (commercial alloy) interfaces. However, Miranda et. al. [115] (a work were the author of this thesis also participated) produced Ni particles reinforced AlSi composites where the formation of $NiAl_3$ was detected. This intermetallic has higher strength than the matrix and Ni particles. It was noticed that this intermetallic contributed to the stress transfer from matrix to reinforcement (Ni). Therefore, it is expected the same behaviour for the CNTs nickel coating, where the formation of this intermetallic not only contributes to load transfer to CNTs but also maintaining CNT integrity. The Ni coating allows the introduction of CNTs on commercial alloys, an advance in current CNT-reinforced metal matrix composites.

2.4 Functionally Graded Materials obtained by powder metallurgy

Nature was the first to produce gradated materials and served as inspiration for the development of new materials designated as Functionally Graded Materials (FGM) [116-119]. Bamboo for instance is a natural FGM, well known by the scientific community [117,

120] due to its mechanical properties. Some other examples of FGMs are teeth, bones, seashells, sedimentary rocks, soils and wood [116-119].

The term Functionally Graded Material emerged in the mid-eighties in Japan, where FGMs were developed for aerospace applications [121]. FGMs are materials in which there is a variation in composition and/or structure which results in material properties change along one axis, at least [122].

The great interest on using FGMs is the possibility of controlling composition or structure and thus obtain components with desired local properties, as regarding mechanical, tribological, thermal properties and other. FGMs have successfully been used to produce thermal barrier coatings, gas turbine blades, chemical reaction vessels, cutting tools, bio-implants and thermoelectric components [123-125].

Scientific community has developed techniques for manufacturing FGMs with spatial variation in composition being introduced during the fabrication. The goal is to avoid abrupt transitions from one material to another, thus avoiding sharp local stress concentrations [126].

According to Erdogan et. al. [127],Yang et. al. [128] and Kokini et. al. [129], the usage of FGMs, can be highly advantageous, namely: i) thermal stresses reduction; (ii) reduction of thermal stresses at critical locations; (iii) diminution of sharp stress transitions at the interface; (iv) reduction of stress intensity factor (driving force for crack propagation) and (v) increase of the interfacial bond strength.

According to Kieback et. al. [130] FGM manufacturing processes usually comprise two different steps: building the spatially inhomogeneous structure (gradation) and transformation of this structure into a bulk material (consolidation).

Gradation processes can be classified into constitutive, homogenizing and segregating processes. Constitutive processes are based on a stepwise build-up of the graded structure from precursor materials or powders. In homogenizing processes a sharp interface between two materials is converted into a gradient by material transport. Segregating processes start with a macroscopically homogeneous material which is converted into a graded material by material transport caused by an external field (for example a gravitational or electric field) [130].

Related with the FGM thickness, according to Ruys et. al. [131], these can be divided in three types: FGM films, interface-FGMs and bulk-FGMs. FGM films are thin graded coatings (10^{-6}–10^{-4} m) which provide an ideal solution to the problem of film-substrate thermomechanical mismatch. Interface-FGMs (10^{-4}–10^{-3} m) are films that are used to bond two dissimilar materials. Bulk-FGMs have large graded cross-sections (10^{-2}–10^{-1} m) and a large volume of each component phase.

The most commonly reported fabrication methods for bulk-FGMs can be grouped as: powder metallurgy processes, casting processes and thermal/chemical processes. Bulk-FGMs produced by powder metallurgy (sintering) will be further explored in this chapter, once these were the type of FGMs used in this work.

According to Kieback et al. [130], FGMs fabrication methods by powder metallurgy can be grouped as follows: gradient of porosity and pore size, chemical and metallurgical composition gradients. These methods are addressed in the following sections.

2.4.1 Gradient of porosity and pore size

Porous structures are highly attractive for energy absorbers, damping devices and biomedical implants [132] to facilitate bone regeneration [133-136] and osteointegration [137, 138]. Porosity can be produced by adding space-holding fillers (space holders and alloy spheres), pressureless sintering, gas entrapment and reactive processing.

By controlling porosity it is possible to manipulate mechanical properties and obtain materials with graded properties. A gradient of porosity can be obtained through the use of space-holding fillers (particles that occupy pre-determined positions). During the burning or sintering step, these space holders disappear, leaving a pore in place. NaCl space holders disappear by dissolution [139-142] as demonstrated in Figure 2.6.

Carbamide (urea) and ammonium hydrogen carbonate space-holders [143, 144] have been used in different matrix alloys, like aluminium [144-146] stainless steel (316L) and several nickel-based super alloys (Hastelloy X, Hastelloy C, Inconel 600, Inconel 625 [145]). These space-holders disappear by sublimation, with the additional advantage of producing uniform and regular pores (in shape and size) that contribute to higher and more predictable mechanical properties [144, 146-149].

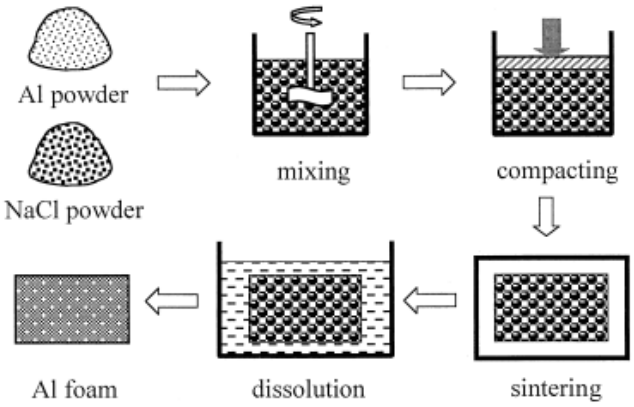

Figure 2. 6 - Schematic representation of the sintering-dissolution process for manufacturing foams by powder metallurgy [139]

Another method to produce controlled porosity is by using hollow spheres [150]. Hollow spheres can be produced by coating polystyrene with metal powders (placing metal powders into a die and heated to sinter the metal powder into a dense, solid shell) followed by the polystyrene and powder binder burning. Another method to produce hollow spheres is by injection of metal through a coaxial nozzle [151] (Figure 2. 8).

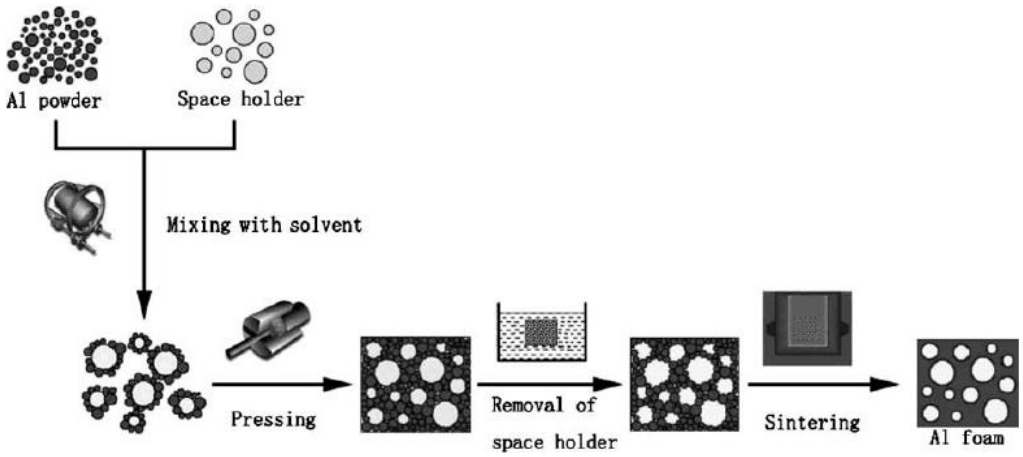

Figure 2. 7 - Schematic representation of the space-holder burning method by powder metallurgy [145].

The advantage of obtaining porous structures from space holders or hollow spheres is that there is a good control of the porosity volume fraction as well as their geometry and size, leading to reproducible structures and properties.

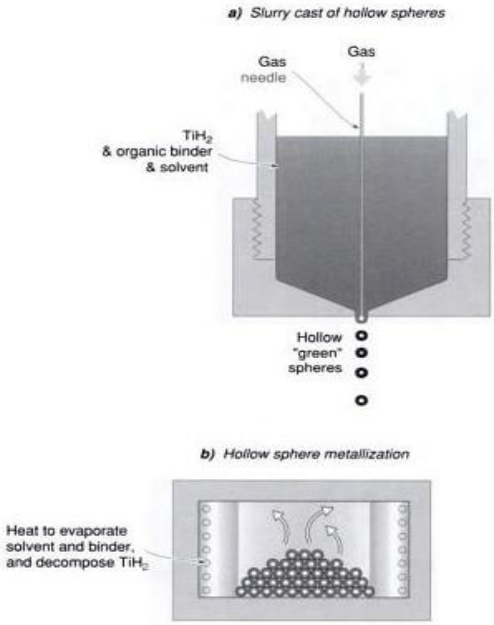

Figure 2. 8 - Prodution method of hollow spheres by injection of metal through a coaxial nozzle [152].

Porosity can also be obtained by pressureless sintering, where insufficient compaction pressure is applied to loose powders. This process is broadly used for filters and self-lubricating bearings production. The porosity obtained by this process is simply derived from the incomplete space filling of powders, when poured and sintered in a die. By controlling the green density of the compact and also sintering parameters like temperature, time and pressure it is possible to manufacture a wide range of FGMs [153].

Another method to produce porosity is by gas entrapment, in which the consolidation of alloy powders is conducted in the presence of argon or another inert gas. After the material consolidation, the material undergoes a thermal treatment for a few hours making the entrapped gas to expand and create pores.

Reactive processing is very similar to gas entrapment, but in this case the gas used for pores formation results from the decomposition reaction of some compounds introduced in the mixture [154] (as shown in Figure 2. 9).

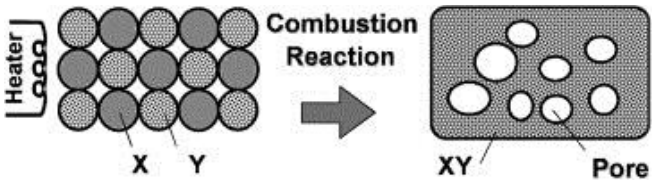

Figure 2. 9 - Schematic representation of the combustion reaction for synthesizing porous materials [154].

2.4.2 Chemical and metallurgical composition gradients

These type of gradients can be obtained by using single-constituent gradation or by using multi-constituents (different phases and/or grain sizes).In these gradients, powders of a single or multiple constituents are sequentially deposited, therefore creating an FGM. Most of the existing literature refers to multi-constituent gradients, varying constituent's volume fraction, as metal-metal, metal-ceramic and ceramic-ceramic. FGMs by power metallurgy are mainly obtained by green compact consolidation (sintering) and additive manufacturing.

Green compact gradient

During the production of a green compact by powder metallurgy, a graded part can be obtained. The formation this gradient can be achieved mainly by varying discrete the composition (Figure 2. 10-a)) or by continuously variation (Figure 2. 10-b)).

a

b

Figure 2. 10 - FGM with a).discrete and b).continuous composition variation.

Green compact gradient with discrete variation can be obtained by compressing different composition layers in a die (powder stacking). The gradient is obtained by stacking powders and manual layers of desired compositions can be selected [155]. These layers can be produced by laminating powder sheets, wet powder spraying and also by slip casting. The final step is the consolidation (sintering) of the graded powder stacked compact. Figure 2. 11 is an example of a FGM obtained by this process. The main disadvantage of this process is the limited number of layers (due to the manual manufacturing).

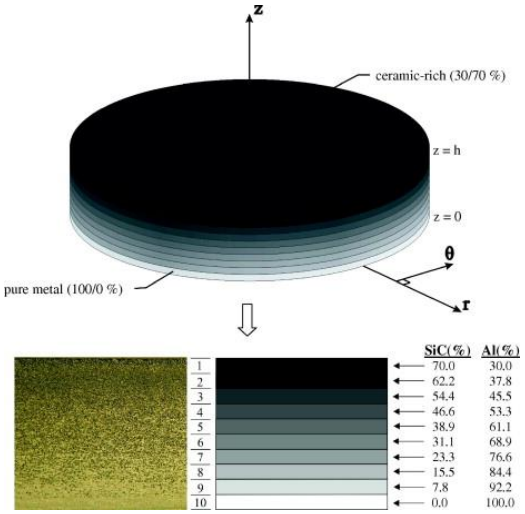

Figure 2. 11 - FGM part obtained by powder stacking [156].

By laminating powder sheets, very thin sheets of different compositions can be produced. This can be obtained by using dry or wet powders, that are forced to pass between two rollers (powder rolling system), leading to compaction [130], like represented in Figure 2. 12. This process is used for obtaining very large and thin sheets although not suited for complex geometries [157].

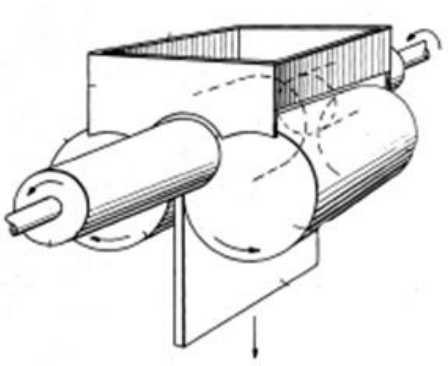

Figure 2. 12 - Schematic representation of powder rolling system [158].

In the wet powder spraying process, a suspension (powder, binder and a volatile carrier) is applied on a substrate by means of an air stream or manual brush [159]. The major steps involved in this process are: preparing the mixture, the spray depositing (coating the surface by painting), drying and sintering. The gradation is obtained by spray deposition of multiple layers with different chemical composition. The main disadvantage of this process is that it is almost exclusively used for the production of FGMs coatings. In Figure 2. 13-a schematic flow diagram of the steps followed in wet powder spraying process are presented.

Using slip casting, various suspensions (water and powder mixture) with different chemical compositions are deposited according to a FGM design, are deposited within porous mould. The water is absorbed by the mould walls, causing the formation of a material layer. The excess of suspension is removed and the body (deposited layer and mould) is dried to have sufficient strength. After dried, the body is sintered [160]. Figure 2. 14 shows the slip casting steps.

The formation of a compact gradient with continuous variation of composition can be produced by continuously varying the powder mixture being deposited in the mould. This deposition can be performed by centrifugal powder forming; gravity sedimentation; centrifugal sedimentation; electrophoretic deposition; pressure filtration/vacuum slip casting.

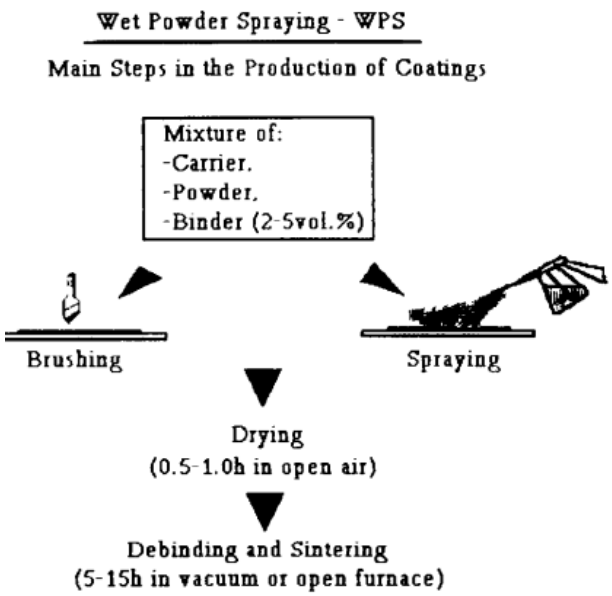

Figure 2. 13 - Schematic flow diagram of wet powder spraying process [159].

In centrifugal powder forming, a powder mixture flux is deposited against the inner walls of a cylinder, using a rotary distributor plate that is computer controlled (Figure 2. 15). The green compact thus formed has sufficient strength for subsequent sintering [161]. The main limitation of this processes is the obtainable geometry, restricted to cylinders, although being fitted for producing different types of gradient with different sizes and shapes powders.

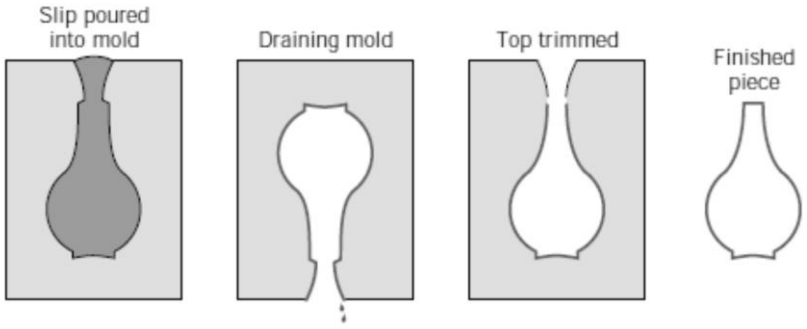

Figure 2. 14 - Schematic representation of slip casting steps [160].

This process seems suited for piston rings manufacturing, one of the demonstrative components used in this thesis.

By using gravity sedimentation (Figure 2. 16), the FGM results from differential sedimentation velocity of powders particles in a suspension, once this velocity results from

equilibrium forces actuating on the different particles. The movement of liquid around the particles, generates three forces: gravitational, drag and impulsion [162]. While the gravitational force is exclusively dependent on the body mass, impulsion depends on the liquid volume displaced by the particle. On the other hand, the drag force (force that opposes the particles sedimentation), depends on the liquid viscosity and particle front area [163]. By controlling mass, shape and fluid viscosity it is possible to achieve a smooth composition transition by this method [162, 164, 165].

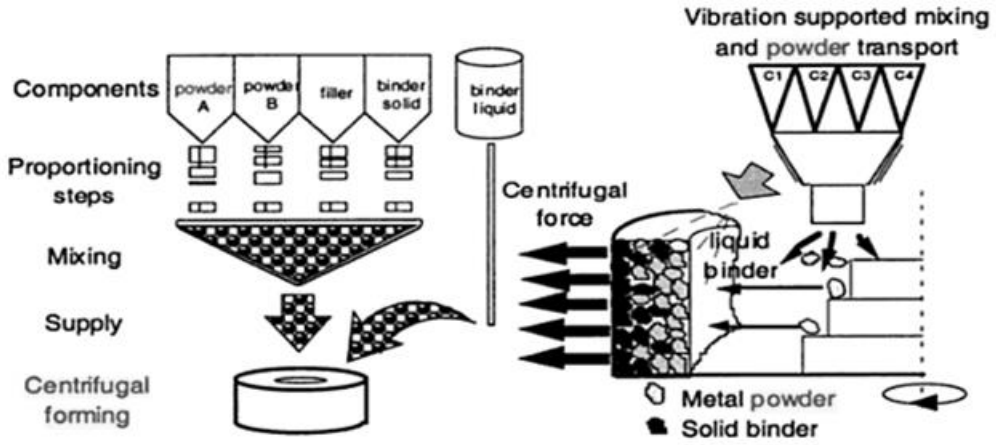

Figure 2. 15 - Schematic representation of centrifugal system powder forming equipment [122] .

After complete particle sedimentation, the sedimented part is dried, compacted and sintered. This technique has some disadvantages, like the interaction between particles during sedimentation and the reduced range of obtainable gradients.

Centrifugal sedimentation is somewhat similar to gravity sedimentation with the exception of another force involved: centrifugal force [166,167].

In electrophoretic deposition, the deposition is carried out from solutions containing more than one constituent. In this process, there is a mixing system that provides suspensions with variable constituent(s) concentrations [168-171]. Figure 2. 17 shows an experimental set up for this technique, that suffered a great evolution, being now possible to produce graded materials in several axis [172].

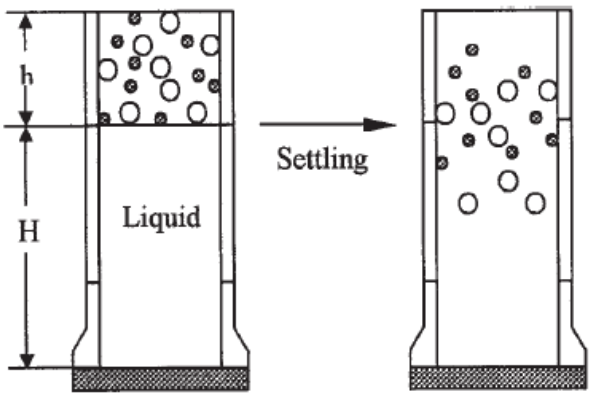

Figure 2. 16 - Schematic representation of gravity sedimentation process [162].

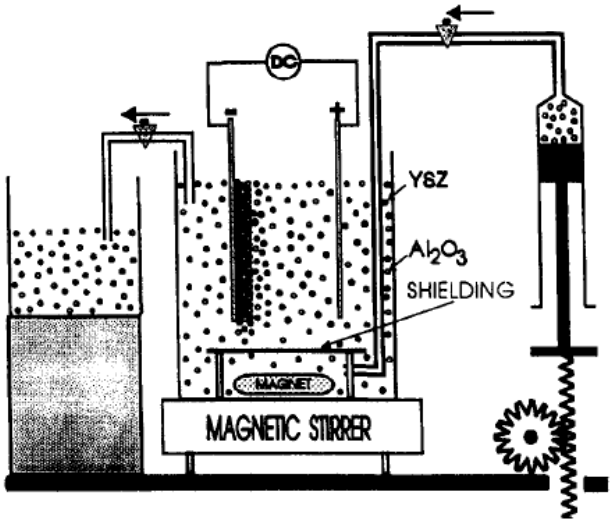

Figure 2. 17 - Schematic representation of the experimental set up for electrophoretic deposition [171]

Pressure filtration/vacuum slip casting is a technique where powders are placed in different suspensions (Figure 2. 18), that are injected using an FGM design assured by a computerized system. These suspensions are forced to pass through a filtration system (by using pressure and vacuum), in order to obtain the continuous variation of composition. This process is very similar to slip casting, although in this case pressure is applied to the fluid while vacuum is made in the ceramic mould [173, 174]. Another difference is the fact that the powders suspensions mixture production is computer controlled.

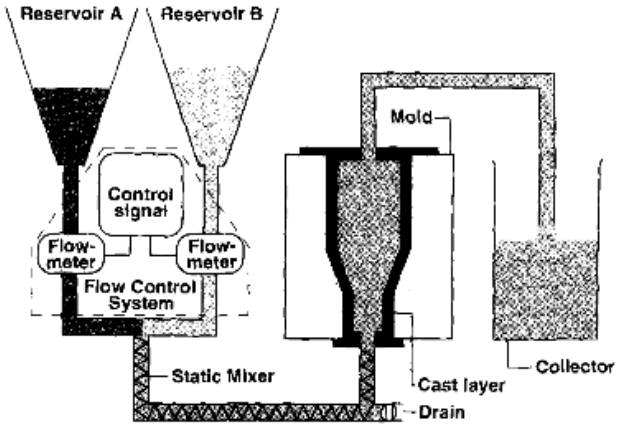

Figure 2. 18 - Schematic representation of computer controled slip casting process [175].

Additive manufacturing

In additive manufacturing, graded parts, as regarding structure (e.g. controlled porosity) and/or composition are build layer by layer. These processes include selective laser sintering (SLS) [176-178] and selective laser powder melting/direct laser forming (DLF) (Figure 2. 19). These processes concept begin by defining the CAD structure that is sent to a prototyping machine that will build the component layer by layer. The first step is to deposit the powder layer with composition and dimension as required. Each of these layers are then sintered according to the CAD information. It is possible to obtain structures (e.g. controlled porosity) by not sintering designated areas of the powder layer.

DLF and SLS represent huge advances in materials processing, once by controlling the composition of each layer and the laser path, structural and compositional structures are possible to be obtained without intermediate stages [180].These processes are viable for high value added products like in the medical field [181-183].

Based on additive manufacturing approaches and also on centrifugal powder forming, a technique for producing FGMs was developed in the scope of this thesis.

In the developed technique a continuous powders mixture is formed (and controlled by computer) being then continuously deposited in a mould. After the deposition of the graded mixture, the powders are afterwards consolidated.

This technique main advantage (comparing with additive manufacturing and centrifugal powder forming) is the ability to control the produced gradient without using a solvent. Additionally, its high production rates makes it more able to be industrially applied. Furthermore, this technique allows to produce controlled porosity gradients using space holders, instead of expendable laser techniques.

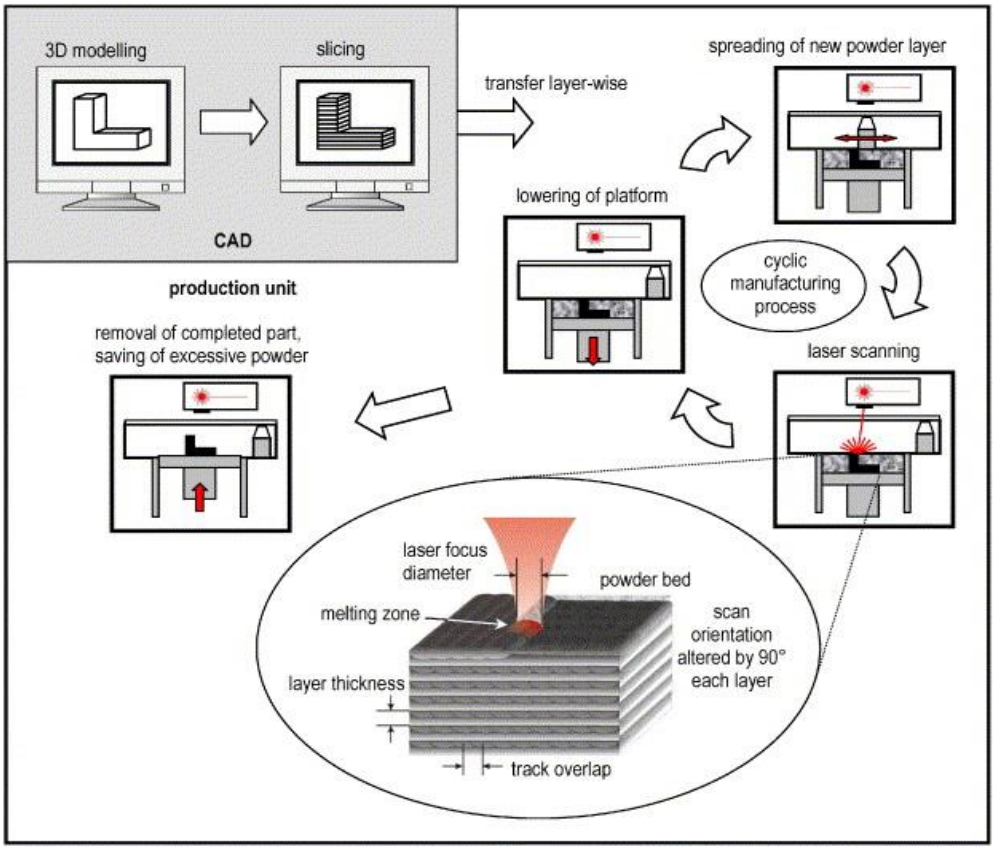

Figure 2. 19 - Schematic representation of rapid prototyping by direct DLF [179].

2.5 Piston rings

Internal combustion engines are made up of three parts: engine head, engine block and crankcase. The engine block is entirely composed by the connecting rod-crank system that includes pistons, piston rods and crankshafts.

This system converts the energy from the air/fuel combustion into mechanical energy. The piston (Figure 2. 20-a) has three functions within the motor: serves as a movable wall of the combustion chamber (ensuring their tightness), receives gas pressure and

transmits it to the connecting rod-crank system and guides the rod [184]. In order to allow the piston movement, a clearance and lubrication must exist between the piston and the cylinder wall.

Piston rings (Figure 2. 21) are inserted in piston grooves (Figure 2. 20-b) in order to: assure the gas tightness of the combustion chamber [186]; transfer heat from the piston to the cylinder walls; control adequately the oil flow to the skirt and to the rings themselves, while preventing oil entrance to the combustion chamber.

Normally piston rings are circular rings made of soft iron (Figure 2. 21), that in some cases may be submitted to electrolytic deposition of hard metals (chromium) to decrease friction against the cylinder walls and increase longevity. To ensure sealing, piston rings have a larger diameter than the cylinder, when not inserted. When introduced into the cylinder, the ring behaves like a spring, pressing the cylinder wall. Ordinarily, internal combustion engines have three different piston rings: compression ring, scraper ring and oil control ring [184].

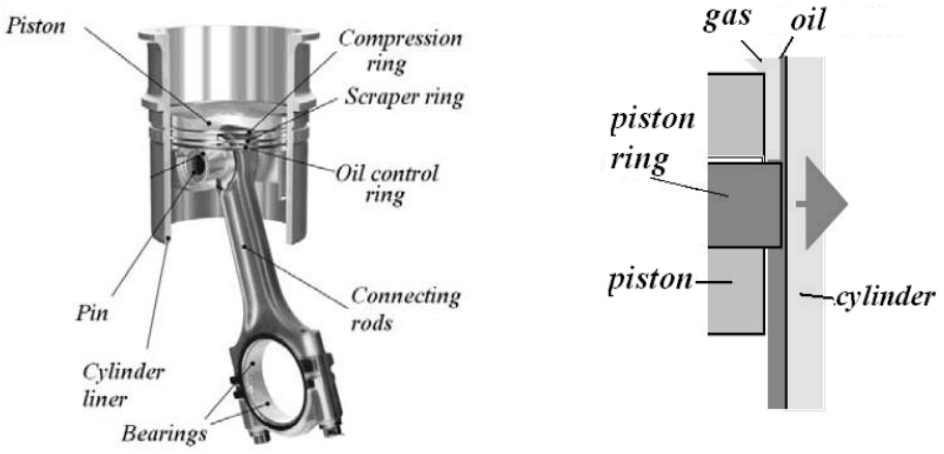

a b

Figure 2. 20 - Power cylinder system a) general view; b) detail view [185].

Piston rings for internal combustion engines or compression engine outer surface is subjected to high temperatures, corrosion and friction against the cylinder walls, therefore they must have high wear resistance as well as good physical (e.g. thermal conductivity) and mechanical properties.

Piston rings can be manufactured by several processes and casting followed by chromium coating by electrodeposition is probably the most conventional one. In this process, a subsequent treatment is made to create cracks on the surface which serve to retain oil.

Figure 2. 21 - Internal combustion engine piston ring.

As mentioned above, some pistons rings are coated with hard metal to reduce friction and increase their longevity [187]. Several patents focus on this direction, offering various types of coatings ranging from chromium carbide, oxides, nitrides and other which are applied on piston rings sliding surfaces. These type of coatings presents some problems mainly related with the metal-ceramic bond, i.e. materials with different thermal expansions leading to de-bonding between metal and ceramic. This problem occurs mostly when the piston ring is covered with materials with reduced thermal conductivity because in this case, the piston rings heat outflow is not so efficient. In addition, when coating only the piston rings sliding surface, welding of the uncoated surfaces to the piston can occur.

Some of the processes used for manufacturing piston rings fall on the powder metallurgy processes group. Special attention will be given to these processes in the following lines.

Dworak et. al. [187] found that piston rings with a homogeneous composition avoid the problem of metal-ceramic bonding, thermally induced destruction as well as the welding between the piston and piston ring. Furthermore, Dworak et. al. obtained a piston ring with greater mechanical and wear resistance by power metallurgy. The obtained piston ring had

a homogeneous structure with partially stabilized zirconium oxide. These authors produced a piston ring with reduced porosity (less than 3%) and improved wear resistance, by using ceramic particles, that led to a weight reduction of 20% (comparing to commercially available piston rings).

Another invention [188] that seeks to eliminate the inherent problems of coating pistons rings with chromium (like delamination),was the development of a piston ring containing a titanium aluminium alloy uniformly dispersed in an iron matrix.

Koehler [189] was pioneer by addressing the piston ring design through the FGM concept. According to this author, a piston ring with homogeneous properties is not an adequate solution for improved mechanical and wear behaviour. Koehler ideal piston ring should have different properties along a cross-section, meeting the requirements (mechanical, wear) of each zone. For instance, high level of porosity in the outer zones can ensure greater lubrication, while no porosity in the inner part is best matched for higher mechanical properties. This controlled porosity allocation is obtained by a differentiated compression at inner and outer zones of the piston ring. The piston ring obtained by Koehler had a density of 7.5 g/cm^3 in the inner, while 6.3 g/cm^3 at the outer zones.

Besides varying porosity, it is also possible to vary piston rings chemical composition, like proposed by Lagradere [190], that designed piston rings by juxtaposition of two rings of two different materials: inner part of cast iron and outer part with low friction coefficient and high melting point metals/alloys like copper, lead and bronze.

Young [191] proposed a piston ring that has physical properties variation (like density) but also chemical (composition) along the piston ring cross-section. These authors produced a piston ring composed from metal powders suitable for nitriding. The presented solution was a method to obtain piston rings whose structure is predominantly pearlitic with dispersed metal particles having a good affinity for nitrogen. After their production a nitride layer is promoted at the outer surface. Different nitriding level can be achieved by controlling the porosity along the cross-section of the piston ring, i.e. higher porosity allows a deeper nitriding layer.

By conjoining the methods of Koehler [189] and Young [191] i.e. combining a differential pressure during compaction of powders and a posterior chemical treatment, it is possible to produce a smooth variation in chemical and physical properties.

This chapter showed that there are many piston rings manufacturing processes by powder metallurgy. Some works looked for joining different materials and allocate them, for specific local requirements. As piston rings undergo higher wear on the outer surface, several attempts were made to increase wear resistance in this zone by placing hard particles or particles that lead to a wear reduction or even by introducing controlled porosity to retain oil. In the majority of these studies, piston rings have a sharp transition from one material to another, with some problems arising as delamination and undesired residual stresses.

The goal of this work is the attainment of a graded composition along the piston ring cross-section by using powder metallurgy. This concept is innovative because most of works produce piston rings with a sharp composition transition. The chosen reinforcements were carbon nanotubes due to their excellent properties. Additionally, silicon carbide particles were used in order to assess the combination effect of two different reinforcements. The selected matrix material was an aluminium silicon alloy due to its thermal stability and lightweight (lighter than steel and cast iron piston rings). The selection of powder metallurgy processes is mainly related with the ability of these processes to introduce reinforcements with a controlled gradation. One of the novelties of this work lies on inserting reinforcements in a controlled manner, in order to obtain controlled gradients as regarding chemical composition as structures, aiming to local mechanical and wear requirements of a piston ring.

2.6 Strengthening mechanisms

A review on Strengthening mechanisms is presented in order to understand the role of reinforcements on composites mechanical behaviour. Thermal mismatch, Orowan looping and shear lag [48, 76] are some of the proposed mechanisms.

Strengthening mechanisms can be grouped in direct and indirect mechanisms. Direct strengthening is when the load is transferred from the soft metallic matrix to the stiff ceramic reinforcement. Shear lag is an example of this type of mechanism. Indirect strengthening is related with the influence of a reinforcement on the matrix microstructure.

The following mechanisms are indirect strengthening ones: Thermal mismatch and Orowan looping.

Shear lag model focuses on the load transfer from the matrix to the reinforcement, when an external load is applied [192, 193]. The continuum shear lag model was first developed to predict the direct strengthening of continuous fibre reinforced composites, by Cox [193]. The predominant direct strengthening factor is the volume fraction of reinforcement.

Aspect ratio is an important parameter in load transfer and higher aspect ratios are known to lead to higher load transfer [194]. For low aspect ratio whiskers or particulates typically used as reinforcements in metal matrix composites, Cox's shear lag model underestimates strength [195].

Nardone and Prewo suggested that a better trade-off could be obtained if the shear lag model was modified to allow for whisker or fibre end loading effects [196]. This model has some limitations, once it assumes that the presence of the reinforcement doesn't affects the matrix and also assumes there is a perfect reinforcement/matrix interface. Nardone and Prewo [196] noticed that the strengthening effect result from load transfer but also from a strengthening effect due to an enhanced work hardening rate of the matrix, that Cox's model ignores.

Another important aspect to consider is fibres orientation. Ho et. al. [197] studied the load-transfer efficiency of this type of reinforcement in MMCs. These authors updated the shear lag model by including geometry and alignment of the reinforcement (introducing a new term for alignment correction - effective aspect ratio parameter). Another aspect that should be considered is the fibres curvature, which influence the composites properties, as suggested by some FEM simulations [198] for composites reinforced with CNTs. Curvature is not taken into account in any of the shear lag models previously mentioned.

Strengthening by dislocations interaction is a mechanism based on the interaction of dislocations with particles [199]. This mechanism, named Orowan looping, claims that when dislocations interact with the particles, an additional stress is necessary to make a dislocation pass between the particles. The applied stress should be sufficiently high to bend the dislocations in a roughly semi-circular form between the particles (Figure 2. 22). If so, the dislocations will extrude between the particles, leaving dislocation loops around them.

Inter-particle spacing reduction leads to higher strengthening effect by Orowan mechanism [200-202], once it is more difficult for dislocations to pass between the particles. Additionally, a reduction in particle size contributes to higher strengthening effect because, for the same volume fraction, there is a reduction in inter-particle spacing. A qualitative comparison of specimens containing whiskers and particles indicates that overall dislocation density tend to be higher in whisker-reinforced composites [203]. For this mechanism, particles of higher aspect ratio are more effective than equiaxial particles (the lowest aspect ratio) [204].

In whisker-reinforced composites, dislocation nucleation takes place initially at whisker ends and spreads along the length of the whisker, as strain increases [205]. A higher dislocation density is find in the sharp corners of the fibre ends [206, 207].

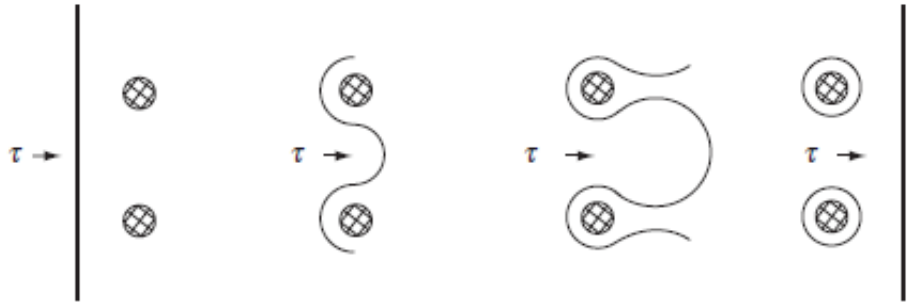

Figure 2. 22 - Schematic representation of Orowan model.

As can be seen in Figure 2. 23, for a given volume fraction, the dislocation density on a composite with spherical reinforcement is lower than for other reinforcements with higher aspect ratio [208].

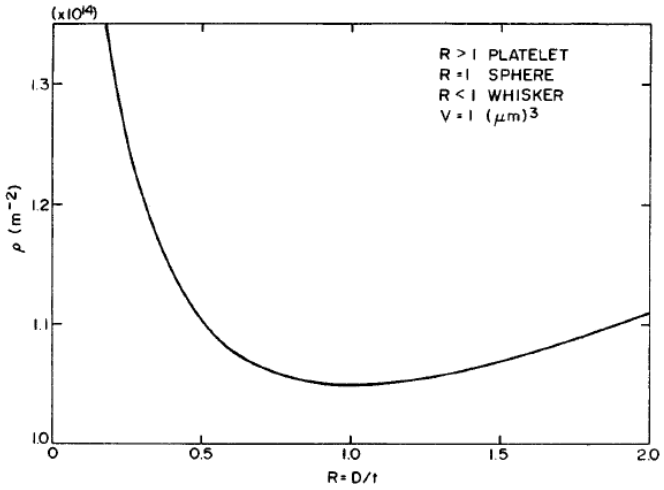

Figure 2. 23 - Calculated dislocation density (ρ) vs. reinforcement aspect ratio (R) [208].

The presence of clusters have also an effect on the dislocation movement, contributing to higher dislocation density near these clusters [205]. High dislocation density in these zones leads to higher void nucleation, contributing to a resistance reduction of the composite.

Concluding, Orowan looping strengthening mechanism is dependent on size, shape, volume fraction of the reinforcement and inter-particle spacing (including dispersion) [209-212].

Thermal mismatch strengthening mechanism results from differential thermal contraction between matrix and reinforcement [213], during cooling from sintering temperature, leading to creation of residual stresses [213, 214]. According to Arsenault and Shi [213], this strengthening effect increases proportionally to the thermal coefficient mismatch between reinforcement and matrix and the reinforcement volume fraction. On the other hand, this effect is inversely proportional to the reinforcing particle size [215].

When comparing composites reinforced by a given volume fraction, smaller particles correspond to greater surface area, therefore generating higher dislocation punching. The dislocation density is also highest in the interface region because the thermal stresses between fibber and matrix, in the interface region, have the highest magnitude [215]. In the case of whisker or fibber reinforcements, aspect ratio should also be considered, with increasing aspect ratios leading to an increase of this strengthening effect.

Additionally, a modulus mismatch strengthening mechanism [216] can be addressed, resulting from elastic modulus mismatch between matrix and reinforcement. This mechanism's contribution increases with higher elastic modulus mismatch and reinforcement volume fraction. On the other hand, this contribution decreases when increasing the reinforcement size.

All the above-mentioned mechanisms contribute to the final yield strength of the composites, however different methodologies have been developed to determine its value: simple summation; Clyne method; Zhang and Chen method and Mirza method.

The simple summation of each of the strengthening contributions can be used for calculating the final strength of the composite. This method neglects the effect of different mechanisms on each other [217] which makes this method more unrealistic. Clyne [217, 218] method proposes the root of the summing of the squares of all the single strengthening contributions. Both these methods consider all the strengthening mechanisms: shear-lag; Orowan looping; thermal and modulus mismatch and also Hall-Petch strengthening. Hall-Petch strengthening mechanism relates to grain size influence on the yield strength [219].

Zhang and Chen model [220, 221] is a modified version of the shear-lag model that takes into account Orowan strengthening mechanism, thermal mismatch mechanism, although not considering the Hall–Petch strengthening and modulus mismatch. In some nanocomposites, Hall–Petch strengthening can have a significant influence, due to this fact Zhang and Chen model can result in less precise predictions.

Mirza et. al. [222] proposed an innovative approach to the calculation of the composite final yield strength, by considering a detrimental aspect: porosity. This effect is introduced in this model by using a porosity factor that is an empirical constant depending on the porosity characteristics such as pore size, geometry, and orientation. This aspect was neglected by any of the other methods. In the present method, all the above mentioned strengthening mechanisms are considered, together with the detrimental effect of porosity.

2.7 Fatigue in Metal Matrix composites

Dieter [223] defines fatigue as the tendency that a material has to break under the application of repetitive or fluctuating stresses, at a stress much lower than that required to

cause fracture on a single application of load. According to Dieter, three basic factors are needed to cause fatigue failure: (1) a sufficiently high maximum tensile stress; (2) a sufficiently large variation of the applied stress and; (3) a sufficiently large number of cycles of the applied stress.

Fatigue damage in a metallic material is caused by plastic (irreversible) deformation which is generally produced by the dislocations motion. This motion is affected by precipitates, impurities and grain boundaries [224].

Fatigue limit is the stress amplitude about zero mean stress, below which fracture does not occur at all, or occurs only after a very large number (10^7) cycles [225] .

According to Boyer [226] fatigue process occurs through three stages (Figure 2. 24): Initial fatigue damage leading to crack nucleation and crack initiation; Progressive cyclic growth of a crack (crack propagation) until the remaining un-cracked cross section of a part becomes too weak to sustain the loads imposed and final, sudden fracture of the remaining cross section.

The fatigue resistance of MMCs are affected by several factors like reinforcement volume fraction, size, shape and distribution; matrix/reinforcement interface; integrity of the reinforcement; matrix properties; presence of inclusions or defects that arise from processing and also the testing environment [228-231].

Crack initiation step starts at a localized point (generally at a notch or stress concentration point) and gradually spreads over the cross section until the member breaks. For non-reinforced materials, these initiation points are mainly located on the surface and include scratches, sharp fillets, keyways and threads. In addition, cyclic loading can produce microscopic surface discontinuities, resulting from dislocation slip steps that may also act as stress raisers and therefore as crack initiation sites [160].

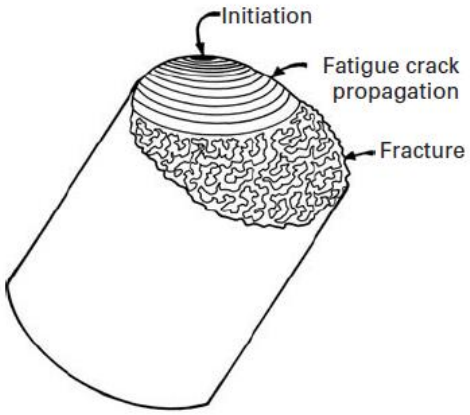

Figure 2. 24 - Schematic representation of a fatigue fracture surface showing the fatigue process stages [227].

Regarding MMCs some possible sites for cracks initiation (or nucleation) are [232]: in a large inclusion; near a porosity; in the reinforcement/matrix interface; at broken fibres regions and clusters. The primary cause for crack initiation can be by reinforcement cracking, void formation in matrix and interfacial de-bonding [233].

For reinforcement cracking to occur it is necessary that load is transferred to the reinforcement and the installed stress should be higher than the reinforcement tensile strength. In the case of fibres, their length has influence on their failure. For instance short fibres are more difficult to fracture [234]. Fibres orientation also influences the fibre cracking [235], with higher inclination from load application reducing their cracking.

In the case of matrix cavitation and interfacial de-bonding, the nucleation of cavities will normally take place in the immediate vicinity of the reinforcement, due to higher strains in these zones. The higher strains are consequence of differential modulus and thermal contraction between matrix and reinforcement. The voids are originated within the matrix, when reinforcements are strongly bonded (interface) and the applied stress exceeds the matrix strength [233]. In case of weak interfaces between matrix and reinforcement, de-bonding is more likely to occur. Higher volume fraction of reinforcement and decreasing particle size results in higher fatigue strength [230]. Irregular shapes (with sharp edges) contribute to void nucleation [236, 237]. A non-uniform distribution of reinforcements and the formation of clusters (agglomerates) can contribute to void nucleation. Porosity can also contribute to crack growth [238].

Matrix work hardening inhibits strain relaxation to take place by deformation. This fact causes the onset of void nucleation at a lower field strain than that observed for an unreinforced material.

Crack propagation in discontinuously-reinforced MMCs results from a void coalescence process. In Figure 2. 25 a schematic illustration of the sequence of events during tensile failure of these MMCs for two reinforcement shapes is presented. This figure shows how voids are formed in regions of high hydrostatic tension and afterwards coalesce by a ductile tearing mechanism.

On a given MMC, crack propagation depends on several factors, as: matrix composition and microstructure; type, size, orientation and distribution of the reinforcement; composite processing and final porosity. Some mechanisms that contribute to slow the crack propagation and thus the fatigue life are: microcracking; crack bowing; crack deflection and crack bridging [227].

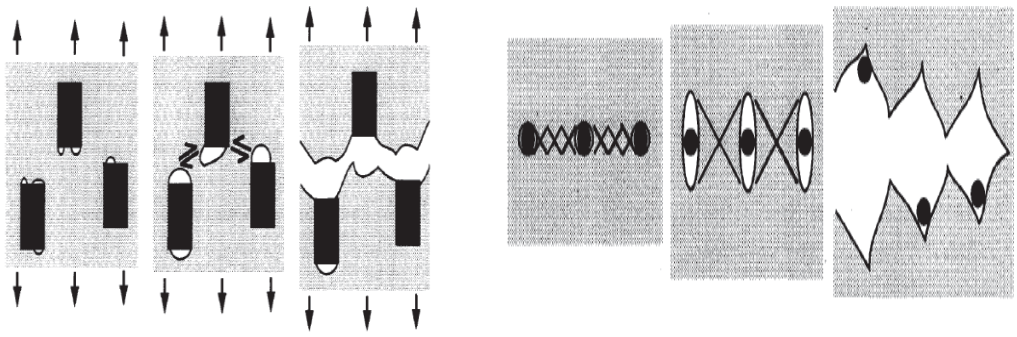

a) b)

Figure 2. 25 - Schematic illustration of the sequence of events during failure of MMCs reinfroced by a) fibres and b) particles [233].

In microcracking mechanism, microcracks form ahead of the main crack, with possible crack branching, distributing this way the strain energy over a large area. The occurrence of crack branching reduces the crack propagation velocity, because the stress required to drive a number of cracks is higher than that required to drive a single crack [239].

The interaction between the cracks and a reinforcing constituent can lead to three phenomenon: bowing, penetration and deflection [240-242]. The crack progressing will always follow the path that offers least resistance.

In the bowing mechanism (Figure 2. 26), when a crack approaches a well bonded reinforcement, the propagation of a part of the crack is hindered. The remainder of the crack bows around this trap site and is consequently retarded (of its propagation process) [243]. A higher adhesion of the fibre to the matrix [243] along with a reduction of distance between fibres [228] and also their higher aspect ratio [243] tend to increase the crack bowing.

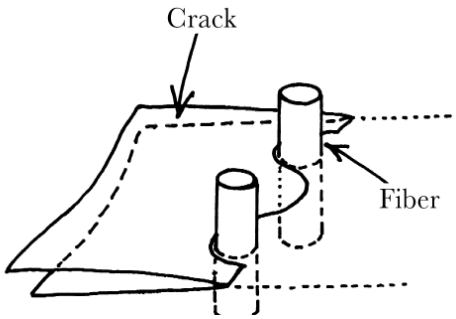

Figure 2. 26 - Schematic representation of crack bowing mechanism [243].

Penetration occurs when the shear force acting on the particle is higher than its tensile strength. A good bonding is necessary to have higher shear force.

Deflection results from thermal misfit stress and delamination between matrix and reinforcement, which introduces residual stresses on matrix that are responsible for crack deflection. In the composite matrix, deflection will happen through planes of higher weakness in the microstructure or by deflection when finding areas of higher resistance (e.g. second phases of higher toughness) [244, 245]. Penetration can also contribute to crack deflection when happening inside the particle (Figure 2. 27) [246].

Finally, in crack bridging (Figure 2. 29), reinforcements act by restricting the opening of cracks, shielding the crack when the matrix fails [249]. In elastic bridging it is assumed that a tightly bonded second phase works as an elastic or elastic-plastic spring. With the increase of crack opening or with the increase of the distance from the crack tip, de-bonding occurs, leading to frictional bridging [250]. Finally the pullout bridging can happen, due to frictional forces between fibre and matrix, with or without fibre rupture.

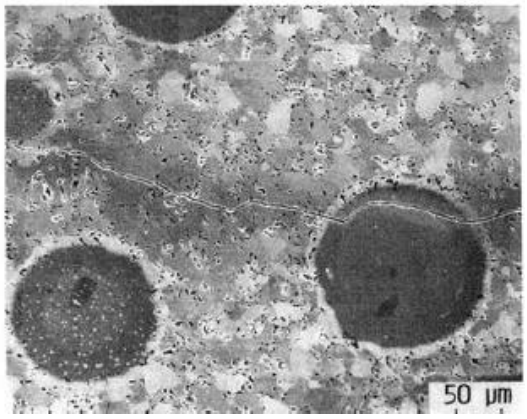

Figure 2. 27 - Crack deflection by cracking of the particle in an MoSI2/Nb composite [246].

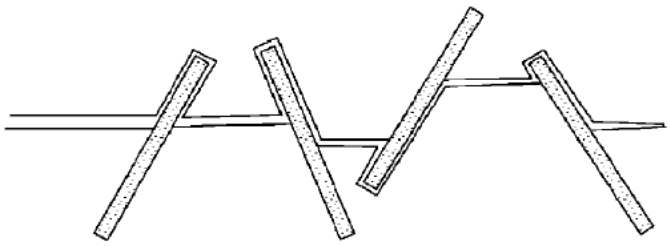

Figure 2. 28 -Schematic representationof crack deflection by delamination [247].

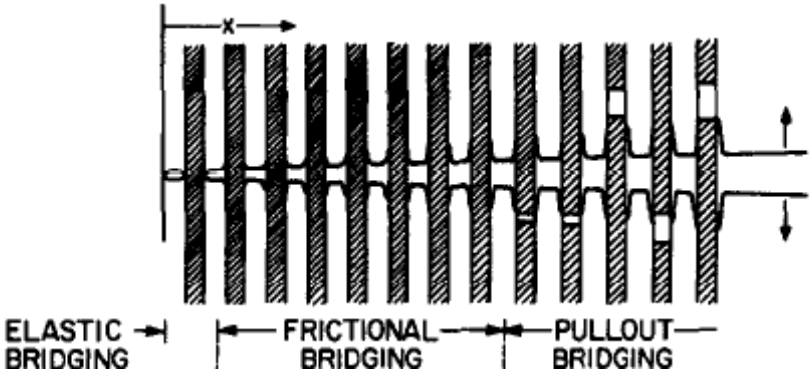

Figure 2. 29 - Schematic representation showing elastic, frictional and pullout bridging [250].

Summarizing, reinforcement characteristics like shape, orientation, size and distribution and also the interface strength [251], affect the fatigue life of MMCs. For instance, angular particles contribute to a higher stress concentration when compared with spherical ones and cracks tends to nucleate in regions with high volume fraction of particles (mainly at clusters) [252]. These aspects affect not only the crack initiation but also their progression (microcracking; crack bowing; deflection and bridging) [253, 254].

Another important aspect to address is the presence of defects (clusters/agglomerates/inclusions can be here included). Murakami studied the effect of small defects on fatigue behaviour and showed that fatigue life is higher for materials with higher static mechanical properties, while lowering when defects, including their size, are present in the material [255].

2.8 Wear

Wear is a phenomenon that results from the contact between two surfaces with relative movement and usually with friction between them. The study of this interaction is very important to understand the wear behaviour. This analysis must regard mechanical, physical and chemical properties of the materials involved. For instance, geometrical characteristics such as shape and surface roughness, mechanical stress, temperature, the existence of lubricant and wear debris must be considered. Additionally, the surface layer metallurgical and mechanical properties (before and also during sliding) influence the tribological interaction. The surface layer is also influenced by its reaction with the environment and with other materials (chemical reactions, as oxidation may occur).

Surfaces relative movement is hampered by the friction force. The fundamental laws that govern the friction of solids can be presented as: static friction is greater than kinetic friction; frictional force is proportional to the applied load; frictional force is independent of the aparent contact area [256-258].

Friction is characterized by the friction coefficient μ, the ratio between the frictional force and the applied normal load. The friction coefficient depends on many parameters such as the cleaning of the surfaces in contact, the real contact area, surface topography, the presence of oxides, etc. Therefore, friction coefficient is not an intrinsic property of a material. Another aspect to consider is that contact surfaces are not completely smooth at the microscopic level (Figure 2. 30). When two surfaces are in contact, by touching the tips of the asperities, the contact pressure leads to plastic deformation at a local level, increasing the contact area (Figure 2. 31) [259, 260].

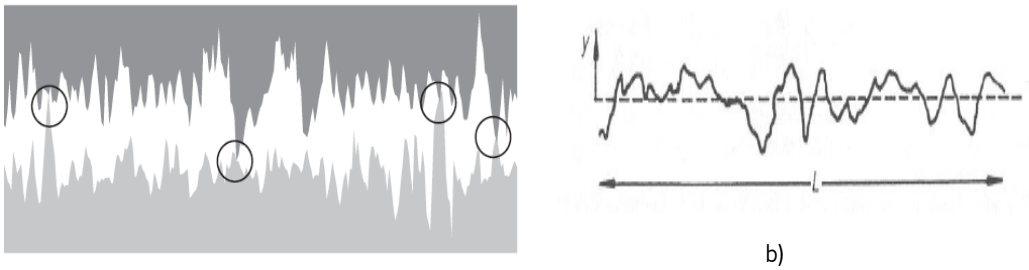

a) b)

Figure 2. 30 - Schematic representation of a) contacts between surfaces asperities [260] and b) roughness profile [257].

Roughness is responsible for the majority of the stick-slip behaviour. Friction-distance records obtained in tribological tests are not smooth curves. Sliding surfaces often exhibit stick-slip behaviour. Figure 2. 32 shows friction coefficient versus sliding distance, where after a maximum friction value during the running-in period, a steady-state is reached, where oscillations are observed due to the stick-slip effect [261-264].

The stick-slip effect results from the surface asperities interlocking (Figure 2. 30), until the driving force is high enough to break the irregularities or slide them over one another. Relative motion does not occur until some critical shear stress is reached. In that moment, the interfaces slip each other to relieve the resultant stress. This occurs when the static frictional force is greater than the kinetic frictional force during sliding.

Stick-slip behaviour depends on surface topography and on the elastic and plastic properties of the sliding materials. Thus the frictional force is the sum of two components: plastic deformation and adhesion. Plastic deformation relates with the force required to deform asperities and ploughing of the softest surface by the hardest surface. Adhesion relates to the force needed to shear the adhesive junctions between opposing materials [265]. Thus, it is not mandatory that higher roughness correspond to higher frictional force. Smoother surfaces and lower roughness lead to greater real contact area between surfaces, and consequently to greater adhesive friction. Conversely, rougher surfaces and sharper and more numerous asperities lead to greater plastic deformation. Between these two extremes, an optimal roughness is found, corresponding to the lower friction coefficient [265].

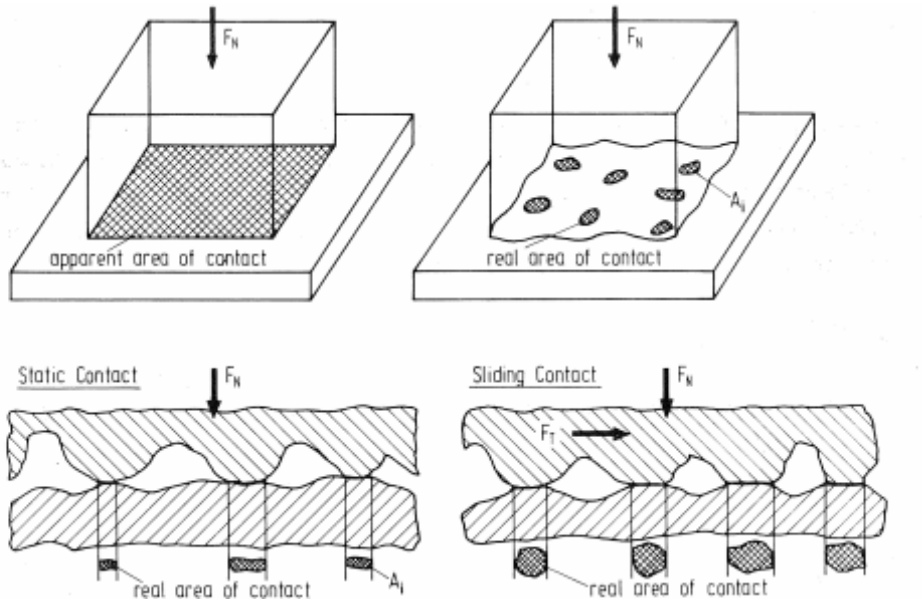

Figure 2. 31 - Aparent and real contact area [259].

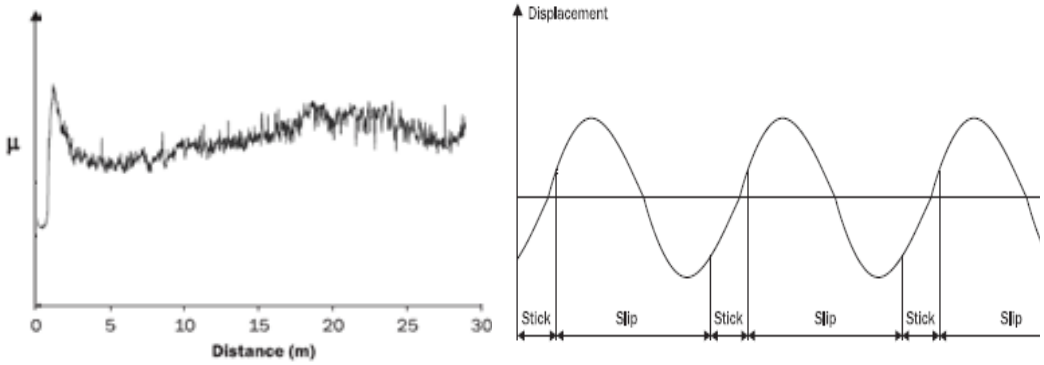

a) b)

Figure 2. 32 - a) Friction coefficient vs sliding distance on a pin-on-disc test for a metal–metal contact under dry conditions b) Stick-slip effect [257].

During sliding, both surfaces are modified, which can lead to an evolution of the friction coefficient. These changes can be chemical, topographical or structural and can include oxidation, allotropic phase transformation, amorphization, crystallization, diffusion, melting, polishing or removal of material. Figure 2. 33 presents a list of variables that can affect the friction coefficient, presented by Budinski [266].

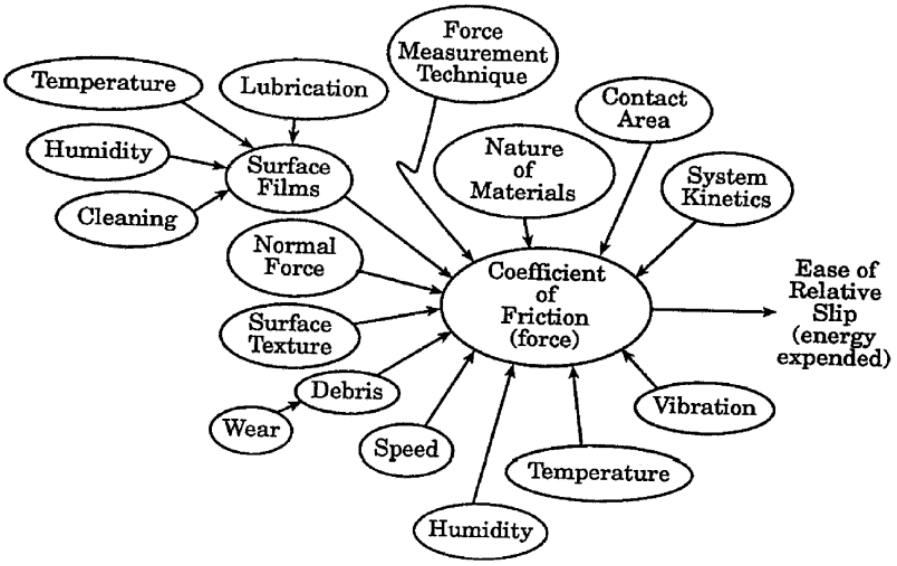

Figure 2. 33 - Factors affecting friction force [266].

The interaction between both surfaces determine the different types of wear that occur: abrasive, adhesive, corrosion, fatigue.

Wear is a complex phenomenon in which debris are produced (with weight loss) due to the relative movement between surfaces. During sliding, topographic, physical and chemical changes occur on the surfaces. Usually friction is accompanied by wear. Similarly to friction, wear is not a property of a material, once it depends on several parameters as testing temperature, normal load, sliding speed, amount of lubrication and also thermal, mechanical, metallurgical and chemical properties of the materials in contact. Materials exhibiting high friction coefficient also exhibit high wear rates, although this is not compulsory. For instance Teflon against steel, has a low friction coefficient but relatively high wear rate [267].

In literature one can find different ways to characterize wear. Ludema [268] lists thirty four different terms to describe wear, like abrasive wear, wear polish, erosion of solid particles, cavitation erosion, adhesive wear, fretting, wear, impact, corrosive wear, among other.

Other authors prefer to be more concise and classify wear in fewer categories, as Neale [269] that presents three categories: adhesive wear, abrasion and surface fatigue.

Rabinowicz [270] and also Katoand Adashi [271] identified four main types of wear: adhesive, abrasive, corrosive and fatigue. Oxidation, erosion, erosion by cavitation and

impact are sometimes classified as types of wear, but Rabinowicz [270] consider that in fact none of them is a form of wear. These types of wear can occur simultaneously and there may be a predominance of one over the others, depending on the sliding conditions.

In this work, only abrasive and adhesive wear (Figure 2. 34) will be addressed, once these were the main types found in the experimental work developed in this thesis.

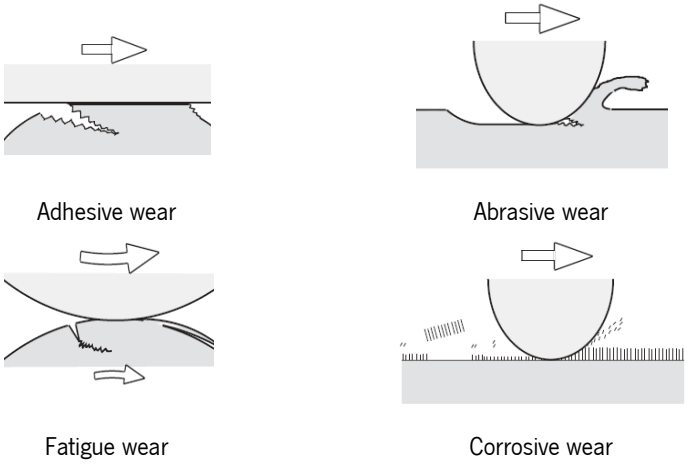

Figure 2. 34 - Schematic representation of a main types of wear [271].

2.8.1 Abrasive wear

According to Hutchings [257], abrasive wear occurs when a solid object is pressed (loaded) against a material having equal or higher hardness. This phenomenon leads to damage of the surface, caused by roughness or by hard particles. Hard particles can be part of the surface (two-body abrasion) or be in between two surfaces in relative motion, freely rotating, since they are not rigidly attached to a surface (three-body abrasion), as shown in Figure 2. 35.

Figure 2.36 shows two surface micrographs that evidence the difference between two bodies (Figure 2.36-a) and three-body wear (Figure 2.36-b) topography.

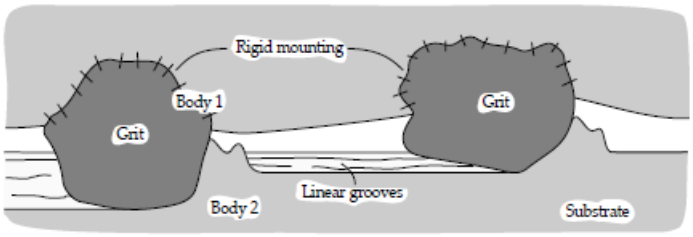

Two-body abrasive wear

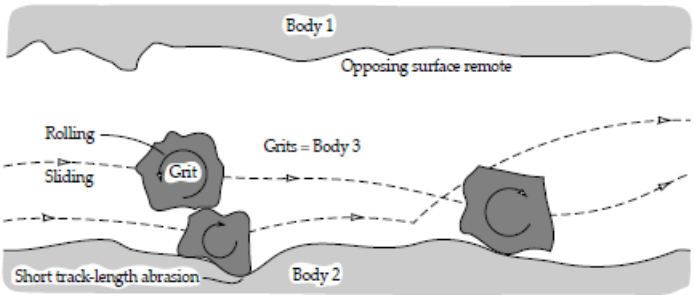

Three-body abrasive wear

Figure 2. 35 -Two-body and three-body abrasive wear [272].

Under two bodies wear, abrasive particles act as indenters, producing a series of parallel groves in the surface. The dimensions of the groves correspond to the dimensions of the abrasive particles. In the case of three body wear, particles are not stuck to one surface, and therefore they can rotate between the two surfaces and produce a highly distorted multiple indented surfaces, with no evidence of wear direction [273].

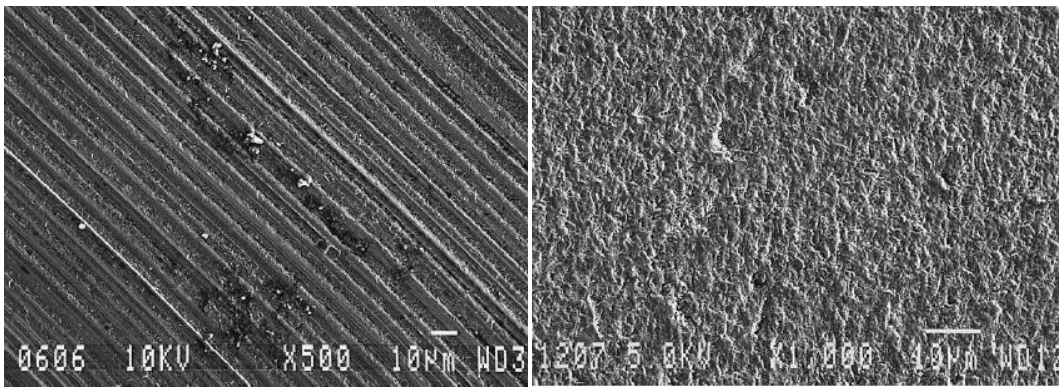

Figure 2.36 - Two-body a) and three-body b) abrasive wear [273].

In abrasive wear, wear losses can occur by cutting, fracture, pull-out of individual grains [274] or accelerated fatigue by repeated deformations. These mechanisms are shown in Figure 2.37.

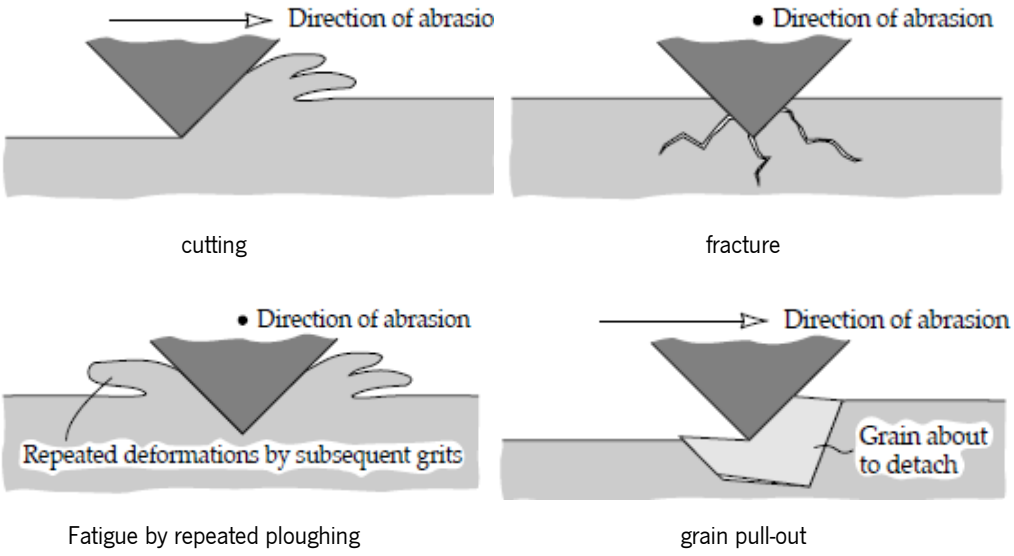

Figure 2.37 - Mechanisms of abrasive wear: microcutting, fracture, fatigue and grain pull-out [272].

Microcuting (Figure 2.37 - a) represents a mode in which the tip of a hard pin cuts a softer surface. The cut is always present but is most marked in fragile materials [272].When the worn material is brittle (e.g. ceramics), fracture of the worn surface may occur (Figure 2.37 - b). In this case wear debris result of cracks convergence. When a ductile material is worn by a blunt grit, then cutting is unlikely and the worn surface is repeatedly deformed (Figure 2.37 - c). In this case, wear debris result of metal fatigue.

The last mechanism illustrated on Figure 2.37-d represents a grain detachment or pull-out. This mechanism occurs mainly in ceramics and MMCs, where the boundary between grains can be relatively weak. By this mechanism the entire grain/particle is lost as wear debris [272].

Toughness and ductility (the ability of the material to deform without forming debris) play an important role in abrasive wear. To create a groove or slot is sufficient that the pin hardness is 20% higher than that of the scratched surface. When the worn material is ductile, a long strip is generated by microcutting. In the case of fragile materials, a wear particle is generated by crack propagation [271].

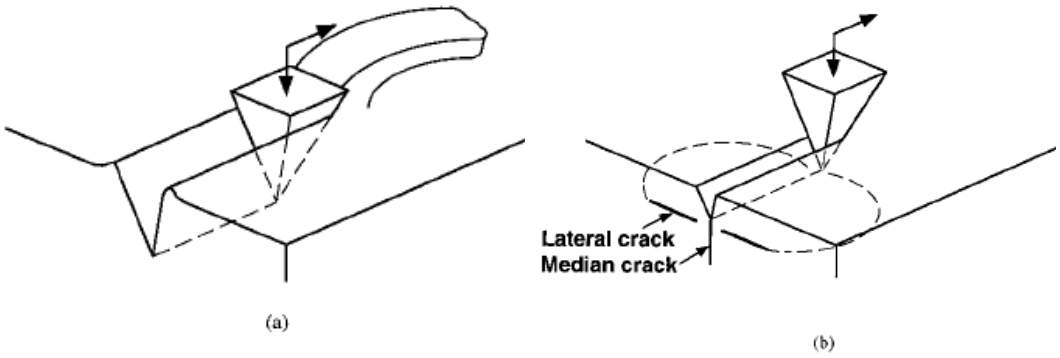

Figure 2.38 -Abrasive wear of a) ductile and b) fragile materials [271].

According to Hutchings [257] the wear of materials can be quantified using a simplified model developed by Archard, which relates the worn volume by unit sliding Q (m^2) with the normal load W (N) and the hardness H (N/m^2) of the softer material according equation: Q=KW/H.

The constant K is called dimensionless wear coefficient. Archard equation is widely used for its simplicity and also by allowing to quantify the wear severity of different systems (by comparing K coefficient). According to Hutchings [257] the determination of K for each system must be studied separately, since it is a characteristic of the tribological system, where the constant K is proportional to the wear.

The dimensionless abrasion wear coefficient (K_{abr}) can vary between 10^{-4} to 10^{-1}.

As above mentioned, wear can occur by two or three body modes. From abrasive wear can result particles. These particles form third bodies in the contact zone. The third body characteristics play an important role on the wear rate: hardness; geometry; size.

Regarding hardness, the ratio between the hardnesses of the abrasive and the worn material can provide an indication of the transition between lower to the higher wear level (Figure 2. 39). Non-homogenous material suffers lower wear in lower wear level, while for higher wear level, homogenous materials suffer less wear.

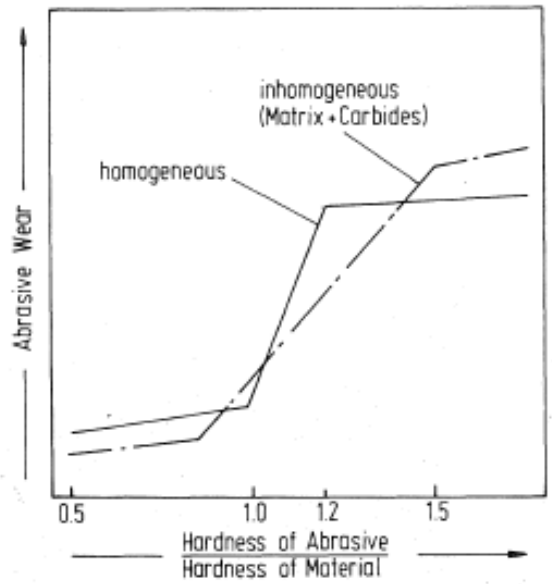

Figure 2. 39 - Abrasive wear as a function of the ratio between hardness of abrasive and hardness of the worn material (steel) for homogeneous material and non-homogeneous [259].

The geometry of the abrasive is another important factor. The material suffers more wear for higher angle of attack of the abrasive particles (Figure 2.40) [275-277]. There is a gradual transition from microploughing to microcutting with increasing angle of attack of the abrasive particles (Figure 2.40).

Abrasive size is also an important factor, with many studies on the influence of this factor on abrasive wear. For small abrasives, the wear rate increases proportionately to the particle size, until a critical size is achieved. After this point, three phenomena may occur: wear increase at a lower rate, wear decrease at a lower rate or wear is independent of the size of the abrasive [278-289].

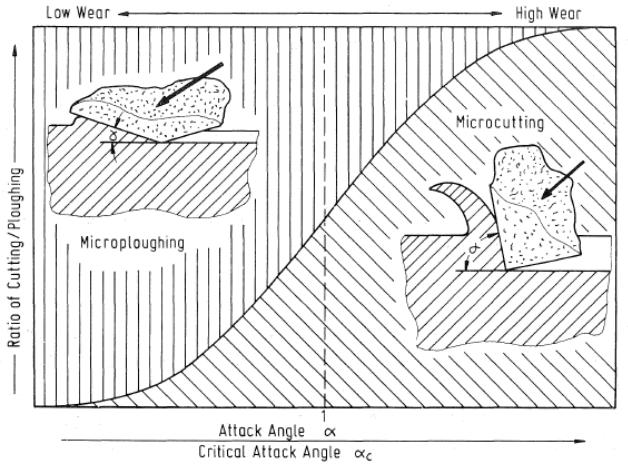

Figure 2.40 - Ratio of microcutting to microploughing as a function of the ratio of the attack angle to the critical attack angle [259].

In addition to abrasive characteristics, also the base materials properties have a relevant influence over the system wear behaviour. Abrasive wear directly relates with the hardness of the abrasive particles and the surface that will be worn. The wear resistance increases with increasing hardness of the material to be worn, as shown in Figure 2.41. However, hardness alone is insufficient to fully predict the wear behaviour of a material.

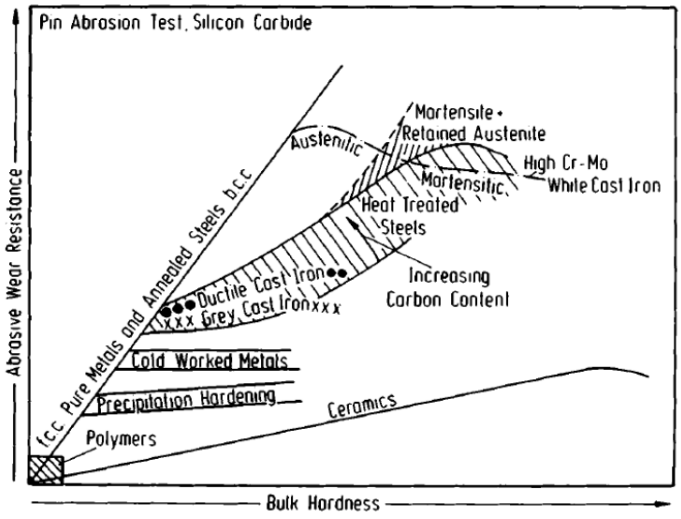

Figure 2.41 - Abrasive wear resistance vs material hardness [259].

Fracture toughness of the worn surfaces is an important factor that also influence the wear behaviour. This parameter effect in the wear resistance is clear when microcracks or microfractures exist [259].

When independently analysed, higher hardness and higher toughness both lead to higher wear resistance. However these properties must be addressed together, once they are connected. Usually, by increasing hardness, toughness is reduced. Regarding the wear process, during sliding the contact between surfaces (two or three body modes) leads to surface hardening by abrasion and plastic deformation of surface roughness. Moreover, the micro-displacement at surface material increases hardness. The overall wear resistance comes from the balance between fracture toughness and hardness [290].

Like surface hardening, also surface softening can occur, although less common. This happens in some materials, when recovery or recrystallization takes place. The recovery or dynamic recrystallization during abrasion may substantially improve its ductility or deformation capacity. Moreover, a lack of work hardening increases the width and depth of the wear grooves [259]. Ductility strongly affects the ratio between microcutting and microploughing. This ratio decreases with ductility increases.

Microstructural characteristics such as: presence of secondary phases, precipitates, crystalline defects and microstructure anisotropy [259] also influence the wear process. These aspects are of utmost importance especially in composite materials. The addition of non-metallic particles can increase abrasive wear resistance of softer materials [259]. The volume fraction, size and mechanical properties of the reinforcing constituents, as well as their orientation and bonding to the matrix, all influence the abrasive wear rate. Reinforcements with smaller than the width or depth of the wear grooves do not have a larger influence on abrasive wear resistance, once they are more easily pulled out from the matrix. The opposite scenario occurs for reinforcements larger than the thickness or depth of the grooves.

Reinforcements act as barriers, by supporting part of the stresses generated during sliding and thus preventing the abrasive wear progression. Figure 2. 42 presents a schematic representation of several reinforcement characteristics influence on the abrasive wear resistance.

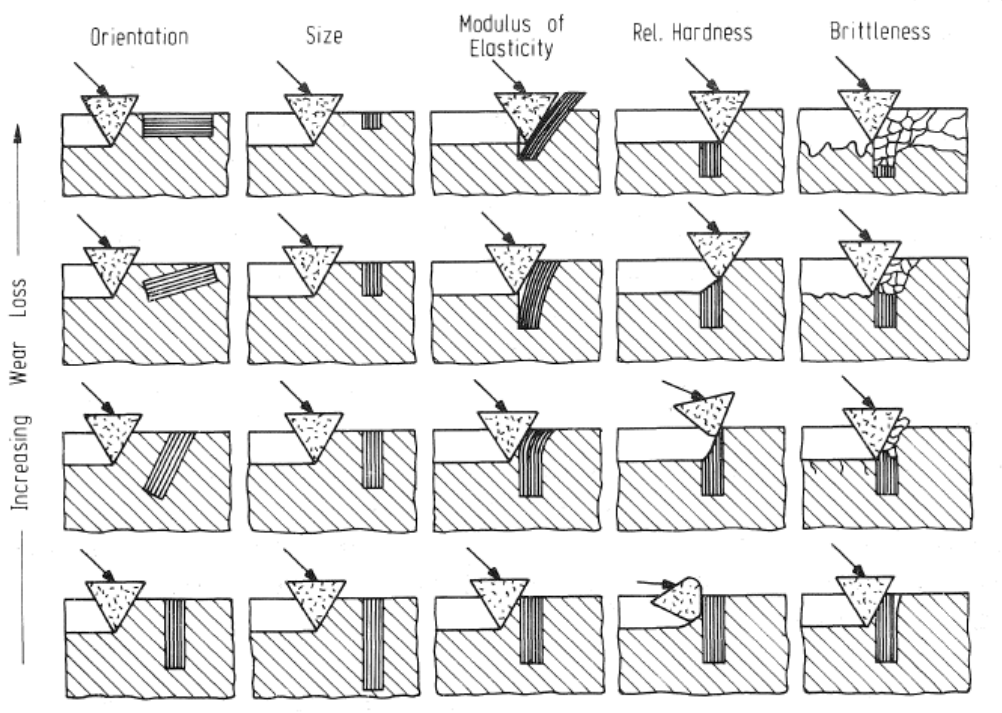

Figure 2. 42 -Schematic representation of reinforcement orientation, size, modulus of elasticity, hardness and brittleness effect on the abrasive wear of composites [259].

2.8.2 Adhesive wear

Adhesion is the ability of atomic structures to form surface bonds with other atoms or surfaces they are in contact during sliding. Microscopically, surfaces present peaks and valleys (roughness) and when two surfaces contact there are "touch points" that concentrate the contact pressure and can lead to cold or hot welding between these points.

Adhesive wear comprehends joining and breaking of junctions (real contact areas) between the sliding surfaces [291]. The welding and breaking is responsible for high wear rates and coefficient of friction instability (stick-slip effect shown in Figure 2. 32). Adhesive joints are sheared and the weakest material is transferred [292] as represented in Figure 2. 43.

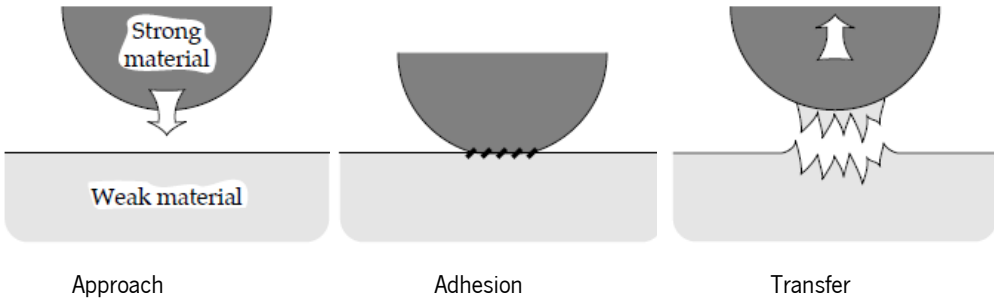

Figure 2. 43 - Schematic representation of adhesive wear [272].

Adhesive wear occurs when surfaces slide and the contact pressure between the asperities is high enough to cause plastic deformation and material adhesion [291]. A strong adhesion between surfaces increases the frictional force [272] (adhesion component).This adhesion is favoured by chemical and structural compatibility and also by cleanliness of the surfaces (e.g. absence of oxidation) [291]. Adhesion may also be reduced by an increase on roughness or hardness of the surface, by reducing the real contact area.

For metals, adhesion attractive forces are covalent, metallic or Van der Waals forces [259]. Higher adhesion rates occur between identical metals (e.g. iron - iron as in Table 2.1) while bimetallic combinations exhibit poor adhesion and therefore lower friction (Table 2.1). From Table 2.1 it is possible to verify that a higher adhesion does not mandatorily corresponds to a higher solubility.

Adhesion between metals is also influenced by their chemical reactivity [293, 294]. The possible reaction products can influence the adhesive wear. The mechanical properties of material also influences the adhesive wear where a higher hardness and modulus of elasticity lower the degree of adhesion [293,295].

Heterogeneous materials such as steel often show lower adhesion because of the interference of inclusions and non-metallic phases that are present in the microstructure [272]. Regarding composites the presence of reinforcements can affects adhesion in a similar way. For instance, for composites with hard reinforcements it is expected a lower adhesion.

Table 2.1 - Adhesion of some metals in contact with iron under vacuum system [293].

Metal	Cohesive energy, kcal/g-atom	Atomic size, A°(10^{-10} m)	Solubility in iron, at.%	Adhesion force to iron[a], mN
Iron	99.4	2.86	-	4
Cobalt	101.7	2.50	35	1.2
Nickel	102.3	2.49	9.5	1.6
Copper	80.8	2.551	<0.25	1.3
Silver	68.3	2.883	0.13	0.6
Gold	87.6	2.877	<1.5	0.5
Platinum	134.8	2.769	20	1
Aluminum	76.9	2.80	22	2,5
Lead	47.0	3.494	Ins.	1.4
Tantalum	186.7	2.94	0.20	2.3

[a] Applied load: 0.2 mN; temperature: 20°C; ambient pressure (0.01315789 atm).

Adhesion force can be much higher than the contact force. For instance iron - iron contact, adhesion force is 20 times higher than the contact force (Table 2.1).

The adhesion can easily occur at moderate or low temperatures [293]. For instance, for iron-other metals contact adhesion at 20°C was assessed (Table 2.1).

Similar to abrasive wear, adhesive wear can also be modelled by Archard law. The Archard adhesive wear coefficient (K_{ad}) ranges from 10^{-8} to 10^{-2}. This large range is due to the vast possible chemical interactions [296].

Additionally, adhesion will also depend on the relative sliding speed and temperature [291].

2.9 References

[1] American Society for M, Committee ASMIH. 1992. ASM Handbook: Properties and selection: nonferrous alloys and special-purpose materials. ASM International.
[2] Clarke J, Sarkar AD. 1979. Wear characteristics of as-cast binary aluminium-silicon alloys. Wear 54:7-16.
[3] Carvalho Ferreira JMG. 2002. Tecnologia da pulverometalurgia. pp 23. Fundação Calouste Gulbenkian.
[4] Fortes MA, Ferreira, P. J. 2003. Materiais 2000. pp 59. Press.
[5] Chang I, Zhao Y. 2013. Advances in Powder Metallurgy: Properties, Processing and Applications. Elsevier Science.

[6] Fuqian Z, Ming X, Jianliang L, Xianyong L, Weiming G, et al. 2001. Study of rapidly solidified atomization technique and production of metal alloy powders. Materials Science and Engineering: A 304–306:579-82.
[7] Chiaverini V. 2001. Metalurgia do pó. pp 18. Associação Brasileira de Metalurgia e Materiais.
[8] Committee ASMH, Klar E, American Society for Metals. Powder Metallurgy C. 1984. Metals handbook: Powder metallurgy. pp 501. American Society for Metals.
[9] German RM. 1996. Sintering Theory and Practice. Wiley.
[10] Lumely RN, Schaffer GB. 1997. Effects of solubility and particle size on liquid phase sintering. Metal Powder Report 53:39.
[11].Schaffer GB, Sercombe TB, Lumley RN. 2001. Liquid phase sintering of aluminium alloys. Materials Chemistry and Physics 67:85-91.
[12].Martín JM, Castro F. 2003. Liquid phase sintering of P/M aluminium alloys: effect of processing conditions. Journal of Materials Processing Technology 143–144:814-21.
[13] Schaffer GB, Huo SH. 1999. On development of sintered 7xxx series aluminium alloys. Powder Metallurgy 42:219-26.
[14] Sercombe TB, Schaffer GB. 1999. On the use of trace additions of Sn to enhance sintered 2xxx series Al powder alloys. Materials Science and Engineering: A 268:32-9.
[15] Schaffer GB, Huo SH, Drennan J, Auchterlonie GJ. 2001. The effect of trace elements on the sintering of an Al–Zn–Mg–Cu ALLOY. Acta Materialia 49:2671-8.
[16] Sercombe TB. 2003. On the sintering of uncompacted, pre-alloyed Al powder alloys. Materials Science and Engineering: A 341:163-8.
[17] Showaiter N, Youseffi M. 2008. Compaction, sintering and mechanical properties of elemental 6061 Al powder with and without sintering aids. Materials & Design 29:752-62
[18] Kang SJL. 2004. Sintering: Densification, Grain Growth and Microstructure. Elsevier Science.
[19] German R. 2014. Sintering: From Empirical Observations to Scientific Principles. Elsevier Science.
[20] Fang ZZ. 2010. Sintering of Advanced Materials. Elsevier Science.
[21] Lumley R. 2010. Fundamentals of Aluminium Metallurgy: Production, Processing and Applications. Elsevier Science.
[22] Trunov MA, Schoenitz M, Dreizin EL. 2006. Effect of polymorphic phase transformations in alumina layer on ignition of aluminium particles. Combustion Theory and Modelling 10:603-23.
[23] Daver EM, Ullrich WJ, Balubhai Patel K. 1991. Aluminium P/M Parts-Materials, Production and Properties. Key Engineering Materials 29:401-28.
[24] Totten GE, MacKenzie DS. 2003. Handbook of Aluminum: Vol. 1: Physical Metallurgy and Processes. CRC Press.
[25] Gutin SS, Panov AA, Khlopin MI. 1972. Effect of oxide films in the sintering of aluminum powders. Soviet Powder Metallurgy and Metal Ceramics 11:280-2.
[26] Balog M, Simancik F, Bajana O, Requena G. 2009. ECAP vs. direct extrusion—Techniques for consolidation of ultra-fine Al particles. Materials Science and Engineering: A 504:1-7.
[27] Moustafa S, Daoush W, Ibrahim A, Neubaur E. 2011. Hot Forging and Hot Pressing of AlSi Powder Compared to Conventional Powder Metallurgy Route. Materials Sciences and Applications 2:1127.
[28] Miracle DB, Donaldson SL, Committee ASMIH. 2001. Asm Handbook: Composites. Asm International. 3-17 pp.

[29] Rawal S. 2001. Metal-matrix composites for space applications. JOM 53:14-7.
[30] Kainer KU. 2006. Metal Matrix Composites. Wiley.
[31] Allison J, Cole G. 1993. Metal-matrix composites in the automotive industry: Opportunities and challenges. JOM 45:19-24.
[32] Agarwal A, Bakshi SR, Lahiri D. 2010. Carbon Nanotubes: Reinforced Metal Matrix Composites. CRC PressINC.
[33] Surappa MK. 2003. Aluminium matrix composites: Challenges and opportunities. Sadhana 28:319-34.
[34] Tang F, Anderson IE, Gnaupel-Herold T, Prask H. 2004. Pure Al matrix composites produced by vacuum hot pressing: tensile properties and strengthening mechanisms. Materials Science and Engineering: A 383:362-73.
[35] Harrigan Jr WC. 1998. Commercial processing of metal matrix composites. Materials Science and Engineering: A 244:75-9.
[36] Hashim J, Looney L, Hashmi MSJ. 1999. Metal matrix composites: production by the stir casting method. Journal of Materials Processing Technology 92–93:1-7.
[37] Rohatgi P. 1991. Cast aluminum-matrix composites for automotive applications. JOM 43:10-5.
[38] Cook AJ, Werner PS. 1991. Pressure infiltration casting of metal matrix composites. Materials Science and Engineering: A 144:189-206.
[39] Gupta M, Mohamed F, Lavernia E, Srivatsan TS. 1993. Microstructural evolution and mechanical properties of SiC/Al2O3 particulate-reinforced spray-deposited metal-matrix composites. Journal of Materials Science 28:2245-59.
[40] Srivatsan TS, Lavernia EJ. 1992. Use of spray techniques to synthesize particulate-reinforced metal-matrix composites. Journal of Materials Science 27:5965-81.
[41].Bakshi SR, Lahiri D, Agarwal A. 2010. Carbon nanotube reinforced metal matrix composites - a review. International Materials Reviews 55:41-64.
[42].Srivatsan TS, Ibrahim IA, Mohamed FA, Lavernia EJ. 1991. Processing techniques for particulate-reinforced metal aluminium matrix composites. Journal of Materials Science 26:5965-78.
[43] Popov VN. 2004. Carbon nanotubes: properties and application. Materials Science and Engineering: R: Reports 43:61-102.
[44] Trojanowicz M. 2006. Analytical applications of carbon nanotubes: a review. TrAC trends in analytical chemistry 25:480-9.
[45] Thostenson ET, Ren ZF, Chou TW. 2001. Advances in the science and technology of carbon nanotubes and their composites: a review. Composites Science and Technology 61:1899-912.
[46] Salvetat JP, Bonard JM, Thomson NH, Kulik AJ, Forro L, et al. 1999. Mechanical properties of carbon nanotubes. Applied Physics A 69:255-60.
[47] Dresselhaus MS, Dresselhaus G, Saito R. 1995. Physics of carbon nanotubes. Carbon 33:883-91.
[48] George R, Kashyap KT, Raw R, Yamdagni S. 2005. Strengthening in carbon nanotube/aluminium (CNT/Al) composites. Scripta Materialia 53:1159-63.
[49] Chen XH, Chen CS, Xiao HN, Liu HB, Zhou LP, et al. 2006. Dry friction and wear characteristics of nickel/carbon nanotube electroless composite deposits. Tribology international 39:22-8.
[50] Chen WX, Tu JP, Gan HY, Xu ZD, Wang QG, et al. 2002. Electroless preparation and tribological properties of Ni-P-Carbon nanotube composite coatings under lubricated condition. Surface and Coatings Technology 160:68-73.

[51] Hertel T, Walkup RE, Avouris P. 1998. Deformation of carbon nanotubes by surface van der Waals forces. Physical Review B 58:13870-3.
[52] Joly-Pottuz L, Dassenoy F, Vacher B, Martin JM, Mieno T. 2004. Ultralow friction and wear behaviour of Ni/Y-based single wall carbon nanotubes (SWNTs). Tribology international 37:1013-8.
[53] Joly-Pottuz L, Vacher B, Le Mogne T, Martin JM, Mieno T, et al. 2008. The role of nickel in Ni-containing nanotubes and onions as lubricant additives. Tribology Letters 29:213-9.
[54] Martin JM, Ohmae N. 2008. Nanolubricants. pp 126-140. Wiley.
[55] Krishnan A, Dujardin E, Ebbesen TW, Yianilos PN, Treacy MMJ. 1998. Young's modulus of single-walled nanotubes. Physical Review B 58:14013.
[56] Treacy MMJ, Ebbesen TW, Gibson JM. 1996. Exceptionally high Young's modulus observed for individual carbon nanotubes.
[57] Collins PG, Avouris P. 2000. Nanotubes for electronics. Scientific American 283:62-9.
[58] Ajayan PM. 1999. Nanotubes from Carbon. Chemical Reviews 99:1787-800.
[59] Ma RZ, Wu J, Wei BQ, Liang J, Wu DH. 1998. Processing and properties of carbon nanotubes–nano-SiC ceramic. Journal of Materials Science 33:5243-6.
[60] Hirsch A, Vostrowsky O. 2005. Functionalization of carbon nanotubes. In Functional molecular nanostructures:193-237: Springer. Number of 193-237 pp.
[61] Ma P-C, Siddiqui NA, Marom G, Kim J-K. 2010. Dispersion and functionalization of carbon nanotubes for polymer-based nanocomposites: A review. Composites Part A: Applied Science and Manufacturing 41:1345-67.
[62] Seo JW, Couteau E, Umek P, Hernadi K, Marcoux P, et al. 2003. Synthesis and manipulation of carbon nanotubes. New Journal of Physics 5:120.
[63] Chen X, Xia J, Peng J, Li W, Xie S. 2000. Carbon-nanotube metal-matrix composites prepared by electroless plating. Composites Science and Technology 60:301-6.
[64] 2004. Tiny tubes boost for metal matrix composites. Metal Powder Report 59:40-3.
[65] Carreno-Morelli E, Yang J, Couteau E, Hernadi K, Seo JW, et al. 2004. Carbon nanotube/magnesium composites. Physica Status Solidi a-Applied Research 201:R53-R5.
[66] Hernadi K, Ljubović E, Seo JW, Forro L. 2003. Synthesis of MWNT-based composite materials with inorganic coating. Acta Materialia 51:1447-52.
[67] de Souza Filho AG, Fagan SB. 2007. Funcionalização de nanotubos de carbono. Química nova 30:1695.
[68] Iijima S. 1991. Helical microtubules of graphitic carbon. nature 354:56-8.
[69] Journet C, Maser WK, Bernier P, Loiseau A, De La Chapelle ML, et al. 1997. Large-scale production of single-walled carbon nanotubes by the electric-arc technique. Nature 388:756-8.
[70] Rinzler AG, Liu J, Dai H, Nikolaev P, Huffman CB, et al. 1998. Large-scale purification of single-wall carbon nanotubes: process, product, and characterization. Applied Physics A: Materials Science & Processing 67:29-37.
[71] Nikolaev P, Bronikowski MJ, Bradley RK, Rohmund F, Colbert DT, et al. 1999. Gas-phase catalytic growth of single-walled carbon nanotubes from carbon monoxide. Chemical physics letters 313:91-7.
[72] Ren ZF, Huang ZP, Wang DZ, Wen JG, Xu JW, et al. 1999. Growth of a single freestanding multiwall carbon nanotube on each nanonickel dot. Applied physics letters 75:1086-8.
[73] Ren ZF, Huang ZP, Xu JW, Wang JH, Bush P, et al. 1998. Synthesis of large arrays of well-aligned carbon nanotubes on glass. Science 282:1105-7.

[74] Huang ZP, Xu JW, Ren ZF, Wang JH, Siegal MP, Provencio PN. 1998. Growth of highly oriented carbon nanotubes by plasma-enhanced hot filament chemical vapor deposition. Applied physics letters 73:3845-7.
[75] Khare R, Bose S. 2005. Carbon nanotube based composites-a review. Journal of Minerals & Materials Characterization & Engineering 4:31-46.
[76] Bakshi SR, Agarwal A. 2011. An analysis of the factors affecting strengthening in carbon nanotube reinforced aluminum composites. Carbon 49:533-44.
[77].Agarwal A, Bakshi SR, Lahiri D. - Carbon Nanotubes: Reinforced Metal Matrix Composites.
[78] Suryanarayana C. 2004. Mechanical Alloying And Milling. pp 292-293. Taylor & Francis
[79] Esawi A, Morsi K. 2007. Dispersion of carbon nanotubes (CNTs) in aluminum powder. Composites Part a-Applied Science and Manufacturing 38:646-50.
[80] Esawi AMK, Morsi K, Sayed A, Gawad AA, Borah P. 2009. Fabrication and properties of dispersed carbon nanotube-aluminum composites. Materials Science and Engineering a-Structural Materials Properties Microstructure and Processing 508:167-73.
[81] Kuzumaki T, Miyazawa K, Ichinose H, Ito K. 1998. Processing of carbon nanotube reinforced aluminum composite. Journal of Materials Research 13:2445-9.
[82] Liao J-z, Tan M-J, Sridhar I. 2010. Spark plasma sintered multi-wall carbon nanotube reinforced aluminum matrix composites. Materials & Design 31:S96-S100.
[83] Esawi AMK, El Borady MA. 2008. Carbon nanotube-reinforced aluminium strips. Composites Science and Technology 68:486-92.
[84] Deng C, Zhang X, Wang D, Lin Q, Li A. 2007. Preparation and characterization of carbon nanotubes/aluminum matrix composites. Materials Letters 61:1725-8.
[85] Perez-Bustamante R, Gomez-Esparz CD, Estrada-Guel I, Miki-Yoshida M, Licea-Jimenez L, et al. 2009. Microstructural and mechanical characterization of Al-MWCNT composites produced by mechanical milling. Materials Science and Engineering a-Structural Materials Properties Microstructure and Processing 502:159-63.
[86] Sridhar I, Narayanan KR. 2009. Processing and characterization of MWCNT reinforced aluminum matrix composites. Journal of Materials Science 44:1750-6.
[87] Mula S, Mondal K, Ghosh S, Pabi SK. 2010. Structure and mechanical properties of Al-Ni-Ti amorphous powder consolidated by pressure-less, pressure-assisted and spark plasma sintering. Materials Science and Engineering a-Structural Materials Properties Microstructure and Processing 527:3757-63.
[88] Deng CF, Wang DZ, Zhang XX, Li AB. 2007. Processing and properties of carbon nanotubes reinforced aluminum composites. Materials Science and Engineering a-Structural Materials Properties Microstructure and Processing 444:138-45.
[89] Perez-Bustamante R, Estrada-Guel I, Antunez-Flores W, Miki-Yoshida M, Ferreira PJ, Martinez-Sanchez R. 2008. Novel Al-matrix nanocomposites reinforced with multi-walled carbon nanotubes. Journal of Alloys and Compounds 450:323-6.
[90] Kwon H, Cho S, Leparoux M, Kawasaki A. 2012. Dual-nanoparticulate-reinforced aluminum matrix composite materials. Nanotechnology 23:225704.
[91] Ci L, Ryu Z, Jin-Phillipp NY, Ruehle M. 2006. Investigation of the interfacial reaction between multi-walled carbon nanotubes and aluminum. Acta Materialia 54:5367-75.
[92] Kwon H, Estili M, Takagi K, Miyazaki T, Kawasaki A. 2009. Combination of hot extrusion and spark plasma sintering for producing carbon nanotube reinforced aluminum matrix composites. Carbon 47:570-7.

[93] Laha T, Chen Y, Lahiri D, Agarwal A. 2009. Tensile properties of carbon nanotube reinforced aluminum nanocomposite fabricated by plasma spray forming. Composites Part a-Applied Science and Manufacturing 40:589-94.
[94] Kwon H, Leparoux M. 2012. Hot extruded carbon nanotube reinforced aluminum matrix composite materials. Nanotechnology 23:415701.
[95] Xu CL, Wei BQ, Ma RZ, Liang J, Ma XK, Wu DH. 1999. Fabrication of aluminum–carbon nanotube composites and their electrical properties. Carbon 37:855-8.
[96] Kwon H, Park DH, Silvain JF, Kawasaki A. 2010. Investigation of carbon nanotube reinforced aluminum matrix composite materials. Composites Science and Technology 70:546-50.
[97] Cho S, Kikuchi K, Kawasaki A, Kwon H, Kim Y. 2012. Effective load transfer by a chromium carbide nanostructure in a multi-walled carbon nanotube/copper matrix composite. Nanotechnology 23:315705.
[98] de Sanctis M, Pelletier S, Bienvenu Y, Guigon M. 1994. On the formation of interfacial carbides in a carbon fibre-reinforced aluminium composite. Carbon 32:925-30.
[99] Vidal-Sétif MH, Lancin M, Marhic C, Valle R, Raviart JL, et al. 1999. On the role of brittle interfacial phases on the mechanical properties of carbon fibre reinforced Al-based matrix composites. Materials Science and Engineering: A 272:321-33.
[100]Besterci M. 2006. Preparation, microstructure and properties of Al–Al4C3 system produced by mechanical alloying. Materials & Design 27:416-21.
[101] Lancin M, Marhic C. 2000. TEM study of carbon fibre reinforced aluminium matrix composites: influence of brittle phases and interface on mechanical properties. Journal of the European Ceramic Society 20:1493-503.
[102] Laha T, Kuchibhatla S, Seal S, Li W, Agarwal A. 2007. Interfacial phenomena in thermally sprayed multiwalled carbon nanotube reinforced aluminum nanocomposite. Acta Materialia 55:1059-66.
[103] Bakshi SR, Singh V, Seal S, Agarwal A. 2009. Aluminum composite reinforced with multiwalled carbon nanotubes from plasma spraying of spray dried powders. Surface and Coatings Technology 203:1544-54.
[104] Aggour L, Fitzer E, Heym M, Ignatowitz E. 1977. Thin coatings on carbon fibers as diffusion barriers and wetting agents in Al composites. Thin Solid Films 40:97-105.
[105] Himbeault DD, Varin RA, Piekarski K. 1989. Tensile properties of titanium carbide coated carbon fibre — aluminum alloy composites. Composites 20:471-7.
[106] Li SN, Song SZ, Yu TQ, Chen HM, Zhang YS, Chen H. 2005. Microstructure and fracture surfaces of carbon nanotubes/magnesium matrix composite. Magnesium - Science, Technology and Applications 488-489:893-6.
[107] Gopa Kumar K, Pavithran C, Rohatgi PK. 1980. Preparation of copper-coated titania particles for composites. Journal of Materials Science 15:1588-92.
[108] Beigi Khosroshahi N, Azari Khosroshahi R, Taherzadeh Mousavian R, Brabazon D. 2014. Effect of electroless coating parameters and ceramic particle size on fabrication of a uniform Ni–P coating on SiC particles. Ceramics International 40:12149-59.
[109] He P, Huang S, Wang H, Huang Z, Hu J, et al. 2014. Electroless nickel–phosphorus plating on silicon carbide particles for metal matrix composites. Ceramics International 40:16653-64.
[110] Mohammadpour M, Azari Khosroshahi R, Taherzadeh Mousavian R, Brabazon D. 2014. Effect of interfacial-active elements addition on the incorporation of micron-sized SiC particles in molten pure aluminum. Ceramics International 40:8323-32.

[111] Chen Y, Cao M, Xu Q, Zhu J. 2003. Electroless nickel plating on silicon carbide nanoparticles. Surface and Coatings Technology 172:90-4.
[112] Kong FZ, Zhang XB, Xiong WQ, Liu F, Huang WZ, et al. 2002. Continuous Ni-layer on multiwall carbon nanotubes by an electroless plating method. Surface and Coatings Technology 155:33-6.
[113] Ang LM, Hor TSA, Xu GQ, Tung CH, Zhao SP, Wang JLS. 2000. Decoration of activated carbon nanotubes with copper and nickel. Carbon 38:363-72.
[114] Yang Z, Xu H, Li M-K, Shi Y-L, Huang Y, Li H-L. 2004. Preparation and properties of Ni/P/single-walled carbon nanotubes composite coatings by means of electroless plating. Thin Solid Films 466:86-91.
[115] Miranda G, Buciumeanu M, Carvalho O, Soares D, Silva FS. 2015. Interface analysis and wear behavior of Ni particulate reinforced aluminum–silicon composites produced by PM. Composites Part B: Engineering 69:101-10.
[116] Niu X, Rahbar N, Farias S, Soboyejo W. 2009. Bio-inspired design of dental multilayers: Experiments and model. Journal of the Mechanical Behavior of Biomedical Materials 2:596-602.
[117] Nogata F, Takahashi H. 1995. Intelligent functionally graded material: bamboo. Composites Engineering 5:743-51.
[118] Suresh S. 2001. Graded materials for resistance to contact deformation and damage. Science 292:2447-51.
[119] Nogata F. Intelligent modelling mechanisms and design concepts of FGMs in natural composites, 308:331-7: Trans Tech Publ.
[120] Ghavami K, Rodrigues CS, Paciornik S. 2003. Bamboo: functionally graded composite material. Asian J. of Civil Engineering, Building and Housing 4:1-10.
[121] Tilbrook MT, Moon RJ, Hoffman M. 2005. Crack propagation in graded composites. Composites Science and Technology 65:201-20.
[122] Miyamoto Y. 1999. Functionally Graded Materials: Design, Processing and Applications. Springer US. 1 pp.
[123] Mortensen A, Suresh S. 1995. Functionally graded metals and metal-ceramic composites: Part 1 Processing. International Materials Reviews 40:239-65.
[124] Suresh S, Mortensen A. 1997. Functionally graded metals and metal-ceramic composites: Part 2 Thermomechanical behaviour. International Materials Reviews 42:85-116.
[125] Sasaki M, Hirai T. 1991. Fabrication and properties of functionally gradient materials. Nippon seramikkusu kyokai gakujutsu ronbunshi 99:1002-13.
[126] Zhu HX, Abbaschian R. 2000. Microstructures and properties of in-situ NiAl–Al2O3 functionally gradient composites. Composites Part B: Engineering 31:383-90.
[127] Erdogan F. 1995. Fracture mechanics of functionally graded materials. Composites Engineering 5:753-70.
[128] Yang YY, Munz D, Schaller W. 1997. Effect of the stress jump at the interface of a joint on the failure behavior. International journal of fracture 87:L113-L8.
[129] Kokini K, Choules BD, Takeuchi YR. 1997. Thermal fracture mechanisms in ceramic thermal barrier coatings. Journal of Thermal Spray Technology 6:43-9.
[130] Kieback B, Neubrand A, Riedel H. 2003. Processing techniques for functionally graded materials. Materials Science and Engineering: A 362:81-106.
[131] Ruys AJ, Popov EB, Sun D, Russell JJ, Murray CCJ. 2001. Functionally graded electrical/thermal ceramic systems. Journal of the European Ceramic Society 21:2025-9.

[132] Köhl M, Bram M, Moser A, Buchkremer HP, Beck T, Stöver D. 2011. Characterization of porous, net-shaped NiTi alloy regarding its damping and energy-absorbing capacity. Materials Science and Engineering: A 528:2454-62.
[133] Karageorgiou V, Kaplan D. 2005. Porosity of 3D biomaterial scaffolds and osteogenesis. Biomaterials 26:5474-91.
[134] Vasconcellos LMRd, Oliveira MVd, Graça MLdA, Vasconcellos LGOd, Carvalho YR, Cairo CAA. 2008. Porous titanium scaffolds produced by powder metallurgy for biomedical applications. Materials Research 11:275-80.
[135] de Vasconcellos LM, Leite DD, Nascimento F-O, de Vasconcellos LG, Graça ML, et al. 2010. Porous titanium for biomedical applications: an experimental study on rabbits. Medicina oral, patología oral y cirugía bucal 15:e407.
[136] Mour M, Das D, Winkler T, Hoenig E, Mielke G, et al. 2010. Advances in porous biomaterials for dental and orthopaedic applications. Materials 3:2947-74.
[137] Miao X, Sun D. 2009. Graded/gradient porous biomaterials. Materials 3:26-47.
[138] Oh I-H, Nomura N, Masahashi N, Hanada S. 2003. Mechanical properties of porous titanium compacts prepared by powder sintering. Scripta Materialia 49:1197-202.
[139] Zhao YY, Sun DX. 2001. A novel sintering-dissolution process for manufacturing Al foams. Scripta materialia 44:105-10.
[140] Sun DX, Zhao YY. 2005. Phase changes in sintering of Al/Mg/NaCl compacts for manufacturing Al foams by the sintering and dissolution process. Materials Letters 59:6-10.
[141] Zhao Y, Han F, Fung T. 2004. Optimisation of compaction and liquid-state sintering in sintering and dissolution process for manufacturing Al foams. Materials Science and Engineering: A 364:117-25.
[142] Sun DX, Zhao YY. 2003. Static and dynamic energy absorption of Al foams produced by the sintering and dissolution process. Metallurgical and Materials Transactions B 34:69-74.
[143] Bram M, Stiller C, Buchkremer HP, Stöver D, Baur H. 2000. High Porosity Titanium, Stainless Steel, and Superalloy Parts. Advanced Engineering Materials 2:196-9.
[144] Jiang B, Zhao NQ, Shi CS, Du XW, Li JJ, Man HC. 2005. A novel method for making open cell aluminum foams by powder sintering process. Materials Letters 59:3333-6.
[145] Jiang B, Zhao NQ, Shi CS, Li JJ. 2005. Processing of open cell aluminum foams with tailored porous morphology. Scripta Materialia 53:781-5.
[146] Bafti H, Habibolahzadeh A. 2013. Compressive properties of aluminum foam produced by powder-Carbamide spacer route. Materials & Design 52:404-11.
[147] Bastawros AF, Bart-Smith H, Evans AG. 2000. Experimental analysis of deformation mechanisms in a closed-cell aluminum alloy foam. Journal of the Mechanics and Physics of Solids 48:301-22.
[148].San Marchi C, Mortensen A. 2001. Deformation of open-cell aluminum foam. Acta materialia 49:3959-69.
[149] Ramamurty U, Paul A. 2004. Variability in mechanical properties of a metal foam. Acta Materialia 52:869-76.
[150] Andersen O, Waag U, Schneider L, Stephani G, Kieback B. 2000. Novel metallic hollow sphere structures. Advanced Engineering Materials 2:192-5.
[151] Vu TV, Takakura H, Wells JC, Minemoto T. 2010. Production of Hollow Spheres of Eutectic Tin-Lead Solder through a Coaxial Nozzle. Journal of Solid Mechanics and Materials Engineering 4:1530-8.
[152] Ashby MF. 2000. Metal foams: a design guide. Butterworth-Heinemann.

[153].Angelo PC, Subramanian R. 2008. Powder Metallurgy: Science, Technology and Applications. PHI Learning.
[154] Kanetake N, Kobashi M. 2006. Innovative processing of porous and cellular materials by chemical reaction. Scripta Materialia 54:521-5.
[155] Bhattacharyya M, Kapuria S, Kumar AN. 2007. On the Stress to Strain Transfer Ratio and Elastic Deflection Behavior for Al/SiC Functionally Graded Material. Mechanics of Advanced Materials and Structures 14:295-302.
[156] Gunes R, Aydin M, Kemal Apalak M, Reddy JN. 2014. Experimental and numerical investigations of low velocity impact on functionally graded circular plates. Composites Part B: Engineering 59:21-32.
[157] Yeo J-G, Jung Y-G, Choi S-C. 1998. Zirconia-stainless steel functionally graded material by tape casting. Journal of the European Ceramic Society 18:1281-5.
[158] Oakley ST. 1979. Powder rolling apparatus. Google Patents.
[159] Ruder A, Buchkremer HP, Jansen H, Malléner W, Stöver D. 1992. Wet powder spraying—a process for the production of coatings. Surface and Coatings Technology 53:71-4.
[160] Callister WD, Rethwisch DG. 2013. Fundamentals of materials science and engineering. Wiley.
[161] Birth U, Joensson M, Kieback B. Powder metallurgical processing and properties of copper/tungsten gradients, 308:766-73: Trans Tech Publ.
[162] Yang Z, Zhang L, Shen Q, Gong D. 2003. Theoretical design of sedimentation applied to the fabrication of functionally graded materials. Metallurgical and Materials Transactions B 34:605-9.
[163] German R. 1994. Powder Metallurgy Science. pp 1-98. Metal Powder Industries Federation.
[164] Yang Z-m, Gong D-r, Zhang L-m. 2004. Design of co-sedimentation experiments used to fabricate functionally graded materials with a continuous change of composition. Journal of Wuhan University of Technology-Mater. Sci. Ed. 19:11-3.
[165] Yang Z-m, Tian F, Zhang L-m. 2002. Fabrication of Ti-Mo functionally graded material with smoothly varying composition. The Chinese Journal of Nonferrous Metals:S1.
[166] Biesheuvel PM, Breedveld V, Higler AP, Verweij H. 2001. Graded membrane supports produced by centrifugal casting of a slightly polydisperse suspension. Chemical engineering science 56:3517-25.
[167] Moritz T, Riedel H, Werner G, Tomandl G. 2000. Simulation and investigation of pore size graded titania layers during sintering. Journal of Materials Science 35:2235-40.
[168] Sarkar P, Huang X, Nicholson PS. 1993. Zirconia/alumina functionally gradiented composites by electrophoretic deposition techniques. Journal of the American Ceramic Society 76:1055-6.
[169] Sarkar P, Haung X, Nicholson PS. 1992. Structural ceramic microlaminates by electrophoretic deposition. Journal of the American Ceramic Society 75:2907-9.
[170] Put S, Vleugels J, Van der Biest O. 2001. Functionally graded WC–Co materials produced by electrophoretic deposition. Scripta Materialia 45:1139-45.
[171] Sarkar P, Datta S, Nicholson PS. 1997. Functionally graded ceramic/ceramic and metal/ceramic composites by electrophoretic deposition. Composites Part B: Engineering 28:49-56.
[172] Pascall AJ, Qian F, Wang G, Li Y, Kuntz JD. Light Directed Electrophoretic Deposition: A New Technique for Patterning Materials in 3D, 36:2304-: The Electrochemical Society.

[173] Katayama T, Sukenaga S, Saito N, Kagata H, Nakashima K. Fabrication of Al2O3-W Functionally Graded Materials by Slipcasting Method, 20, 18:202023: IOP Publishing.
[174] Tomsia AP, Saiz E, Ishibashi H, Diaz M, Requena J, Moya JS. 1998. Powder processing of mullite/Mo functionally graded materials. Journal of the European Ceramic Society 18:1365-71.
[175] Marple BR, Boulanger J. 1994. Graded casting of materials with continuous gradients. Journal of the American Ceramic Society 77:2747-50.
[176] Agarwala M, Bourell D, Beaman J, Marcus H, Barlow J. 1995. Direct selective laser sintering of metals. Rapid Prototyping Journal 1:26-36.
[177] Kumar S, Kruth JP. 2010. Composites by rapid prototyping technology. Materials & Design 31:850-6.
[178] Yan Y, Li S, Zhang R, Lin F, Wu R, et al. 2009. Rapid Prototyping and Manufacturing Technology: Principle, Representative Technics, Applications, and Development Trends. Tsinghua Science & Technology 14, Supplement 1:1-12.
[179] Hollander DA, von Walter M, Wirtz T, Sellei R, Schmidt-Rohlfing B, et al. 2006. Structural, mechanical and in vitro characterization of individually structured Ti–6Al–4V produced by direct laser forming. Biomaterials 27:955-63.
[180] Traini T, Mangano C, Sammons RL, Mangano F, Macchi A, Piattelli A. 2008. Direct laser metal sintering as a new approach to fabrication of an isoelastic functionally graded material for manufacture of porous titanium dental implants. Dental Materials 24:1525-33.
[181] Li JP, Habibovic P, van den Doel M, Wilson CE, de Wijn JR, et al. 2007. Bone ingrowth in porous titanium implants produced by 3D fiber deposition. Biomaterials 28:2810-20.
[182] Simske SJ, Ayers RA, Bateman TA. Porous materials for bone engineering, 250:151-82: Trans Tech Publ.
[183] Oh SH, Park IK, Kim JM, Lee JH. 2007. In vitro and in vivo characteristics of PCL scaffolds with pore size gradient fabricated by a centrifugation method. Biomaterials 28:1664-71.
[184] Martins J. Motores de combustao interna. Publindustria.
[185] Costa N. 2009. Analysis of the influence of processing parameters on the fatigue life of engine piston rings, PhD Thesis.
[186] Newton K, Steeds W, Garrett TK. 1996. The Motor Vehicle. Society of Automotive Engineers.
[187] Dworak U, Olapinski H, Fingerle D, Krohn U. 1985. Piston ring for an internal combustion engine. Google Patents.
[188] F TR, W WE. 1959. Method of forming a sintered powdered metal piston ring. Google Patents.
[189] Koehler M. 1971. Method of making piston ring. Google Patents.
[190] Alberto LB. 1960. Process for manufacturing piston rings. Google Patents.
[191] Young WB. 1998. Nitrided powdered metal piston ring. Google Patents.
[192] Dai LH, Ling Z, Bai YL. 2001. Size-dependent inelastic behavior of particle-reinforced metal–matrix composites. Composites Science and Technology 61:1057-63.
[193] Cox HL. 1952. The elasticity and strength of paper and other fibrous materials. British Journal of Applied Physics 3:72.
[194] Koo MY, Park JS, Park MK, Kim KT, Hong SH. 2012. Effect of aspect ratios of in situ formed TiB whiskers on the mechanical properties of TiBw/Ti–6Al–4V composites. Scripta Materialia 66:487-90.
[195] Arsenault RJ, Wang L, Feng CR. 1991. Strengthening of composites due to microstructural changes in the matrix. Acta Metallurgica et Materialia 39:47-57.

[196] Nardone VC, Prewo KM. 1986. On the strength of discontinuous silicon carbide reinforced aluminum composites. Scripta Metallurgica 20:43-8.
[197] Ryu HJ, Cha SI, Hong SH. 2003. Generalized shear-lag model for load transfer in SiC/Al metal-matrix composites. Journal of materials research 18:2851-8.
[198] Anumandla V, Gibson RF. 2006. A comprehensive closed form micromechanics model for estimating the elastic modulus of nanotube-reinforced composites. Composites Part A: Applied Science and Manufacturing 37:2178-85.
[199] Hull D, Bacon DJ. 2001. Introduction to Dislocations. Elsevier Scienc.e
[200] Manoharan M, Lewandowski JJ. 1992. Effect of reinforcement size and matrix microstructure on the fracture properties of an aluminum metal matrix composite. Materials Science and Engineering: A 150:179-86.
[201] Lewandowski JJ, Liu DS, Liu C. 1991. Observations on the effects of particulate size and superposed pressure on deformation of metal matrix composites. Scripta Metallurgica et Materialia 25:21-6.
[202] Kamat SV, Hirth JP, Mehrabian R. 1989. Mechanical properties of particulate-reinforced aluminum-matrix composites. Acta Metallurgica 37:2395-402.
[203] Barlow CY, Hansen N, Liu YL. 1993. A microstructural investigation of deformation in fine SiC particulate- and whisker-reinforced aluminium-matrix composites. Journal of Microscopy 169:225-32.
[204] Ashby MF. 1970. The deformation of plastically non-homogeneous materials. Philosophical Magazine 21:399-424.
[205] Barlow CY, Hansen N. 1995. Dislocation configurations in metal-matrix composites correlated with numerical predictions. Acta Metallurgica et Materialia 43:3633-48.
[206] Barlow CY, Hansen N. 1991. Deformation structures and flow stress in aluminium containing short whiskers. Acta metallurgica et materialia 39:1971-9.
[207] Christman T, Needleman A, Suresh S. 1989. An experimental and numerical study of deformation in metal-ceramic composites. Acta Metallurgica 37:3029-50.
[208] Taya M, Arsenault RJ. 1989. Metal matrix composites: thermomechanical behavior. Pergamon Press.
[209] Xu XQ, Watt DF. 1994. Basic role of a hard particle in a metal matrix subjected to tensile loading. Acta Metallurgica et Materialia 42:3717-29.
[210] Sarkar J. 1995. Aspects of strengthening and work hardening in particulate metal matrix composites. Scripta Metallurgica et Materialia 32:37-42.
[211] Wu Y, Lavernia EJ. 1992. Strengthening behavior of particulate reinforced MMCs. Scripta Metallurgica et Materialia 27:173-8.
[212] Hall JN, Wayne Jones J, Sachdev AK. 1994. Particle size, volume fraction and matrix strength effects on fatigue behavior and particle fracture in 2124 aluminum-SiCp composites. Materials Science and Engineering: A 183:69-80.
[213] Arsenault RJ, Shi N. 1986. Dislocation generation due to differences between the coefficients of thermal expansion. Materials Science and Engineering 81:175-87.
[214] Dunand DC, Mortensen A. 1991. Dislocation emission at fibers—II. Experiments and microstructure of thermal punching. Acta metallurgica et materialia 39:1417-29.
[215] Chawla KK, Metzger M. 1972. Initial dislocation distributions in tungsten fibre-copper composites. Journal of Materials Science 7:34-9.
[216] Hassan SF, Gupta M. 2006. Effect of different types of nano-size oxide particulates on microstructural and mechanical properties of elemental Mg. Journal of Materials Science 41:2229-36.

[217] Sanaty-Zadeh A. 2012. Comparison between current models for the strength of particulate-reinforced metal matrix nanocomposites with emphasis on consideration of Hall–Petch effect. Materials Science and Engineering: A 531:112-8.
[218] Hull D, Clyne TW. 1996. An Introduction to Composite Materials. Cambridge University Press.
[219] Miller WS, Humphreys FJ. 1991. Strengthening mechanisms in particulate metal matrix composites. Scripta Metallurgica et Materialia 25:33-8.
[220] Zhang Z, Chen DL. 2006. Consideration of Orowan strengthening effect in particulate-reinforced metal matrix nanocomposites: A model for predicting their yield strength. Scripta Materialia 54:1321-6.
[221] Zhang Z, Chen DL. 2008. Contribution of Orowan strengthening effect in particulate-reinforced metal matrix nanocomposites. Materials Science and Engineering: A 483:148-52.
[222] Mirza FA, Chen DL. 2012. An Analytical Model for Predicting the Yield Strength of Particulate-Reinforced Metal Matrix Nanocomposites with Consideration of Porosity. Nanoscience and Nanotechnology Letters 4:794-800.
[223] Dieter GE. 1961. MECHANICAL METALLURGY.
[224] Ellyin F. 1997. Fatigue Damage, Crack Growth and Life Prediction. Springer.
[225] Ashby MF, Shercliff H, Cebon D. 2009. Materials: engineering, science, processing and design. Elsevier Science.
[226] Boyer HE, Metals AS. 1985. Atlas of Fatigue Curves. American Society for Metals.
[227] Meyers MA, Chawla KK. 2009. Mechanical Behavior of Materials. Cambridge University Press.
[228] Kelly A, Zweben CH. 2000. Comprehensive composite materials. Elsevier.
[229] Mortensen A. 2006. Concise Encyclopedia of Composite Materials. pp 367-371. Elsevier Science.
[230] Chawla N, Jones JW, Andres C, Allison JE. 1998. Effect of SiC volume fraction and particle size on the fatigue resistance of a 2080 Al/SiC p composite. Metallurgical and Materials Transactions A 29:2843-54.
[231] Chawla N, Shen YL. 2001. Mechanical Behavior of Particle Reinforced Metal Matrix Composites. Advanced Engineering Materials 3:357-70.
[232] Liu XC, Bathias C. 1992. Fatigue behaviour of Al2O3 short fibre reinforced aluminium alloy. Fatigue & Fracture of Engineering Materials & Structures 15:1113-23.
[233] Clyne TW, Withers PJ. 1993. An introduction to metal matrix composites.
[234] Withers PJ, Stobbs WM, Bourdillon AJ. 1988. Various TEM methods for the study of metal matrix composites. Journal of Microscopy 151:159-69.
[235] Evans AG, He MY, Hutchinson JW. 1989. Interface debonding and fiber cracking in brittle matrix composites. Journal of the American Ceramic Society 72:2300-3.
[236] Qin S, Chen C, Zhang G, Wang W, Wang Z. 1999. The effect of particle shape on ductility of SiCp reinforced 6061 Al matrix composites. Materials Science and Engineering: A 272:363-70.
[237] Spowart JE, Miracle DB. 2003. The influence of reinforcement morphology on the tensile response of 6061/SiC/25p discontinuously-reinforced aluminum. Materials Science and Engineering: A 357:111-23.
[238] Holmes J, Queeney RA. 1985. Fatigue crack initiation in a porous steel. Powder Metallurgy 28:231-5.
[239] Choi S-M, Awaji H. 2005. Nanocomposites—a new material design concept. Science and Technology of Advanced Materials 6:2-10.

[240] Faber KT, Evans AG. 1983. Crack deflection processes—I. Theory. Acta Metallurgica 31:565-76.
[241] Lange FF. 1970. The interaction of a crack front with a second-phase dispersion. Philosophical Magazine 22:0983-92.
[242] Lange FF. 1971. Fracture Energy and Strength Behavior of a Sodium Borosilicate Glass $A_{l2}O_3$ Composite System. Journal of the American Ceramic Society 54:614-20.
[243] Mower TM, Argon AS. 1995. Experimental investigations of crack trapping in brittle heterogeneous solids. Mechanics of Materials 19:343-64.
[244] Lee W, Myoung J-M, Yoo Y-H, Shin H. 2006. Effect of thermal misfit stress on crack deflection at planar interfaces in layered systems. Composites Science and Technology 66:435-43.
[245] Lipetzky P, Knesl Z. 1985. Crack-particle interaction in a two-phase composite Part II: crack deflection. International Journal of Fracture 73:81-92.
[246] Rao KTV, Soboyejo WO, Ritchie RO. 1992. Ductile-phase toughening and fatigue-crack growth in Nb-reinforced molybdenum disilicide intermetallic composites. Metallurgical Transactions A 23:2249-57.
[247] Parmigiani JP, Thouless MD. 2006. The roles of toughness and cohesive strength on crack deflection at interfaces. Journal of the Mechanics and Physics of Solids 54:266-87
[248] He M-Y, Hutchinson JW. 1989. Kinking of a Crack Out of an Interface. Journal of Applied Mechanics 56:270-8.
[249] Evans AG. 1990. Perspective on the development of high toughness ceramics. Journal of the American Ceramic society 73:187-206.
[250] Hsueh C-H, Becher PF. 1991. Some considerations of bridging stresses for fiber-reinforced ceramics. Composites Engineering 1:129-43.
[251] Knowles DM, King JE. 1992. Role of reinforcement/matrix interfacial strength in fatigue crack propagation in particulate SiC reinforced aluminium alloy 8090. Materials science and technology 8:500-9.
[252] Lewandowski JJ, Liu C, Hunt WH. 1989. Effects of matrix microstructure and particle distribution on fracture of an aluminum metal matrix composite. Materials Science and Engineering: A 107:241-55.
[253] Davidson DL. 1988. Plasticity induced fatigue crack closure. Mechanics of fatigue crack closure, ASTM STP 982:44-61.
[254] Flom Y, Arsenault RJ. 1986. Interfacial bond strength in an aluminium alloy 6061 — SiC composite. Materials Science and Engineering 77:191-7.
[255] Murakami Y. 2002. Metal Fatigue: Effects of Small Defects and Nonmetallic Inclusions: Effects of Small Defects and Nonmetallic Inclusions. Elsevier Science.
[256] Committee ASMIH. 1992. ASM Handbook. ASM International.
[257] Hutchings IM. 1992. Tribology: Friction and Wear of Engineering Materials. Edward Arnold.
[258] Williams J. 1994. Engineering Tribology. Cambridge University Press.
[259] Gahr KHZ. 1987. Microstructure and Wear of Materials. Elsevier Science.
[260] Davim JP. 2011. Tribology for Engineers: A Practical Guide. Elsevier Science.
[261] Berman AD, Ducker WA, Israelachvili JN. 1996. Origin and characterization of different stick-slip friction mechanisms. Langmuir 12:4559-63.
[262] Chatelet E, Michon G, Manin L, Jacquet G. 2008. Stick/slip phenomena in dynamics: Choice of contact model. Numerical predictions & experiments. Mechanism and Machine Theory 43:1211-24.

[263] Rapoport L. 2009. Steady friction state and contact models of asperity interaction. Wear 267:1305-10.
[264] Yoshizawa H, McGuiggan P, Israelachvili J. 1993. Identification of a second dynamic state during stick-slip motion. Science 259:1305-8.
[265] Takadoum J. 2013. Materials and Surface Engineering in Tribology. Wiley.
[266] Budinski KG. 2001. Friction of plastic webs. Tribology international 34:625-33
[267] Larsen TØ, Andersen TL, Thorning B, Horsewell A, Vigild ME. 2007. Comparison of friction and wear for an epoxy resin reinforced by a glass or a carbon/aramid hybrid weave. Wear 262:1013-20.
[268] Ludema KC. 2010. Friction, wear, lubrication: a textbook in tribology. CRC press.
[269] Neale MJ. 1995. The tribology handbook. Butterworth-Heinemann.
[270] Rabinowicz E. 1995. Friction and Wear of Materials. Wiley.
[271] Bhushan B. 2000. Modern Tribology Handbook, Two Volume Set. Crc Press.
[272] Stachowiak G, Batchelor AW. 2011. Engineering Tribology. Elsevier Science.
[273] Trezona RI, Allsopp DN, Hutchings IM. 1999. Transitions between two-body and three-body abrasive wear: influence of test conditions in the microscale abrasive wear test. Wear 225:205-14.
[274] Swain MV. 1975. Microscopic observations of abrasive wear of polycrystalline alumina. Wear 35:185-9.
[275] Mulhearn TO, Samuels LE. 1962. The abrasion of metals: a model of the process. Wear 5:478-98.
[276] Sedriks AJ, Mulhearn TO. 1963. Mechanics of cutting and rubbing in simulated abrasive processes. Wear 6:457-66.
[277] Sedriks AJ, Mulhearn TO. 1964. The effect of work-hardening on the mechanics of cutting in simulated abrasive processes. Wear 7:451-9.
[278] Avient BWE, Goddard J, Wilman H. 1960. An experimental study of friction and wear during abrasion of metals. Proceedings of the Royal Society of London. Series A. Mathematical and Physical Sciences 258:159-80.
[279].Rabinowicz E, Dunn LA, Russell PG. 1961. A study of abrasive wear under three-body conditions. Wear 4:345-55.
[280] Rabinowicz E, Mutis A. 1965. Effect of abrasive particle size on wear. Wear 8:381-90.
[281] Nathan GK, Jones WJD. 1966. The empirical relationship between abrasive wear and the applied conditions. Wear 9:300-9.
[282] Larsen-Badse J. 1968. Influence of grit diameter and specimen size on wear during sliding abrasion. Wear 12:35-53.
[283] Larsen-Badse J. 1968. Abrasion resistance of some SAP-type alloys at room temperature. Wear 12:357-68.
[284] Date SW, Malkin S. 1976. Effects of grit size on abrasion with coated abrasives. Wear 40:223-35.
[285] Misra A, Finnie I. 1981. On the size effect in abrasive and erosive wear. Wear 65:359-73.
[286] Misra A, Finnie I. 1981. Some observations on two-body abrasive wear. Wear 68:41-56.
[287] Sasada T, Oike M, Emori N. 1984. The effect of abrasive grain size on the transition between abrasive and adhesive wear. Wear 97:291-302.
[288] Jacobson S, Wallén P, Hogmark S. 1988. Fundamental aspects of abrasive wear studied by a new numerical simulation model. Wear 123:207-23.

[289].Gåhlin R, Jacobson S. 1999. The particle size effect in abrasion studied by controlled abrasive surfaces. Wear 224:118-25.
[290] Hornbogen E. 1975. The role of fracture toughness in the wear of metals. Wear 33:251-9.
[291] Eyre TS. 1978. The mechanisms of wear. Tribology International 11:91-6.
[292] Kerridge M. 1955. Metal transfer and the wear process. Proceedings of the Physical Society. Section B 68:400.
[293] Buckley DH. 1981. Surface effects in adhesion, friction, wear, and lubrication. Elsevier Science.
[294] Buckley DH. 1968. The influence of the atomic nature of crystalline materials on friction. ASLE TRANSACTIONS 11:89-100.
[295] Sikorski ME. 1963. Correlation of the coefficient of adhesion with various physical and mechanical properties of metals. Journal of Fluids Engineering 85:279-85.
[296] Black AJ, Kopalinsky EM, Oxley PLB. 1993. Asperity deformation models for explaining the mechanisms involved in metallic sliding friction and wear—a review. Proceedings of the Institution of Mechanical Engineers, Part C: Journal of Mechanical Engineering Science 207:335-53.

3 Evaluation of CNT dispersion methodology effect on mechanical properties of an Al-Si composite

Carvalho, O[1], Buciumeanu, M[2], Soares, D.[1], Silva, F.S. [1], Miranda, G[1]

[1]CT2M – Centre for Mechanical and Materials Technologies, University of Minho, Azurém, 4800-058 Guimarães, Portugal
[2]Cross–Border Faculty of Humanities, Economics and Engineering, "Dunarea de Jos" University of Galati, Domneasca 47, 800008 Galati, Romania

Published in Journal of Materials Engineering and Performance, 17 Apr2015
DOI 10.1007/s11665-015-1510-5

3.1 Abstract

The aim of this paper was to evaluate the effect of different dispersion methodologies on mechanical properties of the Alumium-Silicon (AlSi) composites reinforced by Multi-Wall Carbon Nanotubes (MWCNTs) coated with Ni. Different mixing procedures of MWCNTs with AlSi powder were tested and AlSi-CNT composites were produced by hot pressing – Powder Metallurgy technique. The shear tests were performed to get the mechanical properties. Scanning electron microscopy (SEM) with X-Ray energy dispersive spectroscopy (EDS) analysis and thermal analysis (DSC) were used to investigate the microstructure of AlSi-CNT composites, interface reactions and fracture morphology after shear tests. The experimental results proved that an improvement of dispersion of CNTs was achieved by using a combination of different mixing processes.

Keywords: Metal-matrix composites (MMC); Carbon nanotube (CNT); Powder processing; AlSi alloy

3.2 Introduction

The properties of carbon nanotubes (e.g. outstanding mechanical properties, low thermal expansion, high thermal conductivity, good electrical properties [1-4] etc.), that

exceed those of any conventional material [5], make them an excellent reinforcement to design high-performance composite materials.

CNTs have been used as a reinforcement for different materials including polymeric [3], metal [5, 6-11] and ceramic matrices [12]. Among CNTs, several materials, such as Al, Ti, Cu, Mg [3-6, 8, 10, 13-20] etc. were used as reinforcement to produce metal-matrix composites.

The enhancement in mechanical properties of the aluminium alloys is the motivation to study different innovative processing routes, and consequently improved composite materials. So far these materials have been produced by dispersing oxides, carbides or nitrides into the metallic matrix. More recently single-walled carbon nanotubes (SWCNTs) and multi-walled carbon nanotubes (MWCNT) are being tested and are raising a great interest in the scientific community as a new kind of reinforcement material for the production of novel MMCs, because of their already mentioned excellent properties [11].

However one of the biggest drawbacks in the field of CNTs reinforced metal matrix composites is the difficulty in the dispersion of CNTs during the mixing process, due to their attractive van der Waals interactions [11]. It is quite difficult to achieve uniform dispersion of CNTs in metal matrix [21-23]. Another potential problem is the possible interfacial reaction between CNTs and metal matrix that might result in the deterioration of composite properties [11]. Thus, the composite processing technique is critical for the composites success.

Different approaches have been used to process MMC reinforced with CNTs such as conventional processes of powder metallurgy, electrochemical processes, thermal spraying, casting processes and other innovative techniques.

Mechanical alloying is the most used powder metallurgy route [6-8, 17, 24, 25]. It has two main stages, such as (i) Mix of the metal powders and the CNTs; (ii) Sintering after cold pressing or pressure-assisted sintering. There are two milling processes: low and high energy milling [9]. Some studies showed that high energy milling process is more efficient in the dispersion process than the low milling process [7, 13, 24, 25], although some degradation may occur on CNTs [5, 18, 25]. Regarding the low energy milling there are two main disadvantages: the process is taking a longer time and the sintering process is more difficult due to the growth of the grains (welding of the particles) [5, 8, 18].

It is well known that the enhancement on mechanical properties of the composites is highly dependent on the dispersion of CNTs, thus on the effectiveness of the CNT's mixing process [5, 8, 18].

In the technical literature is not common to find comparisons between different mixing procedures under similar conditions.

The aim of this paper was to evaluate the effect of different dispersion methodologies on mechanical properties of the Aluminium-Silicon (AlSi) composites reinforced by Multi-Wall Carbon Nanotubes (MWCNTs) coated with Ni. It is shown that an improvement in dispersion of CNTs is achieved by using a combination of different mixing processes.

3.3 Experimental procedure

3.3.1 Materials

An AlSi alloy, powders size < 325 mesh (<44μm) with the following chemical composition (as provided by supplier) is (in weight %): Si 11.0, Fe 0.2, others 1.5 and balance Al, was used as matrix material. Ni coated MWCNTs were used as reinforcement (outer diameter > 50 nm, length 0.5-2.0 μm, purity before coating > 95wt% and ash <1.5wt%). It should be highlighted that the Ni coating does not have a structural effect on CNT molecular structure. The Ni coating was used in order to improve the bonding between CNTs and matrix and to avoid some undesirable chemical reactions.

3.3.2 Methods

Sintering conditions.

The AlSi-matrix composite reinforced by CNTs was processed by the traditional hot pressing (HP) technique. Applied pressure was 35 MPa for 10 minutes at 550°C. The compaction (powder/mixture) was made on a graphite cylindrical die with an internal diameter of 10 mm and 10 mm height. The powder/mixture was then sintered by a pressure-assisted sintering process in a vacuum chamber at 10^{-2} mbar, using a high frequency induction furnace (Fig. 1). The following procedure was used: (1) the mold was placed inside the chamber where the sample powder/mixture were compressed at 1.3 MPa; (2) it was heated up to the stage temperature (T=550°C) with a heating rate of 25°C/min.;

(3) at the stage temperature, the pressure was raised up to 35 MPa and maintained for 10 minutes; (4) then the power was turned off and the system cooled down to room temperature under vacuum.

Mixing processes.

The following five processes were studied in this work:

Process A. AlSi alloy was used for comparison purposes.

Process B. The mixing of powders was made inside a closed stainless steel jar with 10mm diameter steel milling balls. The bottle rotated with constant speed (40 rpm) during 6 days (low-energy ball milling). The milling atmosphere was argon.

Process C. The mixing of powders was made inside a ceramic jar containing 10mm diameter stainless steel milling balls. We used high-energy shaker milling (SPEX-8000M) during 1 minute. The milling atmosphere was argon.

Process D. The mixing of powders was made inside a closed stainless steel jar with 10mm diameter steel milling balls. We used high-energy shaker milling (SPEX-8000M) during 1 minute. The milling atmosphere was ethanol.

Process E. The mixing of powders was made inside a jar with ethanol solution that was placed into an ultrasonic shaker (Axtor CD 4820 – 42 KHz – 170W). The mixing of powders was performed by using simultaneously two techniques: mechanical stirring (120 rpm) and ultrasonic shaking, for 30 min. Then the solution was decanted by vaporizing the ethanol and dried at 100°C in a furnace. After that the mixture was placed in a ceramic mixing jar containing 10 mm diameter stainless steel milling balls. The milling processes used were: a High energy ultrasonic mixing (Axtor CD 4820), followed by high-energy shaker mill (SPEX-8000M) during 1 minute. The atmosphere was ethanol for ultrasonic mixing and Argon for powders milling.

In all the cases studied, the initial ball-to-powder weight ratio was (BPR) = 10:1. In all mixing conditions 2 wt. % of MWCNTs were used. A total mass (AlSi and MWCNTs) of powders used was 5 grams for each mixing condition.

Mechanical testing.

In order to study the mechanical properties of the composites shear tests were performed. The tests were performed at room temperature (23°C) by using a device that is fixed in a universal testing machine (Instron 8874, MA, USA). The shear tests were carried out according to ASTM standard B565, under a loading rate of 0.02 mm/s with five specimens under identical test conditions.

Metallurgical evaluation.

SEM with EDS analysis was used to examine the dispersion of CNTs within the ASi matrix and also to analyze the fracture morphology after shear tests. Thermal analysis (DSC - Differential Scanning Calorimetry) tests were carried out to evaluate the reactivity between CNTs and AlSi matrix. For DSC was used a heating rate of 10°C/min and a constant flow of argon.

3.4 Results and discussion

3.4.1 Microstructural characterization

In Figure 3.1-a is presented the SEM image of CNTs (190x magnification), where can be noticed the presence of agglomerations. In Figure 3.1-a, b and c can be seen amplified images of a CNT agglomerate (30000x and 100000x magnifications). Figure 3.1-d shows an amplified SEM image of a singular CNT (150000x magnification), where can be observed the CNT and the Ni coating.

Figure 3. 2 shows EDS analysis of Ni coated MWCNTs. It can be seen that the composition is essentially carbon and nickel. The other elements can result from the manufacturing process of the MWCNTs.

Microstructures of the unreinforced AlSi alloy (123x magnification) and all produced AlSi - CNTs composites are presented in Figure 3. 3 (123x and 5000x magnifications). As expected, the CNTs are placed at the powders/grains interfaces. It can be observed the presence of the CNT agglomerates in all the studied cases.

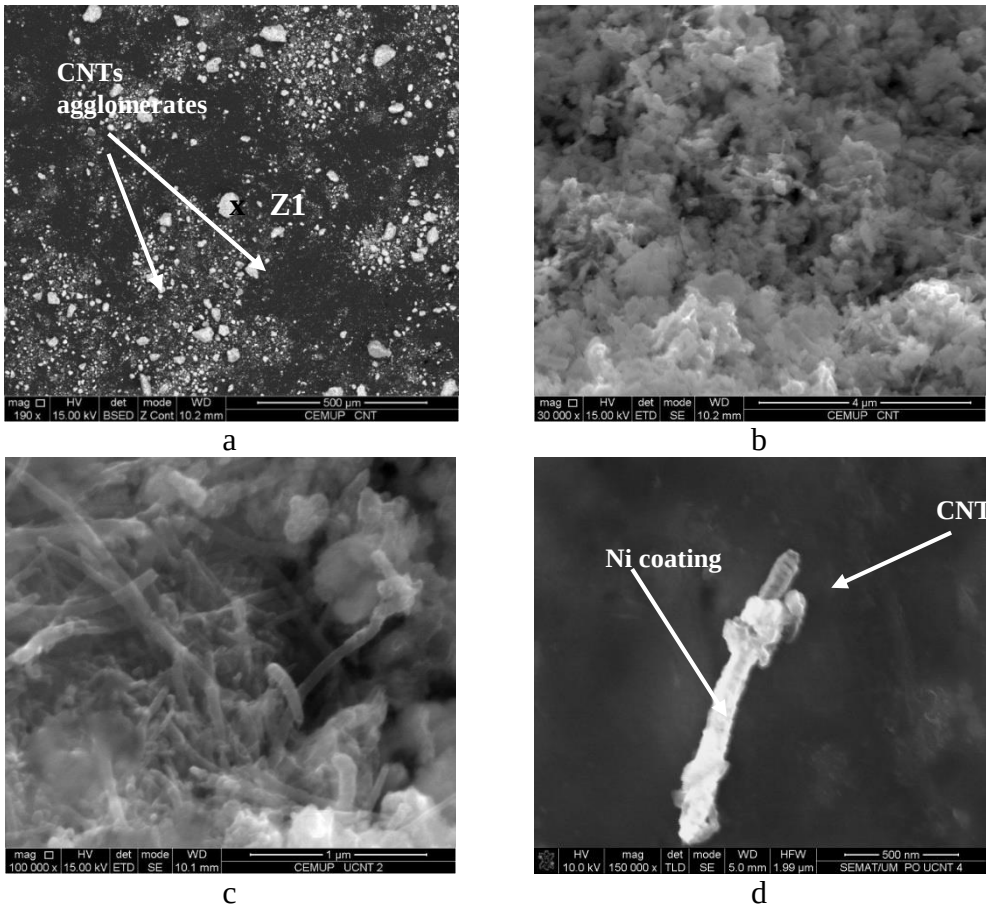

Figure 3. 1 - SEM images showing: a. CNTs (magnification 190x);
b. CNT agglomerate (magnification 30000x); c. CNT agglomerate (magnification 100000x and d. singular CNT (magnification 150000x)

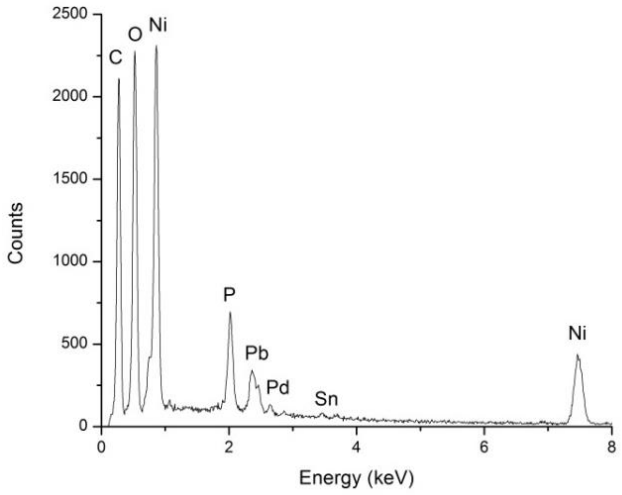

Figure 3. 2 - EDS spectrum of the CNT agglomerates corresponding to zone Z1 (white zone) identified in Figure 3.1-a.

As stated by Zhang [26] the agglomerates are formed due the existence of Van der Waals forces. Due to the nano scale dimensions of CNTs it was expected a better dispersion of the CNTs. This leads to a more isotropic composite material by reducing the stress concentration (the stress is not localized, it is distributed throughout the volume of the composite material) and consequently has a beneficial effect on mechanical properties.

CNTs and CNT agglomerates correspond to the white dots/areas observed Figure 3. 3. Based on a qualitative analysis, it seem that in the case of Process B fewer and smaller agglomerations are formed (Figure 3. 3 b and c) as compared to the other studied processes C, D and E. This means that in the case of Process B there is better distribution of the CNTs in the matrix. A detailed quantification and characterization of CNT agglomerates and dispersion as well as voids quantification is presented elsewhere [27].

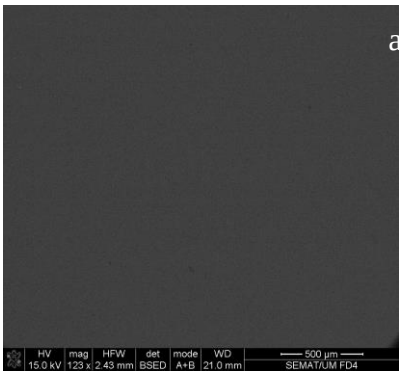

Process A

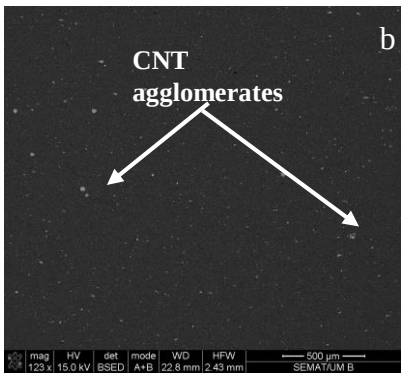

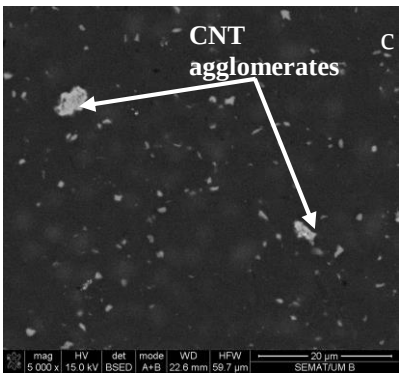

Process B

Figure 3. 3 - SEM images of unreinforced AlSi alloy and AlSi - CNT composites microstructure (cont.)

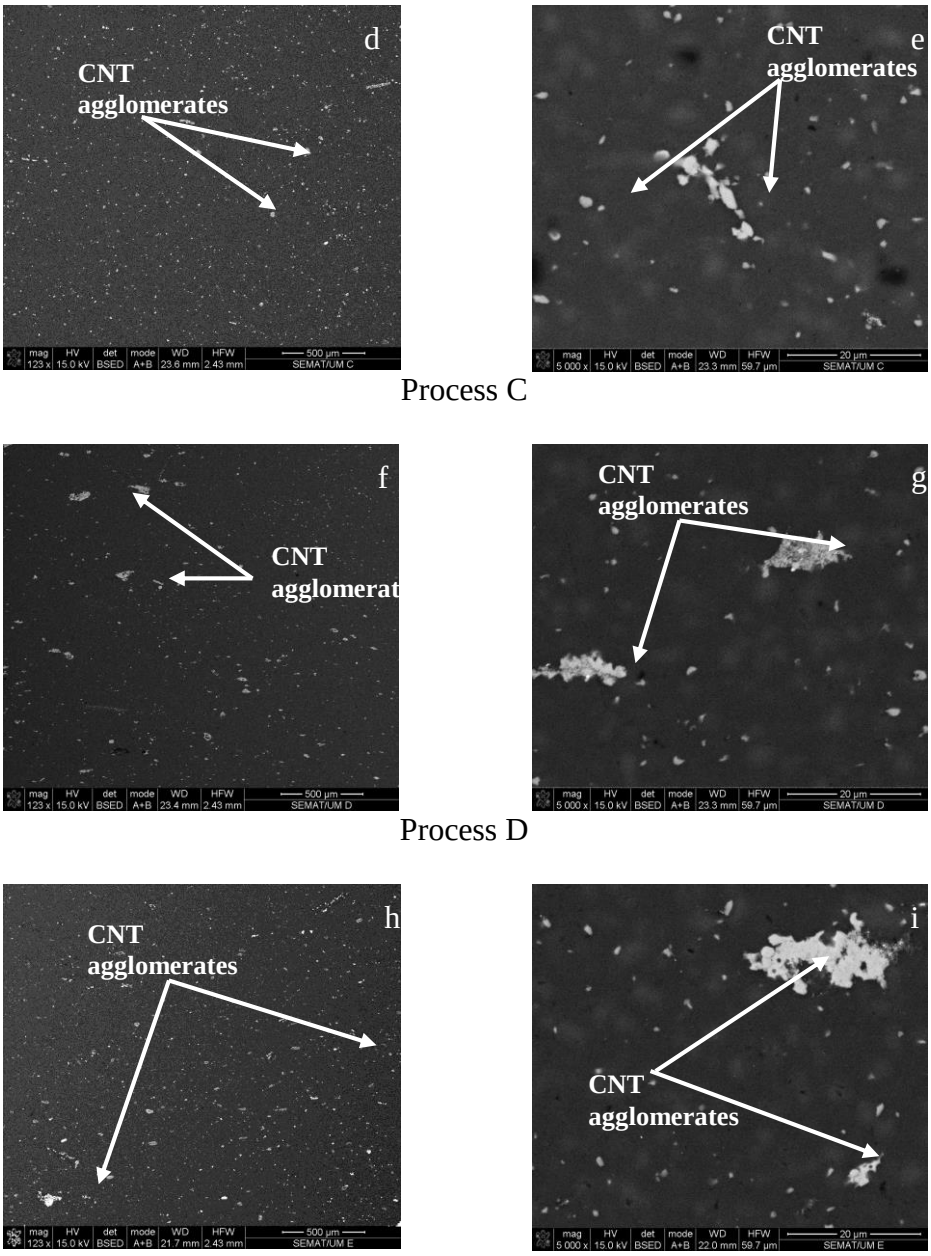

Figure 3. 3 - SEM images of unreinforced AlSi alloy and AlSi - CNT composites microstructure.

3.4.2 Effect of the CNT mixing processing route on mechanical properties

Figure 3. 4 presents the representative stress–strain curves for all studied mixing processes.

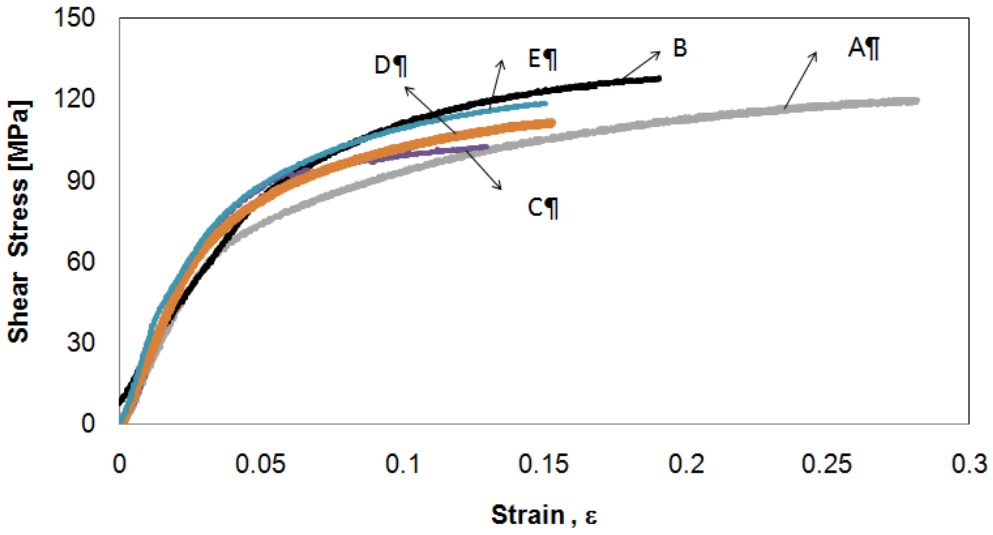

Figure 3. 4 - Stress–strain curves for all studied mixing processes.

Figure 3. 5 shows the shear test results for all studied mixing processes. All studied composites have equal or higher rupture shear (Figure 3. 5-a) and yield shear strength (Figure 3. 5-b) as compared to unreinforced AlSi alloy. Regarding the rupture shear strain there is a substantial decrease for all composites (Figure 3. 5-c) as compared to the unreinforced AlSi alloy.

Regarding the effect of mixing processes on mechanical properties should be highlighted the following: (i) for the same mixing environment (dry mixing) the composites produced with high energy (process C) have lower properties than the ones produced with low energy (process B). This may be explained based on the reduced ability of high energy to disperse the CNTs for the mixing time used (1 minute). However, it has been already proved by several authors [25-29] that a higher mixing time lead to damage and fracture of CNTs; (ii) Regarding the high energy process, if a preliminary mixing step of powders, such as ultrasonic vibration in ethanol was added (compare process C with process E), the dispersion of the CNTs was improved (the rupture strength value in the case of process E is higher than of process C); (iii) if the mechanical mixing of powders was carried out in ethanol solution (process D) instead of in dry conditions (process C) the mechanical properties increased.

If the shear stress results of the present work have to be compared to other results presented in the technical literature (e.g. tensile tests), the rupture shear stress values should be duplicated.

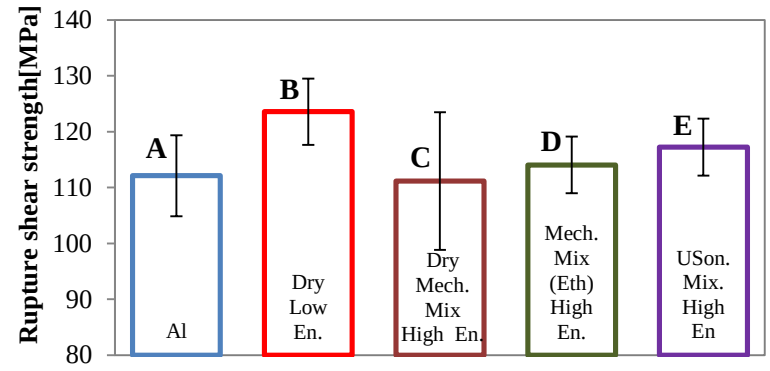

a

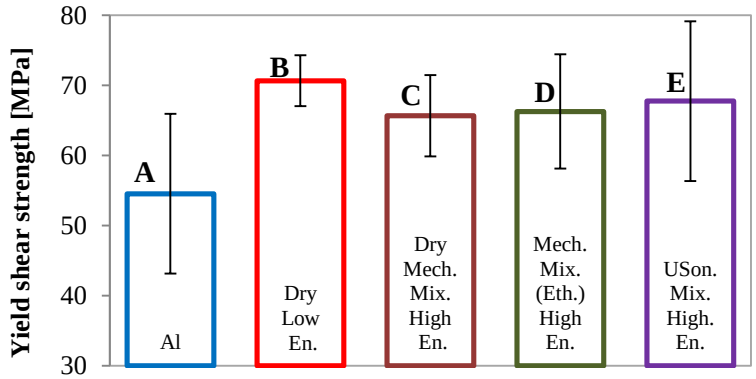

b

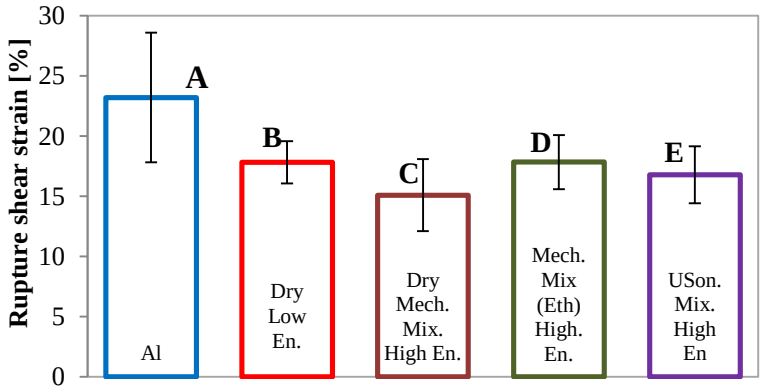

c

Figure 3. 5 - Mechanical properties as obtained on the composites with different mixing processes (A to E on Table 3.2): a. rupture shear strength; b. yield shear strength; c. rupture shear strain.

The ability of the CNTs to improve mechanical properties of Al alloys is well known [13, 28, 29]. As previously mentioned the mixing process is a fundamental step. The low energy mixing process is the most used and studied process because it is simple and has a low cost. The ability of disaggregation mechanisms is essentially based on crushing of agglomerates and on friction ability of spheres to sequentially isolate each fibre from the agglomerate [5, 18]. Concerning the high energy milling mixing process, there are involved two opposing mechanisms: (ii) the improvement of dispersion due to the high velocity [22] and (ii) the degradation of the CNTs due to the high energy involved [25, 30-33].

It can be seen from Figure 3.5 that the mechanical properties did not improve for dry conditions (process C) and slightly improved for the other conditions (processes D and E). Thus, even if some CNTs may be destroyed/damaged during the process, it seems that the improvement in dispersion may compensate it, leading to better mechanical properties in some mixing environments. A longer mixing time, such as 1, 2, and 4 hours were also tested in this work, but there was observed the formation of large particles that does not allow an adequate sintering. This phenomenon of particle growth was also observed by Esawi et al. [5]. It was reported that after 48 hours of mixing, under dry conditions, the CNTs have not suffered any damage. This unexpected result may be due to the lower velocities involved in their mixing process (200 rpm) as compared to the velocities used in the present work, namely 1200 rpm.

It can be observed that the mixing environment used in the case of high energy, has influence on the mechanical properties. As it was previously mentioned, the jar was completely filled with Argon (process C) or with Ethanol (process D). The Ethanol either helps on dispersion of CNTs or reduces the damaging of CNTs. In Figure 3. 5 can be seen that the in the case of process D (Ethanol medium) the properties are slightly higher than in the case of process C (in dry medium-Argon). The slight improvement in the properties may be attributed to the turbulence induced into the liquid medium that may contribute to a better dispersion of CNTs or may be due to the improved damping capacity of the liquid that may reduce the damaging of the CNTs and/or the growth of the powders/granules. To the author's knowledge there are not many studies [24, 34] using this approach. It has been stated that it has potential to improve dispersion of CNTs. There are also studies [7, 8, 11, 18] that used a wet mixing environment, where the powders are only slightly wet in alcohol. Munkhbayar et al. [30, 35] have shown that in the case of a wet mixing environment

(alcohol), there is a reduction on the damaging/breakage of CNTs. It has been proved in another studies [5, 7] that ethanol prevented the growth of the powders/granules. It is worth to mention that the growth of the powders/granules makes the sintering process more difficult [5, 7] and also contributes to a reduction in mechanical properties.

Thus, the effect of wet mixing environment into the jar used in this work may simultaneously contribute to: (i) reduction of damaging of CNTs due to higher damping; (ii) improvement of dispersion of CNTs by improving the turbulence inside the jar, and (iii) reduction on the growth of granules due to lower impact energy. All previous mechanisms would contribute to the improvement of the mechanical properties. This may explain the slightly improvement of mechanical resistance in the case of process D when compared with process C.

Regarding the other high energy approach tested in this work, two dispersion stages were used: (i) a first dispersion stage with an ultrasonic bath (at 42 kHz), (as used for specimens cleaning), along with a mechanical stirrer; (ii) a second dispersion stage, with a high energy milling mixing process. The improvement in mechanical properties is attributed to the better dispersion in the first stage, while the second stage alone does not have any influence (C).

In literature it is not common to see the ultrasonic bath devices, as used in this work, for the dispersion of CNTs. However, horn or wand ultra-sonic devices (≈ 20 kHz) are reported to be very successful in improving the dispersion of CNTs in a liquid phase [1, 21, 36-38] and thus improving the mechanical properties. This has been proved in the case of aluminium composites [6, 10], glass composites [39], and polymer composites [40-43] reinforced by CNTs. Thus, it seems that the previous ultrasonic approach (ultrasonic bath (42 kHz) plus mechanical stirring) was also able to improve the dispersion of CNTs (process E as compared to process C).

The ability of the process to disperse the CNTs, by maintaining their integrity, is the key element to improve mechanical properties. In all studied mixing processes can be observed the existence of CNTs agglomerates (Figure 3. 6). The agglomerates are the reason for mechanical properties deterioration since the agglomerates act as pores/defects [5, 17].

In Figure 3. 6 are presented the SEM micrographs of the fracture surface of the produced unreinforced AlSi alloy (process A) and of all produced composites (processes B,

C, D and E) after the shear tests with two magnifications (150x and 2000x). In Figure 3. 7 are presented the SEM images of the fracture surface of the composite obtained in the case of Process E with a higher magnification (10000x and 50000x magnification). The presence of agglomerates for all the mixing procedures can be noticed. Isolated CNTs and also some small and big agglomerates, located on aluminium powders boundaries, can be observed. This pattern distribution was similar for all the mixing processes. A comprehensive statistical study, quantifying the agglomerates size, for different CNT content, was performed in another study, in order to correlate these factors with the obtained tensile properties of the composite [27]. As previously mentioned less and smaller agglomerates were observed in the case of Process B (Figure 3. 6), while in the case of other processes there are more agglomerates and some of them bigger as compared to Process B (Figure 3. 6).

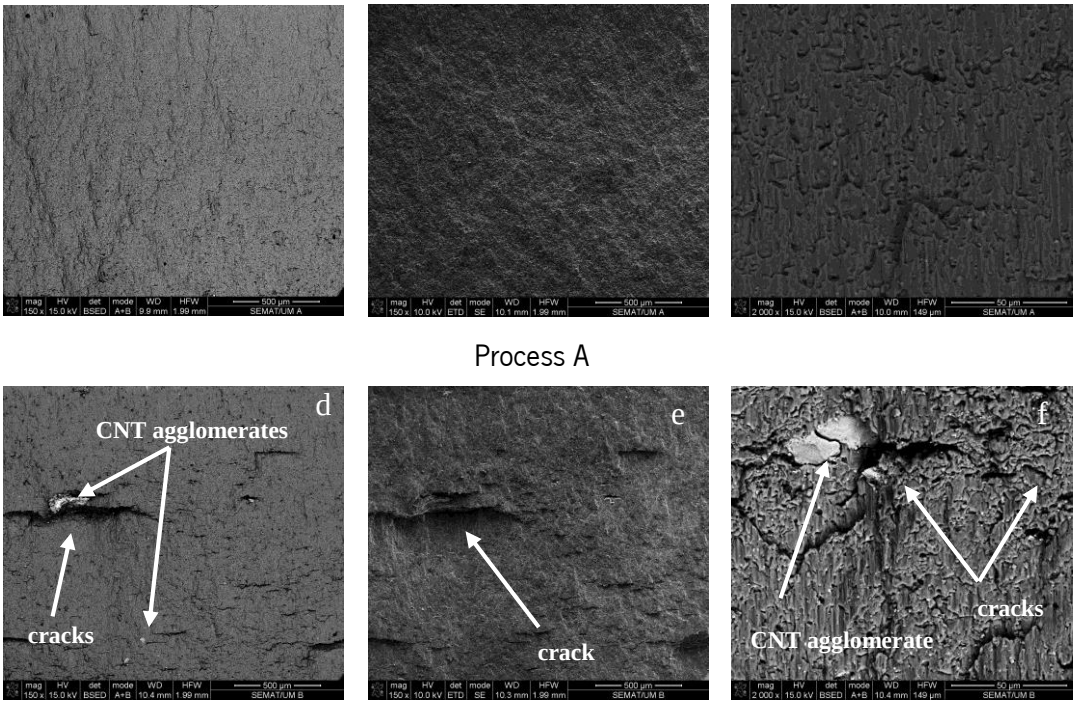

Figure 3. 6 - SEM micrographs of the fracture surface of the composites obtained by different mixing processes (a, d, g, j, n – backscattered images with 150x magnification and c,f,i,l,o – 2000x magnification; and b, e, h, k, m – secondary electron images with 150x magnification).(cont.)

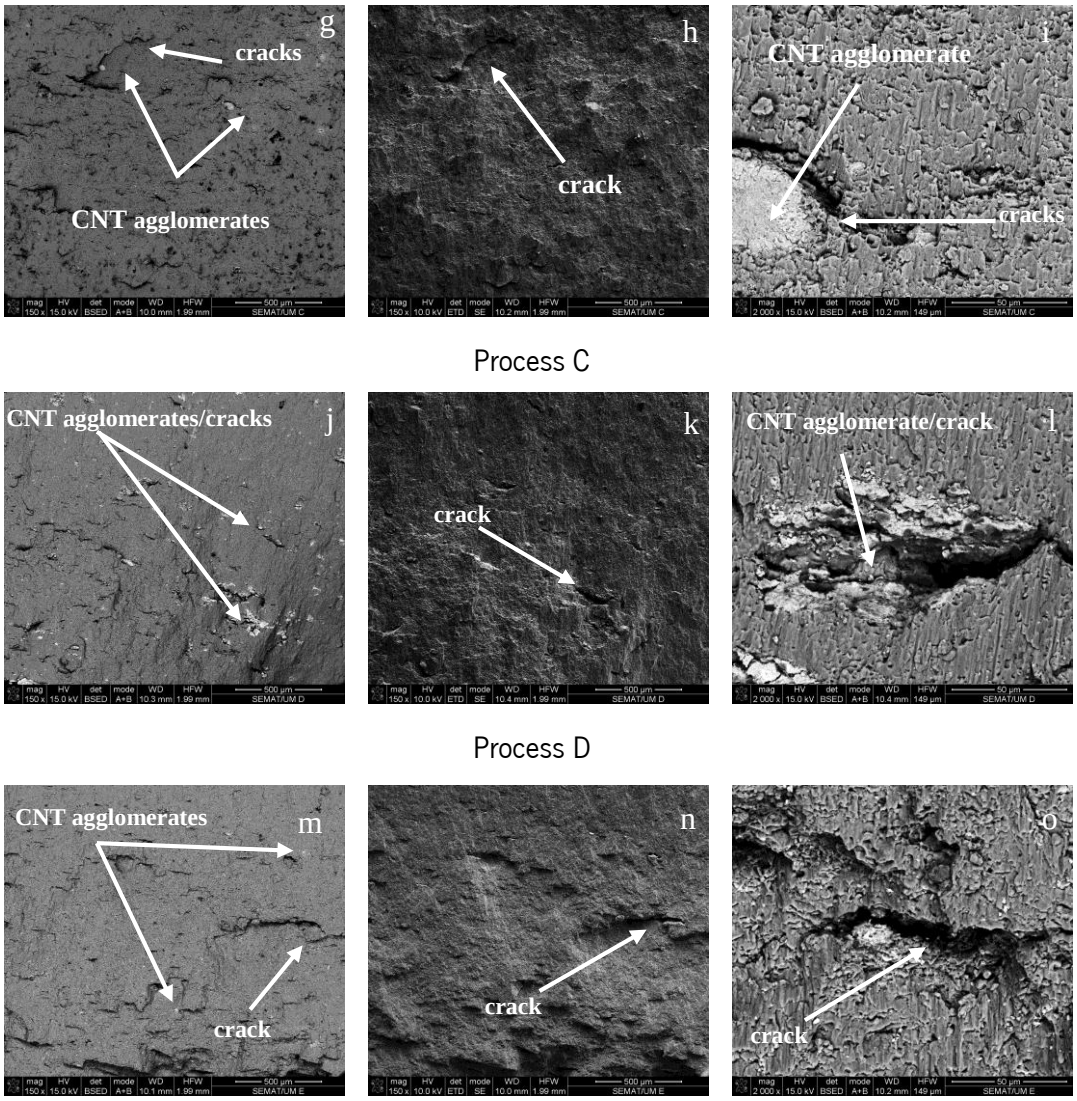

Figure 3. 6 - SEM micrographs of the fracture surface of the composites obtained by different mixing processes (a, d, g, j, n – backscattered images with 150x magnification and c,f,i,l,o – 2000x magnification; and b, e, h, k, m – secondary electron images with 150x magnification).

Regarding the fracture morphology of Process A with different magnifications (Figure 3. 6-a, b and c) can be observed that the surface is very smooth. This is due the fact that the AlSi powders are very well bonded (thus controls the fracture behaviour). Thus, the crack travels through the AlSi grains of the material (intragranular fracture) and it is accompanied by a large amount of plastic deformation.

Regarding the other processes B, C, D and E the fracture behaviour is similar. Cracks may initiate in the regions of agglomerates (stress concentration). If the crack reaches a region where the CNTs are well dispersed it may travel through the AlSi grain

(intragranular fracture), but if the crack reaches zones of weakness (zones where the agglomerates are located, between the AlSi grains), then the crack follows the grain of the material (intergranular fracture). The consequence of this is a rougher region where the agglomerates are formed and a smoother surface when the crack travels through the AlSi powder/grain. The propagation of the crack is accelerated for processes C, D and E because there are zones with bigger agglomerates, as can be observed in Figure 3. 6.

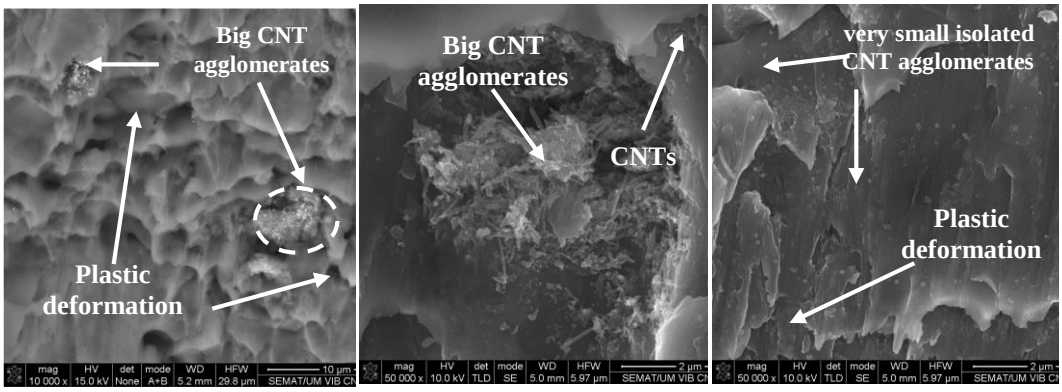

a b c

Figure 3. 7 - SEM micrograph of the fracture surface of the composite obtained by Process E; b. local magnification of zone indicated in a) with dashed line and c. very small isolated CNT agglomerates

These observations are in accordance with the mechanical properties previously presented. Even though there are these zones that behaves like stress concentrations (as called weakness zones), the strengthening effect of CNTs in the zones where the CNTs are well dispersed prevails, thus the mechanical properties of the Process B are higher than the other processes. Thus, the increase in rupture shear (Figure 3. 5-a) and yield shear strength (Figure 3. 5-b) with the addition of the CNTs for all processes studied as compared to Process A is related to the fact that the AlSi powders/grains are bonded with an improved strength due to CNTs interface reinforcement effect, as stated for example by George et al. [44] through the shear lag theory. It is well known that the mechanical properties of the composites are controlled by stress transfer between reinforcement phase and the metal matrix at the interface [45], so the CNTs act like load-bearing element, thus there is a transfer of load from the matrix to the reinforcement by interfacial shear stress does increasing the tensile and yield strength [44, 46, 47].

The increase in the rupture shear strength with the addition of the reinforcement is related to the fact the AlSi grains are bonded with an improved strength in direction of the load, due to CNTs interface reinforcement effect (Figure 3. 7) (shear lag theory). The CNTs act like load-bearing element, thus they protect the matrix (transfer of load from the matrix to the reinforcement by interfacial shear stress), while the CNT agglomerates behave like stress concentrations. In Figure 3. 7 can be observed some isolated CNTs, that may indicates that the CNTs were pulled out from the matrix. It can be seen from Figure 3. 7 that most of these isolated CNTs are oriented in the load direction. It is possible that pull out mechanism occurs due the interfacial de-bonding between the CNT and Al matrix, which leads to a subsequent sliding of the CNTs, orienting these in the load direction.

Based on the previous considerations, the proposed physical mechanism for the fracture surface morphology for shear tests of AlSi-CNTs composites is schematically represented in Figure 3. 8.

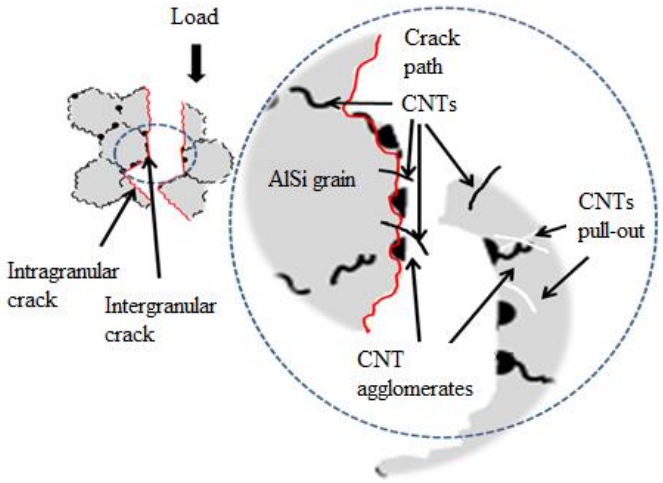

Figure 3. 8 - Schematic representation of the proposed physical model for the shear tests.

In addition to direct strengthening (shear lag), a secondary strengthening (thermal mismatch) can occur due to differential thermal contraction between matrix and reinforcement [48] during cooling from sintering temperature which leads to creation of residual stresses. Another secondary strengthening is the presence of Orowan loops. The high number of volume-fractioned precipitates will effectively inhibit the movement of dislocations, generate more geometrically necessary dislocations and reach the critical dislocation density for fracture earlier during deformation, and thus increase the strength

and decrease the elongation. The nano size of CNTs increases the Orowan strengthening of the grain frontiers [49].

Based on obtained results some considerations may be suggested for futures research/testing:

(i) The high energy process does not seem to bring advantages as compared to the low energy process, at least for one minute test duration. An increase in the mixing time would improve the dispersion but it could also deteriorate the CNTs and increase the grain size [30-32]. In addition, for industrial purposes this is an expensive process. Since the friction among liquid and CNTs may help on dispersion of CNTs a more viscous liquid could be tested.

(ii) The addition of a preliminary ultrasonic mixing in ethanol to the high energy mixing process, does not seem to bring such advantages to overcome the costs associated with the process.

(iii) Processing the mechanical mixing in ethanol instead of in dry condition does not bring substantial advantages to the material although properties are slightly higher than those in dry condition.

(iv) The low energy mixing process seems to be interesting because it is simple, cheap and provide better results. However, the improvement in mechanical properties is still far from what is expected, based on excellent mechanical properties and cost of CNTs. Thus, an agent that would be able to further disperse the CNT agglomerates, such as rubber, cork, or any other material that would have higher friction forces between balls and CNTs would eventually be an advantage on the low energy process. Some experiments have been already carried out [15, 43, 44] and they seem to be promising routes to help on dispersion of CNTs. It should be highlighted that this agent, if necessary, can be easily removed from the obtained mixed composite, before sintering stage.

3.4.3 Reactivity between CNTs and Matrix

Another important aspect is the eventual reactivity between an industrial material acting as a matrix (AlSi alloy) and CNTs. This aspect is still ambiguous in technical literature. Deng et al. [6] reported that in the case of pure aluminium, the reaction between CNTs with

Al matrix has a degradation effect on the composite, while Ci et al. [14] mentioned that it may have a beneficial effect. However, when Al alloys (e.g. AlSi alloy) are used as matrix, several reactions would eventually take place. Undesirable reactions between the reinforcement (in the present case CNTs) and matrix elements should be avoided. These reactions may deteriorate the CNTs or create eventual unwanted interfaces. The Ni coating seems to work perfectly with AlSi alloys.

Figure 3. 9 presents the DSC curves for the unreinforced AlSi alloy and AlSi-CNT composites obtained by processes C and D. It can be seen that no reactions (exothermic and/or endothermic peaks) were detected for any situation. The only endothermic peaks are observed due to melting of the matrix. This means that no degradation of the MWCNTs takes place during the sintering stage (until a temperature of 550 ±2 °C). Thus, it is acceptable that in the case of Ni coated CNTs, the Ni coating protects the CNTs [50]. It can also be seen on fig. 8 that above the working sintering temperature the thermal analysis curves present some differences between the unreinforced AlSi alloy and AlSi-CNT composites. The CNTs seem to reduce the melting temperature from 578°C to approximately 568°C. There is a study that reported [50] that by adding CNTs to Al2024 increased the melting temperature of the composite due to reduction of surfaces of Al2024 particles when CNTs are introduced which becomes more difficult the melting of aluminium alloy powders. In the present case, the opposite was observed. This means that some diffusion of Ni to Al may occur (Ni lowers the melting temperature of Al) and there is no diffusion or reaction between C and Al (C increases the melting temperature of Al). Thus even at the aluminium melting temperature it seems that no reaction between C and Al occurs and thus the shielding effect of Ni coating seems to be very effective.

It has been shown by several authors [4, 7] that by using pure aluminium matrix and similar processing conditions (the mechanical alloying as mixing process, equal quantity of CNTs and similar sintering conditions) there is reactivity between carbon and aluminium, leading to formation of Al_4C. In this work, as has been previously mentioned, this reaction did not happen probably due to several factors such as, the non existence of amorphous carbon, to effectiveness of nickel coating of CNTs or to short sintering times. It has been reported in other studies [6, 10] on aluminium alloys containing silicon that the reaction between aluminium and carbon should occur at temperatures higher than the sintering

temperature used in this work. Thus this could be another explanation for the non formation of Al_4C in the present study.

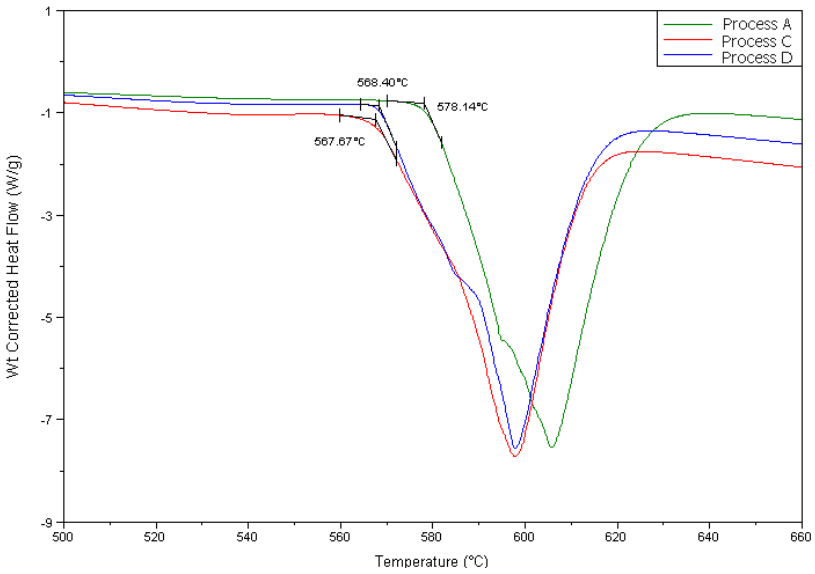

Figure 3. 9 - DSC curves obtained for samples with and without CNTs.

As the AlSi matrix contains silicon, reactions between silicon and carbon could occur, leading to the formation of SiC. It has been reported [16, 17, 51] that this reaction may increase the wetability between matrix and CNTs. The DSC results (Figure 3. 9) did not indicate the occurrence of this reaction. Another possible reaction would be between Silicon and Nickel [52-56]. At temperatures up to 300° C the formation of Ni_2Si is possible [53, 56]. Around 300°C there is a possible formation of NiSi [53, 56]. This last compound could lead, at higher temperatures (750°C) [53, 54], to the formation of $NiSi_2$. In the present study none of these reactions were detected by DSC analysis (Figure 3. 9). Qian et al. [57] reported that reactions between Aluminium and Nickel may lead to formation of Al_3Ni at temperatures lower than the temperatures used in sintering in this work. Also in this case, the DSC results did not indicate the occurrence of this reaction. The formation of this phase could be beneficial in order to improve the bonding between the CNTs and the AlSi matrix increasing the reinforcement strengthening effect.

Thus, no reactions between Ni coated CNTs and AlSi matrix occurred[1]. There occurred only some diffusion of Ni into the matrix, which caused a decrease on the melting temperature. Thus, concerning reactivity, this pair of materials (AlSi alloy and CNTs) seems to be adequate for the production of composites.

3.5 Conclusions

From the present investigation the following conclusions can be drawn:

- Ni coated CNTs improved the mechanical properties of AlSi alloys;

- The mechanical properties of the composites are dependent on the mixing process;

- CNT agglomerates were found in all mixing procedures;

- The low energy mixing process is to be more effective on dispersion of CNTs than the high energy processes;

- A preliminary ultrasonic mixing step improved the dispersion of CNTs;

- A wet environment (ethanol) during the mixing slightly improved the dispersion of CNTs;

- The presence of Ni coating on CNTs prevents the reactions between the CNTs and AlSi matrix;

- The combination of different mixing processes improved the dispersion of CNTs.

3.6 Acknowledgements

This work was supported by the Portuguese *Foundation* of *Science and Technology* through the project references PTDC/EME-PME/68664/2006 and EXCL/EMS-TEC/0460/2012.

3.7 References

[1] X. Lu, Z. Hu. 2012. Mechanical property evaluation of single-walled carbon nanotubes by finite element modeling, Compos. Part B-Eng. 43: 1902-1913.

[1]The term "occurred" should be replaced by "not detected". A more detailed study about reactivity between Ni coated MWCNT and AlSi matrix can be found on Chapter 10.

[2] M.D. Ganji, A. Fereidoon, M. Jahanshahi, M.G. Ahangari. 2012. Investigation of the Mechanical Properties of Multi-Walled Carbon Nanotubes Using Density Functional Theory Calculations. J. Comput. Theor. Nanos. 9: 980-985.
[3] M.J. O'Connell. 2006. Carbon nanotubes: properties and applications. CRC press Taylor & Francis Group.
[4] Y.Y. Huang, E.M. Terentjev. 2012. Dispersion of carbon nanotubes: mixing, sonication, stabilization, and composite properties. Polymers, 4: 275-295.
[5] A. Esawi, K. Morsi. 2007. Dispersion of carbon nanotubes (CNTs) in aluminum powder, Compos Part A-Appl S. 38: 646-650.
[6] C. Deng, X. Zhang, D. Wang, Q. Lin, A. Li. 2007. Preparation and characterization of carbon nanotubes/aluminum matrix composites. Mater. Lett., 61: 1725-1728.
[7] R. Perez-Bustamante, C.D. Gomez-Esparz, I. Estrada-Guel, M. Miki-Yoshida, L. Licea-Jimenez, et al. 2009. Microstructural and mechanical characterization of Al-MWCNT composites produced by mechanical milling. Mater. Sci. Eng. A., 502: 159-163.
[8] A.M.K. Esawi, K. Morsi, A. Sayed, A.A. Gawad, P. Borah. 2009. Fabrication and properties of dispersed carbon nanotube-aluminum composites. Mater. Sci. Eng. A, 508: 167-173.
[9] S. El-Eskandarany. 2013. Mechanical Alloying: For Fabrication of Advanced Engineering Materials. Elsevier Science.
[10] C.F. Deng, D.Z. Wang, X.X. Zhang, A.B. Li. 2007. Processing and properties of carbon nanotubes reinforced aluminum composites, Mater. Sci. Eng. A. 444: 138-145.
[11] R. Perez-Bustamante, I. Estrada-Guel, W. Antunez-Flores, M. Miki-Yoshida, P.J. Ferreira, R. Martinez-Sanchez. 2008. Novel Al-matrix nanocomposites reinforced with multi-walled carbon nanotubes, J. Alloys Compd. 450: 323-326.
[12] K.G. Dassios. 2014. Carbon nanotube-reinforced ceramic matrix composites: processing and properties. Ceram. Trans., 248 DOI: 10.1002/9781118932995.ch15.
[13] S.R. Bakshi, A. Agarwal. 2011. An analysis of the factors affecting strengthening in carbon nanotube reinforced aluminum composites, Carbon. 49: 533-544.
[14] L. Ci, Z. Ryu, N.Y. Jin-Phillipp, M. Ruehle. 2006. Investigation of the interfacial reaction between multi-walled carbon nanotubes and aluminum, Acta Mater. 54: 5367-5375.
[15] H. Kwon, M. Estili, K. Takagi, T. Miyazaki, A. Kawasaki. 2009. Combination of hot extrusion and spark plasma sintering for producing carbon nanotube reinforced aluminum matrix composites, Carbon. 47: 570-577.
[16] T. Laha, S. Kuchibhatla, S. Seal, W. Li, A. Agarwal. 2007. Interfacial phenomena in thermally sprayed multiwalled carbon nanotube reinforced aluminum nanocomposite, Acta Mater 55: 1059-66.
[17] T. Laha, Y. Chen, D. Lahiri, A. Agarwal. 2009. Tensile properties of carbon nanotube reinforced aluminum nanocomposite fabricated by plasma spray forming, Composites Part A. 40: 589-594.
[18] K. Morsi, A. Esawi. 2007. Effect of mechanical alloying time and carbon nanotube (CNT) content on the evolution of aluminum (Al)–CNT composite powders, J. Mater. Sci. 42: 4954-4959.
[19] K.S. Munir, P. Kingshott, C. Wen. 2014. Carbon Nanotube Reinforced Titanium Metal Matrix Composites Prepared by Powder Metallurgy––A Review, Crit. Rev. Solid State Mater. Sci., DOI: 10.1080/10408436.2014.929521, 1-18.
[20] C.D. Li, X.J. Wang, K. Wu, W.Q. Liu, S.L. Xiang, C. Ding, X.S. Hu, M.Y. Zheng. 2014. Distribution and integrity of carbon nanotubes in carbon nanotube/magnesium composites. J. Alloys Compd. 612: 330-336.

[21] T. Premkumar, R. Mezzenga, K.E. Geckeler. 2012. Carbon nanotubes in the liquid phase: addressing the issue of dispersion, Small, 8: 1299-1313.
[22] J.S. Oh, K.H. Ahn, J.S. Hong. 2010. Dispersion of entangled carbon nanotube by melt extrusion, Korea-Aust. Rheol. J. 22: 89-94.
[23] W. Salas, N.G. Alba-Baena, L.E. Murr. 2007. Explosive shock-wave consolidation of aluminum powder/carbon nanotube aggregate mixtures: optical and electron metallography. Metall. Mater. Trans. A 38 () 2928-2935.
[24] T. Peng, I. Chang. 2014. Mechanical alloying of multi-walled carbon nanotubes reinforced aluminum composite powder. Powder Technol. 266: 7-15.
[25] Z.D. Tao, H.R. Geng, K. Yu, Z.X. Yang, Y.Z. Wang. 2004. Effects of high-energy ball milling on the morphology and the field emission property of multi-walled carbon nanotubes. Mater. Lett. 58: 3410-3413.
[26] Q. Zhang. 2012. Carbon nanotubes and their applications. RC Press, Taylor & Francis Group, ed.
[27] O. Carvalho, G. Miranda, D. Soares, F.S. Silva. 2014. Carbon nanotube dispersion in aluminum matrix composites – quantification and influence on strength, Accepted to Mech. Adv. Mat. Struct. DOI: 10.1080/15376494.2014.929766.
[28] S.R. Bakshi, D. Lahiri, A. Agarwal. 2010. Carbon nanotube reinforced metal matrix composites - a review, Int. Mater. Rev. 55: 41-64.
[29] C. M. Efraín. 2009. Carbon Nanotube-Metal Matrix Composites. In Dekker Encyclopedia of Nanoscience and Nanotechnology, Second Edition, null:611-619: Taylor & Francis, 611-619.
[30] B. Munkhbayar, M. Nine, J. Jeoun, M. Bat-Erdene, H. Chung, H. Jeong. 2013. Influence of dry and wet ball milling on dispersion characteristics of the multi-walled carbon nanotubes in aqueous solution with and without surfactant, Powder Technol. 234: 132-140.
[31] N. Al-Aqeeli, K. Abdullahi, C. Suryanarayana, T. Laoui, S. Nouari. 2013. Structure of mechanically milled CNT-reinforced Al-alloy nanocomposites. Mater. Manuf. Processes. 28: 984-990.
[32] Z.Y. Liu, S.J. Xu, B.L. Xiao, P. Xue, W.G. Wang, Z.Y. Ma. 2012. Effect of ball-milling time on mechanical properties of carbon nanotubes reinforced aluminum matrix composites. Compos Part A-Appl S. 43: 2161-2168.
[33] Y.B. Li, B.Q. Wei, J. Liang, Q. Yu, D.H. Wu. 1999. Transformation of carbon nanotubes to nanoparticles by ball milling process. Carbon. 37: 493-497.
[34] S. Yoshio, J. Tatami, T. Yamakawa, T. Wakihara, K. Komeya. 2011. Dispersion of carbon nanotubes in ethanol by a bead milling process. Carbon. 49: 4131-4137.
[35] B. Munkhbayar, M.J. Nine, S. Hwang, J. Kim, K. Bae. 2012. Effect of grinding speed changes on dispersibility of the treated multi-walled carbon nanotubes in aqueous solution and its thermal characteristic. Chem. Eng. Process. 61: 36-41.
[36] K.S. Park, J.R. Youn. 2012. Dispersion and aspect ratio of carbon nanotubes in aqueous suspension and their relationship with electrical resistivity of carbon nanotube filled polymer composites. Carbon 50: 2322-2330.
[37] G. Pagani, M.J. Green, P. Poulin, M. Pasquali. 2012. Competing mechanisms and scaling laws for carbon nanotube scission by ultrasonication. Proc Natl Acad Sci. 109: 11599-604
[38] A. Lucas, C. Zakri, M. Maugey, M. Schoo Pvd Pasquali, P. Poulin. 2009. Kinetics of nanotube and microfiber scission under sonication. J. Phys. Chem. C. 113: 20599-20605.

[39] J.W. Ning, J.J. Zhang, Y.B. Pan, J.K. Guo. 2003. Fabrication and mechanical properties of SiO2 matrix composites reinforced by carbon nanotube, Mater. Sci. Eng. A. 357: 392-396.
[40] B. Safadi, R. Andrews, E.A Grulke. 2002. Multiwalled carbon nanotube polymer composites: Synthesis and characterization of thin films. J. Appl. Polym. Sci. 84: 660-2669.
[41] R.A. Graff, J.P. Swanson, P.W. Barone, S. Baik, D.A. Heller, M.S. Strano. 2005. Achieving Individual Nanotube Dispersion at High Loading in Single Walled Carbon Nanotube Composites. Adv. Mater. 17: 980-984.
[42] T.R. Frømyr, F.K. Hansen, T. Olsen. 2012. The Optimum Dispersion of Carbon Nanotubes for Epoxy Nanocomposites: Evolution of the Particle Size Distribution by Ultrasonic Treatment. Nanotechnology, 2012: 1-14.
[43] A. Ilcham, A. Srisurichan, A. Soottitantawat, T. Charinpanitkul. 2009. Dispersion of multi-walled carbon nanotubes in poly(p-phenylene) thin films and their electrical characteristics. Particuology, 7: 403-407.
[44] R. George, K.T. Kashyap, R. Rahul, S. Yamdagni. 2005. Strengthening in carbon nanotube/aluminium (CNT/Al) composites. Scripta Mater. 53: 1159–1163
[45] H.J. Ryu, S.I. Cha, S.H. Hong. 2003. Generalized shear-lag model for load transfer in SiC/Al metal-matrix composites. J. Mater. Res. 18: 2851-2858.
[46] S.J. Yoo, S.H. Han, W.J. Kim. 2013. Strength and strain hardening of aluminum matrix composites with randomly dispersed nanometer-length fragmented carbon nanotubes. Scripta Mater. 68:711–714.
[47] H.J. Ryu, S.I. Cha, S.H. Hong. 2003. Generalized shear-lag model for load transfer in SiC/Al metal-matrix composites. J. Mater. Res. 18: 2851-2858.
[48] R.J. Arsenault, N. Shi. 1986. Dislocation generation due to differences between the coefficients of thermal expansion. Materials Science and Engineering 81: 175-178.
[49] Z. Zhang, D.L. Chen. 2006. Consideration of Orowan strengthening effect in particulate-reinforced metal matrix nanocomposites: A model for predicting their yield strength. Scripta Mater. 54: 1321–1326.
[50] C.F. Deng, X.X. Zhang, D.Z. Wang, Y.X. Ma. 2007. Calorimetric study of carbon nanotubes and aluminum. Mater. Lett., 61: 3221-3223.
[51] S.R. Bakshi, R.R. Patel, A. Agarwal. 2010. Thermal conductivity of carbon nanotube reinforced aluminum composites: A multi-scale study using object oriented finite element method. Comp. Mater. Sci., 50: 419-428.
[52] E.G. Colgan, M. Mäenpää, M. Finetti, M.A. Nicolet. 1983. Electrical characteristics of thin Ni2Si, NiSi, and NiSi2 layers grown on silicon. J. Electron. Mater. 12: 413-422.
[53] J. Foggiato, W.S. Yoo, M. Ouaknine, T. Murakami, T. Fukada. 2004. Optimizing the formation of nickel silicide. Mater. Sci. Eng. B.,114 : 56-60.
[54] F.F. Zhao, J.Z. Zheng, Z.X. Shen, T. Osipowicz, W.Z. Gao, L.H. Chan. 2004. Thermal stability study of NiSi and NiSi2 thin films. Microelectron. Microelectron. Eng. 71: 104-111.
[55] D.C. Dunand. 1994. NiAl formation by annealing of infiltrated aluminium-nickel precursors. J. Mater. Sci, 29: 4056-4060.
[56] H. Okamoto. 1993. Al-Ni (aluminum-nickel). J Phase Equil, 14: 257-259.
[57] Qian, J. Li, J. Xiong, F. Zhang, X.Lin. 2012. In situ synthesizing Al3Ni for fabrication of intermetallic-reinforced aluminum alloy composites by friction stir processing. Mater. Sci. Eng. A. 550: 279-285.

4 Carbon nanotube dispersion in aluminum matrix composites – quantification and influence on strength

O. Carvalho, G. Miranda, D. Soares and F.S. Silva

University of Minho, Azurém, 4800-058 Guimarães, Portugal

Published in Mechanics of Advanced Materials and Structures, 10 Sep 2014
DOI 10.1080/15376494.2014.929766

4.1 Abstract

CNT incorporation in metal matrix composites is hampered by the development of attractive van der Waals forces, which lead to the formation of CNT agglomerates. Therefore, a detailed quantification and characterization of CNT agglomerates and consequently CNT dispersion can enlighten their influence in composites strength. This work presents a comprehensive study, quantifying agglomerates by size, for three different composites (2, 4 and 6 CNT vol. %), made with an aluminium-silicon matrix by a powder metallurgy route. From the obtained experimental data, an empirical model that attempts to predict the tensile strength of these composites from CNT agglomerates analysis is presented.

Keywords: Carbon nanotube (CNT), dispersion, aluminium alloys, powder metallurgy, tensile strength.

4.2 Introduction

Carbon nanotubes exceptional mechanical properties [1, 2], extremely low thermal expansion and high thermal conductivity [3], are leading to the development of new CNT-reinforced composites, using polymeric [4, 5], metal [6-17] or ceramic [18] matrices. Concerning metal matrix composites (MMC), both single-walled carbon nanotubes (SWCNTs) and multi-walled carbon nanotubes (MWCNT) are being used as reinforcements, mainly in aluminium alloys [6-10], but also in titanium [11], copper [12-16] and magnesium

alloys [17].This way, CNT excellent mechanical properties combined with their low density make them suitable as reinforcement in aluminium composites.

The main challenge concerning the production of CNT-reinforced metal matrix composites is to disperse nanotubes in the matrix and thus obtain a homogenous distribution. Attractive van der Waals forces between nanotubes lead to nanotube agglomeration, hampering the enhancement of the composite mechanical properties by incorporating CNTs [19, 20]. Additionally, when using powder metallurgy (PM), as the matrix powder average size is usually much larger than that of CNTs, it is difficult to achieve their homogeneous distribution in the composite [8]. Therefore, disperse CNTs in metal matrix composites using PM processing routes is not a fully accomplished task, especially for the most widely used CNTs mixing techniques, namely ball milling [2,7,8, 12, 23-26]. In this technique, matrix metal powders and nanotubes are placed in stainless steel jars containing stainless steel spheres. Normally the jars are filled with argon to avoid the oxidation of metal powders and then agitated with a certain rotation speed, using a mechanic system.

Some processing techniques have demonstrated to be able to take a significant advantage of CNTs by substantially increasing composite properties. C. N. He et al., [19] obtained a 184% improvement in ultimate tensile strength, when compared with base material, with an addition of 5 wt. % CNTs. The composite was produced by using the chemical vapour deposition (CVD) technique. These CNTs were produced in situ, in aluminium powder, achieving, this way, a good dispersion. In order to compare these results with those obtained by a traditional route of mixing aluminium powders with CNTs, the same authors also produced specimens by ball-milling CNTs in the aluminium alloy powder. They verified that the improvement in ultimate tensile strength was 52% [19]. C. N. He et al., in another work [27] and using the same CVD process to produce aluminium CNTs composites, tried different amounts of carbon nanotubes (1.5; 3.5; 5 and 6.5 wt. %) and verified that the 5 wt. % samples presented the best mechanical properties (tensile strength and young modulus). Although effective at laboratory level, the CVD processing technique [19, 27] does not seem suitable for large-scale production. The most capable techniques for large-scale industrial implementation are still based on mechanical mixture of CNTs to metal powders following PM processing routes already used in industries. Hence efforts should be allocated in optimizing this process in order to achieve a homogeneous CNTs dispersion.

There are some studies concerning the dispersion of carbon nanotubes in aluminium nanocomposites that go beyond simple qualitative methods to quantify dispersion, such as visual observation of micrographs images. In Yazdanbakhsh A. et al. [28] work, dispersion is measured based on the amount of work required to translate inclusions so they form the state of maximum uniformity, quantifying dispersion with a single parameter, but not correlating dispersion with mechanical properties. Bakshi S. R.et. al. [29] quantify the quality of nanotubes distribution using two different parameters, based on image analysis technique. Although these authors correlate CNT distribution to elastic modulus, this correlation is only presented for one CNT volume fraction (0.6 vol. %) and the elastic modulus measurements of are made by nanoindentation, giving this way a local mechanical property and not an overall mechanical property of the composite material. Yazdanbakhsh A. et al. and Bakshi S. R. et. al. methods where developed to quantify dispersion of carbon nanotubes in Al coatings.

This work attempts to understand how CNT volume fraction influences the formation of agglomerates (number and size) and establish a correlation between these factors and the overall mechanical properties of the produced composites (obtained with standard testing techniques). Based on the obtained experimental data, an empirical model that intends to predict the ultimate tensile strength as a function of CNTs vol.% in the composite is presented.

4.3 Experimental procedure

4.3.1 Fabrication of CNT-reinforced Al-Si composites

Aluminium Silicon powder (Al-Si 88-12 wt. %, 99% pure - 325 mesh) purchased from AlfaAesar - Germany, and Multi-Wall Carbon Nanotubes (MWCNTs) Nickel coated, grown by CCVD, from CheapTubes.com - USA, were used to produce Al-Si based nanocomposites. Al-Si powder had a measured average particle diameter of 8 μm, while the MWCNT had a length between 0.5 and 2.0 μm and a diameter higher than 50 nm (information given by the supplier).

Powder metallurgy technique was used to obtain three types of composites, with different MWCNT additions: 2, 4 and 6 wt. %. Unreinforced samples (Al-Si 88-12 wt. %) were also produced by the same PM technique, for comparison purposes.

Al-Si powders and MWCNTs mixture was made inside a closed stainless steel jar, together with 12 steel milling balls with 10 mm diameter, presenting a ball-to-powder weight ratio of 10:1. The jar was placed in a rotation device and the mixing was made with a constant rotation speed of 40 rpm, during 6 days (low-energy ball milling).

Afterwards the Al-Si/MWCNT mixture was introduced in a rectangular profile graphite die (Figure 4. 1-a) and slightly compacted. The die was then placed in a vacuum chamber (Figure 4. 1b), where it was heated until 550°C.

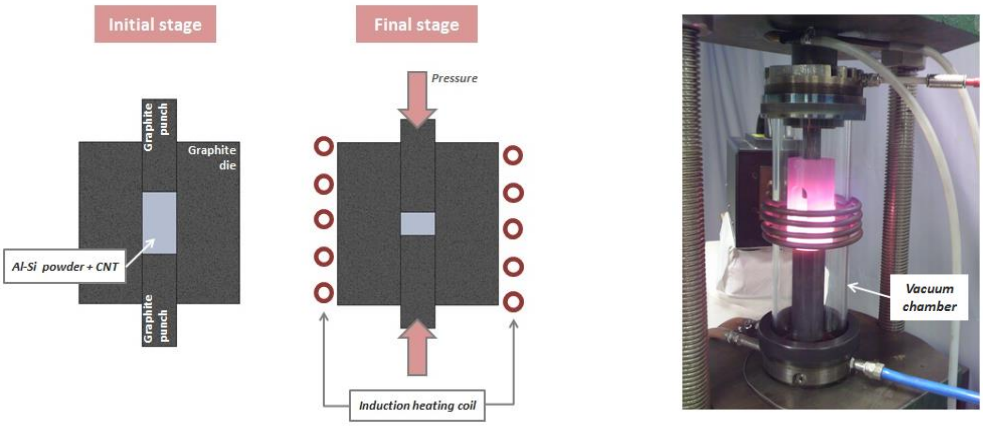

a b

Figure 4. 1 - Hot pressing (a) schematic representation and (b) vacuum chamber detail.

The samples were produced applying uniaxial load pressure of 35 MPa and a temperature of 550 °C during 10 minutes (hot pressing). The obtained samples had average dimensions of 44 x 3.4 x 6 mm.

4.3.2 Characterization techniques and image analysis

The produced composites were characterized regarding the distribution of MWCNT in the matrix, especially concerning the presence of agglomerates, by means of Scanning Electron Microscopy (SEM), in backscattered view. Figure 4. 2 shows the presence of agglomerates due to the fact that the CNT's are nickel coated and easily observed in backscattered view (CNTs white colour comes from the nickel coating). Table 4. 1 presents

the chemical composition of the white areas, observed in Figure 4. 2, showing that the white areas are CNT's. This fact allows an easy agglomerates size observation and quantification. Without the nickel coating, CNTs observation with these lower amplifications was not possible.

The obtained images were then processed, applying a threshold filter in order to further highlight the agglomerates (Figure 4. 3-b) and be able to count and measure them, as described in Figure 4. 4.

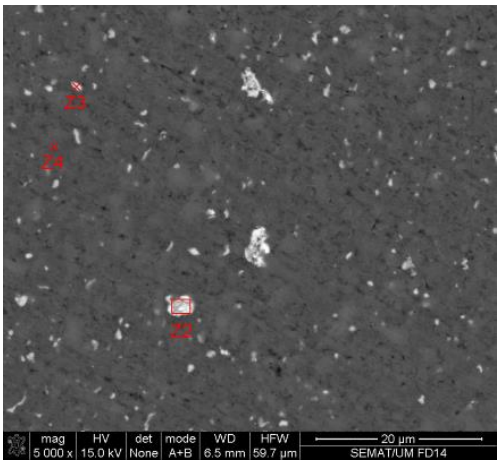

Figure 4. 2 - SEM image in backscattered view of an Al-Si/2%CNT composite sample.

Table 4. 1 - Chemical composition of zones Z2 and Z4 presented in Figure 4. 2.

Element	Concentration (wt. %)	
	Z2	Z4
Al	60.8	89
Si	3.6	11
Ni	30	-
C	5.6	-

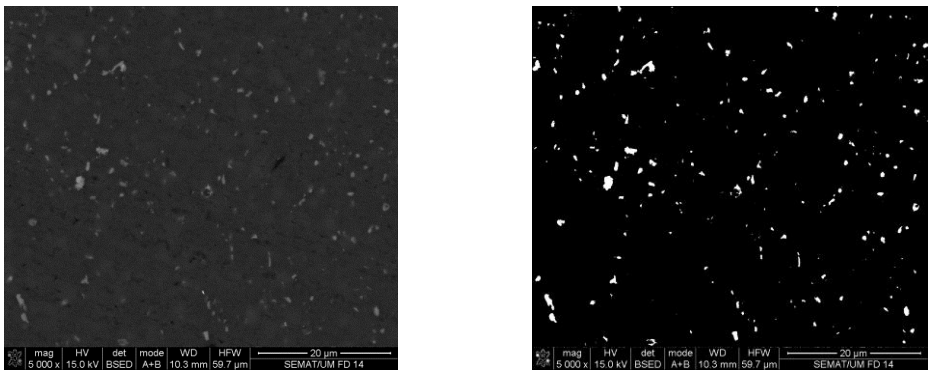

a b

Figure 4. 3 - Figure 1.SEM image in backscattered view: (a) Al-Si/CNT composite with 2 wt. % MWCNT and (b) same SEM image, with threshold filter, enhancing the carbon nanotubes distribution and presence of agglomerates.

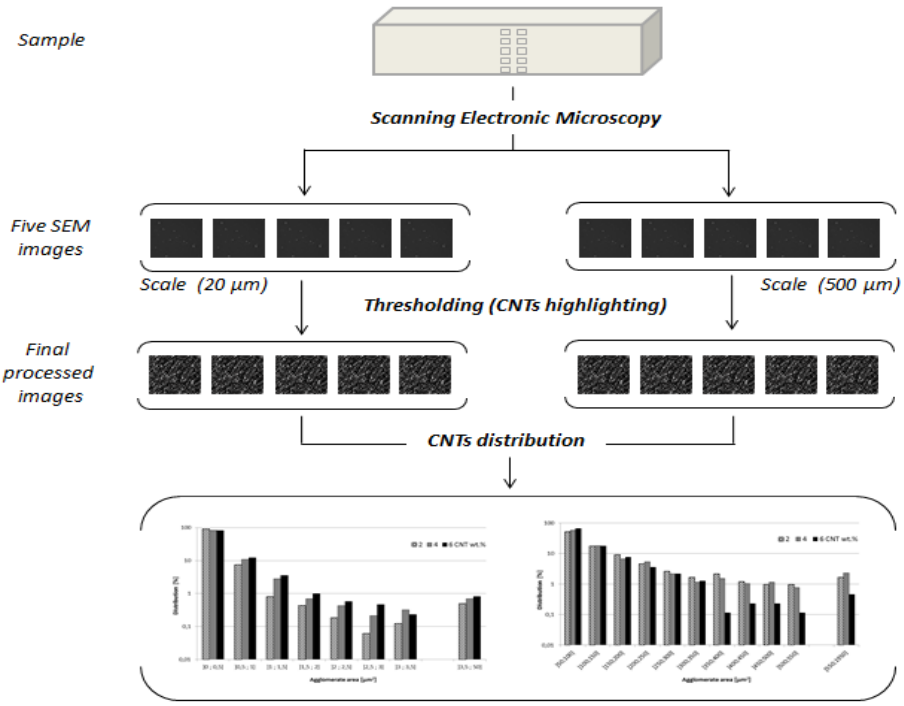

Figure 4. 4 -Implemented procedure for SEM images analysis, for CNT agglomerates quantification.

4.3.3 Mechanical testing

Dog-bone shaped tensile test specimens were machined from the produced samples, in order to perform tensile tests, in a servo hydraulic universal tensile testing machine (Instron 8874), equipped with a 25 kN capacity load cell. Tests were performed at room temperature (≈23 °C), with a crosshead speed of 0.05 mm.s-1.

4.4 Results and discussion

Results regarding tensile strength, as well as CNT distribution as a function of the CNT content in the matrix, for 2, 4, and 6 CNT vol. % are presented.

4.4.1 Tensile Strength

Figure 4. 5 shows the experimental results of tensile strength for the Al-Si/CNT composites produced in this work, as a function of CNT's content. It can be seen that there is an increase of about 25% in tensile strength with incorporation of CNT's (2% CNTs) but for CNT's weight content higher than 2% the properties suffer a decrease.

In Figure 4. 6 are presented the results achieved by C.N. He et. al. [27], for Al/CNT composites produced using in situ chemical vapour deposition. It can be seen that properties increase until an amount of about 5% of CNT's and tensile strength increases in about 185% as compared to the matrix properties. In the former work it is assumed that CNT's are ideally distributed in the matrix (with no agglomerates) and these results will be used in this study for comparison purposes.

C. N. He et. al. [27] produced the CNT-reinforced aluminium composites by synthesizing CNTs into the aluminium powders in situ by a chemical vapour deposition (CVD) process. Post-processing analysis allowed concluding that the formed CNTs have a diameter between 5 and 25 nm, and a length between 1 and 3 μm. These as-grown CNTs are well-graphitized multiwalled nanotubes, with the presence of Ni. According to the authors, a homogenous distribution is obtained, and no agglomerates are formed. Concerning the mechanical properties, assessed by means of tensile tests, the authors concluded that a strong interfacial bonding was obtained between CNTs and the matrix; once most CNTs are ruptured in the fracture surface, and few are pulled out.

The present work uses Nickel coated Multi-Wall Carbon Nanotubes (MWCNTs), with length between 0.5 and 2.0 μm and a diameter of approximately 50 nm, while the matrix alloy is an Al12Si alloy in powder form.

Although there exists some differences between both studies, namely on the matrix material (aluminium in C. N. He et. al. [27] work and aluminium-silicon in this work) and on the processing route that in the present study was by mixture of the CNTs and the matrix alloy by low-energy ball milling, followed by hot pressing, there are strong similarities between studies, allowing to make, on the opinion of the authors of this work, to some extent, a comparison between them in terms of the effect of the agglomerates in the composite tensile strength, since in both works, MWCNTs, with similar dimensions, are used in the composites. Thus, C. N. He et. al. work can be used as a reference, setting the influence of CNTs in aluminium composites in an ideal scenario - when agglomerates are not formed and a good dispersion is obtained, and the present work will allow taking conclusions about the influence of agglomerates in these composites.

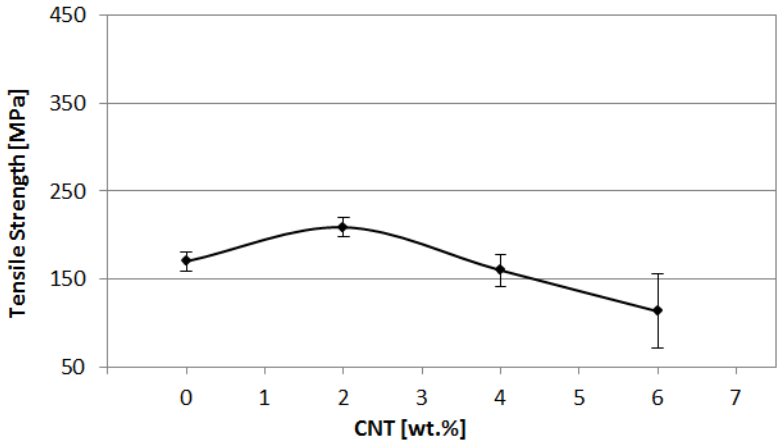

Figure 4. 5 -Tensile strength for different Al-Si/CNT composites, with 0; 2; 4 and 6 wt. % CNT,produced and tested in the present work.

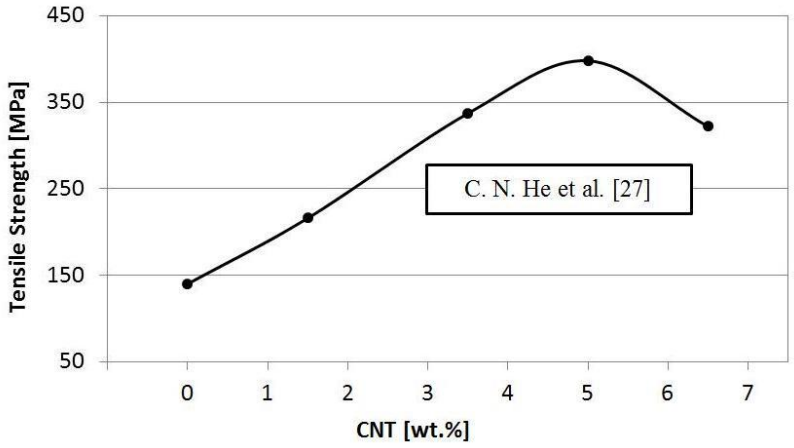

Figure 4. 6 - Tensile strength of different Al/CNT composites, with 0; 1.5; 3.5; 5 and 6.5 wt. % CNT,produced and tested by C. N. He et al. Data extracted from [27].

While in the present work (Figure 4. 5) the highest tensile strength value is achieved with a CNT content of 2 wt. %., in C.N. He et. al. work, the highest value is obtained for 5 wt. % CNT (Figure 4. 6). Moreover the improvement in mechanical properties is of about 25% in the present work and of about 185% in ref. 27. The decrease in tensile strength improvement (25% as compared to 185%) as well as the CNT content for which it is obtained (2% as compared to 5%) will be considered a cause of the CNT's agglomerates formation, commonly accepted as the main detrimental effect on CNTs reinforced aluminium based composites [21, 22].

4.4.2 CNT distribution

In order to clarify the influence of CNTs agglomerates in the composite mechanical properties (namely on tensile strength), an agglomerates distribution study, by size, in the produced Al-Si/CNT composites was performed. The obtained results allow a quantification of CNT's dispersion as a function of CNT's content in the produced composites. Results are shown in Figure 4. 7 to Figure 4. 10.

Figure 4.7 relates to measurements of agglomerates with areas up to 50 μm^2, representing well dispersed CNTs, as well as agglomerates of one to few CNTs (amplifications of 5000 times were used in used pictures). These results show a similar pattern in agglomerates distribution, for all the produced Al-Si/CNT composites (with 2, 4 and 6 wt. % CNTs). In all of them it is verified that more than 93% of the agglomerates are less than 1 μm^2 in area (Figure 4. 8). Considering the representativeness of these small agglomerates ([0, 1] μm^2) in all of the produced composites, they will be, hereafter, named as Type A agglomerates (Figure 4. 8).

Figure 4. 9 presents measurements of agglomerates with areas up to 1950 μm^2. All Al-Si/CNT composites, with 2, 4 and 6 wt. % CNT, show a similar pattern in agglomerates distribution, however, agglomerates with area above 350 μm^2 are less represented in the composite with 6 wt. % CNT (amplifications of 123x were used in these pictures).

In all of the produced composites, more than 93% of the agglomerates have area above 50 μm^2 and less than or equal to 550 μm^2 (Figure 4. 10). Considering the representativeness of these agglomerates in all of the produced composites, agglomerates with area within the range]50, 550] μm^2 are named hereafter as Type B agglomerates (Figure 4. 10).

It is worth to mention that different magnifications were used for the different measurements. Type A agglomerates were measured in pictures with 5000x magnification and type B agglomerates were measured with 123x magnification. In the type A pictures it was not possible to properly quantify big agglomerates due to higher amplification and in type B pictures it was not possible to properly observe the very small agglomerates due to the lower amplification.

Figure 4. 8 shows that Type A agglomerates are more represented in Al-Si/2%CNT composite, decreasing for greater CNTs contents. On the other hand, Type B agglomerates are more represented in Al-Si/6%CNT composite (Figure 4. 10).

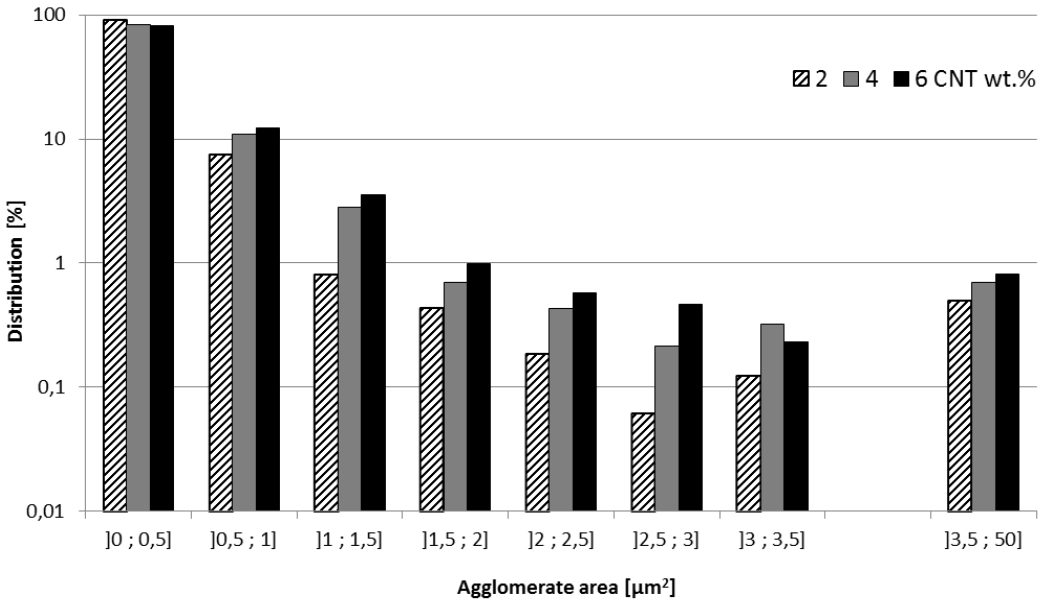

Figure 4. 7 - CNTs agglomerates distribution, determined in pictures with 5000 times magnification - percentage of agglomerates by size classes (y-axis withlogarithmic scale).

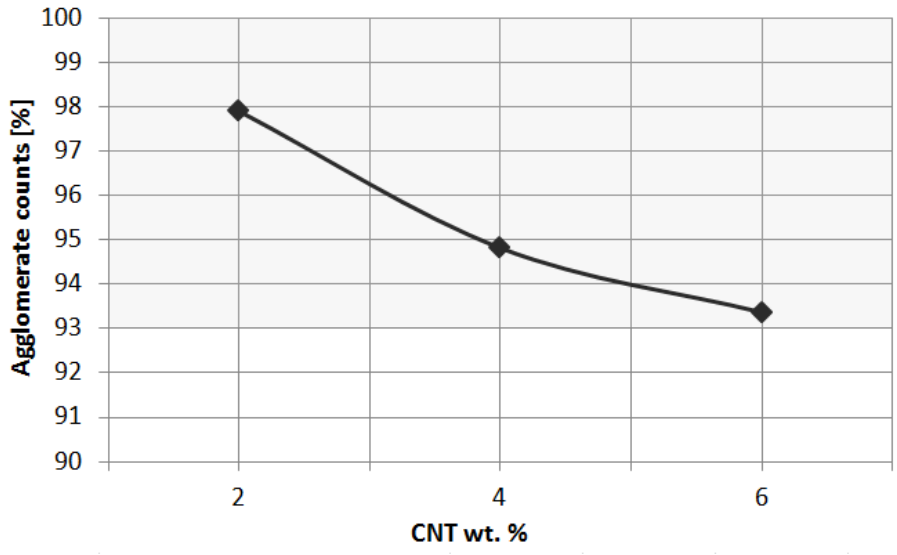

Figure 4. 8 - Type A agglomerates ([0, 1] µm²) counts for Al-Si/CNT composites with 2, 4 and 6 wt.% CNT.

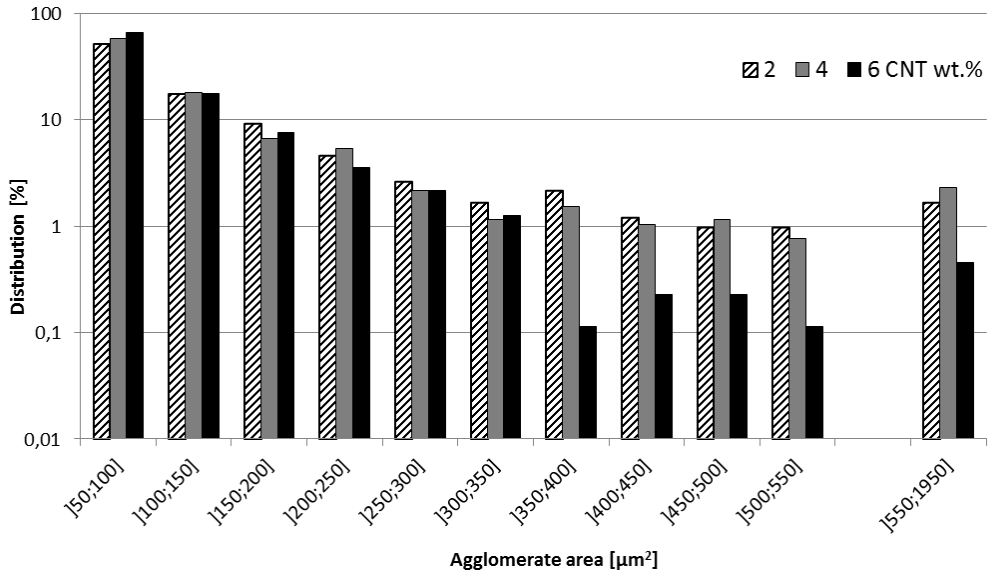

Figure 4. 9 - CNTs agglomerates distribution, determined in pictures with 123 times magnification - percentage of agglomerates by size classes (y-axis withlogarithmic scale).

The first main observation from the previous results is that as the volume fraction of CNT's increases in the composites (from 2 to 6 wt. %), the ability to disperse the CNTs decrease. There are less small agglomerates (Figure 4. 8) and more big agglomerates (Figure 4. 10) with increasing CNTs volume fraction in the composite.

In order to quantify the influence of the agglomerates in the produced composites, the area occupied (as measured in photographs) by the agglomerates was measured. The results are presented as the area fraction of the agglomerates in the whole material. Figure 4. 11 shows the results for the different CNT contents and type of agglomerate.

It can be seen in Figure 4. 11 that both type A and type B agglomerates area fraction increase with CNT's content in the composite. An interesting conclusion is that with increasing CNT's content, the type A agglomerates area fraction increases, while the measured counts of these agglomerates decrease. This trend is explained by the fact that that with increasing CNT content, the agglomerates area tend to approximate the upper limit (1 μm^2), indicating a tendency to agglomerate with higher CNT content.

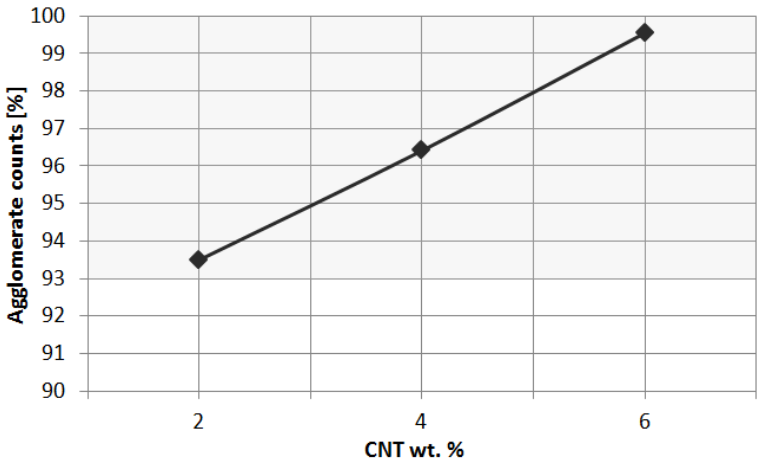

Figure 4. 10 - Type B agglomerates ( ]50, 550] μm²) counts for Al-Si/CNT composites with 2, 4 and 6 wt.% CNT.

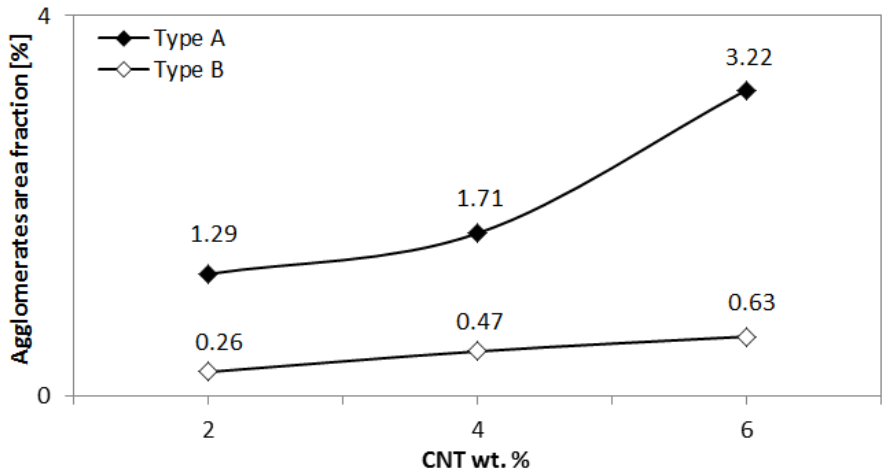

Figure 4. 11 - Type A and type B agglomerates area fraction (in percentage) for Al-Si/CNT composites with 2, 4 and 6 wt. % CNT.

4.4.3 Proposed empirical model

With the gathered results, a quantification of CNTs agglomerates effect on tensile strength as a function of CNTs content in the composite is proposed. In order to assess the influence of the different types of agglomerates in the tensile strength of the composite, all the obtained information was gathered in Figure 4. 12: C.N. He et. al. tensile strength results (with assumed complete CNTs dispersion) and the results obtained in this work concerning tensile strength and type A e type B agglomerates area fraction for all the produced Al-Si/CNT composites (2, 4 and 6 wt. % CNT).

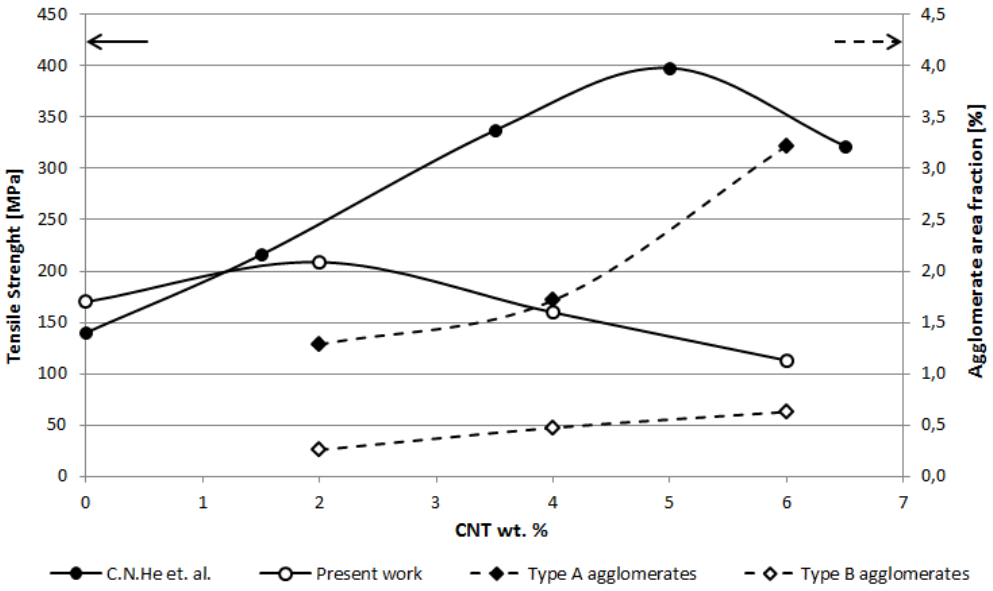

Figure 4. 12 - Tensile strength (C.N. He et. al. results and present work) and agglomerate area fraction for produced Al-Si/CNT composites.

Analyzing Figure 4. 12, it can be concluded that when no agglomerates are formed (C.N. He et. al. curve), the optimum point concerning tensile strength is reached at 5 wt. % CNT. In the present work, where CNTs agglomeration occurs, the 2 wt. % CNT composite revealed the higher tensile strength. As previously mentioned, the leading mechanism behind this difference lies in the formation of agglomerates.

Based on the gathered information, an empirical model is proposed, where the influence of agglomerates in the final composite tensile strength is quantified. The ideal curve (without agglomerates), and the curve that includes the agglomerates influence are presented in Figure 4. 13. Also type A and type B agglomerates area fraction, for different CNT contents are included in Figure 4. 13.

The agglomerates area fraction as a function of CNT content (in wt. %) in an Al-Si/CNT composite is presented in Table 4. 2, for type A and type B agglomerates. This way, knowing the CNT content in the composite, it is possible to predict the amount of agglomerates, of each type, that will be formed.

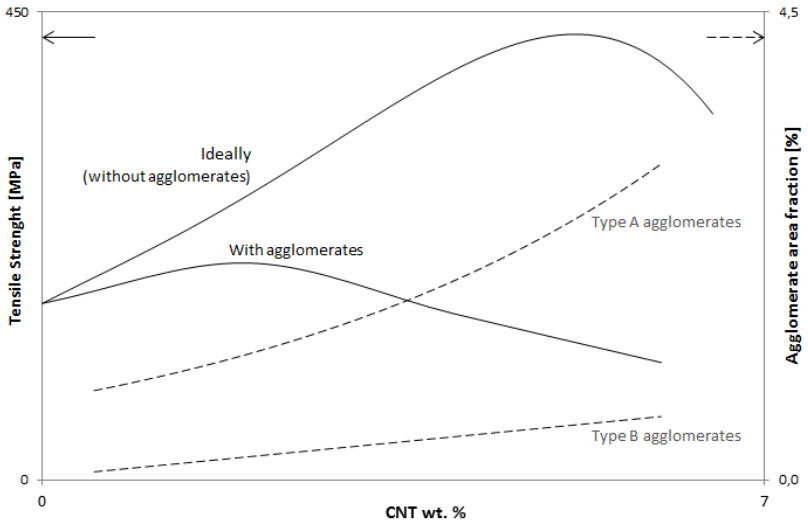

Figure 4. 13 - Tensile strength (without and with agglomerates) and agglomerate area fraction (for types A and B) in Al-Si/CNT composites.

Table 4. 2 - Agglomerates area fraction of: type A (*y*) and type B (*z*) agglomerates, as a function of CNT content (wt. %) (*x*) in an Al-Si/CNT composite.

	Agglomerates area fraction	
	Type A [*y*]	Type B [*z*]
CNT wt.% [*x*]	$y = 0.7671e^{0.2296x}$	$z = 0.0928x + 0.0814$

Based on the curves presented in Figure 4. 13, the tensile strength of an Al-Si/CNT composite obtained by powder metallurgy (using low-energy ball milling to mixture CNTs with Al-Si alloy powder), can be obtained, from the ideal composite results, without agglomerates, (modelled from C. N. He et. al. results), by the following equation:

$$\sigma_{With\ agglomerates} = \sigma_{Without\ agglomerates} + (315y^{1.5} - 4380z^2 - 178) \Leftrightarrow$$

$$\Leftrightarrow \sigma_{with\ agglomerates} = 170 + 50.7x - 3.9x^2 + 3.3x^3 - 0.5x^4 + 315y^{1.5} - 4380z^2 - 178$$

Eq. (1)

where *x* is the CNT content (wt.%) in the Al-Si/CNT composite, *y* is the area fraction occupied by type A agglomerates and *z* the area fraction for type B agglomerates (both area fractions can be obtained by image analysis (measurements) or in alternative using the equations presented in Table 4. 2). This empirical model should now be tested under other different processing conditions, in order to evaluate its validity.

4.5 Conclusions

The main conclusions that can be drawn from this work are as follows:

- CNTs dispersion in the matrix depends on CNT content in the matrix;

- The higher the CNT content in the matrix the higher the amount of big agglomerates;

- A correlation between CNT agglomerates and CNT content in the matrix is possible to be established;

- An empirical correlation of tensile strength as a function of CNT's content in the matrix is possible to be established.

4.6 Acknowledgements

This work was supported by an FCT (Fundação para a Ciência e a Tecnologia) grant (SFRH/BD/44077/2008).

4.7 References

[1] Y. Min-Feng, O. Laurie, M.J. Dyer, K. Moloni, T.F. Kelly and R.S. Ruoff. 2000. Strength and breaking mechanism of multiwalled carbon nanotubes under tensile load. Science 287: 637.
[2] R. Pérez-Bustamante, I. Estrada-Guel, W. Antúnez-Flores, M. Miki-Yoshida, P. J. FerreiraandR. Martínez-Sánchez. 2008. Novel Al-matrix nanocomposites reinforced with multi-walled carbon nanotubes. J. Alloy Compd. 450: 323–326.
[3] Y. Tang, H. Cong, R. Zhong and H. Cheng. 2004. Thermal expansion of a composite of single-walled carbon nanotubes and nanocrystalline aluminium. Carbon 42: 3260–3262.
[4] E. T. Thostenson, C. Li and T. Chou. 2005. Nanocomposites in context. Compos. Sci. Technol 65: 491–516.
[5] E. T. Thostenson, Z. Ren and T. Chou. 2001. Advances in the science and technology of carbon nanotubes and their composites: a review. Compos. Sci. Technol 61: 1899–1912.
[6] D. S. Lim, D. H. You, H. Choi, S. Lim and H. Jang. 2005. Effect of CNT distribution on tribological behavior of alumina–CNT composites. Wear 259: 539–544.
[7] R. George, K. T. Kashyap, R. Rahul and S. Yamdagni. 2005. Strengthening in carbon nanotube/aluminium (CNT/Al) composites. Scripta Mater 53: 1159–1163.
[8] C. F. Deng, D. Z. Wang, X. X. Zhang and A. B. Li. 2007. Processing and properties of carbon nanotubes reinforced aluminum composites. Mat. Sci. Eng. A 444: 138–145.
[9] R. Zhong, H. Cong andP. Hou. 2003. Fabrication of nano-Al based composites reinforced by single-walled carbon nanotubes. Carbon 41: 848-851.
[10] K. Morsi and A. Esawi. 2007. Effect of mechanical alloying time and carbon nanotube (CNT) content on the evolution of aluminum (Al)–CNT composite powders. J Mater Sci 42: 4954–4959.
[11] T. Kuzumaki, O. Ujiie, H. Ichinose and K. Ito. 2000. Mechanical characteristics and preparation of carbon nanotube fiber-reinforced Ti composite. Adv. Eng. Mater 2: 416-418.

[12] E. Carreño-Morelli. 2006. Carbon Nanotubes: Metal Matrix Composites, in: C. I. Contescu and K. Putyera (eds.). Dekker Encyclopedia of Nanoscience and Nanotechnology: 611–619. Taylor & Francis, Boca Raton.
[13] S. R. Dong, J. P. Tu and X. B. Zhang. 2001. An investigation of the sliding wear behavior of Cu-matrix composite reinforced by carbon nanotubes. Mater. Sci. Eng. A 313: 83-87.
[14] J. P. Tu, Y. Z. Yang, L. Y. Wang, X. C. Ma and X. B. Zhang. 2001. Tribological properties of carbon-nanotube-reinforced copper composites. Tribol. Lett. 10: 225-228.
[15] K. T. Kim, S. I. Cha, S. H. Hong and S. H. Honga. 2006. Microstructures and tensile behavior of carbon nanotube reinforced Cu matrix nanocomposites. Mat. Sci. Eng.A 430: 27-33.
[16] H. Li, A. Misra, Y. Zhu, Z. Horita, C. C. Koch andT. G. Holesinger. 2009. Processing and characterization of nanostructured Cu-carbon nanotube composites. Mat. Sci. Eng. A 523: 60-64.
[17] E. Carreño-Morelli, J. Yang, R. Schaller and C. Bonjour. 2003. Tiny tubes boost for metal matrix composites. Metal Powder Report 2004, vol. 59: 40-43. Proceedings of European Conference on Powder Metallurgy, Valencia, Spain.
[18] A.Peigney, Ch. Laurent, E. Flahaut and A. Rousset. 2000. Carbon nanotubes in novel ceramic matrix nanocomposites. Ceram. Int. 26: 677-683.
[19] C. He, N. Zhao, C. Shi, X. Du, J. Li, H. Li and Q. Cui. 2007. An Approach to Obtaining Homogeneously Dispersed Carbon Nanotubes in Al Powders for Preparing Reinforced Al-Matrix Composites, Adv. Mater. 19: 1128-1132.
[20] S. R. Bakshi and A.Agarwal. 2011. An analysis of the factors affecting strengthening in carbon nanotube reinforced aluminum composites. Carbon 49: 533–544.
[21] A. M. K. Esawi and M. A.El Borady. 2008. Carbon nanotube-reinforced aluminium strips. Compos. Sci. Technol. 68: 486-492.
[22] A. M. K. Esawi, K. Morsi, A.Sayed, M.Taher and S. Lanka. 2010. Effect of carbon nanotube (CNT) content on the mechanical properties of CNT-reinforced aluminium composites. Compos. Sci. Technol. 70: 2237-2241.
[23] N. Darsono, D. H. Yoon and J. Kim. 2008. Milling and dispersion of multi-walled carbon nanotubes in texanol. Appl. Surf. Sci. 254:3412-3419.
[24]Z. Tao, H. Geng, K. Yuc, Z. Yang and Y. Wang. 2004. Effects of high-energy ball milling on the morphology and the field emission property of multi-walled carbon nanotubes. Mater. Lett. 58: 3410-3413.
[25]A. M. K. Esawi, K. Morsi, A. Sayed, A. Abdel Gawad and P. Borah. 2009. Fabrication and properties of dispersed carbon nanotube–aluminum composites. Mat. Sci. Eng. A. 508: 167-173.
[26] C. Deng, X. Zhang, D. Wang, Q. Lin and A. Li. 2007. Preparation and characterization of carbon nanotubes/aluminum matrix composites. Mater. Lett. 61: 1725-1728.
[27] C. N. He, N. Q. Zhao, C. S. Shi and S. Z. Song. 2009. Mechanical properties and microstructures of carbon nanotube-reinforced Al matrix composite fabricated by in situ chemical vapor deposition. J. Alloy Compd. 487: 258-262.
[28] A.Yazdanbakhsha, Z.Grasleyb, B. Tysonc and R. K. Abu Al-Rubd. 2011. Dispersion quantification of inclusions in composites. Composites Part A: Applied Science and Manufacturing 42: 75–83.
[29] S. R. Bakshi, R. G. Batista and A. Agarwal. 2009. Quantification of carbon nanotube distribution and property correlation in nanocomposites. Composites: Part A. 40: 1311–1318.

5 Improvement on sliding wear behaviour of Al/cast iron tribopair by CNTs reinforcement of an Al alloy

Oscar Carvalho[1], Mihaela Buciumeanu[2], Delfim Soares[1], Jose Gomes[1], Filipe S. Silva[1]

[1]CT2M – Centre for Mechanical and Materials Technologies, University of Minho, Azurém, 4800-058 Guimarães, Portugal

[2]Cross–Border Faculty of Humanities, Economics and Engineering, "Dunarea de Jos" University of Galati, Domneasca 47, 800008 Galati, Romania

Published in Tribology Transactions 58, 2015, 643-653
, DOI: 10.1080/10402004.2014.1002143

5.1 Abstract

The results presented in this work show the wear characterization of an AlSi-matrix composites reinforced by Multi-Wall Carbon Nanotubes (MWCNTs) under dry reciprocating sliding conditions against a grey cast iron (GCI). The wear resistance is investigated as a function of the CNT content that varied from 2 wt. % to 6 wt. %. The results demonstrated that the CNT content plays a relevant role on wear behaviour by substantially reducing the wear loss of AlSi-CNT composites. Further, it also reduces the wear loss of the grey cast iron counterface. A physical model able to explain the improved behaviour in both mating materials is depicted from experimental results.

Keywords: Carbon nanotubes (CNTs); AlSi-matrix composite; Wear

5.2 Introduction

Several studies exist on the use of CNTs as reinforcement to produce metal matrix composites (MMC) for wear purposes [1-13]. The tribological properties of the MMC can be enhanced by several factors such as: (i) the matrix [1, 4-6]; (ii) reinforcement phase [7-12]; (iii) production methods [13, 14] etc. Regarding the used CNTs as reinforcement to produce composites that can be used in tribological application, several metal matrix materials were used such as Cu [4, 5], Mg [6, 13], Ti [7], Zn [8] and Al [2, 5, 9–12]. CNTs are an effective reinforcement for improving wear characteristics of Al based composites [2, 5, 9-12]. To the authors knowledge

only one study, conducted by Bakshi et al. [2], investigated the wear response of AlSi alloy as a function of a CNT content [5 and 10 wt.% of CNTs) by plasma spraying. They observed that there is an improvement on wear resistance of the 5wt.% CNT, while in the case of 10 wt.% CNT the wear resistance decreased. This wear behaviour is explained based on CNTs dispersion, CNTs' agglomeration size and fraction and carbide formation. In the present work is used a different production method: powder metallurgy. The main advantage of this technique in comparison to the plasma spraying is that it is possible to produce structural materials while the plasma spraying is effective to produce coatings.

The degree of dispersion of CNTs plays an important role in wear resistance not only in the case of metal matrix composites [4-8,13] but also in other composites like non-metal composites (e.g. MWNTs/Carbon) [14].

Aluminium-based metal matrix composites are characterized by low density and high specific stiffness [15], but the poor wear resistance of the aluminium and its alloys is still a problem for its application in situations involving sliding contacts [4,5]. As CNTs are characterized by extraordinarily low thermal expansion and high thermal conductivity [16–18], it is supposed that the aluminium-based metal matrix composites reinforced with CNTs are good candidates to meet the necessary qualities for components under sliding contact.

AlSi alloys reinforced with CNTs may be, for example, applied in automotive components where low weight is a key factor [19]. Two examples of components where wear characteristics may be important are the case of compression piston rings and engine pistons. In order to minimize the wear loss between the engine piston or the piston rings and cylinder the material pairs play an important role. For example, in practice the piston rings damage is attributed first to wear (as there are parts in contact and in relative motion), then to lubrication and fatigue [20]. The up and down movement against the cylinder wall makes wear properties of piston or piston ring a key requirement. Moreover, it is also important that the counterpart (cylinder wall - usually made in grey cast iron) is itself preserved from wear loss. Not only the piston ring or engine piston but also the cylinder wall (counterpart) must be wear resistant. The materials used to manufacture the engine piston or the piston rings must have the following properties: low weight, high strength, high wear resistance (under dry [21-24] and lubricated conditions) and good thermal conductivity. It is well known that the automotive piston tribological system is essentially lubricated [25, 26], but there are also situations when the lubrication system fails. So, the authors consider that it is

important first to improve the wear of the tribopair in the dry situations. Another possible application of AlSi- CNTs is the self-lubricating composite bearings.

This paper investigates the wear behaviour of an AlSi matrix composite reinforced by MWCNTs, coated with Nickel, under dry reciprocating sliding conditions. The MWCNTs content ratios studied are 2 wt. %, 4 wt. % and 6 wt. % and it is shown that the carbon nanotubes content is very effective in reducing the wear loss of the composite, as well as of the grey cast iron counterpart.

5.3 Experimental Procedure

5.3.1 Fabrication of AlSi-CNTs composites

An AlSi alloy, powders size < 325 mesh (< 44 μm), with chemical composition as listed in Table 5. 1, was used as matrix material. Ni coated MWCNTs were used as reinforcement (outer diameter > 50 nm, length 0.5-2.0 μm, purity before coating > 95wt% and ash < 1.5wt%). It should be highlighted that the Ni coating does not have a structural effect on CNT molecular structure. The Ni coating was used in order to improve the bonding between CNTs and matrix and to avoid some undesirable chemical reactions.

The AlSi-matrix composite reinforced by CNTs was processed by the traditional hot pressing (HP) technique. Applied pressure was 35 MPa for 10 minutes at 550°C under vacuum (10^{-2} mbar). The mixing of the AlSi powders was made inside a closed stainless steel jar along with steel milling balls (10 mm in diameter). The ball powder ratio is 10:1. The bottle rotated with constant speed (40 rpm) during 6 days (low-energy ball milling).

Table 5. 1 - Chemical composition of AlSi alloy (wt%)

Al	Si	Fe	Others
87.3	11	0.20	1.5

Microstructures of an unreinforced AlSi alloy and of AlSi-CNT composites (after etching) for all CNT content are presented in Figure 5. 1. It can be seen that CNTs, as expected, are placed in the grain interfaces and also that there are some agglomerates. More than 93% of the agglomerates are less than 1 μm^2 in area. There are also some bigger agglomerations, in composites with a

higher CNT content, with areas ranging from 50 μm^2 to 550 μm^2 and some voids. A detailed quantification and characterization of CNT agglomerates and dispersion as well as voids quantification is presented elsewhere [27]. The CNTs correspond to the white dots/areas (see explanation later in 3.4 discussion section). The average AlSi grain size is around 6 µm. As the grains are deformed due to the hot pressing processing technique the grain size was measured as an average size in two directions - horizontal and vertical).

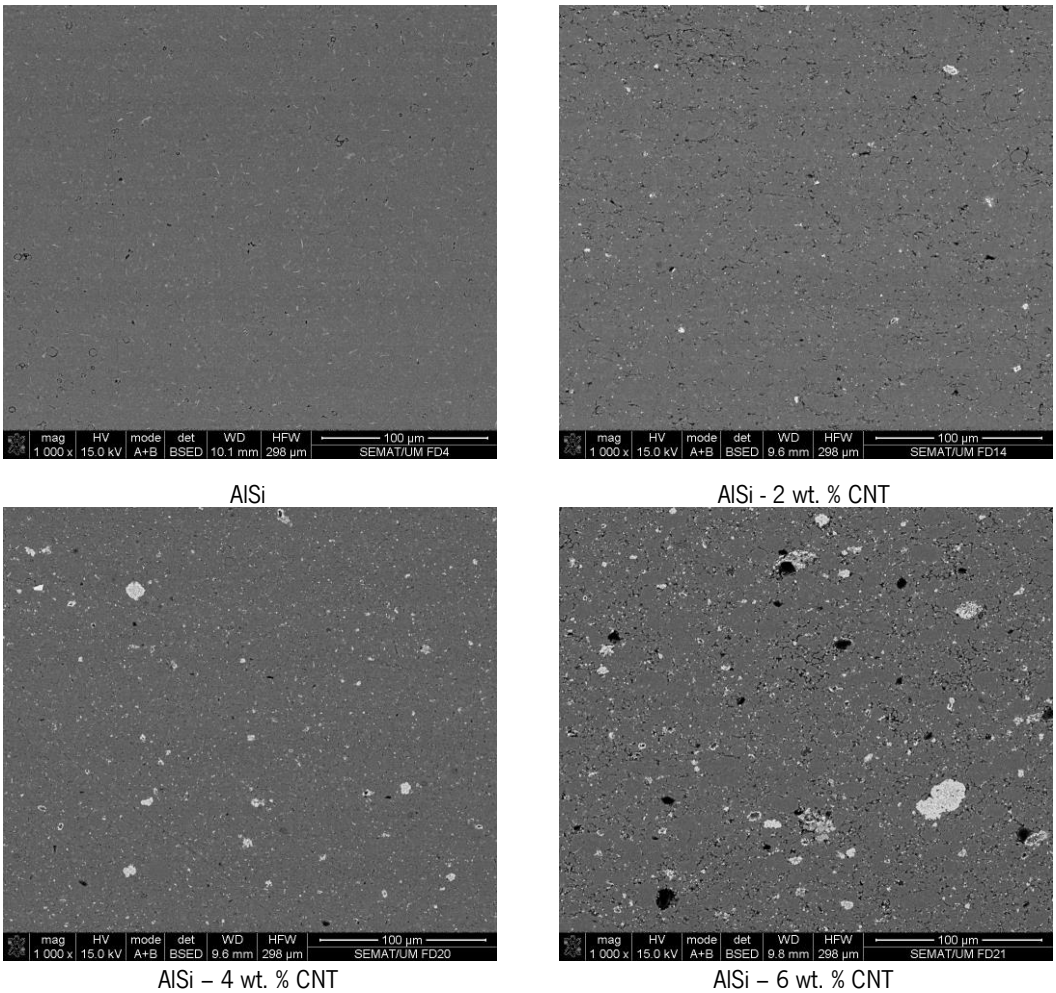

Figure 5. 1 - SEM images of unreinforced AlSi alloy and AlSi - CNT composites microstructure.

Figure 5. 2 presents SEM images where CNT agglomerates are in evidence, with two magnifications. In the first picture (magnification 190x and backscattered view) different agglomerates can be seen, and in the second picture (magnification 30000x) an amplified image of one agglomerate of CNTs is presented (see more details in 3.4 discussion section where a chemical analysis was performed).

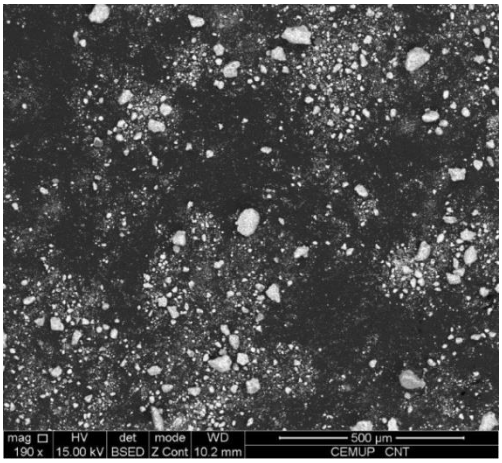

Magnification 190x

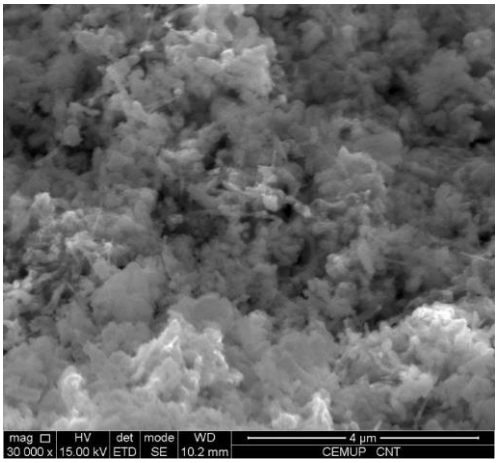

Magnification 30000 x

Figure 5. 2 - SEM images of CNTs.

5.3.2 Chemical characterization

The obtained specimens were characterized in terms of chemical composition by means of Scanning Electron Microscopy (SEM) / Energy Dispersive Spectrometer (EDS).

5.3.3 Hardness measurements

Hardness measurements were conducted in the produced composites and unreinforced matrix material. Vickers hardness measurements were obtained as a mean of 16 indentations per sample using a Shimadzu microhardness tester with a load of 200 gf during 15 s.

5.3.4 Details of the reciprocating wear test

A reciprocating pin-on-plate tribometer PLINT-TE67/R was used to evaluate the wear characteristics of AlSi-CNT composite/cast iron sliding pairs. Pins were machined from the AlSi matrix composites reinforced with CNTs. The CNT content of the pins varied from 2, 4 to 6 wt. %. An unreinforced AlSi alloy was used for comparison purposes. The content ratios of this paper have been chosen based on a previous work [27]. The effect of CNT content on the mechanical behaviour of AlSi-CNT composites was studied. It was concluded that in the case AlSi–2wt.% CNT's

composite, there is an optimal improvement in all studied mechanical properties; while, with increasing CNT content, a drop in the mechanical properties was observed. Pins have the shape shown in Figure 5. 4. The dimensions of the pins are: radius of curvature 40 mm, thickness 3.5 mm and the arc length 20 mm. This AlSi composite can eventually be used for engine pistons or compression piston rings.

The counterpart consisted in flat plates (40×18×5 mm) that were machined from grey cast iron (GCI) with a hardness of 338 HV. Table 5. 2 presents the chemical composition of GCI and Figure 5. 3 shows the microstructure of GCI.

Table 5. 2 - Chemical Composition of GCI.

Fe	C	Mn	Si	P	Cr	Ni	Cu	S	Mo	Others
90,4	3,59	0,392	2,37	0,624	0,249	1,52	0,28	0,023	0,007	0,545

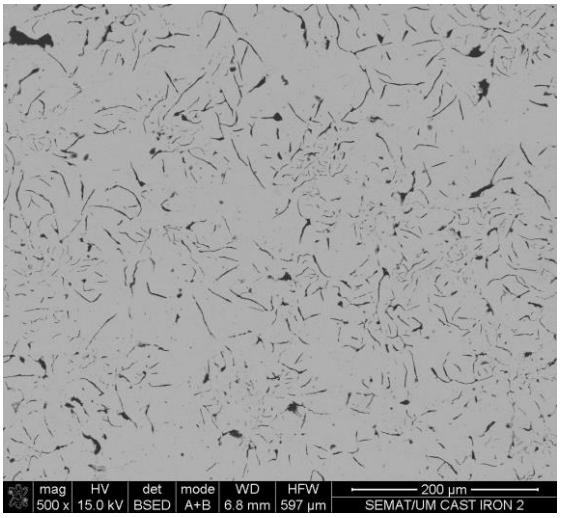

Figure 5. 3 - SEM image of cast iron microstructure.

Figure 5. 4 shows, schematically, the test performed in this work: applied normal load (Fn) on the pin and alternative displacement (d) of the flat specimen. Experiments were carried out with a normal load of 10 N and relative displacement amplitude of 10 mm, for a sliding distance of 148 m (for 2 hours), at a sliding speed of about 0.02 m/s. During the test compressed air was fed to the contact zone in order to remove loose wear debris. The frequency of the reciprocating motion was 1 Hz for all tests. All wear tests were carried out under the same conditions. All tests were performed in laboratory environment (20 ± 2°C).

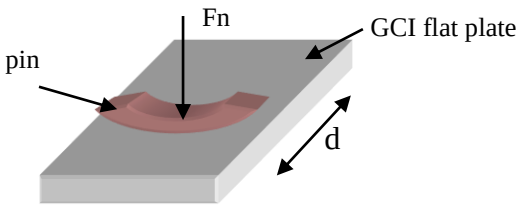

Figure 5. 4 - Schematic test configuration: Fn – Normal applied load; d – alternated displacement amplitude.

The data acquisition system associated to the tribometer recorded different testing variables including coefficient of friction and sliding distance. Both pin and flat specimens were cleaned ultrasonically in alcohol before and after the tests and the amount of wear was measured by weight loss. The dominant wear mechanisms were characterized by scanning electron microscopy (SEM) with X-Ray energy dispersive spectroscopy (EDS) analysis.

5.4 Results and Discussion

Coefficient of friction, hardness, wear loss, and wear mechanisms will be discussed subsequently both for the pin and for the flat plate counterpart.

5.4.1 Coefficient of friction as a function of the CNT content

Figure 5.5 shows the evolution of the coefficient of friction (COF) with sliding distance in the case of unreinforced AlSi alloy and of AlSi - CNT composites against GCI. It is observed a typical evolution of the COF with the sliding distance for a reciprocating sliding wear test. After a first period corresponding to the running-in regime (where surfaces adapt to each other and COF changes significantly during the first period of sliding, increasing with the sliding distance) the COF enters in steady-state conditions and remains approximately constant during the whole test.

Figure 5. 6 presents the average COF as a function of the CNT content. It can be seen that there is a slight decrease of COF with the addition of the 2 wt. % CNT (that may be due to the self lubrication effect of CNTs), but after that the values of the coefficient of friction obtained in this study are approximately the same no matter the CNT content.

It has been reported in other studies [2, 5, 8-12, 28] that COF decreases with CNT content. In those studies it is said that the CNT content causes a reduction on COF possibly due to the self lubrication effect of carbon content. In the current work, the counterpart is a grey cast iron and, consequently, there is a substantial amount of free carbon compared to the eventual contribution of carbon due to the CNT content. Thus, the effect of carbon present in the GCI overlaps any possible influence on COF provided by the CNTs in the AlSi - based composites. It should be highlighted that the carbon graphite present in the GCI is different from the CNTs. It was expected that there would be a different lubricant effect between graphite in the GCI and in CNTs because they have different chemical structure. So, the graphite in GCI is only expected to work like a solid lubricant and this does not contribute to the enhancement of the properties of the GCI (in this case the nodular graphite reduces the mechanical properties of the GCI because it behaves like pores - stress concentration). In this case the CNTs have more than one effect on the tribological behaviour of the composite: self lubrication effect and strengthening effect (increase the bonding between the grains on the Al matrix), so it is more difficult to remove them as the mechanical properties have confirmed [27]. Due to their shape and size, mainly the CNTs that come from the agglomerates could roll between the mating surfaces. A comparison can be made between the graphite in GCI and the agglomerates in the composites.

In both cases these two do not have a beneficial effect on mechanical properties but could have a beneficial effect on wear behaviour. The agglomerates could have a higher effect on tribological properties because when these agglomerates are released into the contact there is a disaggregation of these agglomerations due to the shear forces, leading to the appearance of individual CNTs that could roll into the sliding contact [29]. Once the CNTs are released, they may behave as a third body that contribute to wear. The graphite does not have this ability. Some researchers tried to introduce the CNTs in the lubricants in order to [30] decrease both friction and wear. The possible rolling effect of the CNTs could be higher if the debris were not removed by the permanent air flow. Thus, the CNTs have a double effect on the wear behaviour: self lubrication effect between the mating surface and strengthening effect on the pin.

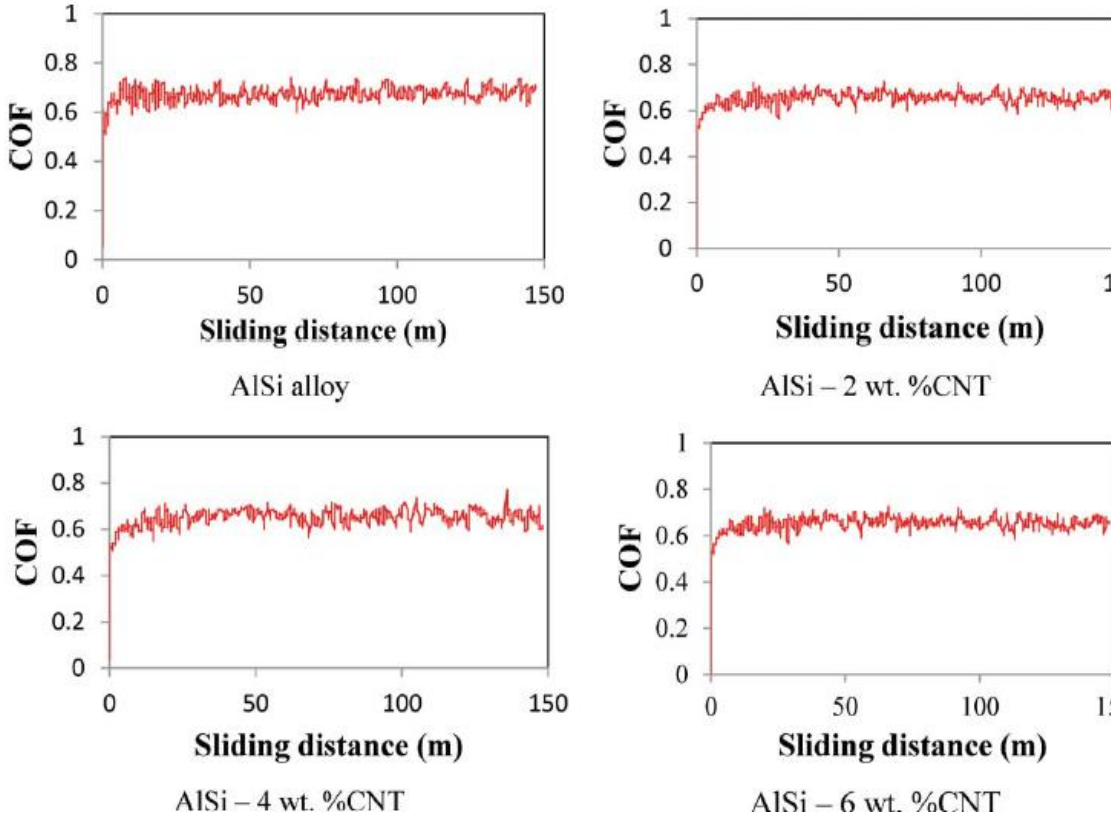

Figure 5. 5- Evolution of coefficient of friction with sliding distance for unreinforced AlSi alloy and all AlSi- CNT composites (AlSi - CNT against GCI.

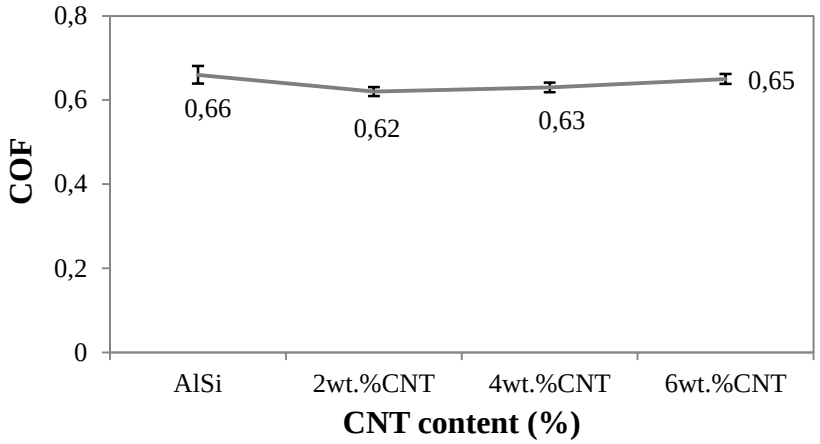

Figure 5. 6 - COF as a function of the CNT content.

5.4.2 Hardness values as a function of the CNT content

Figure 5. 7 shows the hardness results as a function of CNT content in all AlSi-CNT composites.

As expected, the hardness increases with increasing CNT content. As compared to the unreinforced AlSi alloy (pin), the CNT composites show an increase of about 26% to 41%. This behaviour may eventually be explained based on the fact that the CNTs, placed in the grain interfaces, create barriers to dislocations thus increasing strain hardening during plastic deformation [31]. There are also some other strengthening mechanisms that contribute to the increase of mechanical properties, such as hardness: shear lag (load is transferred to the reinforcement via shear stresses at the interface between the matrix and the CNTs) [32] and thermal mismatch (due to differential thermal contraction between matrix and CNTs during cooling from sintering temperature leads to creation of residual stresses) [33]. In all mentioned studies [2, 4, 5, 7, 9, 12] it is reported that hardness increases with CNT content.

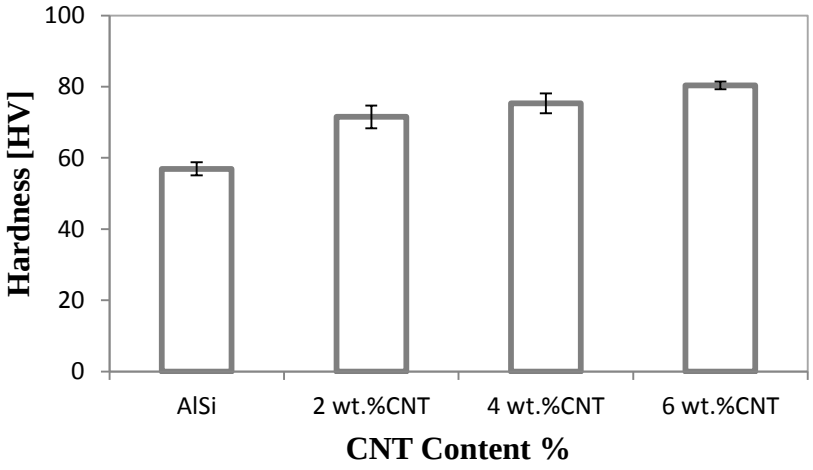

Figure 5. 7 - Hardness as a function of the CNT content.

5.4.3 Wear loss as a function of the CNT content

The wear characteristics (weight loss) according to the CNT content in AlSi alloy matrix composite pins and also for the mating GCI plate are shown in Figure 5. 8.

It can be seen in Figure 5. 8 that the wear loss of both contact surfaces (pin and counterpart) decreases with increasing CNT content. In the case of AlSi-2% wt. CNT/GCI tribopair the wear loss decreased about 26% for the GCI plate and about 9% for the AlSi-2% wt. CNT composite (pin), as compared with the contact involving unreinforced AlSi alloy/GCI. For AlSi – 4 wt. % CNT/GCI tribopair the wear loss decreased about 41% for the GCI plate and 38% for the AlSi – 4 wt. % CNT composite (pin). In the case of AlSi-6 wt. % CNT/GCI tribopair the decrease of wear

was about 51% for the GCI plate and 67% for the pin (AlSi-6 wt. % CNT composite). It is worth highlighting that the wear resistance was improved for both materials (pin and counterpart) involved in the sliding contact.

The pin wear loss results are in line with some previous studies [5, 7, 9-12] where wear loss decreases with CNT content but only until a certain CNT content. Some studies show an inflection curve on wear behaviour above certain CNT content. For example for contents above 4.5 wt. % CNT [9] the wear loss starts to gradually increase. They mentioned that there is a critical point. It is also interesting to observe that it was mentioned that while wear loss changed its behaviour the hardness values kept its increasing behaviour with CNT content. The decrease of wear resistance in spite of increasing hardness was also confirmed by Bakshi and co-authors [2]. Working with an Al-Si alloy, they attributed the improvement on wear resistance for AlSi - 5 wt. % CNT composite to an increase in hardness. But in the case of AlSi - 10 wt. % CNT composite, the wear resistance decreased in spite of the increased hardness. They explained this phenomenon by the existence of CNT agglomerates and on their poor adhesion to the matrix.

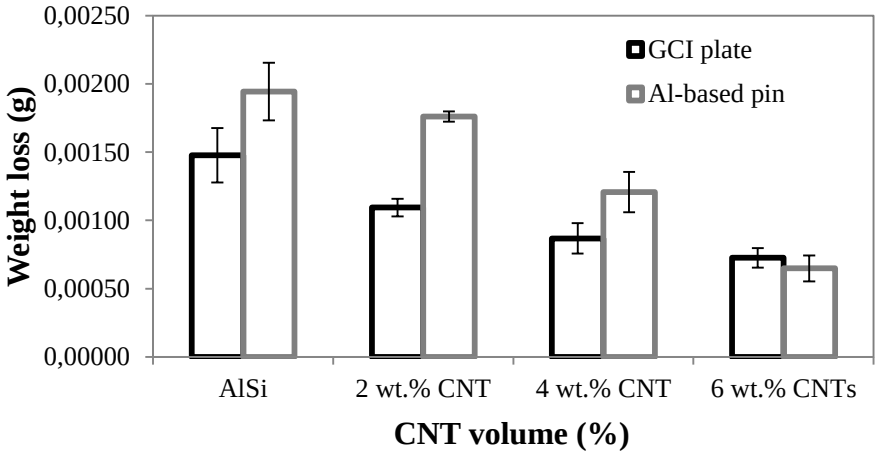

Figure 5. 8 - Wear loss as a function of the CNT content.

Thus, although hardness generally increases with CNT content, wear does not necessarily follow the hardness evolution. Even if hardness is usually considered the main material parameter governing the wear behaviour it seems that in this case the dominant factor affecting the wear behaviour of the AlSi – CNT composites is the CNT content.

In order to understand the mechanisms responsible for the reported wear behaviour, SEM and EDS analysis were performed on the surfaces of the unreinforced AlSi alloy and on the produced AlSi-CNTs composites.

A novelty and important observation of the present study, when comparing to previous studies, is that the counterpart also improves its wear behaviour. To the author's knowledge in previous studies [4, 6, 9-11] nothing is said about the counterpart wear response.

5.4.4 Analysis of wear track (SEM and EDS analysis)

High resolution images and the EDS spectrums (obtained by SEM) are shown in Figure 5. 9– Figure 5. 12 for Al-Si - based pins (unreinforced AlSi alloy and AlSi-CNT composites) and GCI plate.

GCI plates

Figure 5. 9 shows SEM images of the worn surface of GCI plates after sliding against unreinforced AlSi pin and AlSi-based pins with different CNT content.

It can be clearly observed that there is a difference in the wear track morphology between the plates used for sliding against unreinforced AlSi alloy (Figure 5. 9-a) and the ones sliding against AlSi-CNTs composites (Figure 5. 9-b, c and d). On the SEM image of the wear track of the GCI plate when this is sliding against unreinforced AlSi alloy (Figure 5. 9-a) can be observed the destructive effects of delamination marks. This is the main wear mechanism observed in the case of unreinforced AlSi alloy, but there can also be observed a few tiny grooves. Regarding the worn surface morphology of GCI plates among the different CNT content, it can be seen from Figure 5. 9-b, c and d that there is no substantial difference between them in terms of the dominant wear mechanisms. All the surfaces presented similar abrasion deeper grooves. The presence of these deeper grooves on the plates sliding against AlSi-CNT pins will be explained later in this paper (see section AlSi-based pins). However, the degree of GCI surface damage tends to decrease by the presence of CNTs at the mating surface (by increasing the CNTs content), as revealed by the increased extension of smooth plateaus at GCI worn surface from Figure 5. 9-a to d.

This observation is in good correlation with the weight loss results presented in Figure 5. 8.

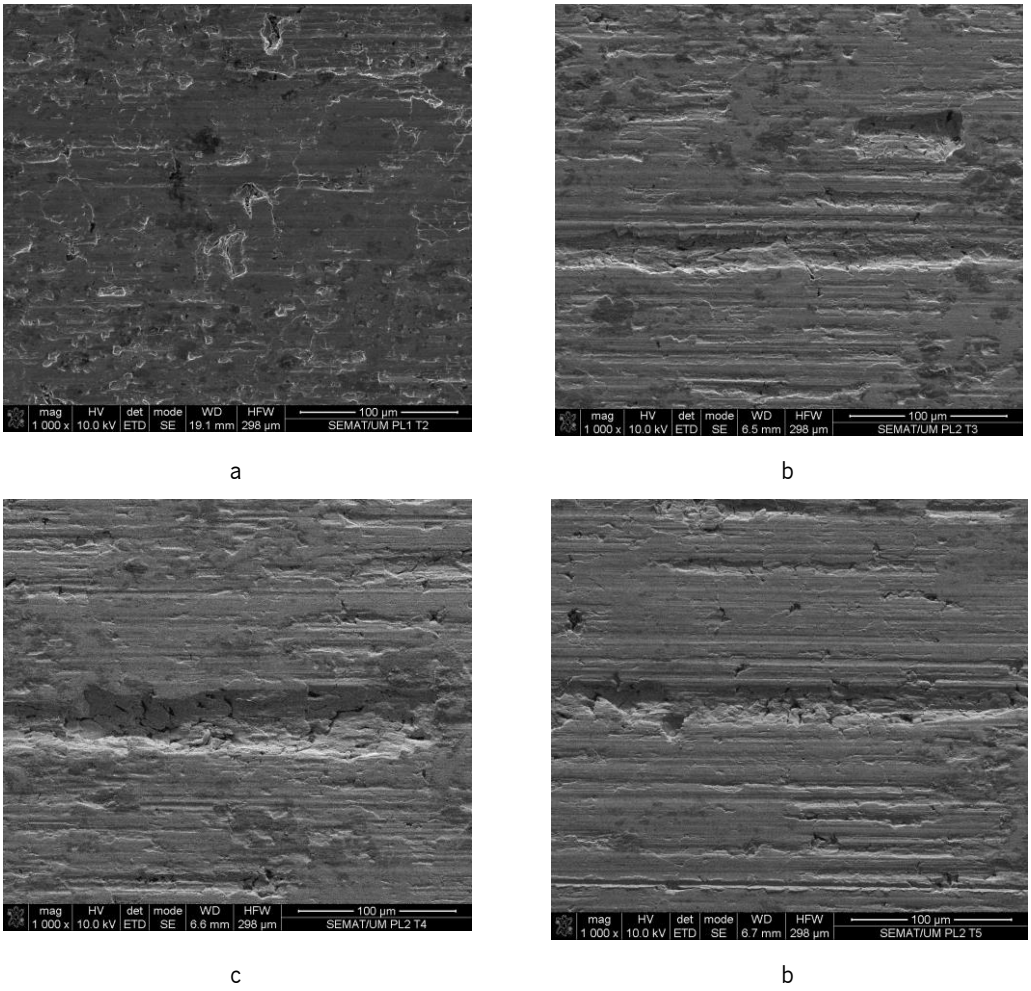

Figure 5. 9 - SEM images of the worn surface of GCI plates after sliding against AlSi-based pins with different CNT content: (a) unreinforced AlSi alloy; (b) AlSi - 2 wt. % CNT; (c) AlSi – 4 wt. % CNT and (d) AlSi – 6 wt. % CNT.

Figure 5. 10-a shows a backscattered SEM image of GCI plate worn surface (1000x magnification) after sliding against AlSi – 2 wt.% CNT composite (pin). This image shows that that material transfer occurred from the pin to the GCI plate (dark zones in backscatter images correspond to material transfer, while the lighter areas correspond to GCI). In order to identify the composition of the transferred material, EDS analysis was performed in the dark zones present in Figure 5. 10-b. The composition of these transferred layers revealed some transfer of aluminium and silicon derived from the pin counterface. The same transfer of aluminium was also found for

all test conditions in this work. For all GCI plates used for sliding against unreinforced AlSi alloy and AlSi-CNTs composites, EDS analysis revealed the presence of oxygen. This high oxygen content may indicate the presence of some aluminium oxides. The transfer of Al and Si from the pin to the GCI plate means that the wear mechanisms of GCI also included adhesion. Besides aluminium, silicon (coming from the matrix alloy) and aluminium oxides, there were found iron and carbon (coming from the GCI).

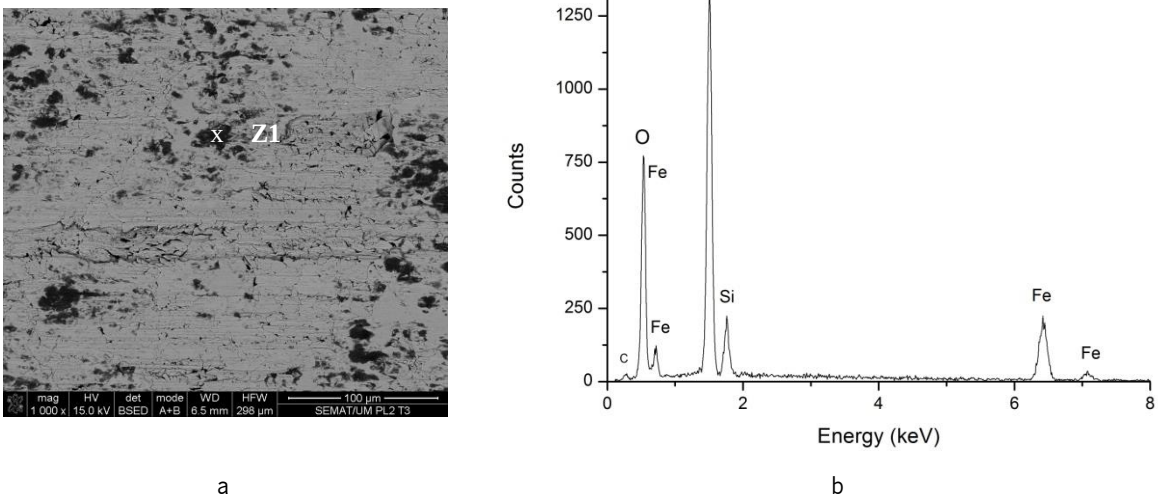

a b

Figure 5. 10 - a.Backscattered SEM image of GCI plate worn surface after sliding against AlSi -2 wt. % CNT pin;b. and EDS spectrum representative of the dark zones in the micrograph.

AlSi-based pins

Figure 5. 11 presents SEM images of the worn surface of unreinforced AlSi alloy and AlSi-based pins with different CNT content. The surface morphology is emphasized at different magnifications (130x, 1000x and 5000x). There is observed a clear evolution in the worn surface morphology from unreinforced AlSi to AlSi-CNTs pins.

In the case of unreinforced AlSi pins surface (Figure 5. 11-a) adhesive wear is present, due to the fact that the surface is under the influence of applied stresses. In the sliding direction the surface material is removed layer by layer, with deeper craters than the AlSi-CNTs pins.

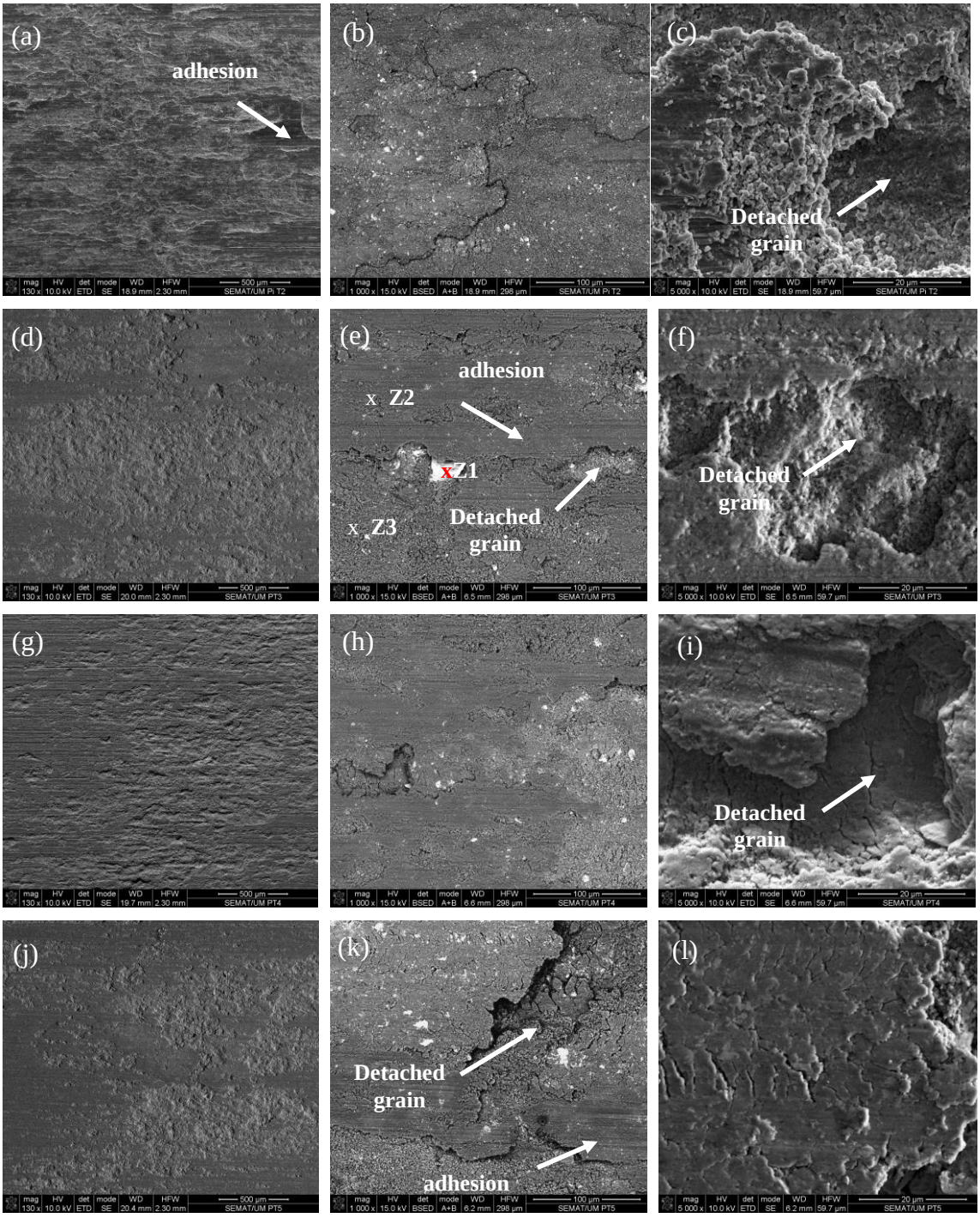

Figure 5. 11 - SEM images of the worn surface of unreinforced AlSi alloy (a), (b) and (c); AlSi -2 wt. % CNT (d), (e) and (f); AlSi – 4 wt. % CNT (g), (h) and (i) and AlSi – 6 wt. % CNT (j), (k) and (l). Global (130x) view (a), (d), (g) and (j); close-up (1000x) backscattered view (b), (e), (h) and (k); high magnification (5000x) view (c), (f), (i) and (l).

SEM images of the worn surface of AlSi-CNT pins (see Figure 5. 11 d, g and j) reveal that by increasing the CNT content (from 2 wt.% to 6% wt. CNT) the pin contact surfaces seem to have less voids but deeper. This can indicate a lower material loss in the AlSi-CNTs composites, when comparing to unreinforced AlSi.It can be observed on the contact region after sliding two types of plateaus: a smooth plateaus and others with more peaks and valleys. The smoother plateaus are increasing with the increase of the CNT content. This observation may be explained based on the anisotropy of the AlSi-CNT composite pins. Based on the microstructural images of the AlSi composites (Figure 5. 1) and on another study by the same authors [20], where the characterization and quantification of CNT agglomerates and dispersion were studied, it can be seen (Figure 5. 1) that there are zones where the CNTs are very well dispersed and zones with a poor dispersion (where the CNT agglomerations are located). By increasing the CNT content there is an increase in the number of macro-agglomerates and a reduction in the micro-agglomerates [27]. The smoother plateaus correspond to the regions where the CNTs are better dispersed and the rougher regions to the regions where there is a poor distribution of CNTs (where the agglomerates are located). These rougher regions are areas of weakness from which failure was initiated to cause wear of the AlSi-composites. It can be observed that the areas of weakness are decreasing with increasing the CNT content. This happens simultaneously with improved diminished wear loss (Figure 5. 8). It is expected that on the zones with good CNT dispersion, the hardness is higher and is responsible for the grooves that can be observed on the plates (Figure 5. 9-b ,c and d). It seems that there is a competition between these two zones, so between adhesion and abrasion.

Figure 5. 12 shows the EDS analysis corresponding to distinct zones of the pin worn surface of AlSi - 2 wt. % CNT composite. Three zones were examined: Z1, Z2 and Z3, which are identified in Figure 5. 11-e. It can be seen from Figure 5. 12-a that Z1 (white zone) corresponds to iron-rich transfer of material from the mating GCI plate and that Z2 and Z3 (dark zones) show the base material of the pin, namely Al and Al2O3. It is worth mentioning at this stage that some white spots in Figure 5. 11 (the biggest ones) correspond to Fe-rich transfer from the GCI plate. However, as can be seen in detail in Figure 5. 13 and Figure 5. 14 the smallest white points correspond to CNTs. This will be explained later in this paper.

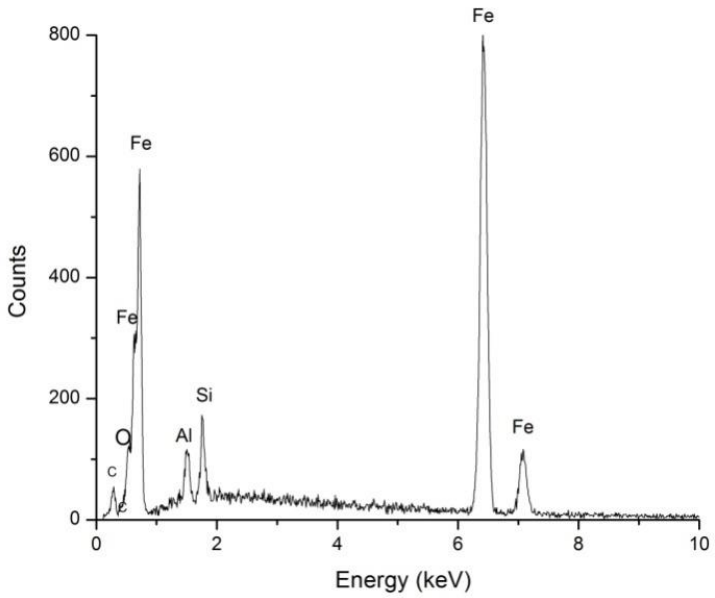

a

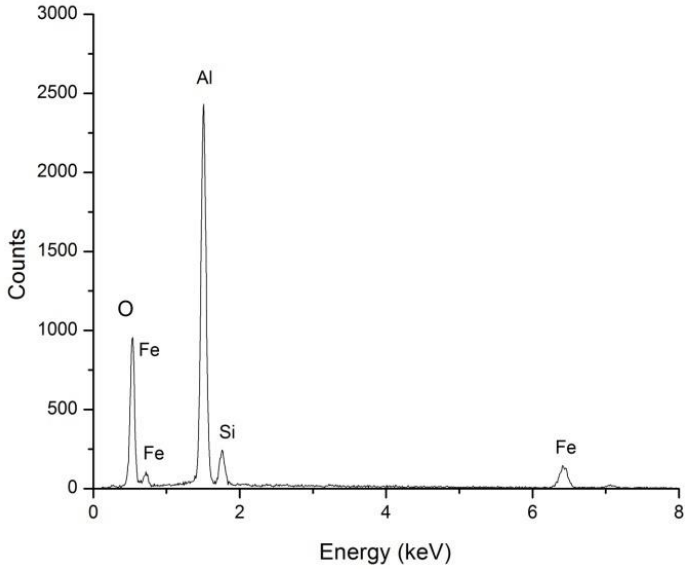

b

Figure 5. 12 - EDS spectra of the pin worn surface with AlSi – 2 wt. % CNT content corresponding to three zones, Z1, Z2 and Z3, identified in Figure 5. 11-e: (a) spectrum from the analysis in Z1 (white zone); (b) spectrum representative of Z2 and Z3.

From Figure 5. 11 with higher magnifications it seems that the powders/grains seem to be detached from the bulk and the void shows the grain/powder boundaries. The voids are formed from agglomerations (where there is a poor distribution of CNTs). Some grains are plastically deformed while some other grains detached from bulk. Thus, it can be concluded that wear damage of AlSi-based pins seems to be controlled essentially by two mechanisms: adhesive wear

that includes material transfer between the mating surfaces, as evidenced by EDS analysis (Figure 5. 10-b and Figure 5. 12-a) and pull-out of grains/particles or agglomerates (Figure 5. 11). Regarding the pull-out mechanism correlation with CNT content, it can be verified that by increasing the CNT content there is an increase in macro-agglomerates, thus the detached grains/powders are less, but deeper. This is in agreement with the fact that CNTs and CNT agglomerates are located at the interfaces between Al-Si powders/grains.

The strengthening mechanism of CNTs in Al-Si sintered parts takes place (increasing the strength or cohesion between AlSi powder or grain interfaces) [34-37] on the regions with well dispersed CNTs (on the smoother plateaus). This is why less detached powders are found when CNT content increases (6 wt. % CNT), as can be seen in Figure 5. 11-j, where there are smoother plateaus.

On zones laden with agglomerates (Figure 5. 11-k), one notices multiples cracks on the sliding surface, as a consequence of the lower properties of the zones. The consequence of the cracks is the formation of debris and consequently of a surface with cavities.

It can be seen in Figure 5. 11 that with increasing the CNT content, the number of cracks increases (with increasing number of macro-agglomerates), which may be due to the lower mechanical properties, as proved in [27]. In spite of the reduction of mechanical properties with the increase of the CNTs [27], there is an improvement in the wear response. This can be explained based on the self lubrication effect of CNTs and on the well dispersed zones, where the properties are higher in the composites with a higher amount of CNTs. So, the agglomerates have detrimental effect on void nucleation, but they may have a beneficial effect on wear behaviour if they are released into the contact, as has been already previously mentioned.

The detaching mechanism is evident in Figure 5. 11 b, e, h, k. on the backscattered view. It clearly shows the CNT agglomerates are located on the interface of the detached grains.

Figure 5. 13 shows SEM image of the AlSi-based pins with 2 wt. % CNT's (5000× magnification) backscattered view before the wear tests and Figure 5. 14 shows the EDS analysis corresponding to distinct zones of the pin Z1, Z2 (white zones) and Z3 (grey zone). In Figure 5. 13 the marked zone Z3 shows the base material of the pin, namely aluminium and silicon. The marked zones Z1 and Z2 reveal besides the aluminium and silicon (base material of the pin) and aluminium oxides, the presence of carbon and nickel. So based on the chemical composition, the small white points (Z1 and Z2) are mainly CNTs and the white colour comes from the nickel CNT coating.

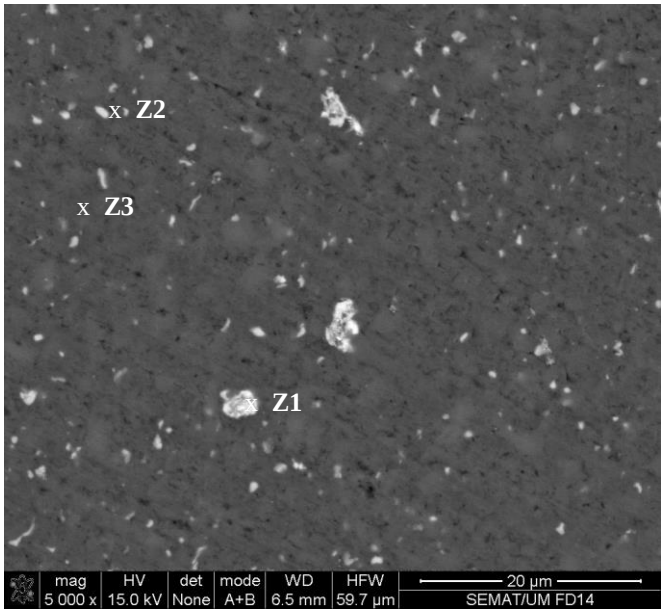

Figure 5. 13 - SEM image of the AlSi-based pins with 2 wt. % CNT (1000×) backscattered view.

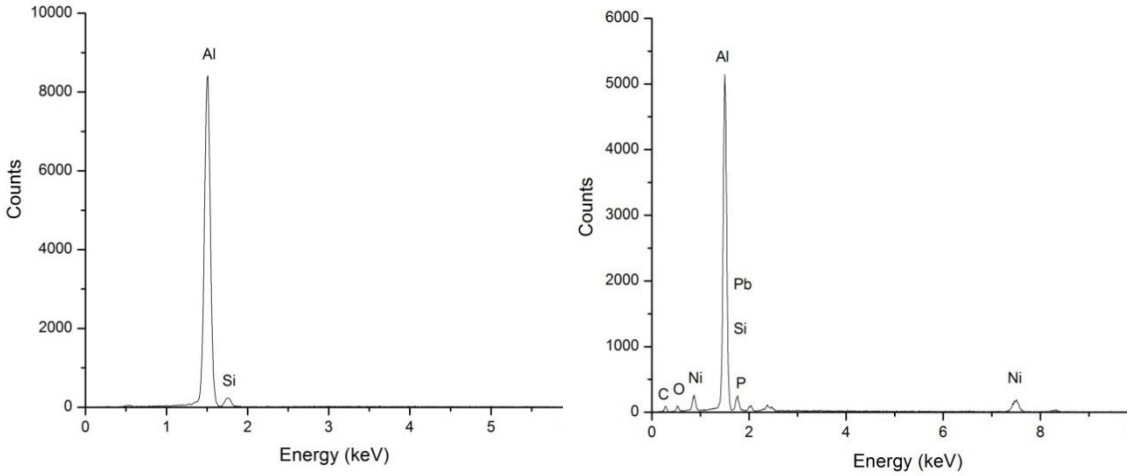

a) b)

Figure 5. 14 - EDS spectra of an AlSi surface with 2 wt. % CNT content corresponding to three zones, Z1 and Z3, identified in Figure 5. 13: (a) spectrum from the analysis in Z3; (b) spectrum from the analysis in Z1 (white zone)(this is equal to zone Z2).

It is worth noting that while in Figure 5. 11 and Figure 5. 12, the mentioned white points corresponded to iron-rich transfer of material from the mating GCI plate to the pin, in this case (also in Figure 5. 11 to Figure 5. 14) the white points are CNTs, in the isolated form or in agglomerates. And if CNTs are found on the voids it means that those are grain boundaries since

the powder metallurgy processing only allows the CNTs to be placed at the grain boundaries. As there is no abrasion/plastic deformation inside the voids if a grain is detached/pull-out the CNTs appear in the grain boundaries. This is a physical evidence that the voids are grain boundaries created by detached/pull-out grains. It should be highlighted that the voids can also result from the agglomerates.

Based on previous reasoning it may also explain the improvement in the GCI wear response and, consequently, in the AlSi-CNT composite/GCI tribopair. As the pin surface has smoother plateaus (less detached grains) the counterpart surface suffers less abrasion. Fewer voids (even if they are deeper with increasing the CNT content) mean a higher contact surface and, consequently, large load-bearing capacity and lower contact stresses. This means less material transfer by adhesion between both mating surfaces and thus an improved wear resistance of the tribopair. In line with those explanations, it seems clear by observing Figure 5. 9 that the deformation is less plastic as CNT content increases in AlSi -based composites.

It seems that the main mechanisms, as observed in the fracture morphologies of wear test results, are: (i) Strengthening effect of CNTs: A stronger bonding between AlSi grain interfaces due to the CNTs, and the effect of the CNT's reinforcement on the matrix most probably due to restrictions on matrix dislocations (mainly in the zones where the CNTs are well dispersed). This is basically in accordance with some of the proposed mechanisms, by George et al. [34], namely, thermal mismatch, Orowan looping and shear lag theory, or also with Zang and co-authors [38], or even with Bustamante et al. [39] suggested mechanisms. Also, it should be mentioned that the CNT agglomerations have detrimental effect on the strengthening, and they are responsible for voids nucleation. (ii) Self-lubrication effect. The CNTs and the CNT agglomerates are released into the contact where there is a disintegration of these agglomerations due to the shear forces, leading to the appearance of individual CNTs that could roll into the sliding contact.

An important aspect to highlight is that previous papers on metallic bulk with CNT as reinforcements [4, 6, 9-11] either with Cu, Mg, Ti, Zn or Al, do not refer to counterparts wear behaviour. Reinforcements introduced in the composite improve its wear behaviour but depending on the counterface material, contact situation, reinforcement type etc. [40] it may reduce the counterpart wear behaviour. In this study one clearly sees the improvement of the wear response of the tribopair by reinforcing the AlSi alloy with CNTs.

When increasing the CNT content, there is clearly a tendency for improvement in the wear behaviour of the AlSi-CNT composites. Moreover also the wear of counterface material improved. Thus, the wear response of the tribopair by reinforcing AlSi alloy with CNTs is improved, when comparing it with unreinforced AlSi/GCI system.

5.5 Conclusions

From the present investigation on the sliding wear behaviour of AlSi-CNT composites/GCI tribopairs when increasing the CNT content, the following conclusions can be drawn:

- All AlSi-CNT composites experienced a substantial improvement in the wear behaviour when compared to unreinforced AlSi alloy.

- Wear mechanisms of AlSi-CNT composites were characterized dominantly by adhesive wear and by grain detachment. The grain detachment is responsible for the wear resistance improvement with increasing CNT content. The main wear mechanisms in the case of grey cast iron were abrasion and delamination.

- It is shown that by reinforcing AlSi alloy with CNTs, the wear behaviour of tribopair (AlSi-CNT/GCI) is improved, when compared with unreinforced AlSi alloy/GCI tribopair.

5.6 Acknowledgments

This work was supported by the Portuguese Foundation of Science and Technology through the project references PTDC/EME-PME/68664/2006 and EXCL/EMS-TEC/0460/2012.

5.7 References

[1] Balani, K., Agarwal, A. 2008. Multiscale wear of plasma-sprayed carbon-nanotube-reinforced aluminum oxide nanocomposite coating. Acta Mater 56, 20: 5984–5994.
[2] Bakshi, S.R., Keshri A.K., Agarwal, A. 2011. A comparison of mechanical and wear properties of plasma sprayed carbon nanotube reinforced aluminum composites at nano and macro scale. Mater. Sci. Eng. A 52, 9: 83375–3384.
[3] Carpenter, C.R., Shipway, P.H., Zhu, Y. 2011. Electrodeposition of nickelcarbon nanotube nanocomposite coatings for enhanced wear resistance. Wear 271, 9-10: 2100–2105.
[4] Dong, S.R., Tu, J.P., Zhang, X.B. 2001. An investigation of the sliding wear behavior of Cu-matrix composite reinforced by carbon nanotubes. Mater. Sci. Eng. A 313, 1-2: 83–87.
[5] Bakshi, S.R., Lahiri, D., Agarwal, A. 2010. Carbon nanotube reinforced metal matrix composites – a review. Int. Mater. Rev. 55, 1: 41-64.

[6] Umeda, J., Kondoh, K., Imai, H. 2009. Friction and wear behavior of sintered magnesium composite reinforced with CNT-Mg2Si/MgO. Mat. Sci. Eng. A 504, 1-2: 157–162.
[7] Threrujirapapong, T., Kondoh, K., Umeda, J., Imai, H. 2008. Friction and wear behavior of titanium matrix composite reinforced with carbon nanotubes under dry conditions. Trans. of JWRI 379, 2: 51-56.
[8] Si, L., Chao, W., Lin, S., Shuangchun, Y. 2013. The research state of CNTs reinforced mental matrix composites. Int. J. of Adv. in Res. & Technol. 2: 243-245.
[9] Choi, H.J., Lee, S.M., Bae, D.H. 2010. Wear characteristic of aluminium-based composites containing multi-walled carbon nanotubes. Wear 270, 1-2: 12–18.
[10] Kim, I.Y., Lee, J.H., Lee G.S., Baik S.H., Kim Y.J., Lee Y.Z. 2009. Friction and wear characteristics of the carbon nanotube–aluminium composites with different manufacturing conditions. Wear 267, 1-4: 593–598.
[11] Zhou, S., Zhang, X., Ding, Z., Min, C., Xu, G., Zhu, W. 2007. Fabrication and tribological properties of carbon nanotubes reinforced Al composites prepared by pressureless infiltration technique. Compos Part. A-Appl. S 38: 301–306.
[12] Al-Qutub, A.M., Khalil, A., Saheb, N., Hakeem, A.S. 2013. Wear and friction behavior of Al6061 alloy reinforced with carbon nanotubes. Wear 297, 1-2: 752–761.
[13] Jamshidijam, M., Fakhrabadi, A. A., Masoudpanah, S. M., Hasani, G. H., Mangalaraja, R. V. 2013. Wear Behavior of Multiwalled Carbon Nanotube/AZ31 Composite Obtained by Friction Stir Processing. Tribol T 56: 827-832.
[14] Men, X.-H., Zhang, Z.-Z., Yan, J., Zhu, X.-T., Wang, K., Jiang, W. 2011. Effect of Different Functional Carbon Nanotubes on the Tribological Behaviors of Poly (Furfuryl Alcohol)–Derived Carbon Nanocomposites. Tribol T 54: 265-274.
[15] Bustamante, R.P., Guel, I.E., Flores, W.A., Yoshida, M.M., Ferreira, P.J., Martínez-Sánchez, R. 2008. Novel Al-matrix nanocomposites reinforced with multi-walled carbon nanotubes. J. Alloy. Compd. 450, 1-2: 323–326.
[16] Tang, Y., Cong, H., Zhong, R., Cheng, H.M. 2004. Thermal expansion of a composite of single-walled carbon nanotubes and nanocrystalline aluminium. Carbon 42: 3260–3262.
[17] Esawi, A.M.K., Morsi, K., Sayed, A., Abdel Gawad, A., Borah, P. 2009. Fabrication and properties of dispersed carbon nanotube–aluminium composites. Mater. Sci. Eng. A 508, 1-2: 167–173.
[18] Deng, C., Zhang, X.X., Wang, D., Lin, Q., Li, A. 2007. Preparation and characterization of carbon nanotubes/aluminium matrix composites. Mater. Lett. 61, 8-9: 1725–1728.
[19] Presting, H., Konig, U. 2003. Future nanotechnology developments for automotive applications. Mater. Sci. Eng. C 23, 6-8: 737–741.
[20] Silva, F.S. 2006. Fatigue on engine pistons – A compendium of case studies. Eng. Fail. Anal. 13, 3: 480–492.
[21] Mohammed Jasim K., Dwarakadasa, E.S. 1987. Wear in Al-Si alloys under dry sliding conditions. Wear 119, 1: 119–130.
[22] Deuis, R.L., Subramanian, C., Yellup, J.M. 1997. Dry sliding wear of aluminium composites-a review. Compos. Sci. Technol. 57, 4: 415-435.
[23] Abouei, V., Shabestari, S.G., Saghafian, H. Dry sliding wear behaviour of hypereutectic Al–Si piston alloys containing iron-rich intermetallics. Mater. Charact. 61, 11: 1089–1096.
[24] Douglas, R.M., Steel, J.A., Reuben, R.L. 2006. A study of the tribological behaviour of piston ring/cylinder liner interaction in diesel engines using acoustic emission. Tribol. Int. 39, 12: 1634–1642.
[25] Truhan, J.J., Qu, J., Blau, P.J. 2005. A rig test to measure friction and wear of heavy duty diesel engine piston rings and cylinder liners using realistic lubricants. Tribol. Int. 38: 211–218.

[26] Kapsiz, M., Durat, M., Ficici, F. 2011. Friction and wear studies between cylinder liner and piston ring pair using Taguchi design method. Adv. Eng. Softw. 42, 8: 595–603.
[27] Carvalho, O., Miranda, G., Soares, D., Silva, F. S. 2014. Carbon nanotube dispersion in aluminum matrix composites – quantification and influence on strength. Mech. Adv. Mat Struct. DOI: 10.1080/15376494.2014.929766.
[28] Peña-Parás, L., Taha-Tijerina, J., García, A., Maldonado, D., González, J. A., Molina, D., Palacios, E., Cantú, P. 2014. Anti-wear and extreme pressure properties of nanofluids for industrial applications. Tribol T. DOI: 10.1080/10402004.2014.933937.
[29] Falvo, M. R., Taylor II, R.M., Helser, A., Chi, V., Brooks Jr, F.P., S., Washburn, Superfine, R. 1999. Nanometre-scale rolling and sliding of carbon nanotubes. Nature 397: 236-238.
[30] Dassenoy, F., Joly-Pottuz, L., Martin, J.M., Mieno, T. 2006. Carbon nanotubes as advanced lubricant additives," V.N. Popov and P. Lambin (eds.), Carbon Nanotubes: 237–238, Springer, Netherlands.
[31] Lahiri, D., Bakshia, S.R., Keshria, A.K., Liub, Y., Agarwal, A. 2009. Dual strengthening mechanisms induced by carbon nanotubes in roll bonded aluminum composites. Mater. Sci. Eng. A 523, 1-2: 263–270.
[32] Nardone V.C., Prewo K.M. 1986. On the strength of discontinuous silicon carbide reinforced aluminum composites. Scripta. Metall. Mater. 20, 1: 43-8.
[33] Arsenault R.J., Shi N. 1986. Dislocation generation due to differences between the coefficients of thermal expansion. Materials Science and Engineering 81: 175-87.
[34] George R, Kashyap KT, Rahul R, Yamdagni S. 2005. Strengthening in carbon nanotube/aluminium (CNT/Al) composites. Scripta Mater. 53, 10: 1159–1163.
[35] Bakshi, S.R., Agarwal A. 2011. An analysis of the factors affecting strengthening in carbon nanotube reinforced aluminum composites. Carbon 49, 2: 533– 544.
[36] Yoo S.J., Han S.H., Kim W.J. 2013. Strength and strain hardening of aluminum matrix composites with randomly dispersed nanometer-length fragmented carbon nanotubes. Scripta Mater. 68, 9: 711–714.
[37] Lahiri D., Bakshi S.R., Keshri A.K, Agarwal A. 2009. Dual strengthening mechanisms induced by carbon nanotubes in roll bonded aluminum composites. Mater. Sci. Eng. A. 523, 1-2: 263–270.
[38] Zhang, Z., Chen, D.L. 2006. Consideration of Orowan strengthening effect in particulate-reinforced metal matrix nanocomposites: A model for predicting their yield strength. Scripta Mater. 54, 7: 1321–1326.
[39] Pérez-Bustamante, R., Gómez-Esparza, C.D., Estrada-Guel, I., Miki-Yoshida, M., Licea-Jiménez, L., Pérez-García, S.A., Martínez-Sánchez, R. 2009. Microstructures and tensile behavior of carbon nanotube reinforced Cu matrix nanocomposites. Mater. Sci. Eng. A. 502: 159–163.
[40] Veeresh Kumar, G.B., Rao, C.S.P., Selvaraj, N. 2011. Mechanical and Tribological Behavior of particles reinforced aluminium metal matrix xomposites – a review. J. Miner. Mater. Charact. Eng. 10, 1: 59-91.

6 Mechanisms Governing the Tensile, Fatigue and Wear Behaviour of Carbon Nanotube reinforced Aluminum Alloy

Carvalho, O.[1], Buciumeanu, M.[2], Miranda, G.[1], Costa, N.[3], Soares, D.[1], Silva, F.S.[1]

[1]CT2M – Centre for Mechanical and Materials Technologies, University of Minho, Azurém, 4800-058 Guimarães, Portugal;
[2]Cross–Border Faculty of Humanities, Economics and Engineering, "Dunarea de Jos" University of Galati, Domneasca 47, 800008 Galati, Romania; 3FIA - Fédération Internationale de l'Automobile, Chemin de Blandonnet 2, 1215 Geneve 15, Switzerland

Published in Mechanics of advanced materials and structures

6.1 Abstract

This work is concerned with understanding the influence of reinforcement mechanisms of carbon nanotubes (CNTs) on mechanical, wear, and fatigue tests on an Aluminium-Silicon (AlSi) alloy. The reinforcement mechanism is presented through the observation of fracture morphology of the different tests. Results of mechanical properties, fatigue life performance and wear loss is presented and discussed. It is shown that the CNTs reinforcement effect is active simultaneously in all previous properties and the reinforcement physical mechanism seems to be essentially due to a reinforcement effect of the interface that seems to be similar in all mentioned mechanical solicitations.

Keywords: carbon nanotubes (CNTs); Al-matrix composite; static properties; fatigue life; wear; fracture morphologies.

6.2 Introduction

Aluminium alloys are widely used in engineering applications where components weight is a key factor (e.g. automotive industry) [1] mainly due to their low density, high thermal conductivity and high specific strength and stiffness [1-3].

It is well known that the carbon nanotubes are hollow cylinders consisting of single or multiple sheets of graphite wrapped into a cylinder with remarkable mechanical (Young's modulus is over 1 TPa and the tensile strength is an estimated 200 GPa), electrical, and thermal properties [4] that are used as reinforcements to increase the strength and stiffness of different materials [5-9]. Due to the expected high potential of CNT's as reinforcement, several studies exist on the use of CNT's, mainly by using the powder metallurgy processing route, for mechanical [7,10-14] and wear [10, 15-20] enhancement purposes. Some of them are related to metal matrix composites and mainly Al based composites [10-13, 15-19].

To better understand the physical mechanisms involved in the reinforcing effect of CNTs some authors proposed different strengthening mechanisms [7,9,21-25], such as: thermal mismatch [7,21], Orowan looping [21,25], shear lag theory [21,25,26], dislocation density model [7,22,25,27], grain-size refinement [25], etc. The proposed mechanisms are correlated to mechanical properties of the specimens including hardness and static properties, Young's modulus, tensile strength, yield strength and rupture strain.

In the technical literature, the increase of mechanical properties with the addition of CNTs [8,11,13,14,24,27,28] was directly related to several factors such as the amount of the CNT's content [13,14,22], size of nanoparticles [22,28], dispersion/orientation of CNTs in matrix [14,22], the difference in the coefficients of thermal expansion between the matrix and nanoparticles, and the temperature change after processing [22].

To the author's knowledge research work concerning the fatigue behaviour of metal matrix composites reinforced with CNTs is scarce and the results presented in technical literature are contradictory [29-33]. Some of the researchers observed an increase of the fatigue strength [32, 33] with the CNTs content, while other reported a decrease of the fatigue strength with the CNTs content [29]. The increase on fatigue strength with CNTs was related with the separation and uniform distribution of CNTs in the matrix, by the formation of voids [33] and with the fact that CNTs can effectively suppress crack propagation generated under high stress loading (e. g. due to the CNT bridging mechanism) [31,32]. The decrease of the fatigue life has been attributed to the CNTs agglomerates that behave like local stress concentrations (crack growth rate is accelerated) [29].

The studies regarding the wear behaviour have demonstrated that CNTs in the case of Al-matrix composite are an effective reinforcement for improving wear characteristics [8, 10, 15-18].

The improvement in wear behaviour was explained in terms of bimodal CNT dispersion (well dispersed and agglomerations) in AlSi matrix, CNT agglomeration size and fraction [8], and on self lubricating effect of carbon content [15]. It has also been observed that an extensive increase in CNT content (more than 5 wt.%) causes the wear to increase [16]. This behaviour was explained based on the weak coherence between formed Al_4C_3 and conglomerated carbon as competing mechanisms.

The present study proposes the understanding of the reinforcing mechanism effect of CNT's based on fracture morphology observation in three different types of tests: tensile, fatigue and wear tests. It is shown that the reinforcement physical mechanisms are similar in all mentioned mechanical solicitations, although different mechanisms must act simultaneously in the composite.

6.3 Experimental procedure

6.3.1 Materials

An AlSi alloy, powders size < 325 mesh (< 44 μm), with chemical composition as listed in Table 6. 1, was used as matrix material. As reinforcement, Ni coated MWCNT's were used with outer diameter > 50 nm, length 0.5-2.0 μm, purity before coating > 95wt% and ash < 1.5wt%.

The Al-matrix composite reinforced by CNTs was processed through traditional hot pressing technique. The pressure was 35 MPa, applied for 10 minutes at a temperature of 550°C under vacuum (10^{-2} mbar). The mixing of the Al powders was performed inside a closed stainless steel jar with the powders mixture and steel milling balls (10 mm diameter). The ball/powder ratio was 10:1 and the atmosphere was argon. The jar was placed in a rotation machine and he mixing was made with a constant rotation speed of 40 rpm during 6days (low-energy ball milling).

The obtained samples had average dimensions of 44 x 3.7 x 6 mm.

The flat plates prepared for the wear tests were machined from grey cast iron (GCI). Table 6. 2 presents the chemical composition of GCI.

Table 6. 1 - Chemical composition of AlSi alloy (wt%).

Al	Si	Fe	Others
87.3	11	0.20	1.5

Table 6. 2 – Chemical composition of GCI

Fe	C	Mn	Si	P	Cr	Ni	Cu	S	Mo	Others
90.4	3.59	0.392	2.37	0.624	0.249	1.52	0.28	0.023	0.007	0.545

Microstructures of CNTs are presented in Figure 6. 1 with 190x magnification (a) and of AlSi-2 wt.% CNTs (after etching) with 5000x magnification (b). In the first picture (Figure 6. 1-a) can be noticed the presence of some CNTs agglomerates and in Figure 6. 1-b can be seen that the average Al grain size is around 6 µm (< 40 µm) and that the CNT agglomerates are located between the grains.

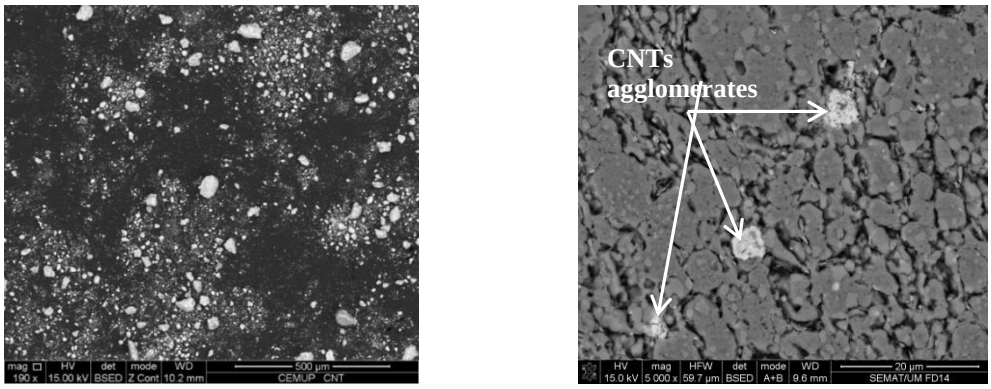

a b

Figure 6. 1 - SEM images showing: (a) microstructure of CNT (magnification 190x) and (b) microstructure of AlSi-2 wt.% CNTs composite (magnification 5000x).

6.3.2 Methods

Tensile tests.

Tensile testing was carried out in order to obtain the mechanical properties, such as tensile strength, σ_r, yield strength σ_y and tensile strain ε_r. The flat-dog-bone shaped tensile specimens were machined from the produced samples. Tensile tests were carried out using a servo-hydraulic universal testing machine Instron 8874, equipped with a load cell capacity of 25 kN (tension). Tests were performed at room temperature (≈23 °C), with a crosshead speed of 0.05 $mm.s^{-1}$ and 5 specimens were used for each condition.

Fatigue tests.

In order to get the influence of the CNT content on the fatigue life (S-N curve), several fatigue tests were carried out at a stress ratio *R=0.1* using a servo-hydraulic universal testing machine Instron 8874. All tests were performed at ambient temperature, in laboratory environment, and at a cyclic frequency of 16 Hz. Tests were performed until final fracture.

Figure 6. 2 shows the geometry of the specimen used in tensile and fatigue tests. A single edge notched configuration was adopted only for the fatigue tests.

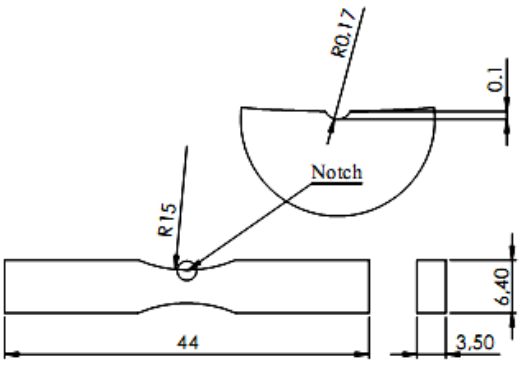

Figure 6. 2 - Geometry of the specimen for tensile and fatigue tests.

Wear tests.

A reciprocating pin-on-plate tribometer PLINT-TE67/R was used to evaluate the wear characteristics of unreinforced AlSi alloy/GCI and AlSi - 2 wt.% CNTs composite/GCI sliding pairs. This is a very simplified test for piston ring and cylinder liner materials with the pin representing the ring and the plate representing the cylinder. Figure 6. 3 shows schematically the test performed in this work: applied normal load (F_n*=10 N*) on the pin and alternative displacement (*d=10 mm*) of the flat specimen. The flat plates (40×18×5 mm) prepared for the wear tests were machined from cast iron. Pins were machined from the unreinforced AlSi alloy and AlSi matrix composites reinforced with 2% wt. CNTs, which can be used for engine piston rings. The dimensions of the pin are: radius of curvature 40 mm, thickness 3.5 mm and the arc length 20 mm.

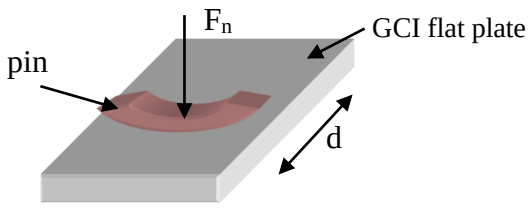

Figure 6. 3 - Schematic test configuration: F_n – Normal applied load; d – alternated displacement amplitude. All tests have been stopped after a sliding distance of 148 m. During the tests compressed air was flown to the contact zone in order to remove loose.

6.4 Results and discussion

The reinforcement mechanisms governing the tensile, fatigue and wear behaviour of CNTs reinforced aluminium alloy (AlSi–2 wt.% CNTs composite) will be discussed subsequently. An unreinforced AlSi alloy is used for comparison purposes.

The AlSi–2 wt.% CNTs composite has been selected for this study based on a previous research works of the same authors [34,35]. It was studied the effect of CNT content (from 2 wt.% to 6 wt.% CNT) over the mechanical behaviour of AlSi-CNT composites. It was concluded that in the case AlSi–2 wt.% CNTs composite there is an optimal improvement in all studied mechanical properties. Similar behaviour was reported by several authors [7, 13, 19, 20]. Esawi et al. [13] stated that the mechanical properties improve with the increase in CNT content. The best results were obtained in the case of 2% wt. CNT content, while with increasing the CNT content it was observed a drop in the mechanical properties. The explanation was based on the dispersion of CNTs and on the strain-hardening powders. Also, Bikiaris et al. [20] observed that the mechanical properties are reducing after the addition of more than 2-3 wt. % CNTs. The explication was based on fact that the CNTs tend to aggregate into bundles and it is difficult to be dispersed homogeneously in matrix. Bustamante et al. [7] showed that the CNTs content has a significant effect over the mechanical properties of AlSi composites. They also observed a maximum on the mechanical properties (such as yield strength σ_y and maximum strength σ_{max}) for the composites with 2% wt. CNTs.

6.4.1 Mechanical properties (Tensile tests)

Figure 6. 4 presents the representative tensile stress–strain curves of both unreinforced AlSi alloy and AlSi-2% wt. CNTs composite. The mechanical properties (tensile strength σ_r, yield

strength σ_y and tensile strain ε_r) are listed in Table 6. 3. It is observed that the tensile strength, σ_r, of AlSi-2% wt. CNT composite improved by about 23% as compared to unreinforced AlSi alloy. The yield strength σ_y of AlSi-2% wt. CNTs composite improved by 26% as compared to unreinforced AlSi alloy. However, the rupture strain decreases [11] with the addition of CNTs by about 46% as compared to unreinforced AlSi alloy.

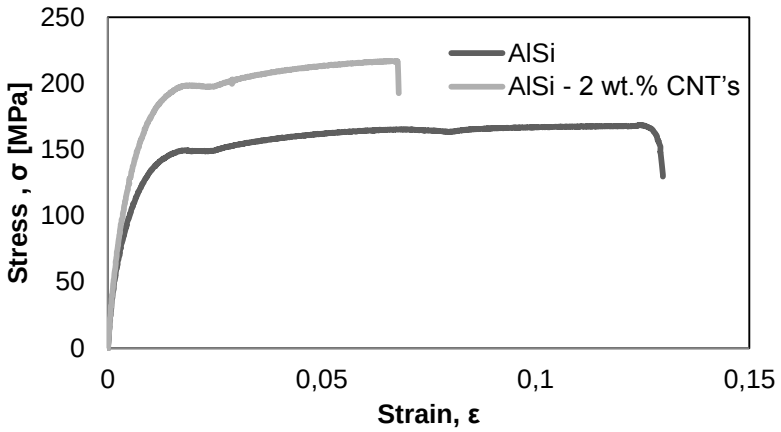

Figure 6. 4 - Stress–strain curves from tensile testing of unreinforced AlSi alloy and AlSi – 2 wt.% CNT's composite.

Table 6. 3 - Results of tensile testing of unreinforced AlSi alloy and AlSi-2 wt. % CNT's composite.

Material	σ[MPa]	σ[MPa]	ε[%]
AlSi	170	152	13
AlSi-2 wt. % CNT's	209	192	7

Figure 6. 5 presents the SEM images of the fracture surface after tensile test of (a) unreinforced AlSi alloy and (b) AlSi-2% wt. CNTs composite, with two magnifications, 1000x and 5000x.It can be observed that the surface of unreinforced AlSi alloy (Figure 6. 5-a) seems to be slightly smoother, while the surface of AlSi-2% wt. CNTs composite seems to have a mixture of two regions (Figure 6. 5-b): smoother regions and a few rougher regions.

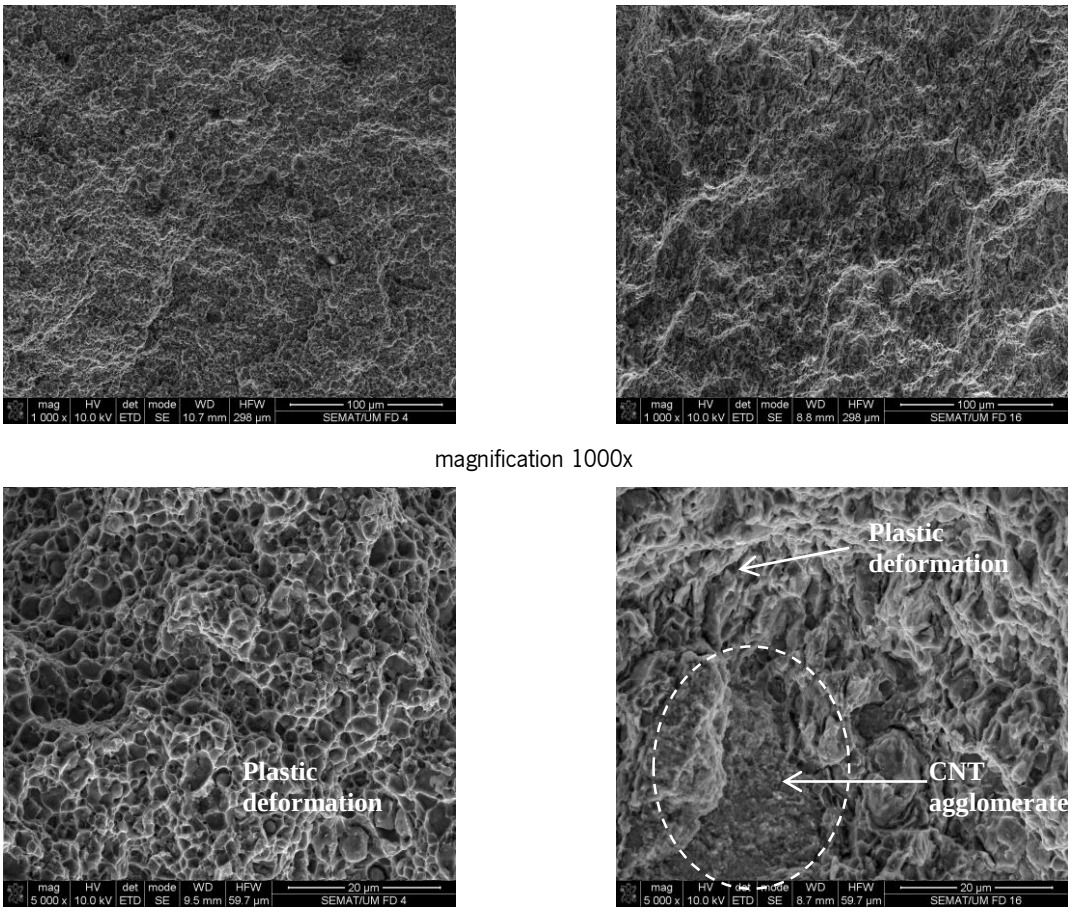

magnification 1000x

a magnification 5000x b

Figure 6. 5 - SEM images of the fracture surface after tensile test of: (a) unreinforced AlSi alloy and (b) AlSi-2 wt. % CNT's composite (with different magnifications).

Figure 6. 5 a shows typical fracture surface morphology of aluminium alloys. The smother fracture surface (Figure 6. 5-a) observed in the case of the unreinforced AlSi alloy is due the fact that the AlSi grains are very well bonded (control the fracture behaviour). Thus, the crack travels through the AlSi grains of the material (intragranular fracture) and it is accompanied by a large amount of plastic deformation (can be observed the dimple appearance of the fractured surface - ductile fracture).

Regarding the surface fracture of AlSi-2% wt. CNTs composite (Figure 6. 5-b), as it was previously mentioned, there can be well observed smoother regions and a few regions with more pronounced shaped peaks and valleys. The smoother regions are due to the fact that the AlSi grains are bonded with an improved strength due to CNTs interface reinforcement effect, while the

rougher regions are due to the poor dispersion of CNTs leading to agglomerations. The presence of agglomerations can be better observed in Figure 6. 6.

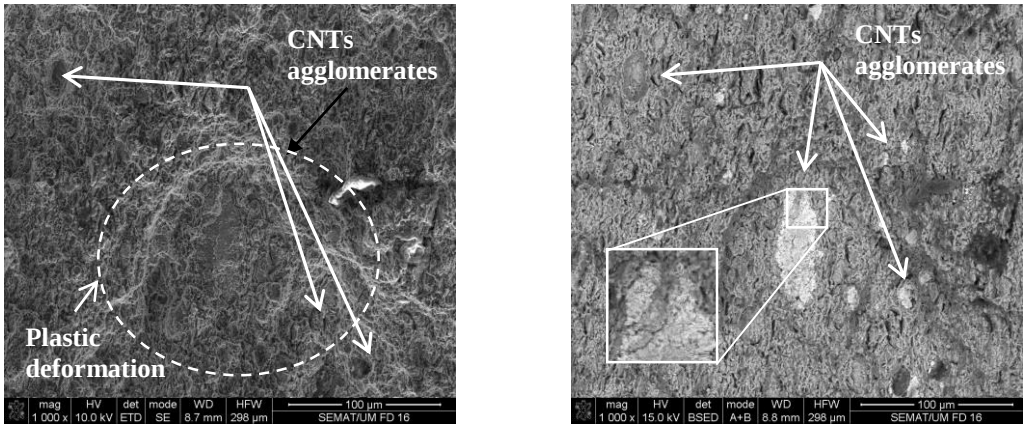

Figure 6. 6 - SEM images of the fracture surface after tensile test showing the presence of CNTs agglomerates (AlSi-2 wt. % CNT's composite –with magnification 1000x)

It has been demonstrated in another study of the same authors that the CNT agglomerates have a big influence on the mechanical properties of the composites [34]. The agglomerations of CNTs act like stress concentration zones and thus decrease the mechanical properties. This is in accordance with several authors [11, 29, 31]. For example, Jen et al. [31] showed that a high CNT content has an adverse effect on the strength because the stress concentration effects caused by the CNT agglomerates reduce the tensile strength of the nanocomposites.

As a result in the case of AlSi-2% wt. CNTs composite the fracture (crack) may initiates in the regions of agglomerates (stress concentration). If the crack reaches a region where the CNTs are well dispersed it may travel through the AlSi grain (intragranular fracture), but if the crack reaches zones of weakness (the zones where the agglomerates are located, between the AlSi grains), then the crack follows the grain of the material (intergranular fracture). The consequence of this is a rougher region where the agglomerates are formed and a smoother surface when the crack travels through the AlSi grain.

Even though there are these zones that behaves like stress concentrations (as called weakness zones), the strengthening effect of CNTs in the zones where the CNTs are well dispersed prevails, thus the overall properties of the AlSi 2% wt. CNT composite are higher that unreinforced AlSi alloy.

Thus, the increase in the tensile strength and yield strength with the addition of the CNTs is related to the fact that the AlSi grains are bonded with an improved strength due to CNTs interface reinforcement effect (Figure 6. 5-b), as stated for example by George et al [21] through the shear lag theory. It is well known that the mechanical properties of the composites are controlled by stress transfer between reinforcement phase and the metal matrix at the interface [26], so the CNTs act like load-bearing element, thus they protect the matrix (transfer of load from the matrix to the reinforcement by interfacial shear stress) [21,25,26].

The substantial decrease in rupture strain with addition of the CNTs suggests that there was an embrittlement of the composite. This means that the aluminium-silicon matrix (AlSi) suffered also from the other mechanisms, namely thermal mismatch (coefficient of thermal expansion of CNTs is $\approx 10^{-6}K^{-1}$ [21], while the measured value for AlSi alloy is $23x10^{-6}K^{-1}$) and/or Orowan looping or an enhanced dislocation density [21, 22, 25]. Thus, not only the reinforcing mechanism of the CNTs is present at the interface but also an effect of the CNTs in the matrix properties is active.

The proposed physical mechanisms for the fracture surface morphology for tensile tests for both unreinforced AlSi alloy and AlSi-2% wt. CNTs composite are schematically represented in Figure 6. 7.

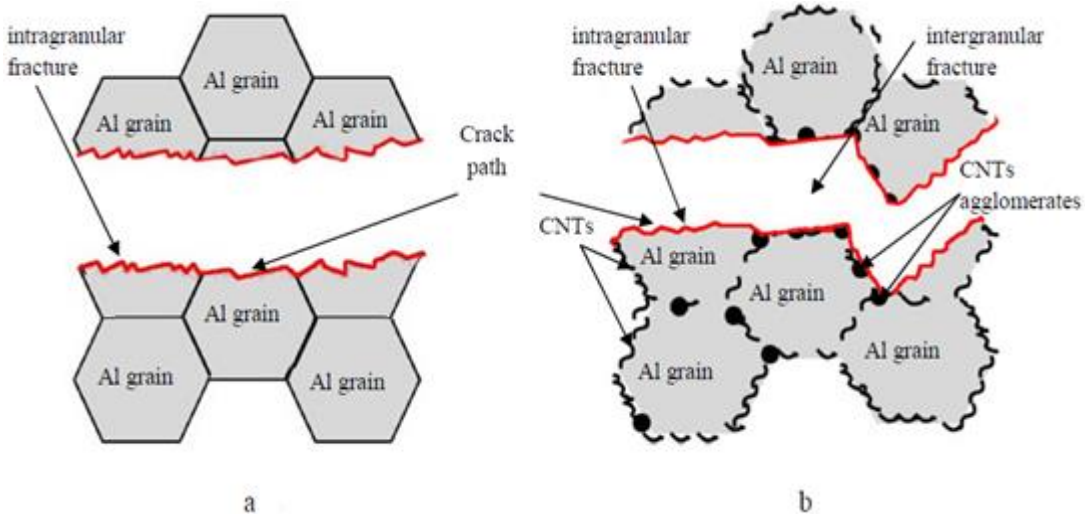

Figure 6. 7 - Schematic representation of the proposed physical model for the tensile tests: a. unreinforced AlSi alloy (intragranular crack) b. AlSi -2 wt. % CNT's composite (intragranular and intergranular crack).

6.4.2 Fatigue properties

The fatigue analysis reveals that it is possible to increase fatigue behaviour with the addition of CNTs. Figure 6. 8 shows the fatigue results obtained as S-N curves. It should be noted that the specimens contained a pre-notch, so life contains not only the initiation life bus also the propagation life.

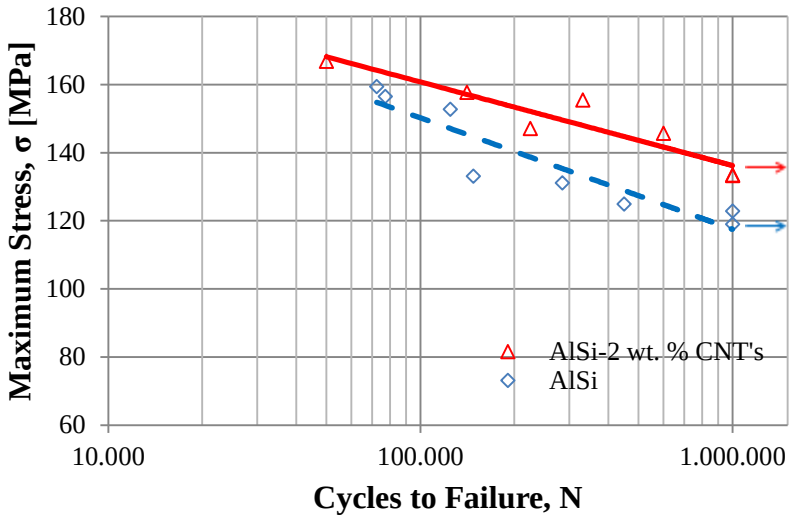

Figure 6. 8 - Maximum stresses (σ_{max}) vs. number of cycles to failure for unreinforced AlSi alloy and AlSi-2 wt. % CNT's composite.

It can be seen from Figure 6. 8 that under identical loading conditions the AlSi-2 wt. % CNTs composite has longer fatigue lives (continuous line – Figure 6. 8) and a higher fatigue life than the unreinforced AlSi alloy (dashed line – Figure 6. 8). It can be seen that at a stress level of about 140 MPa the fatigue life of AlSi-2% wt. CNT's composite increased by 270% compared to unreinforced AlSi alloy. The fatigue life is approximately 15% higher for the CNTs composite. These results are in line with some studies [31-33] where the fatigue life increased with the addition of CNTs. However, some other studies stated the opposite [29].

Figure 6. 9 presents the SEM images of the fracture surface morphologies of both the (a) unreinforced AlSi alloy and (b) AlSi-2% wt. CNT's composite (with different magnifications 500x and 5000x).

It can be clearly seen from Figure 6. 9-a that the crack path is very straight in the case of unreinforced AlSi alloy (smother surface), while in the case of AlSi-2% wt. CNTs composite (Figure 6. 9-b) the crack path is very tortuous (slightly rougher surface).

This observation indicates that in the case of the unreinforced AlSi alloy the crack travels through the grains of the material (intragranular fracture), due to the fact that the AlSi grains are very well bonded.

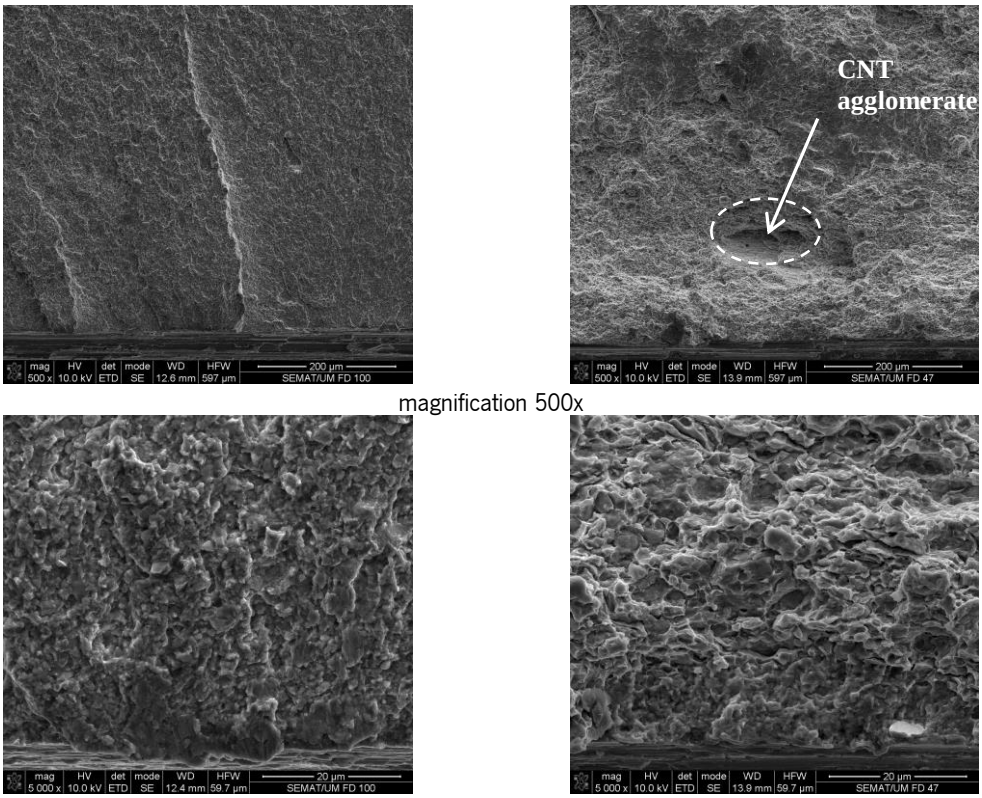

Figure 6. 9 - SEM images of the fracture surface after fatigue test of: (a) unreinforced AlSi alloy and (b) AlSi-2 wt. % CNT's composite(with different magnifications).

In the case of AlSi-2% wt. CNTs composite the fatigue crack may initiate in the region with agglomerations (fatigue cracks frequently initiates from the stress concentrated regions). If the crack reaches a region where the CNTs are well dispersed, the crack is deflected due to the stronger interface between matrix and CNT, then may travel through the AlSi grain (intragranular fracture). Crack deflection is a common effect in metal matrix composites [37]. If the crack reaches a region with agglomerates (zones of weakness) the propagation of the crack is accelerated. So, in the case of composite there is a mixture/competition between intragranular fracture and intergranular fracture. Thus, even though in the case of AlSi-2% wt. CNTs composite there are these weak regions (CNTs agglomerates) that may accelerate the crack propagation, CNTs act as interface barriers to crack propagation [31,32], increasing the fatigue life of the AlSi-2% wt. CNTs composite.

Figure 6. 10 presents a schematic representation of the proposed physical mechanisms for the fatigue tests for AlSi-2 wt. % CNTs composite.

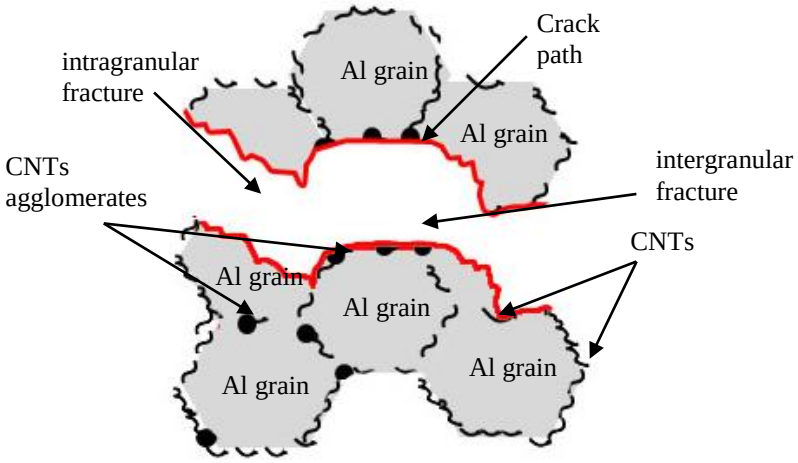

Figure 6. 10 - Schematic representation of the proposed physical model for fatigue tests for AlSi-2 wt. % CNT's composite.

6.4.3 Wear properties

The wear loss of both unreinforced AlSi alloy and AlSi-2% wt. CNTs composite are presented in Figure 6. 11.

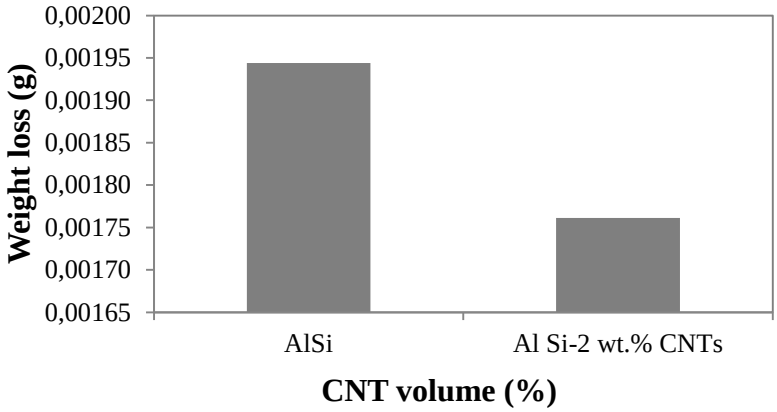

Figure 6. 11 - Wear loss as a function of the CNT content

It can be seen in Figure 6. 11 that a lower wear loss was obtained for AlSi-2% wt. CNT pin when comparing to unreinforced AlSi pin. This is in accordance with some previous studies [14,15-18,38] where wear loss substantially decreases with CNT content.

High resolution images (obtained by SEM) of the worn surfaces are shown in Figure 6. 12 for both AlSi and AlSi-2% wt. CNT pins. SEM images of the worn surfaces (Figure 6. 12 a and b - magnification 130x) reveal that there is a clear evolution in the worn surface topography from AlSi to AlSi-CNTs pins. The worn surface of AlSi pin (Figure 6. 12-a) is clearly rougher than the AlSi-2% wt. CNT pin (Figure 6. 12-d). On a closer view (Figure 6. 12-b and e - magnification 1000x – backscattered view) it seems that the roughening of the worn surface is closely related to the plastic deformation (adhesive wear) but also to the substantial number of voids that seem to be material detached from the bulk. Voids are in a bigger quantity on the worn surface of AlSi pin. In the higher magnification (Figure 6. 12-c and f – magnification 5000x) it is possible to observe the voids and what seems to be the grain/powder boundaries. It is interesting to observe that the voids, mainly in the AlSi-2% wt. CNTs composite, have about the size of the Al powders (≈20-40 μm) used for sintering. Thus the detached areas are aluminium grains. In the unreinforced AlSi alloy it seems that various grains may be detached together. This happens simultaneously with improved wear resistance (Figure 6. 11) for the AlSi-2% wt. CNTs composite.

Thus, it can be concluded that wear damage of reinforced AlSi alloy - based pins seems to be controlled essentially by two mechanisms: adhesive wear that includes material transfer between the mating surfaces, and pull-out of grains/particles (Figure 6. 12). Regarding the pull-out mechanism correlation with CNTs content it can be verified that by introducing CNTs it becomes more difficult to grains/powders to be detached from the bulk. They are detached in a smaller quantity. This is in agreement with the shear lag theory and the fact that CNTs are located at the interfaces between Al powders/grains. The strengthening mechanism of CNTs in AlSi sintered parts takes place by increasing the strength or cohesion between Al powder or grain interfaces. This grain detachment mechanism is schematically represented in Figure 6. 13.

The proposed grain detaching mechanism seems to be evident of Figure 6. 12 on the backscattered view ((b) and e)). It shows clearly the CNTs on the grains interface of the detached grains. The small white points are mainly CNTs and the white colour comes from the nickel CNT coating/functionalization [35]. It is worth to mention that some white points (both in unreinforced AlSi alloy and also in AlSi-2% wt. CNTs composite) correspond to iron-rich areas that result from transfer of material from the mating GCI plate (grey cast iron) to the pin. However in the AlSi-2% wt. CNTs composite case (Figure 6. 12-e) the white points are mainly CNTs, in the isolated form or in agglomerates, as shown in a previous work [35].

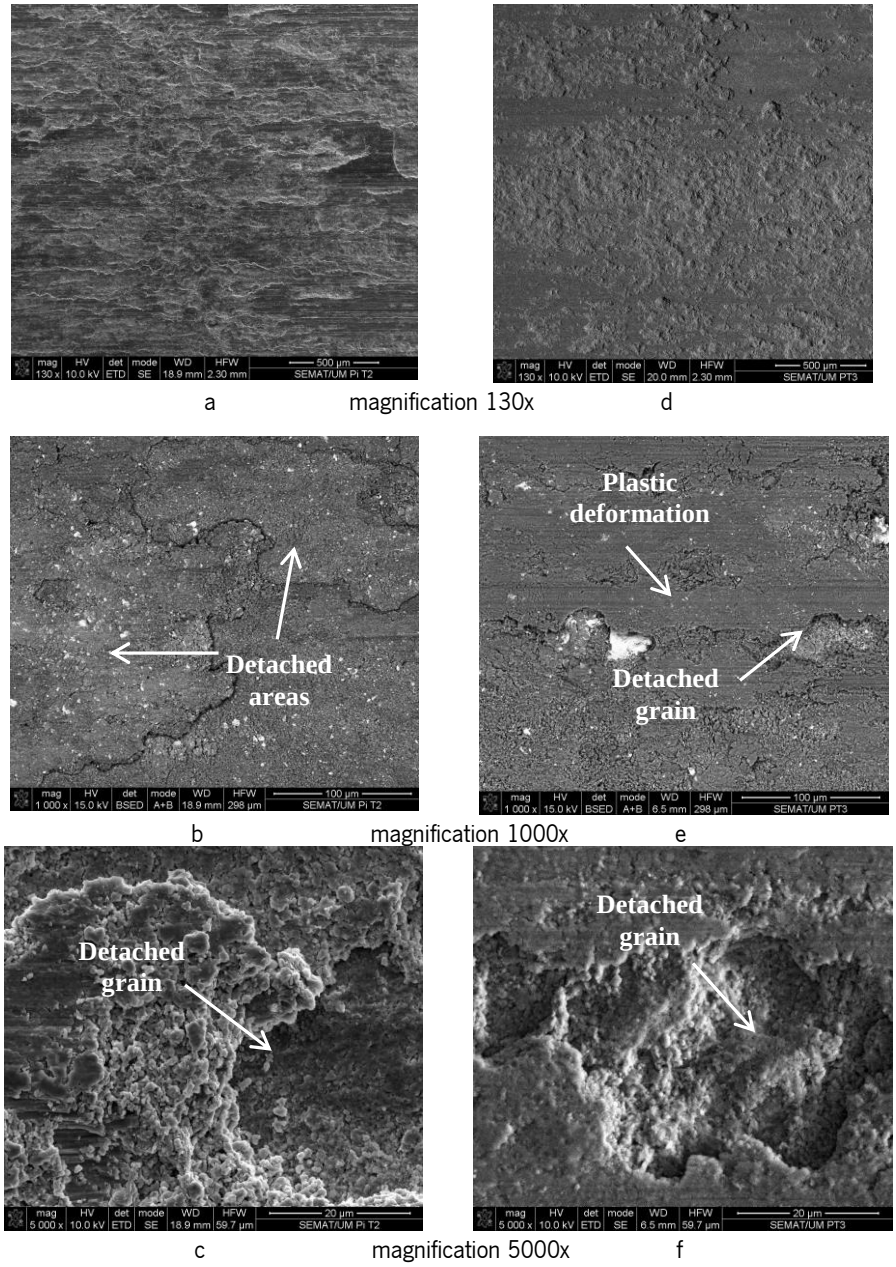

Figure 6. 12 - SEM images of the worn surface of unreinforced AlSi alloy (a), (b) and (c); and AlSi-2 wt.% CNT's composite (d), (e) and (f); b) and e) is a backscattered view.

Based on the previous results it seems that the main mechanisms, as observed in the fracture morphologies of tensile, fatigue, and wear test results, are: a stronger adhesion between AlSi grain interfaces due to the CNTs, and the effect of the CNT's reinforcement on the matrix most probably due to restrictions on matrix dislocations. This is basically in accordance with some of the proposed mechanisms, by George et al [21] namely thermal mismatch, Orowan looping and shear

lag theory or also with Zang and co-authors [22] or even with Bustamante et al. [7] suggested mechanisms.

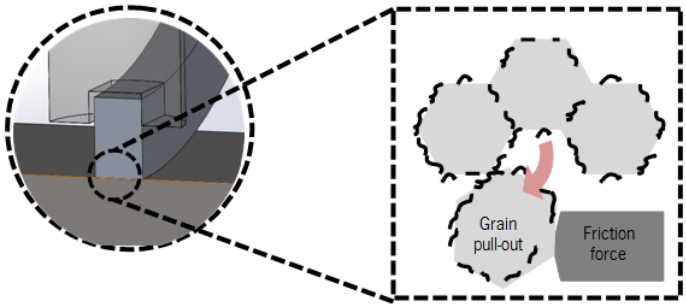

Figure 6. 13 - Schematic representation of the proposed physical model for the wear test: AlSi grains are bonded with an improved strength due to CNT's interface reinforcement effect. Friction force (pin) cause pull-out of the grains.

6.5 Conclusions

From the present investigation on mechanisms governing the tensile, fatigue and wear behaviour of CNT's reinforced AlSi alloy, the following conclusions can be drawn:

- Compared to unreinforced AlSi alloy the tensile strength, σ_r and yield strength σ_y of AlSi – 2 wt. % CNTs composite was enhanced. The mechanisms responsible for improvement on the mechanical performance are based on the interface reinforcement and also on the matrix hardening;

- Compared to unreinforced AlSi alloy the fatigue life of AlSi – 2 wt. % CNTs composite was notably increased. This can be attributed to the strengthening of the interfaces and to the crack path deflection due to CNTs that are placed at the interfaces;

- Compared to unreinforced AlSi alloy the wear behaviour of AlSi – 2 wt. % CNTs composite was improved. Wear mechanisms of AlSi-CNT composites were characterized dominantly by adhesive wear and also by an improved resistance to grain detachment, being this last responsible by wear resistance improvement due to the CNT content. This means that a stronger interface between grains was promoted by the CNTs.

CNTs seem to be a good choice as reinforcement on AlSi alloy to improve mechanical, wear, and fatigue behaviours of AlSi-CNT composites. CNT's reinforcement effect is active simultaneously in all previous properties and the reinforcement physical mechanism seems to be essentially due to a reinforcement effect of the interface that seems to be similar in all mentioned mechanical solicitations.

6.6 Acknowledgements

This work was supported by the Portuguese Foundation of Science and Technology through the project references PTDC/EME-PME/68664/2006 and EXCL/EMS-TEC/0460/2012.

6.7 References

[1] H. Presting, and U. Konig. 2003. Future nanotechnology developments for automotive applications.Mater. Sci. Eng. C. 23: 737–741.
[2] R.P. Bustamante, I.E. Guel, W.A. Flores, M.M. Yoshida, P.J. Ferreira, and R. Martínez-Sánchez. 2008. Novel Al-matrix nanocomposites reinforced with multi-walled carbon nanotubes. Alloy Compd. 450: 323–326.
[3] R.S. Rana, R. Purohit and S. Das. 2012. Review of recent Studies in Al matrix composites, IJSER 3: 1-16.
[4] V.N. Popov. 2004. Carbon nanotubes: properties and application, Mat. Sci. Eng. R. 43: 61-102.
[5] S.R. Dong, J.P. Tu and X.B. Zhang. 2001. An investigation of the sliding wear behavior of Cu-matrix composite reinforced by carbon nanotubes. Mater. Sci. Eng. A 313: 83–87.
[6] W.X. Chen, J.P. Tu, L.Y. Wang, H.Y. Gan, Z.D. Xu and X.B. Zhang. 2003. Tribological application of carbon nanotubes in a metal-based composite coating and composites. Carbon 41: 215-222.
[7] R. Pérez-Bustamante, C.D. Gómez-Esparza, I. Estrada-Guel, M. Miki-Yoshida, L. Licea-Jiménez, S.A. Pérez-García and R. Martínez-Sánchez. 2009. Microstructural and mechanical characterization of Al–MWCNT composites produced by mechanical milling. Mater. Sci. Eng. A. 502: 159–163.
[8] S.R. Bakshi, A.K. Keshri and A. Agarwal. 2011. A comparison of mechanical and wear properties of plasma sprayed carbon nanotube reinforced aluminum composites at nano and macro scale. Mater. Sci. Eng. A. 528: 3375–3384.
[9] S.E. Shin and D.H. Bae. 2013. Strengthening behaviour of chopped multi-walled carbon nanotube reinforced aluminum matrix composites. Mater. Charact. 83: 170– 177.
[10] K. Balani and A. Agarwal. 2008. Multiscale wear of plasma-sprayed carbon-nanotube-reinforced aluminum oxide nanocomposite coating. Acta Mater. 56: 5984–5994.
[11] T. Laha, Y. Chen, D. Lahiri and A. Agarwal. 2009. Tensile properties of carbon nanotube reinforced aluminum nanocomposite fabricated by plasma spray forming. Composites: Part A. 40: 589–594.
[12] A.M.K. Esawi, K. Morsi, A. Sayed, A.A. Gawad and P. Borah. 2009. Fabrication and properties of dispersed carbon nanotube–aluminum composites. Mater. Sci. Eng. A. 508: 167–173.

[13] A.M.K. Esawi, K. Morsi, A. Sayed, M. Taher and S. Lanka. 2010. Effect of carbon nanotube (CNT) content on the mechanical properties of CNT-reinforced aluminium composites. Compos Sci. Technol.70: 2237–2241.
[14] K.T. Kim, S.I. Cha, S.H. Hong and S.H. Hong. 2006. Microstructures and tensile behaviour of carbon nanotube reinforced Cu matrix nanocomposites. Mater. Sci. Eng. 430: 27-33.
[15] H.J. Choi, S.M. Lee and D.H. Bae. 2010. Wear characteristic of aluminium-based composites containing multi-walled carbon nanotubes. Wear 270: 12–18.
[16] I.Y. Kim, J.H. Lee, G.S. Lee, S.H. Baik, Y.J. Kim and Y.Z. Lee. 2009. Friction and wear characteristics of the carbon nanotube–aluminium composites with different manufacturing conditions. Wear 267: 593–598.
[17] S. Zhou, X. Zhang, Z. Ding, C. Min, G. Xu and W. Zhu. 2007. Fabrication and tribological properties of carbon nanotubes reinforced Al composites prepared by pressureless infiltration technique. Compos Part A-Appl S. 38:301–306.
[18] A.M. Al-Qutub, A. Khalil, N. Saheb and A.S. Hakeem, Wear and friction behaviour of Al6061 alloy reinforced with carbon nanotubes, Wear, vol. 29, pp. 7752–761, 2013.
[19] I. Sridhar and K.R. Narayanan. 2009. Processing and characterization of MWCNT reinforced aluminum matrix composites. J. Mater. Sci. 44: 1750–1756.
[20] D. Bikiaris. 2010. Microstructure and Properties of Polypropylene/Carbon Nanotube Nanocomposites. Materials 3: 2884-2946.
[21] R. George, K.T. Kashyap, R. Rahul, S. Yamdagni. 2005. Strengthening in carbon nanotube/aluminium (CNT/Al) composites. Scripta Mater 53: 1159–1163.
[22] Z. Zhang and D.L. Chen. 2006. Consideration of Orowan strengthening effect in particulate-reinforced metal matrix nanocomposites: A model for predicting their yield strength. Scripta Mater 54: 1321–1326.
[23] H.J. Choi and D. Bae. 2011. Strengthening and toughening of aluminum by single-walled carbon nanotube. Mater. Sci. Eng. A. 528: 2412–2417.
[24] H.J. Choi, B.H. Min, J.H. Shin and D.H. Bae. 2011. Strengthening in nanostructured 2024 aluminum alloy and its composites containing carbon nanotubes. Composites: Part A 42: 1438–1444.
[25] S.J. Yoo, S.H. Han and W.J. Kim. 2013. Strength and strain hardening of aluminum matrix composites with randomly dispersed nanometer-length fragmented carbon nanotubes. Scripta Mater 68: 711–714.
[26] H.J. Ryu, S.I. Cha and S.H. Hong. 2003. Generalized shear-lag model for load transfer in SiC/Al metal-matrix composites. J. Mater. Res.18: 2851-2858.
[27] D .Lahiri, S.R. Bakshi, A.K. Keshri and A. Agarwal. 2009. Dual strengthening mechanisms induced by carbon nanotubes in roll bonded aluminum composites. Mater. Sci. Eng. A. 523: 263–270.
[28] M. Paramsothy, J. Chan, R. Kwok and M. Gupta. 2011. Addition of CNTs to enhance tensile/compressive response of magnesium alloy ZK60A. Composites: Part A. 42: 180–188.
[29] C.S. Goh, J. Wei, L.C. Lee and M. Gupta. 2008. Ductility improvement and fatigue studies in Mg-CNT nanocomposites. Compos Sci. Technol. 68: 1432–1439.
[30] Y.M. Jen and Y.H.Yang. 2010. A study of two-stage cumulative fatigue behaviour for CNT/epoxy composites. Procedia Eng. 2: 2111–2120.
[31] Y.M. Jen and Y.C. Wang. 2012. Stress concentration effect on the fatigue properties of carbon nanotube/epoxy composites. Composites: Part B. 43: 1687–1694.
[32] M.R. Loos, J. Yang, D.L. Feke, I. Manas-Zloczower, S. Unal and U. Younes. 2013. Enhancement of fatigue life of polyurethane composites containing carbon nanotubes. Composites: Part B. 44: 740–744.

[33] N. Yu, Z.H. Zhang and S.Y. He. 2008. Fracture toughness and fatigue life of MWCNT/epoxy composites. Mater. Sci. Eng. A. 494: 380–384.
[34] O. Carvalho, G. Miranda, D. Soares and F.S. Silva.2013. CNT-reinforced aluminium composites: processing and mechanical properties. Conference of Sociedade portuguesa de Materiais, 25-27 March, Coimbra, Portugal.
[35] O. Carvalho, M. Buciumeanu, D. Soares, J Gomes and F.S. Silva. 2014. Optimizing the wear behaviour of Al/cast iron tribopair by reinforcing an Al alloy with CNT's, Submitted to Tribol Trans.
[36] J.A. Williams. 1994. Engineering tribology. Oxford University Press.
[37] J.K. Shang, W. Yu and R.O. Ritchie. 1988. Role of silicon carbide particles in fatigue crack growth in SiC-particulate-reinforced aluminum alloy composites. Mater. Sci. Eng. A 102: 181–192.
[38]T. Threrujirapapong, K. Kondoh, J. Umeda and H. Imai. 2008. Friction and wear behaviour of titanium matrix composite reinforced with carbon nanotubes under dry conditions. Intra of JWRI. 37: 51-56.

7 Dry sliding wear behaviour of AlSi-CNTs-SiCp hybrid composites

O. Carvalho[1], M. Buciumeanu[2], S. Madeira[1], D. Soares[1], F. S. Silva[1], G. Miranda[1]

[1]CT2M – Centre for Mechanical and Materials Technologies, University of Minho, Azurém, 4800-058 Guimarães, Portugal

[2]Cross–Border Faculty of Humanities, Economics and Engineering, "Dunarea de Jos" University of Galati, Domneasca 47, 800008 Galati, Romania

Published in Tribology International, 90 (2015) 148–156

7.1 Abstract

The aim of this paper was to examine the wear behaviour of a hybrid AlSi-2wt. %CNTs-5wt.%SiCp composite. For comparison purposes the unreinforced AlSi alloy, AlSi-2%wt.CNTs and AlSi-5wt.%SiCp composites were used. A powder metallurgy processing route was used to produce the unreinforced AlSi alloy and AlSi composites. Dry reciprocating pin-on-plate wear tests were performed and the results showed that the wear behaviour was improved for all produced composites when compared to the unreinforced AlSi alloy. However the best wear behaviour was achieved in the case of AlSi hybrid composite. This improvement is attributed to the combine effects of both constituent reinforcements. The dominant wear mechanisms were characterized by scanning electron microscopy with X-Ray Energy Dispersive Spectrometry analysis.

Keywords: CNTs; AlSi- hybrid composites; SiCp; sliding wear.

7.2 Introduction

It is well known that the specific strength of the materials used in the aerospace, aircraft and automotive industries is a key factor [1, 2]. Besides, these materials should exhibit a good compromise between mechanical, physical and tribological properties. For example, in practice the piston rings damage is attributed first to wear, then to lubrication and fatigue [2]. Aluminium-silicon (AlSi) alloy is a good choice for engine components [1, 3], due to their satisfactory

mechanical and wear properties. The reinforcements incorporated in the Al alloys are used to increase desired properties, which make them attractive for specific applications. Some of reinforcements used in the case of Al alloys are SiCp [4-6], Al_2O_3 [7], TiC [8], TiAl [9], B_4C [10], TiB_2 [11], CNTs [12-15], graphite [16], etc. Regarding the processing route, it is well known that by powder metallurgy (PM) it is possible to obtain a very good distribution of the particles. It should me also mentioned that the hot pressing allows a good densification process [17].

Regarding aluminium (Al) alloy reinforced by carbon nanotubes (CNTs), and to the authors' knowledge, there are only few studies [12-15, 17-20] that are concerned with their wear behaviour. Most of the previous studies demonstrated that the CNTs are an effective reinforcement for improving wear characteristics of Al based composites [12-15]. The wear behaviour is explained based on CNT dispersion, CNT agglomeration size and fraction and carbide formation [12]. Regarding the coefficient of friction (COF) as reported by other studies [12-15, 17-20] it decreases with CNTs content, possibly due to the self lubrication effect of carbon content. Also, it was observed a reduction on COF when the agglomerations are formed (improving the wear resistance), as they act as a lubricant between the contacting surfaces [12]. It has been reported that there is a critical CNTs agglomeration concentration, above which starts the well known detrimental effect. Regarding the effect of CNTs content (from 2 wt.% to 6 wt.% CNTs) over the mechanical and wear behaviour of AlSi-CNTs composites, it was concluded on a previous research work of the same authors [21,22] ,that in the case 2wt.%CNTs content there is an equilibrium among improvement in mechanical properties in the different tests namely tensile, fatigue and wear. It was concluded that the 2wt.%CNTs was the optimal CNTs content for tensile properties.

Thus, in order to improve wear properties without reducing tensile values, another reinforcement, that would introduce a different strengthening mechanism or the some strengthening mechanism, but at a different scale, would be necessary. SiCp as a second reinforcement, was used in the present work. SiCp as reinforcement of Al alloys, has been tested by several authors [4-6,23]. According to Mondal et al. [23] there are some factors that may explain improvement on wear resistance such as: (1) the hard SiCp are protruded on the surface, and thus it will lead to a rougher surface; (2) the debris get accumulated around the SiCp.

So, by adding SiCp to the AlSi-2%wt.CNTs composite, it may lead to new advanced composite materials so-called hybrid metal matrix composites (HMMC) [16,24-26]. The increase in wear resistance in the case of hybrid composites was reported by several authors [16, 25, 26].

It has been proved that by adding graphite to an AlSi- SiCp [23] as a second reinforcement, the wear rates of the hybrid composite compared to SiCp reinforced composite decreased. As reported by Aruri et al. [26] the increase on wear resistance of both hybrid composites studied (Al-SiCp/Al_2O_3 and Al-SiCp/graphite) was attributed to the presence of both reinforcements. SiC particles acted like load bearing elements, while graphite acts like a solid lubricant. Also, Ames et al. [16] reported the improvement of wear behaviour when two reinforcements were added to an aluminium alloy (3 % graphite-20 % SiCp-A356). The higher wear rate was attributed also to the load bearing effect of SiC particles, but they reported that SiCp may also act as abrasives and can machine the counterface.

This paper investigates the wear behaviour of an AlSi alloy reinforced by Multi-Wall Carbon Nanotubes (MWCNT) and SiC particles. The main purpose was to determine the combined effects (the advantages) of both constituent reinforcements (CNTs and SiCp) on wear behaviour in dry reciprocating sliding conditions. The purpose is to clarify if, when a certain reinforcement reached its optimal beneficial effect, another reinforcement could further increase the composites properties without compromising other relevant properties.

7.3 Experimental procedure

7.3.1 Fabrication of AlSi composites

An AlSi alloy, powders size < 325 mesh (< 44 μm), with chemical composition as listed in Table 7. 1, was used as matrix material. AlSi powder was purchased from AlfaAesar – Germany.

Ni coated MWCNTs (outer diameter > 50 nm, length 0.5-2.0 μm, purity before coating>95wt% and ash < 1.5wt%), and SiC particles (with 13 μm in size) were used as reinforcements. Ni coated MWCNTs were purchased from CheapTubes.com – USA.

The AlSi-matrix composites were processed by the traditional hot isostatic pressing (HIP) technique. Applied pressure was $35x10^6$ Pa for 10 minutes at 550°C under vacuum (10^{-2} mbar). The mixing of the AlSi powders was made inside a closed stainless steel jar along with 12 steel milling balls (10 mm in diameter). The ball powder ratio is 10:1. The bottle rotated with constant speed (40 rpm) during 6 days (low-energy ball milling).

Table 7. 1 - Chemical composition of AlSi alloy (wt.%)

Al	Si	Fe	Others
87.3	11	0.20	1.5

7.3.2 Microstructural and chemical characterization

The obtained AlSi composites and the worn surfaces (to observe the dominant wear mechanisms) were characterized by means of Scanning Electron Microscopy (SEM) / Energy Dispersive Spectrometry (EDS).

7.3.3 Hardness tests

Vickers hardness tests were conducted according to standards, using a Shimadzu microhardness tester. Hardness measurements were conducted for all AlSi composites. Sixteen readings were taken for each condition from which the average value was calculated. The hardness tests were carried out with a load of 200 gf during 15 s.

7.3.4 Details of the reciprocating wear tests

A reciprocating pin-on-plate tribometer PLINT-TE67/R was used to evaluate the wear characteristics of AlSi composites/GCI sliding pairs. Pins were machined from the unreinforced AlSi alloy and AlSi matrix composites (AlSi-2wt.%CNTs, AlSi-5wt.%SiCp and AlSi-2wt.%CNTs-5wt.%SiCp).

The dimensions of the pins are: radius of curvature 40 mm, thickness 3.5 mm and the arc length 20 mm. This AlSi composite can eventually be used for engine pistons or compression piston rings.

The counterpart consisted of plates (40×18×5 mm) that were machined from grey cast iron (GCI) with a hardness of 338 HV. Table 7. 2 presents the chemical composition of GCI.

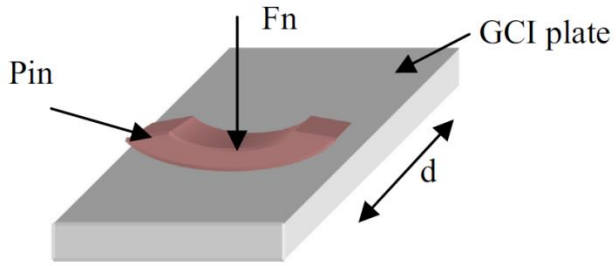

Figure 7. 1- Schematic test configuration: Fn – Normal applied load; d – alternated displacement amplitude

Table 7. 2 - Chemical Composition of GCI

Fe	C	Mn	Si	P	Cr	Ni	Cu	S	Mo	Others
90.4	3.59	0.392	2.37	0.624	0.249	1.52	0.28	0.023	0.007	0.545

Figure 7. 1 shows a schematic representation of the test performed in this work: applied normal load (Fn) on the pin and alternative displacement (d) of the GCI plate. Experiments were carried out with a normal load of 10 N and relative displacement amplitude of 10 mm, for a sliding distance of 148 m (for 2 hours), at a sliding speed of about 0.02 m/s. During the tests compressed air was flown to the contact zone in order to remove loose wear debris. The frequency of the reciprocating motion was 1 Hz for all tests. All wear tests were carried out under the same conditions. The only variable was the material of the pins (the reinforcement – CNTs, SiCp or CNTs-SiCp). An unreinforced AlSi alloy was used for comparison purposes. All tests were performed in environment temperature (20 ± 2°C).

The data acquisition system associated to the tribometer recorded different testing variables including coefficient of friction and sliding distance. Both pin and GCI plate were cleaned ultrasonically in alcohol before and after the tests and the amount of wear was measured by weight loss. The dominant wear mechanisms were characterized by SEM/EDS analysis.

7.4 Results and discussion

7.4.1 Microstructural characterization

Microstructures of the unreinforced AlSi alloy and all AlSi matrix composites (after etching) are presented in Figure 7. 2.

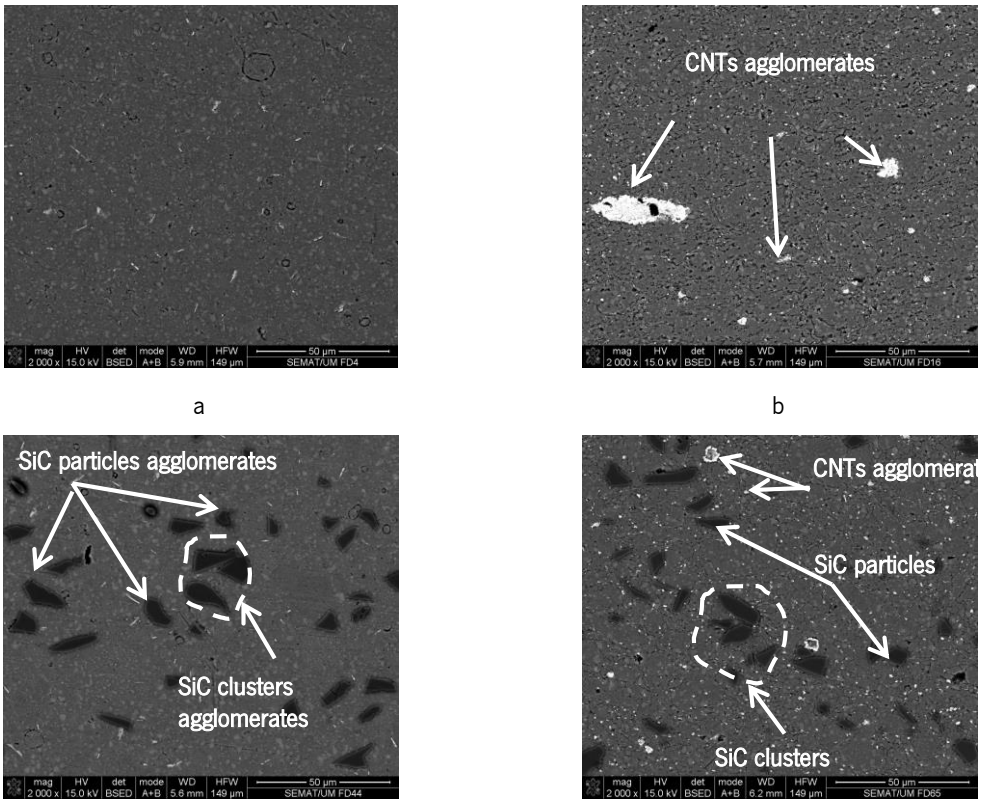

a b

c d

Figure 7. 2 - SEM images of the composites microstructures: a. unreinforced AlSi alloy; b. AlSi-2%wt.CNTs; c. AlSi-5wt.%SiCp and d. AlSi-2%wt.CNTs-5% wt.SiCp.

SEM images revealed that CNTs, as expected are placed at the grain interfaces and also that there are some CNTs agglomerates (Figure 7. 2-b). In a previous work of the same authors [31] it has been shown that more than 93% of the agglomerates are less than 1 μm^2 in area. The CNTs correspond to the white dots/areas. The average AlSi grain size is around 6 μm.

Figure 7. 2-c shows the AlSi microstructure for 5wt.%SiCp, where can be seen the black SiC particles distributed in AlSi matrix. The SiC particles are visible at the grain interfaces as reported also by Balani et al. [27] and no interface was formed between SiC particles and AlSi matrix. Walczak et al. [28] reported that there can be formed interface between SiC particles and AlSi matrix, but if the processing route is other then HIP technique (e.g. squeeze casting route [27, 29]).

Figure 7. 2-d shows the microstructure of the hybrid composite (Al-2wt.%CNTs-5wt.%SiCp). It can be observed the composite reinforcement (black SiC particles and the CNTs). There can be

observed some CNTs agglomerates. The addition of SiCp seems that does not have any influence on the distribution of the CNTs.

In both AlSi-5wt.%SiCp and Al-2wt.%CNTs-5wt.%SiCp composites can be observed that some SiC particles can form also clusters (Figure 7. 2-c and d). These clusters can act like stress concentrations leading to microplasticity, as stated by other authors [30,31].

7.4.2 Hardness values

Figure 7. 3 shows the hardness results in the case of unreinforced AlSi alloy and of AlSi-composites.

As expected, the hardness increases with addition of the reinforcements (CNTs or SiCp). As compared to the unreinforced AlSi alloy, the AlSi-2%wt.CNT composite shows an increase on hardness of about 25%, as reported in another study of the same authors [22], while in the case of AlSi-5%wt.SiC composite of about 27%. The increase of hardness was higher in the case of hybrid composite, about 36%.

The hardness results are in accordance with the other studies [32-34] and the main factor that governs the increase of hardness in both cases seems to be the volume fraction of the reinforcement.

The increase in hardness with the addition of the CNTs may eventually be explained based on the fact that the CNTs placed at the grain interfaces, create barriers to dislocations thus increasing strain hardening during plastic deformation, as reported by D.P. Mondal et al. [33].

Regarding the increase in hardness of AlSi-5wt.%SiCp compared to unreinforced AlSi alloy is in accordance to other previous studies [32, 35]. The increase in hardness was attributed to the high dislocation density in matrix induced by thermal mismatch between the matrix and the reinforcement [27] and to the harder reinforcements that impeded the movement of dislocations [24].

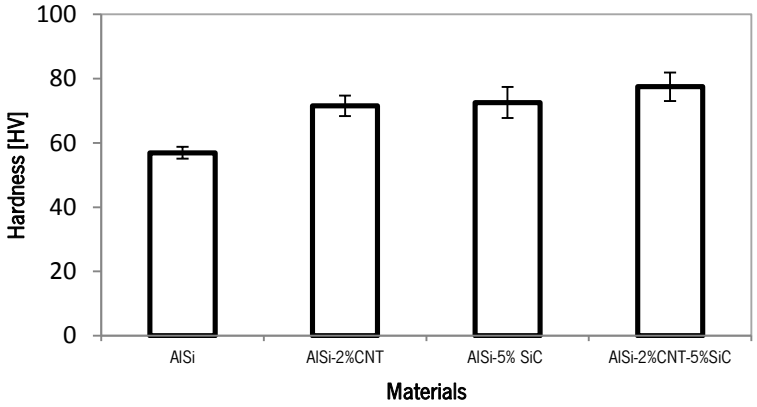

Figure 7. 3 - Hardness of the unreinforced AlSi alloy and all AlSi composites.

In the case of the hybrid composites the hardness increased as compared to unreinforced AlSi alloy and to studied AlSi composites (Figure 7. 3). These results are in accordance with the other studies [24, 26, 36]. The increase of hardness is due to strengthening effects of both reinforcements SiCp and CNTs (Shear lag [37], Thermal mismatch [25, 27] and Orowan looping [38,39]). Due to different properties, shape and size of both reinforcements, it is expected that they have different contribution on the previously mentioned models. The behaviour of hybrid composites is a sum of inherent advantages and disadvantages of both reinforcements. Some other authors have been already proved the additional effect of the reinforcements on mechanical properties [24, 27].

7.4.3 Wear loss

The volume losses of the AlSi pins (unreinforced AlSi alloy and AlSi - composites) and also of the mating GCI plates are shown in Figure 7. 4.

When comparing all AlSi composites with the unreinforced AlSi alloy it can be clearly seen that the wear of all studied composites is less than that of unreinforced alloy.

The wear volume decreased with the addition of CNTs or SiCp, and it further decreased with the incorporation of both reinforcements (CNTs and SiCp).

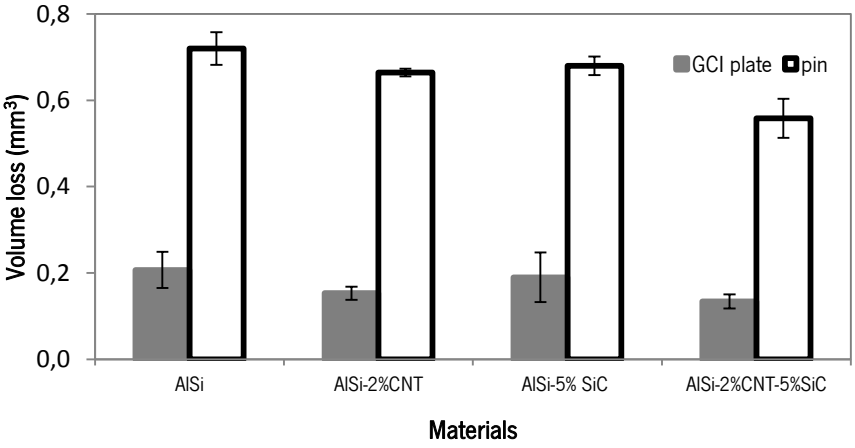

Figure 7. 4 - Variation on volume loss for unreinforced AlSi and AlSi - composites

In the case of AlSi-2wt.%CNTs/GCI tribopair the volume loss decreased with about 8% for the AlSi-2wt.%CNTs composite (pin) and 29% for the GCI plate, as compared with the contact involving unreinforced AlSi alloy/GCI [21]. As demonstrated by other studies [12-15, 18, 40], CNTs in the case of Al-matrix composite are an effective reinforcement for improving wear characteristics. The improvement in wear behaviour is explained in terms of CNTs dispersion in the matrix [15], CNTs agglomeration size and fraction [19], and on self lubricating effect of carbon content [13].

In the case of AlSi-5wt.%SiCp/GCI tribopair the volume loss decreased about 6 % for the pin and 10% for the GCI plate, as compared with the contact involving unreinforced AlSi alloy/GCI. The improvement on wear behaviour when SiCp are incorporated into the AlSi alloy is in accordance with some other studies [4-6, 23].

In the case of AlSi-2wt.%CNTs-5wt.%SiCp/GCI tribopair the volume loss decreased about 22% for the pin and 38% for the GCI plate, as compared with the contact involving unreinforced AlSi alloy/GCI. The combine effect of both reinforcements CNTs and SiCp in the AlSi matrix seem to have a beneficial role, once both pin and counterface material exhibited a reduction in wear volume, as compared to unreinforced AlSi/GCI tribopair and also to the AlSi composites/GCI tribopairs.

Also in the present study the SiCp act like load bearing element and the CNTs have self-lubrification effect. These effects will be later explained in the paper. Both reinforcements have a strengthening effect on the AlSi matrix, which also contributes to a better wear behaviour.

It is worth to highlight that in the present work, by improving the wear resistance of all studied AlSi composites (pins), it was also improved the wear resistance of other part involved in the sliding contact (GCI plate). In practice it is desirable to achieve optimal operating condition of the system (as called tribosystem optimization).

7.4.4 Coefficient of friction

Figure 7. 5 shows the evolution of the coefficient of friction (COF) with sliding distance in the case of AlSi-2wt.%CNTs-5wt.%SiCp hybrid composite against GCI. It is observed a typical evolution of the COF with the sliding distance for a reciprocating sliding wear test. After a first period corresponding to the running in regime (where surfaces adapt to each other and COF changes significantly during the first period of sliding, increasing with the sliding distance) the COF enters in steady-state conditions and remains approximately constant during the whole test.

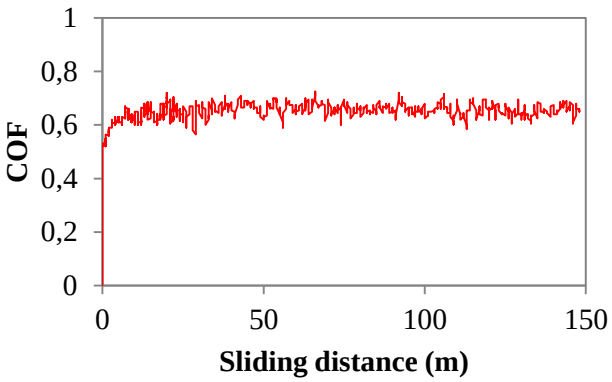

Figure 7. 5 - Evolution of COF with sliding distance of AlSi-2wt.%CNTs-5wt.%SiCp hybrid composite.

Figure 7. 6 presents the average COF for unreinforced AlSi alloy and of AlSi - composites. It can be seen that there is a slight decrease of COF values of the AlSi-composites as compared to unreinforced AlSi alloy. The COF values obtained in this study for AlSi – composites are approximately the same.

Regarding the slight decrease of COF with the addition of CNTs, as reported in another study of the same authors [22], as the counterpart is a GCI and, consequently, there is a substantial amount of free carbon compared to the eventual contribution of carbon due to the CNTs content.

The CNTs have two contributions on tribological behaviour of the composite: self lubrication effect and strengthening effect (increase the bonding between the grains on the Al matrix), so it is more difficult to remove them as confirmed by the mechanical properties results from another study of the same author [21]. Due to their shape and size, mainly the CNTs that come from the agglomerates could roll between the mating surfaces [41]. The agglomerates would have a higher effect on tribological properties if are released into the contact. There can be a disaggregation of these agglomerations due to the shear forces, leading to the appearance of individual CNTs that could roll into the sliding contact [41]. Once the CNTs are released may behave as a third body that contributes to wear.

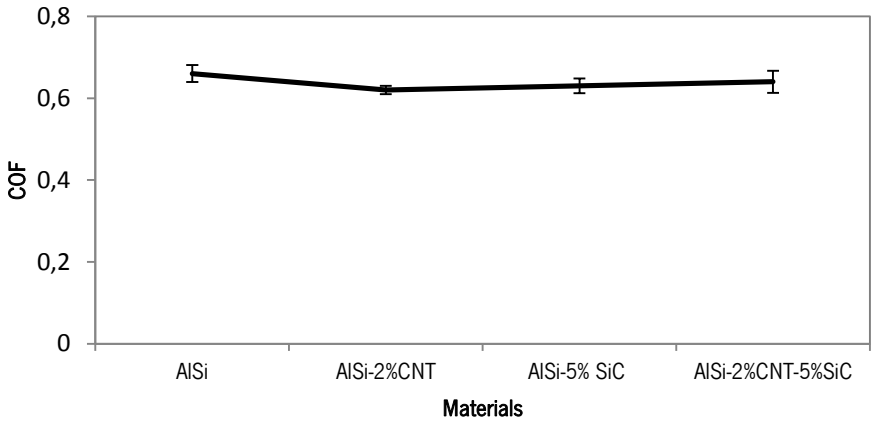

Figure 7. 6 - Average COF of the unreinforced AlSi alloy and of the Al-Si composites.

The slight decrease of COF value observed in the case of AlSi alloy reinforced with SiCp as compared to unreinforced AlSi alloy can be explained based on the two mechanisms adhesion and abrasion. Related to adhesion there are two factors that may contribute to reduction of COF values: (i) the higher hardness of the matrix due to the presence of hard SiCp. Therefore, it is expected less adhesion between the pin composites and GCI plate; (ii) the presence of SiCp which work as load bearing elements [26, 42] protect the matrix from wear. Regarding the second mechanism, abrasion, it is expected a higher COF values because the harder SiCp may penetrate the counter surface, as stated in [23]. The presence of the SiCp also increases the hardness of the composite and is more difficult to cut down the picks of roughness, thus it is expected more abrasion of the SiCp and a harder matrix, as stated by Zhou et al. [15]. Therefore, due to the combination of less adhesion and more abrasion, there is only a slight decrease on COF value. Later in this paper these mechanisms will be better explained based on the morphological analysis of both contact pairs.

7.4.5 Wear mechanism - SEM and EDS analysis

GCI plates

Figure 7. 7 shows SEM images of the worn surfaces of GCI plates after sliding against unreinforced AlSi alloy and AlSi composites.

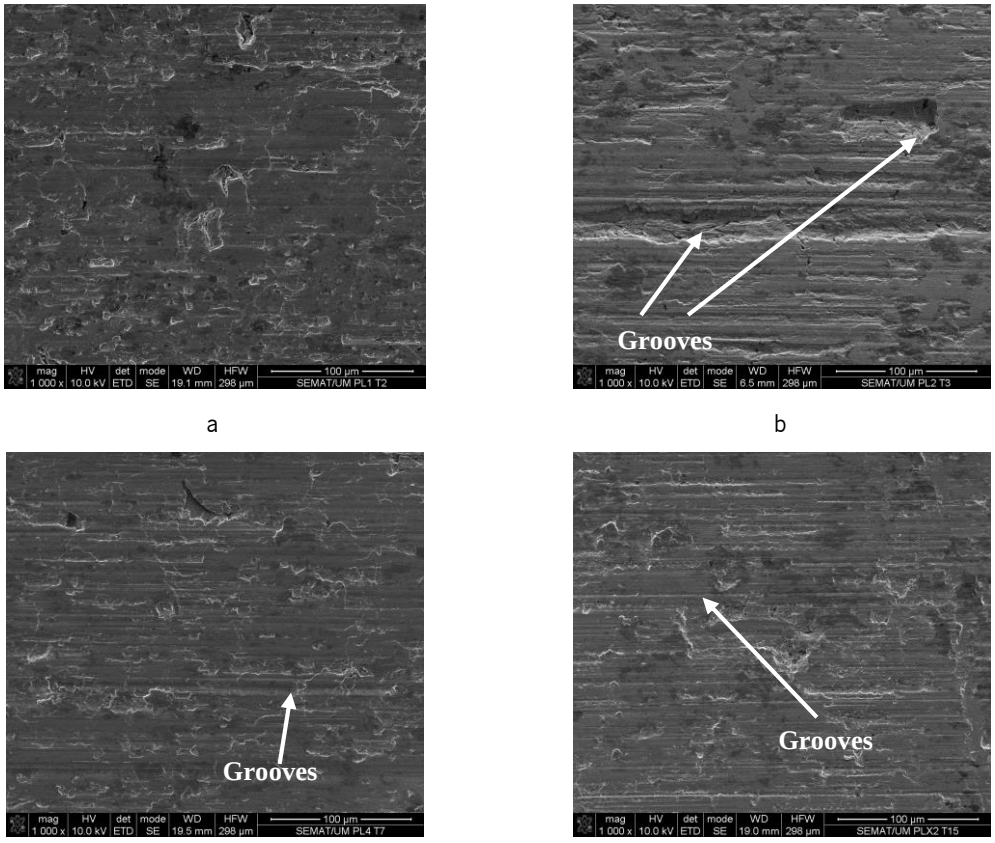

a b

c d

Figure 7. 7 - SEM images of the worn surfaces of GCI plates after sliding against AlSi-based pins: a. unreinforced AlSi alloy; b. AlSi-2wt.%CNT; c. AlSi-5wt.%SiC and d. AlSi-2wt.%CNT-5wt.%SiC.

Figure 7. 8 shows a backscattered SEM images of GCI plates worn surface after sliding against AlSi-2wt.%CNTs-5wt.%SiCp hybrid composite) and the EDS spectrum representative of the dark zones in the micrography.

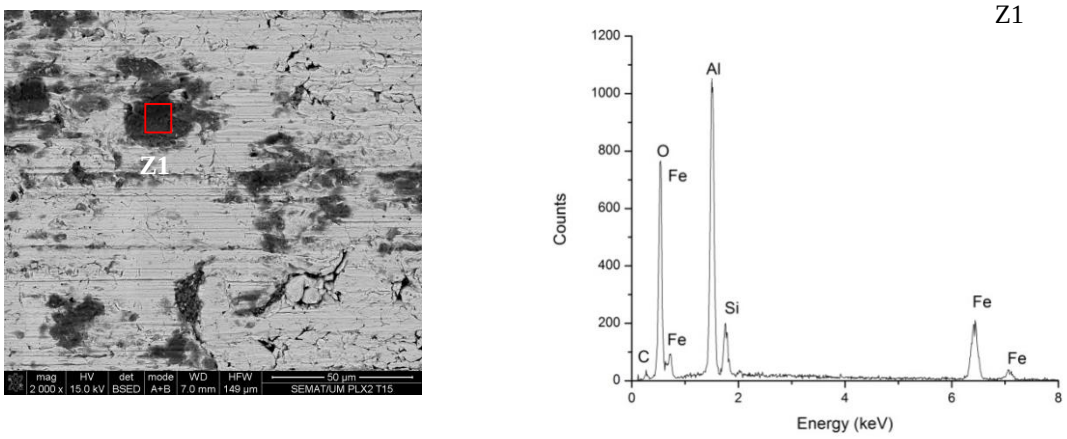

Figure 7. 8 - Backscattered SEM image of GCI plate worn surface and EDS spectrum after sliding against (representative of the dark/grey zones in the micrograph) AlSi-2wt.%CNTs-5wt.%SiCp hybrid composite.

Regarding the worn surface morphology of GCI plates among the different materials used in this study, it can be seen from Figure 7. 7 that even if the dominant wear mechanisms seems to be the same, such as: abrasion grooves (due to the reinforcement particles) and delamination marks, can be highlighted some differences.

The GCI surface damage tends to decrease by the presence of CNTs or/and SiCp at mating surface, as revealed by the increased extension of smooth plateaus at GCI worn surface from (Figure 7. 7a-d).

In the case of the hybrid composite it can be observed (Figure 7. 7) that the groove size decreases in width indicating less plastic deformation (less abrasion) and also less delamination (less adhesion).

These observations are in accordance with the volume wear loss between the plates used for sliding against unreinforced AlSi alloy and AlSi composites (Figure 7. 4– decreasing tendency of the volume loss of the GCI plates).

The EDS analysis performed in the dark zones (Z1) presented in Figure 7. 8 revealed some transfer of Al and Si derived from the pin counterface. EDS analysis in zone Z1 revealed the presence of the following elements: 19% O, 59% Al, 2% Si and 20% Fe. This oxygen content may indicate the presence of some aluminium oxides. The transfer of Al and Si from the pin to the GCI plate means that the wear mechanisms of GCI also included adhesion. Besides Al, Si (coming from the matrix alloy) and O, there were found Fe and C (from the GCI).

So, the main wear mechanism that governs the wear of the plates seems to be abrasion due to hard reinforcement particles and also adhesion as the AlSi matrix is softer then the GCI plate.

AlSi composites (pins)

Figure 7.9 presents SEM images (130x magnification) of the worn surface of unreinforced AlSi alloy and of AlSi-composites pins (Figure 7.9 a1, b1, c1, d1) and also of the mating GCI pins (Figure 7.9 a2, b2, c2, d2).

Figure 7. 10 presents SEM images of the worn surface of AlSi-2wt.%CNTs-5wt.%SiCp hybrid composite with higher magnifications (1000x and 5000x).

Figure 7. 11 shows the EDS analysis corresponding to distinct zones of the pin worn surface for the hybrid composite. It can be seen that zone Z1 shows the based material of pin, namely Al, Si and O. There is also Fe-rich and a small quantity of Mn transfer of material from the mating GCI plate.

SEM images of the worn surfaces (Figure 7. 9- magnification 130x) revealed that there is a clear difference in the worn surface topography of unreinforced AlSi alloy and AlSi composites (Figure 7. 9- a1, b1, c1, d1).

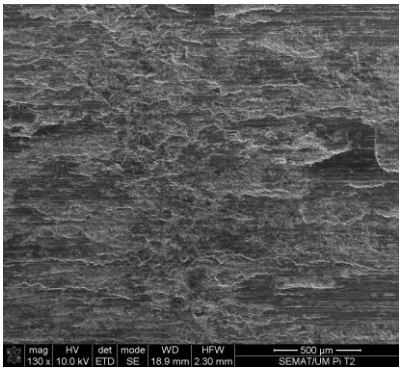

a1

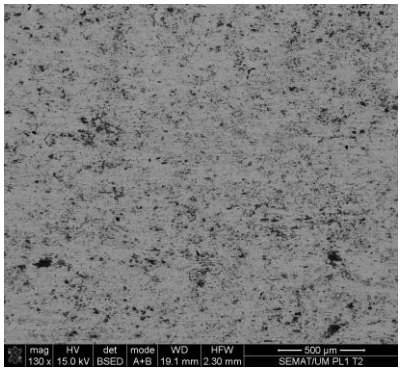

a2

Figure 7. 9 - SEM images of the worn surface of AlSi-based pins (130x magnification) and mating GCI plates (backscattered): a1/a2 - unreinforced AlSi alloy/GCI plate; b1/b2 - AlSi-2wt.%CNTs/GCI plate; c1/c2 - AlSi-5wt.%SiCp/GCI plate and d1/d2 AlSi-2wt.%CNTs-5wt.%SiCp/GCI plate (cont.).

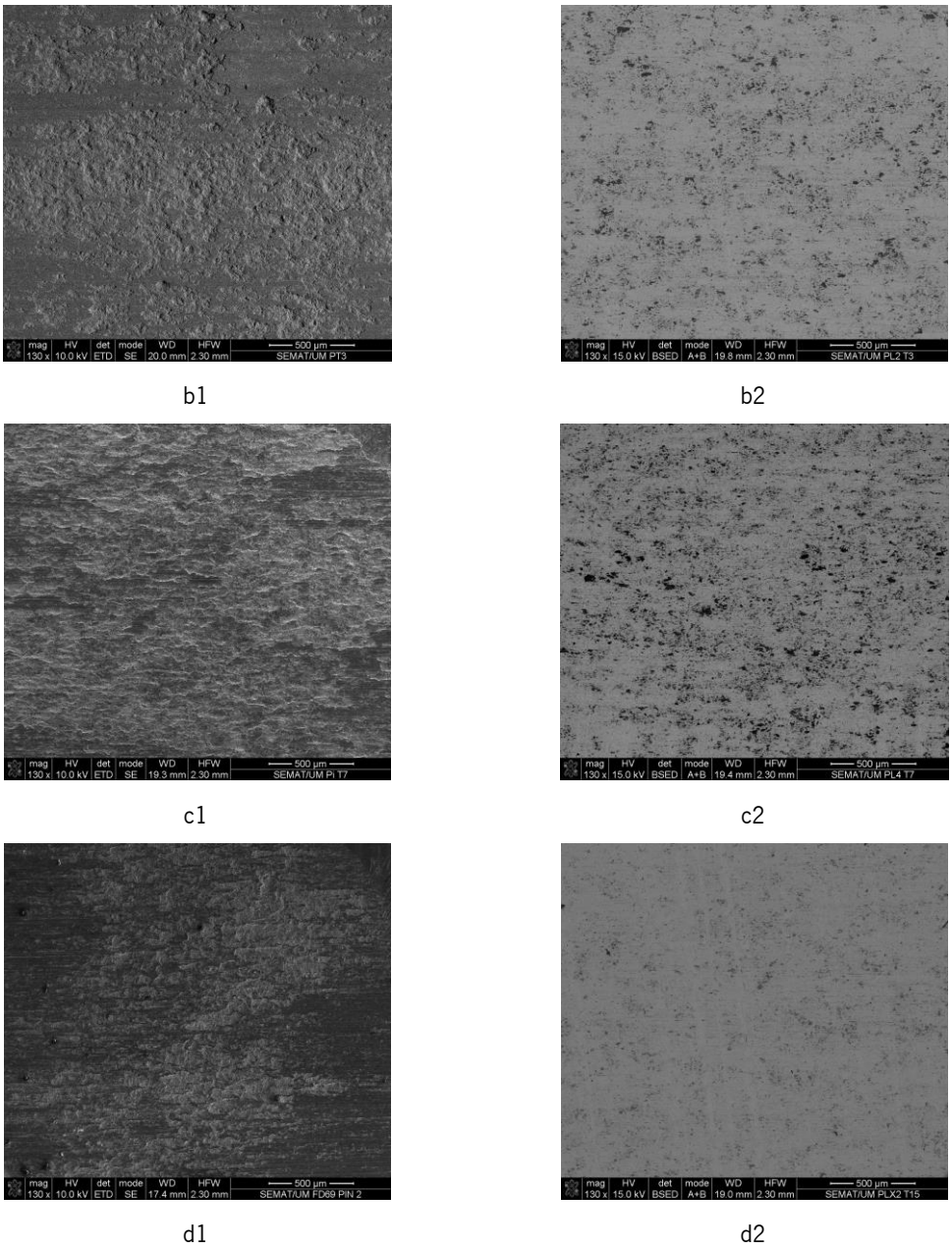

Figure 7. 9 - SEM images of the worn surface of AlSi-based pins (130x magnification) and mating GCI plates (backscattered): a1/a2 - unreinforced AlSi alloy/GCI plate; b1/b2 - AlSi-2wt.%CNTs/GCI plate; c1/c2 - AlSi-5wt.%SiCp/GCI plate and d1/d2 AlSi-2wt.%CNTs-5wt.%SiCp/GCI plate.

It can be clearly seen from the worn surface topography of the unreinforced AlSi alloy (Figure 7. 9- a1) is more uniform as compared to AlSi composite reinforced with CNTs (Figure 7. 9- b1).

SEM images of the worn surface of AlSi-2wt.%CNTs pins (Figure 7. 9-b1) reveals that with the addition of the CNTs, on the pin contact surfaces can be observed two types of plateaus: a smooth plateaus and the other one with more voids, as reported in [23]. More details regarding

the worn surface topography of unreinforced AlSi alloy and AlSi-CNTs composite is given elsewhere [23].

The strengthening mechanism of CNTs in AlSi sintered parts takes place (increasing the strength) [33, 34, 43, 44] on the regions with well dispersed CNTs (on the smoother plateaus).

Regarding the worn surface of AlSi-5%wt.SiCp composite (Figure 7. 9-c1), it can be observed that is very similar to the worn surface of unreinforced AlSi alloy (Figure 7. 9-a1). It can be observed a large plastic deformation, but it is lower as compared to unreinforced AlSi alloy and much lower than AlSi-2wt.%CNTs composite (Figure 7. 9-b1). In Figure 7. 2-c can be observed that there was formed a SiCp cluster that is considered a weakness point (lower bonding strength), so it is easier for the SiC particles to be pulled out. Generally, the pulled out particles may increase the abrasive wear of the composite due to the third body effect [5,25], but in our case they were taken off from the sliding area by the permanent air flow, so they will not have a significant effect on the wear behaviour of the AlSi composites based pins. This is in accordance with other studies [45] that stated that the pull out mechanism increases the effect of abrasive wear, and consequently increased the wear loss.

Regarding the worn surface of the AlSi-2wt.%CNTs-5 wt.%SiCp hybrid composite can be observed (Figure 7. 9-d1) similar plateaus as the ones observed in the case of unreinforced AlSi alloy: a smooth plateaus (adhesive wear) and the other one with more voids (abrasive wear).

It seems that during sliding it is a competition between these two mechanisms, thus between abrasive and adhesive wear (Figure 7. 9-d1). It has been observed that the smoother region corresponds to the region where there is a good distribution of the CNTs and SiCp into the AlSi matrix. It can be seen that in the rougher regions (that seems to be less than the smoother ones) a layer of material has been removed as debris from the surface. The smother plateaus seems to be larger than in the case of AlSi-2wt.%CNTs composite, may be because the volume fraction is higher in the case of AlSi-2wt.%CNTs-5wt.%SiCp hybrid composite.

It should be also mentioned that the amount of the transferred material is less in the case of AlSi-2wt.%CNTs-5wt.%SiCp hybrid composite from the pin to the plate (less dark zones in backscatter images – Figure 7. 9-d2) as compared to the unreinforced AlSi alloy and AlSi composites (Figure 7. 9-a2, b2 and c2).

It can be seen that no pull out mechanism can be observed in the case of hybrid composite (Figure 7. 10). On Figure 7. 10 can be observed a SiC particle that is debonded, and it is also

fractured. It can be observed a lower level of plastic deformation in the case of AlSi hybrid composite as compared to the unreinforced AlSi alloy and AlSi composites. These happened simultaneously with the improvement on wear resistance (Figure 7. 4) of the AlSi - hybrid composite as compared to unreinforced AlSi alloy. Thus, it can be concluded that wear damage of unreinforced AlSi and AlSi composites based pins seems to be controlled essentially by two mechanisms: abrasive wear (with delamination/pull-out of grains/particles) and adhesive wear that includes plastic deformation and material transfer between the mating surfaces. The AlSi hybrid composite seems to be controlled by the same mechanisms, but with wear that includes plastic deformation and material transfer between the mating surfaces.

magnification 1000× magnification 5000x

Figure 7. 10 - SEM images of the worn surface of AlSi-2wt.%CNTs-5wt.%SiCp hybrid composite

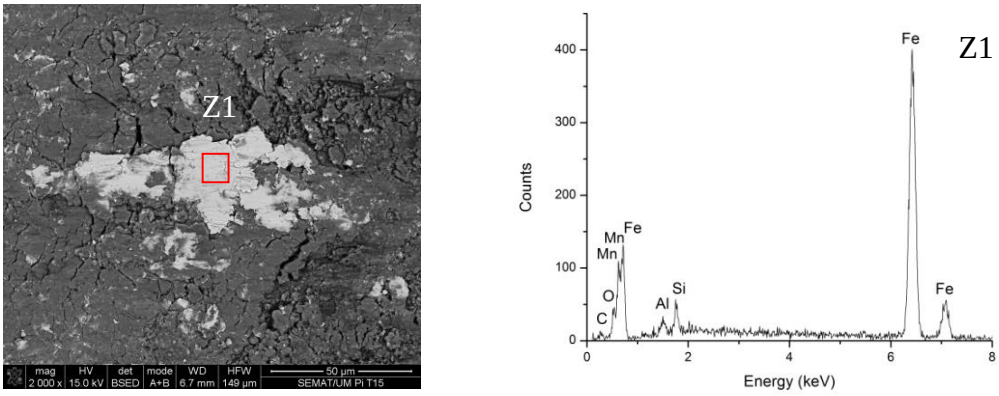

Figure 7. 11 - SEM image (backscattered view) and EDS spectra (corresponding to Z1) of 2wt.%CNTs-5wt.%SiCp hybrid composite.

The introduction of both reinforcements (CNTs and SiCp) in the AlSi matrix seems to have a beneficial role, as AlSi-hybrid composite/GCI tribopair exhibited an improvement on wear

resistance, as compared to unreinforced AlSi alloy/GCI and AlSi alloy- composites/GCI tribopairs. As referred above, the main contribution of the reinforcements are:

(i) Strengthening effect of CNTs: A stronger bonding between AlSi grain interfaces due to the CNTs. This is basically in accordance with some of the proposed mechanisms, by George et al. [41] namely thermal mismatch, Orowan looping and shear lag theory or also with Zang and co-authors [42] or even with Bustamante et al. [45] suggested mechanisms. Also, it should be mentioned that the CNTs agglomerations have detrimental effect on the strengthening, and they are responsible for voids nucleation.

(ii) Self-lubrication effect of CNTs. The CNTs and the CNTs agglomerates are released into the contact and there is a disintegration of these agglomerations due to the shear forces, leading to the appearance of individual CNTs that could roll into the sliding contact;

(iii) Strengthening effect of SiCp: the strengthening of the matrix by SiC particles (SiC_p increased the hardness of the composite);

(iv) Load bearing elements: SiC particles act like load bearing elements (during sliding the SiC particles support the load and prevent the contact between the AlSi matrix and the GCI plate).

Finally it should be emphasized that the approach based on two distinct reinforcements with different reinforcement mechanisms or the same reinforcement mechanism but acting at different scales (nano-scale or micro-scale) seems to be effective. As a fact the tensile strength with CNTs as reinforcement, presented its peak with 2% of CNTs, as shown in a previous paper [21]. The same happened with the SiCp reinforcement that presented its saturation point, for tensile strength, at 5% of reinforcement. Thus, increasing the reinforcement content, in both cases, would allow to increase the wear behaviour but it would substantially decrease the tensile strength. It was also reported that when the peak of tensile strength was achieved with one reinforcement (CNTs), it was possible to further increase the tensile strength by adding another type of reinforcement (SiCp).

Thus it is concluded that the use of two reinforcements, by using two different reinforcement mechanisms or the same mechanism but at different scales, may provide better overall properties than by using one reinforcement alone. Thus, hybrid composites, as proposed in the present paper, provide better overall properties.

7.5 Conclusions

From the present investigation on the sliding wear behaviour of AlSi-composites/GCI tribopairs, the following conclusions can be drawn:

- AlSi-2wt.%CNTs, AiSi-5wt.%SiCp and AiSi-2wt.%CNTs-5wt.%SiCp reinforced composites were successfully produced by hot-pressing technique.

- Hardness of the all produced AlSi composites increased, and the hardness of the hybrid composite was higher as compared to unreinforced and also to the composites. Hardness of the hybrid composites increased due to the strengthening effect of both reinforcements CNTs and SiCp.

- Both AlSi-2wt.%CNTs and AiSi-5wt.%SiCp composites experienced an improvement in the wear behaviour when compared to unreinforced AlSi alloy. The wear behaviour of AlSi-composites is controlled essentially by abrasive wear (with delamination/pull-out of grains/particles) and adhesive wear that includes plastic deformation and material transfer between the mating surfaces.

- The addition of both reinforcements (CNTs and SiCp) in AlSi matrix improved the wear behaviour of the AiSi-2wt.%CNTs-5wt.%SiCp hybrid composite when comparing to AlSi- composites. The wear behaviour of AlSi hybrid composite is controlled essentially by two mechanisms: abrasive wear and adhesive wear.

- It is shown that by reinforcing AlSi alloy with both reinforcement the wear behaviour of tribopair (AlSi-hybrid composite/GCI) is improved, when compared with unreinforced AlSi /GCI and AlSi alloy- composites /GCI tribopairs, due to the strengthening effect of CNTs, self-lubrication effect of CNTs and CNTs agglomerates, strengthening effect of SiCp and load bearing elements of SiC particles.

7.6 Acknowledgements

This work was supported by the Portuguese Foundation of Science and Technology through the project references PTDC/EME-PME/68664/2006, EXCL/EMS-TEC/0460/2012 and through the PhD grant with the reference SFRH/BD/44077/2008.

7.7 References

[1] S.V. Prasad, R. Asthana. 2004. Aluminum metal–matrix composites for automotive applications: tribological considerations. Tribol. Lett. 17: 445-453.
[2] F.S. Silva. 2006. Fatigue on engine pistons – A compendium of case studies. Eng. Fail. Anal. 13: 480–492.
[3] R.L. Deuis, C. Subramanian, J. M. Yellup. 1997. Dry sliding wear of aluminium composites-a review. Compos. Sci. Technol. 57: 415-435.
[4] R.N. Rao, S.Das, D.P. Mondal, G. Dixit. 2009. Dry sliding wear behaviour of cast high strength aluminium alloy (Al–Zn–Mg) and hard particle composites. Wear 267: 1688–1695.
[5] M. Walczak, D. Pieniak, M. Zwierzchowski. 2014. The tribological characteristics of SiC particle reinforced aluminium composites. ACME. http://dx.doi.org/10.1016/j.acme.2014.05.003.
[6] R.N. Rao, S. Das. 2010. Effect of matrix alloy and influence of SiC particle on the sliding wear characteristics of aluminium alloy composites. Mater. Des. 31: 1200–1207.
[7] K. Umanath, S. T. Selvamani. 2011. Friction and wear behaviour of al6061alloy (SiCp +Al2O3p) hybrid composites. Int. j. innov. res. sci. eng. Technol. 3: 5441-5451.
[8] K. Borodianskiy, A. Kossenko, M. Zinigrad. 2013. Improvement of the Mechanical Properties of Al-Si Alloys by TiC Nanoparticles. Metall. Mater. Trans. A 44A: 4948-4953.
[9] C. E. da Costa, L. de Aguiar, E.L. de Carvalho, V. A. Borras. 2003. Properties of AA6061 aluminum alloy reinforced with different intermetallics and ceramics particles, Proceedings of COBEM 2003, 17 International Congress of Mechanical Engineering Nov. 10-14. Sao Paulo.
[10] M. O. Shabani, A. Mazahery. 2011. Prediction of wear properties in A356 matrix composite reinforced with B4C particulates. Synth. Met 161: 1226–1231.
[11] A.P. Sannino, H.J. Rack. 1995. Dry sliding wear of discontinuously reinforced aluminum composites: review and discussion. Wear 189: 1-19.
[12] S.R. Bakshi, A.K. Keshri, A. Agarwal. 2011. A comparison of mechanical and wear properties of plasma sprayed carbon nanotube reinforced aluminum composites at nano and macro scale. Mater. Sci. Eng. A 52: 3375–3384.
[13] H.J. Choi, S.M. Lee, D.H. Bae. 2010. Wear characteristic of aluminium-based composites containing multi-walled carbon nanotubes. Wear 270: 12–18.
[14] I.Y. Kim, J.H. Lee, G.S. Lee, S.H. Baik, Y.J. Kim, Y.Z. Lee. 2009. Friction and wear characteristics of the carbon nanotube–aluminium composites with different manufacturing conditions. Wear 267: 593–598.
[15] S. Zhou, X. Zhang, Z. Ding, C. Min, G. Xu, W. Zhu. 2007. Fabrication and tribological properties of carbon nanotubes reinforced Al composites prepared by pressureless infiltration technique. Compos Part. A-Appl. S 38: 301–306.
[16] W. Ames, A.T. Alpas. 1995. Wear Mechanisms in Hybrid Composites of Graphite-20 SiC in A356 Aluminum Alloy (Al-7 Pct Si-0.3 Pct Mg). Metall. Mater. Trans. A, 26A: 85-98.
[17] S.R. Bakshi, D. Lahiri, A. Agarwal. 2010. Carbon nanotube reinforced metal matrix composites – a review. Int. Mater. Rev. 55: 41-64.
[18] A.M. Al-Qutub, A. Khalil, N. Saheb, A.S. Hakeem. 2013. Wear and friction behaviour of Al6061 alloy reinforced with carbon nanotube. Wear 29: 752–761.
[19] L. Si, W. Chao, S. Lin, Y. Shuangchun. 2013. The research state of CNTs reinforced mental matrix composites. Int. J. of Adv. in Res. & Technol. 2: 243-245.
[20] L. Peña-Parás, J. Taha-Tijerina, A. García, D. Maldonado, J. A. González, D. Molina, E. Palacios, P. Cantú. 2014. Anti-wear and extreme pressure properties of nanofluids for industrial applications. Tribol. T. DOI: 10.1080/10402004.2014.933937.

[21] O. Carvalho, G. Miranda, D. Soares, F. S. Silva. 2014. Carbon nanotube dispersion in aluminum matrix composites – quantification and influence on strength. Mech. Adv. Mat Struct. DOI: 10.1080/15376494.2014.929766.
[22] O. Carvalho, M. Buciumeanu, D. Soares, J. Gomes, F. S. Silva. 2014. Improvement on sliding wear behaviour of Al/cast iron tribopair by CNT's reinforcement of an Al alloy. Tribology Transactions. DOI: 10.1080/10402004.2014.1002143.
[23] D.P. Mondal, S. Das, R.N. Rao, M. Singh. 2005. Effect of SiC addition and running-in-wear on the sliding wear behaviour of Al–Zn–Mg aluminium alloy. Mater. Sci. Eng.A 402: 307–319.
[24] L. Poovazhagan, K. Kalaichelvan, A. Rajadurai, V. Senthilvelan. 2013. Characterization of Hybrid Silicon Carbide and Boron Carbide Nanoparticles-Reinforced Aluminum Alloy Composites. Procedia Eng. 64: 681 – 689.
[25] S. Basavarajappa, G. Chandramohan. 2005. Dry Sliding Wear Behaviour of Hybrid Metal Matrix Composites. Mater. Sci. Medžig. 11: 253-257.
[26] D. Aruri, K. Adepu, K. Adepu, K. Bazavada. 2013. Wear and mechanical properties of 6061-T6 aluminum alloy surface hybrid composites [(SiC + Gr) and (SiC + Al2O3)] fabricated by friction stir processing. J. Mater. Res.Technol. 2: 362–369.
[27] D. S. Prasad, C. Shoba. 2014. Hybrid composites – a better choice for high wear resistant materials. J. Mater. Res.Technol. 3: 172-178.
[28] X.N. Zhang, L. Geng, G.S. Wang. 2006. Fabrication of Al-based hybrid composites reinforced with SiC whiskers and SiC nanoparticles by squeeze casting. J. Mater. Process. Technol 176: 146–151.
[29] B. Ralph, H.C. Yuen, W.B. Lee. 1997. The processing of metal matrix composites — an overview. J. Mater. Process. Technol. 63: 339-53.
[30] G.P. Tandon, G.J. Weng. 1986. Stress Distribution in and Around Spheroidal Inclusions and Voids at Finite Concentration. J. Appl. Mech. 53: 511-518.
[31] S.F. Corbin, D.S.Wilkinson. 1994. The influence of particle distribution on the mechanical response of a particulate metal matrix composite. Acta Metall. Mater. 42: 1311-1318.
[32] A.A. Cerit, M.B. Karami, Ş, F. Nair, K. Yildizli. 2008. Effect of Reinforcement Particle Size and Volume Fraction on Wear Behaviour of Metal Matrix Composites. Tribology in industry 30, No. 3&4.
[33] D.P. Mondal, N.V. Ganesh, V.S. Muneshwar, S.Das, N. Ramakrishnan. 2006. Effect of SiC concentration and strain rate on the compressive deformation behaviour of 2014Al-SiCp composite. Mater. Sci. Eng. A 433:18–31.
[34] A. Mazahery, M. O. Shabani. 2012. Characterization of cast A356 alloy reinforced with nano SiC composites. Trans. Nonferrous Met. Soc. China 22:275280.
[35] G. E. Kiourtsidis, S. M. Skolianos, G. A. Litsardakis. 2004. Aging response of aluminium alloy 2024/silicon carbide particles (SiCp) composites. Mater. Sci. Eng. A 382: 351–361.
[36] D. S. Prasad, C. Shoba, N. Ramanaiah. 2014. Investigations on mechanical properties of aluminum hybrid composites. J. Mater. Res. Technol. 3: 79–85.
[37] V.C. Nardone, K.M. Prewo. 1986. On the strength of discontinuous silicon carbide reinforced aluminum composites. Scripta. Metall. Mater. 20: 43-48.
[38] R. George, K.T. Kashyap, R. Rahul, S. Yamdagni. 2005. Strengthening in carbon nanotube/aluminium (CNT/Al) composites. Scripta Mater. 53: 1159–1163.
[39] Z. Zhang, D.L. Chen. 2006. Consideration of Orowan strengthening effect in particulate-reinforced metal matrix nanocomposites: A model for predicting their yield strength. Scripta Mater 54: 1321–1326.
[40] K. Balani, A. Agarwal. 2008. Multiscale wear of plasma-sprayed carbon-nanotube-reinforced aluminum oxide nanocomposite coating. Acta Mater 56: 5984–5994.

[41] F. Dassenoy, L. Joly-Pottuz, J.M. Martin, T. Mieno. 2006. Carbon nanotubes as advanced lubricant additives, V.N. Popov and P. Lambin (eds.). Carbon Nanotube: 237–238, Springer, Netherlands.
[42] A.T. Alpas, J. Zhang. 1992. Effect of SiC particulate reinforcement on the dry sliding wear of aluminium-silicon alloys (A356). Wear 155: 83–104.
[43] S.R. Bakshi, A. Agarwal. 2011. An analysis of the factors affecting strengthening in carbon nanotube reinforced aluminum composites. Carbon 49: 533– 544.
[44] S.J. Yoo, S.H. Han, W.J. Kim. 2013. Strength and strain hardening of aluminum matrix composites with randomly dispersed nanometer-length fragmented carbon nanotubes. Scripta Mater 68: 711–714.
[45] R. Pérez-Bustamante, C.D. Gómez-Esparza, I. Estrada-Guel, M. Miki-Yoshida, L. Licea-Jiménez, S.A. Pérez-García, R. Martínez-Sánchez. 2009. Microstructures and tensile behaviour of carbon nanotube reinforced Cu matrix nanocomposites. Mater. Sci. Eng. A. 502: 159–163.

8 Mechanical, wear and fatigue behaviour of an AlSi-CNTs-SiCp hybrid composite

Carvalho, O.[1], Buciumeanu, M.[2], Madeira S.[1], Soares, D.[1], Silva, F.S.[1], Miranda, G.[1]

[1]MEMS-UMinho, University of Minho, Azurém, 4800-058 Guimarães, Portugal
[2]Cross–Border Faculty of Humanities, Economics and Engineering, "Dunarea de Jos" University of Galati, Domneasca 47, 800008 Galati, Romania

Submitted to Journal of Materials Engineering and Performance

8.1 Abstract

The aim of this paper was to study the mechanical, fatigue and wear behaviours of a hybrid AlSi-2wt. %CNTs-5wt.%SiCp composite. For comparison purposes the unreinforced AlSi alloy, AlSi-2%wt.CNTs and AlSi-5wt.%SiCp composites were used. A powder metallurgy processing route was used to produce the unreinforced AlSi alloy and AlSi composites. Tensile, fatigue and dry reciprocating pin-on-plate wear tests were performed and the results showed that the hybrid composite AlSi-2wt.%CNTs-5%wt.SiCp proposed in the present paper, provided better overall properties than the single reinforcement composites. The improvement is attributed to the simultaneous effect of two different reinforcement mechanisms or on the same mechanisms but acting at different scales.

Keywords: Composites, Metallic Matrix; Aluminum; Powder Metallurgy; Hybrid; Mechanical properties; Fatigue; Wear.

8.2 Introduction

Due to their mechanical properties (e.g. high specific stiffness, low density; high strength to weight ratio, improved damping capabilities, good corrosion resistance etc.) aluminium matrix composites are used in various industrial applications, such as: brake drums, cylinder liners, pistons, cylinder blocks, connecting rods etc. [1].

Different fabrication techniques were developed to produce metal matrix composites (MMC) such as: liquid metallurgy, powder metallurgical, diffusion bonding of filaments and foils, and vapour phase infiltration techniques [1]. The technique used in this work to produce the AlSi based composites is powder metallurgy. This technique is very versatile because it allows fabrication of a wide variety of composites. It permits to achieve a better distribution of the reinforcement mainly discontinuous reinforcements. The main advantages of discontinuous reinforced metal matrix composites (DRMMCs) are improved strength, specific modulus, high toughness, and good wear resistance property even at elevated temperatures, controlled co-efficient of thermal expansion, increased fatigue resistance and superior dimensional stability at elevated temperatures etc. when compared with other materials [2].

The most used reinforcements in MMCs are ceramics which can be continuous, in the form of fibres or discontinuous, in the form of whisker, platelets or particles embedded in a ductile metal matrix. The reinforcements are ranging from soft materials, such as graphite, talc, etc., to harder ceramic particles such as Silicon carbide (SiCp), Al_2O_3 etc. [3-5]. The SiCp is used as reinforcement primarily in aluminium matrix composites [1,4]. It has been already proved that it reduces the wear of the MMCs. In the dry sliding and abrasive wear conditions, this reinforcement supports the applied load by restricting surface deformations [6]. There are also some other reinforcement phases incorporated in aluminium alloys to improve their characteristics, such as: metals or other compound such as carbon nanotubes (CNTs). CNTs are also used in aluminium matrix composites due to their properties. CNTs have excellent mechanical properties [7-17], such as elastic modulus as high as 1 TPa and strengths 10 to 100 times higher than the strongest steel at a fraction of the weight.

When there is an addition of different types of reinforcements (at least two types) in a metal matrix a new kind of MMCs are created, known as Hybrid MMCs. These are unique materials fabricated by reinforcements of at least two types of ceramic or metals particles into a metal matrix [18]. The purpose is to combine different reinforcement mechanisms and thus have an overall result better than the ones achieved with a single reinforcement.

The advantage of hybrid composites, due to different properties of both reinforcements, shape and size, is that it is expected that they have different contributions on the previously mentioned models. The behaviour of hybrid composites is a sum of inherent advantages and

disadvantages of both reinforcements that cannot be achieved with the use of a single reinforcement.

The main purpose of this paper is to understand the combined effects of (the advantages) both reinforcements (CNTs and SiCp) on the tensile, fatigue, and wear behaviour of a hybrid AlSi-2wt.%CNTs-5wt.%SiCp composite. For comparison purposes the unreinforced AlSi alloy, and the single reinforced composites, AlSi-2wt.%CNTs and AlSi-5wt.%SiCp, were also tested.

8.3 Experimental procedure

8.3.1 Fabrication of AlSi composites

An AlSi alloy, powders size < 325 mesh (< 44 μm), with chemical composition as listed in Table 8. 1, was used as matrix material. Ni coated Multi-Wall Carbon Nanotubes (MWCNTs) (outer diameter > 50 nm, length 0.5-2.0 μm, purity before coating > 95wt.% and ash < 1.5wt.%), and SiCp particles (with 13 μm in size) were used as reinforcements.

The AlSi-matrix composites were processed by the traditional hot isostatic pressing (HIP) technique. Applied pressure was 35 MPa for 10 minutes at 550°C under vacuum (10^{-2} mbar). The mixing of the AlSi powders was done inside a closed stainless steel jar along with 12 steel milling balls (10 mm in diameter). The ball powder ratio is 10:1. The bottle rotated with constant speed (40 rpm) during 6 days (low-energy ball milling). The flat plates prepared for the wear tests were machined from grey cast iron (GCI). Table 8. 2 presents the chemical composition of GCI.

Table 8. 1 - Chemical composition of AlSi alloy (wt.%).

Al	Si	Fe	Others
87.3	11	0.20	1.5

Table 8. 2 - Chemical composition of GCI.

Fe	C	Mn	Si	P	Cr	Ni	Cu	S	Mo	Others
90.4	3.59	0.392	2.37	0.624	0.249	1.52	0.28	0.023	0.007	0.545

In Figure 8. 1-a is presented the SEM image of CNTs (190x magnification), where can be notice the presence of agglomerations. Figure 8. 1-b shows the SEM images of the SiC_p (2000x magnification), where can be observed their irregular shape.

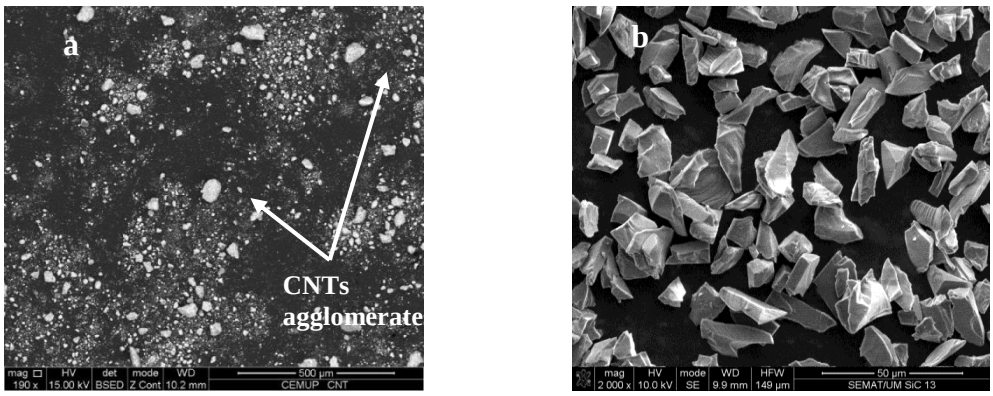

Figure 8. 1 - SEM images showing: a. CNTs and b. SiCp.

8.3.2 Methods

Tensile tests

Tensile tests were carried out using a servo-hydraulic universal testing machine Instron 8874, equipped with a load cell capacity of 25 kN (tension). Tests were performed at room temperature (≈23 °C), with a crosshead speed of 0.05 $mm.s^{-1}$ and five specimens were used for each condition.

Fatigue tests

In order to get the influence of the CNT content on the fatigue life (S-N curve), several fatigue tests were carried out at a stress ratio $R=0.1$ using a servo-hydraulic universal testing machine Instron 8874. All tests were performed at ambient temperature, in laboratory environment, and at a cyclic frequency of 16 Hz. Tests were performed until final fracture. More details regarding the tensile and fatigue tests are given elsewhere [19].

Wear tests

A reciprocating pin-on-plate tribometer PLINT-TE67/R was used to evaluate the wear characteristics. Experiments were carried out with a normal load of 10 N and relative displacement amplitude of 10 mm. All tests have been stopped after a sliding distance of 148 m. During the tests compressed air was flown to the contact zone in order to remove loose. The flat plates (40×18×5 mm) prepared for the wear tests were machined from grey cast iron (GCI). Pins were machined from the unreinforced AlSi alloy and AlSi composites. The dimensions of the pin are: radius of curvature 40 mm, thickness 3.5 mm and the arc length 20 mm. More detailed regarding the wear test procedure is give elsewhere [20,21].

8.4 Results and discussion

8.4.1 Microstructural characterization

In Figure 8. 2 are presented the SEM images of the unreinforced AlSi alloy and of the AlSi-composites (after etching). It can be observed that there is no porosity, proving the effectiveness of the hot-pressing process for the production of these composites.

In the SEM images of the AlSi-2 wt.%CNTs composite (Figure 8. 2-b) and AlSi-2wt.%CNTs-5wt.%SiCp hybrid composite (Figure 8. 2-d) can be observed the presence of the CNT agglomerates. A uniform dispersion without formation of CNTs agglomerates would be the ideal situation in terms of mechanical properties. However, due to the existence of Van der Waals forces [22] is not possible to achieve a uniform distribution with the used technique, and this results in the formation of agglomerates which have a negative effect on the final properties of the composites.

It can be observed in Figure 8. 2-c that there are some SiCp fractured particles. The fracture of these particles resulted from their high modulus. In zones with clusters the fracture of the SiCp is less probable to occur and interfacial rupture between the particles and the matrix is the common occurrence. In Al-SiCp composites, microplasticity can occur due to stress concentrations in the matrix at the poles of the reinforcement and/or at sharp corners of the reinforcing particles [23, 24]. When these reinforcements are in form of clusters, these places are more favourable to crack growth [25]. The presence of silicon content contributes to the absence of reaction between AlSi matrix and SiCp. This fact resulted from the reaction of AlSi matrix with

SiCp in which reaction products are Al_4C_3 and Si. In this way higher the content of Si, lowers the reaction probability [26].

In Figure 8. 3 is presented the amplified SEM image of the hybrid composite. The preferable etching on samples with CNTs is due to strain hardening effect of the well dispersed CNTs. The higher strain effect is between the powders because are zones where the CNTs are localized and thus there is higher dislocation density. It can be observed a higher corrosion in these zones after etching. Another explanation could be the formation of galvanic pairs between the reinforcements and the matrix and even between reinforcements.

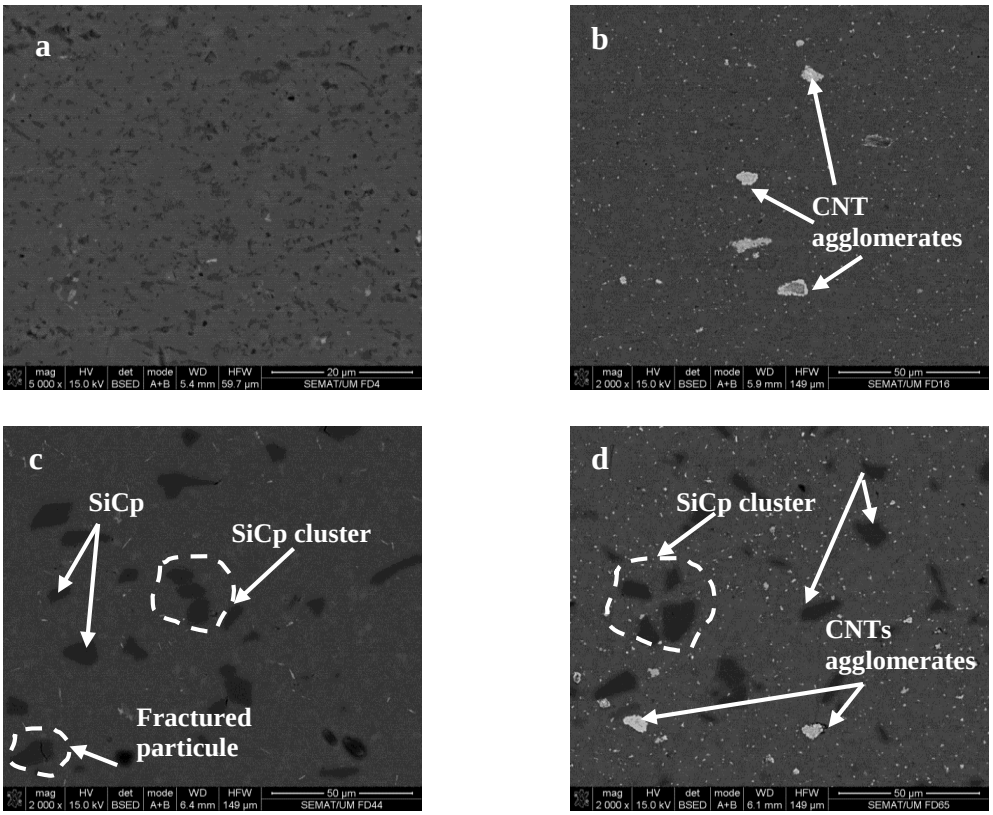

Figure 8. 2 - SEM images of: a. unreinforced AlSi alloy; b. AlSi-2wt.%CNT; c. AlSi- 5wt.%SiCp and d. AlSi-2wt.%CNT-5wt.%SiCp composites.

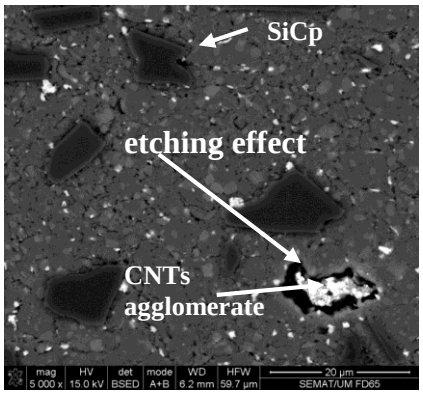

Figure 8. 3 - SEM images of AlSi-2%wt.CNTs-5%wt.SiCp hybrid composites.

8.4.2 Mechanical properties (Tensile tests)

Figure 8. 4 presents the representative tensile stress–strain curves of the unreinforced AlSi alloy and all produced composites. The mechanical properties (tensile strength, σ_r, yield strength σ_y and tensile strain ε_r) are listed in Table 8.3.

The results of the tensile tests revealed that all composites presented higher tensile strength and yield strength than the unreinforced AlSi alloy. The best results were obtained in the case of AlSi-2wt.%CNTs-5wt.%SiCp hybrid composite. The tensile strength in the case of hybrid composite increased with about 37%, while the yield strength increased with about 53% as compared to the unreinforced AlSi alloy. However, the rupture strain decreased for all the composites as compared to unreinforced AlSi alloy. The hybrid composite exhibited the highest rupture strain reduction (about 89% as compared to the unreinforced AlSi alloy) which may be explained based on work hardening due to geometric constraints imposed by the presence of both reinforcements (CNTs and SiCp). Another factor that may contribute to the reduction of the rupture strain of the composites is the presence of CNT agglomerates or/and SiCp clusters.

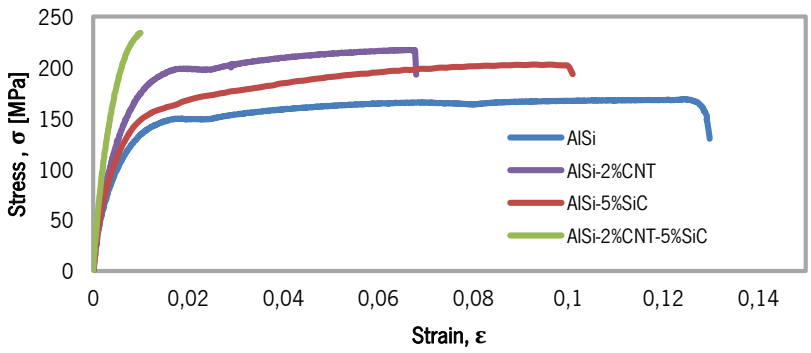

Figure 8. 4 - Stress–strain curves from tensile testing of unreinforced AlSi alloy and of the AlSi composites

Table 8. 3 - Results of tensile testing of unreinforced AlSi alloy and of the AlSi composites.

Material	σr [MPa]	σy [MPa]	εr [%]
AlSi	170±11.1	152±4	13±1.1
AlSi-2%CNTs	209±10.5	192±7.9	7±1.3
AlSi-5%SiCp	200±9.3	165±5.4	10±1.1
AlSi-2%CNTs-5%SiCp	233±7.8	233±4.8	0.7±1.4

Figure 8. 5 presents the SEM images of the fracture surface after tensile test of unreinforced AlSi alloy and of all AlSi composites. More details regarding the fracture morphology of the unreinforced AlSi alloy and of the AlSi-2%wt.CNTs composite are given elsewhere [19].

The fracture surface of the AlSi-5wt.%SiCp composite (Figure 8. 5-c) seems to be very similar with the one the unreinforced AlSi alloy (Figure 8. 5-a), but with more picks and valleys. The deeper valleys are formed due to the fact that the crack travels through the AlSi grains/particles of the material (intragranular fracture) between the SiCp. The AlSi-5wt.%SiCp presents large plastic deformation with a longer dimple size. In Figure 8. 6-a can be also be observed some fractured SiCp particles. The fracture of the particles means that shear strength at the interface was higher than the particle fracture strength. Also, can be observed some pull out SiCp particles. In this case, the bonding between SiCp particles and AlSi matrix has less resistance than particles fracture resistance. Another aspect that was already mentioned, the presence of SiCp clusters, as were observed in Figure 8. 3-c, have detrimental effect on mechanical properties of the composite.

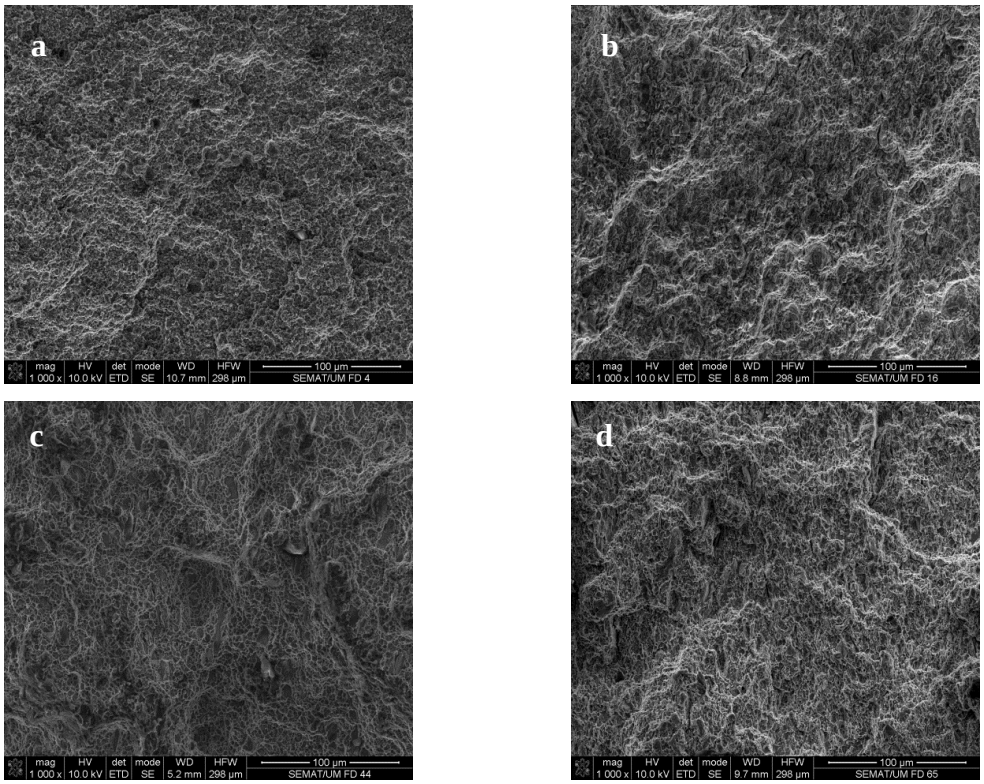

Figure 8. 5 - SEM images of the fracture surface after tensile test: a unreinforced AlSi alloy; b. AlSi - 2wt.%CNTs; c. AlSi - 5wt.%SiCp and d. Al-2wt.%CNTs-5wt.%SiCp.

Regarding the fracture morphology of AlSi-2wt.%CNT-5wt.%SiCp hybrid composite (Figure 8. 5-d) there can be observed a mixture between two types of regions: a smooth region and the other one with more voids, but there are more voids as compared to AlSi-2wt.%CNTs composite. In this case the crack propagation is a combined effect between both reinforcements (Figure 8. 6-b), such as debonding of SiCp -AlSi grains, fracture of SiCp and also from the presence of CNT agglomerates (it can be well seen in Figure 8. 6-b the voids from the CNT agglomerates). The crack in this case can nucleate from the CNTs agglomerates or from the interface between the SiCp particles and AlSi matrix (stress concentration points). In well dispersed zones the crack propagates thought AlSi matrix grains/powders and when reaches to SiCp particles the crack may have two possibilities to go: (i) if there is not boding between the SiCp particle and the AlSi matrix (that is the common case) then the crack may travel around the SiCp particle; (ii) if there is bonding between the SiCp particle and AlSi matrix (few cases) the crack may travel through the particle (there can be observed some fractured particles- Figure 8. 6-b). If the crack reaches zones with agglomerates, then the crack follows the agglomerates (as these are zones of stress concentrations).

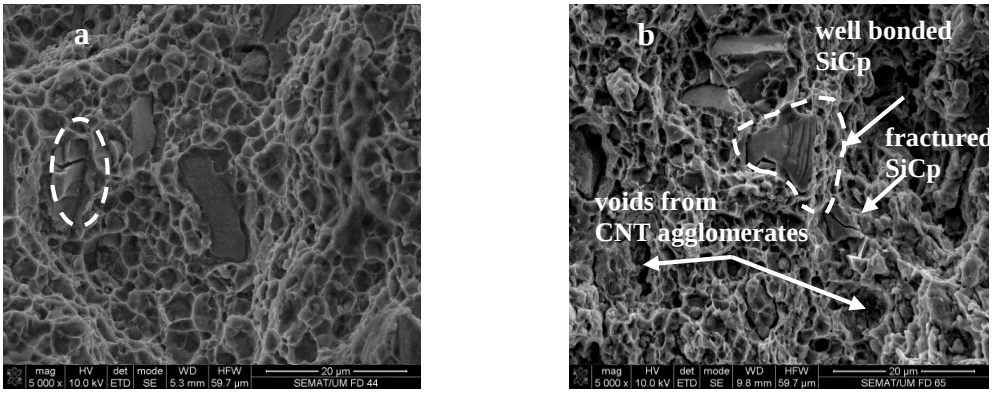

Figure 8. 6 - SEM images of the fracture surface after tensile test of: a. AlSi - 5wt.%SiCp and b. Al-2wt.%CNTs-5wt.%SiCp

Based on tensile tests results and on the fracture morphologies there seems to be three main mechanisms of reinforcement in composites:

(i) Shear lag model. In this model the higher ultimate tensile strength [22] results from the load that is transferred to the reinforcement via shear stresses at the interface between the components (shear lag theory - direct strengthening [27]). The presence of agglomerates decreases the efficiency of load transfer from the matrix for reinforcement [28], thereby not all CNTs contribute to shear lag strengthening mechanism. The clusters of SiCp are less thus this problem should be less prevalent with SiCp reinforcement. It should be stated that the largest number of CNT agglomerates results not only due to the presence of Van der Walls forces, but also due to the difference in size of the CNTs and AlSi powder [29]. The reduction in relative particle size ratio (RPS) contributes to probability in agglomerations formation [30, 31]. These agglomerations during the sintering process prevent the AlSi matrix to deform and fill in the voids in agglomerates zones. Thus, these zones are favourable to earlier start of void nucleation [23, 25, 32] and also there is a reduction in load transfer from matrix to reinforcement [32] and consequently reduction of mechanical properties like hardness and stiffness [24, 32]. Another aspect to consider is that this model depends on the orientation of reinforcement. The strengthening effect is greater if the reinforcement is aligned in the direction of the load [33]. No statistical study was made for both reinforcements but it is expected that not all CNTs contribute in same manner.

The most important aspect to consider in this strengthening mechanism is the effectiveness of the bonding between the reinforcement and matrix. In case of SiCp as can be observed in Figure 8. 3-c and Figure 8. 6-a, no reaction has been detected for most of the SiCp. It

seems that SiCp are only entrapped in AlSi matrix. It should be mentioned that there are also some cases where it was observed a bonding between the reinforcement (SiCp) and the matrix (see Figure 8. 5and Figure 8. 6). Regarding this strengthening mechanism, it is expected that SiCp has a lower contribution to strengthening of composite by this mechanism as compared to the CNT's effect.

In the case of CNTs because they are nickel coated, it is expected a good bonding between the CNTs and AlSi matrix, so between Nickel and silicon the intermetallic Ni_2Si and NiSi can be generated [34-38]. Other studies [39] reported that reactions between Al and Ni may occur forming Al_3Ni at temperatures lower than the temperatures used in sintering in this work. The formation of intermetallic contributes to better load transfer. Based on another study of the same authors [40], no reactivity was detected between Al and Ni. The reduced thickness of the nickel coating on CNTs could justify the non-detection of this reaction. The diffusion of nickel to matrix since also cannot occur because there is reduced amount of Ni on CNTs and the matrix can dissolve the existent Ni. If Ni is totally dissolved in matrix and the CNT is expose to matrix, a reaction between the CNTs and matrix can occur leading to formation of SiC and Al_4C_3 [41,42]. It has been reported that the formation of SiC may have a beneficial effect in loading transfer [41]. The shear lag model should be adjusted and take in consideration the two new product formed between the AlSi matrix and CNTs [43]. In this case it is expected that the effect of shear reinforcement is less because the properties of these intermetalics are worst than CNTs. Another aspect that should be considered is the high probability of CNT to breakdown/damage during mixture, which can reduced the length of CNTs [44, 45]. This reduction contributes to a lower strengthening by shear lag [46,47]. It should be mentioned that the shear lag model does not take into account the effect of the CNTs curvature on the composite which have an influence on properties of the CNT composites as suggested by some FEM simulations [48].

(ii) Thermal mismatch. In addition to direct strengthening (shear lag), it can occur a secondary strengthening due to differential thermal contraction between matrix and reinforcement [49] during cooling from sintering temperature. This leads to creation of residual stresses. This strengthening should be higher in the case of SiCp reinforcement due to higher value of coefficient of thermal expansion (CTE). The CTE of CNTs [50] is close to zero 10^{-6} K^{-1}, the CTE of SiCp is 4.0×0^{-6} K^{-1}, while the AlSi have a higher CTE (24×10^{-6} K^{-1}) than both reinforcements and thus both contribute to this strengthening mechanism. According to Arsenault et al. [49] indirect strengthening due to thermal mismatch is directly proportional to volume fraction and aspect ratio

and inversely proportional to particle size. It is expected an enhanced dislocation punching with larger degree of interfacial area (i.e., smaller particle size) and due to this it is expected that CNTs have a larger contribution to strengthening by CTE reduced size in higher aspect ratio and also higher difference in CTE between the CNTs and the matrix.

(iii) Orowan strengthening mechanism. Another secondary strengthening is the presence of Orowan loops. The high number of volume-fractioned precipitates will effectively inhibit the movement of dislocations, generate more geometrically necessary dislocations and reach the critical dislocation density for fracture earlier during deformation, and thus increase the strength and decrease the elongation. The nanosize of CNTs increases the Orowan strengthening of the grain frontiers [51, 52]. Orowan strengthening can be related with the thermal mismatch because the difference in CTE between the matrix and reinforcements can introduce stress around the particles, that can be enough to cause plastic deformation in the matrix and dislocation loops around the vicinity of the particles [53]. CNTs may act as impenetrable obstacles similar to non-shearable precipitates and increase the yield stress through an Orowan mechanism [54].

8.4.3 Fatigue properties

Figure 8. 7 shows the fatigue results obtained as S-N curves for the unreinforced AlSi alloy and also for all AlSi composites. It should be noted that the specimens contained a pre-notch, so life contains mainly the propagation life.

It can be seen from Figure 8. 7 that under identical loading conditions the AlSi-2wt.%CNT composite (red continuous line – Figure 8. 7) has higher fatigue life than the unreinforced AlSi alloy (small blue dashed line – Figure 8. 7). More details regarding the fatigue behaviour of the unreinforced AlSi alloy and o AlSi-2%wt.CNTs composite are given elsewhere [19].

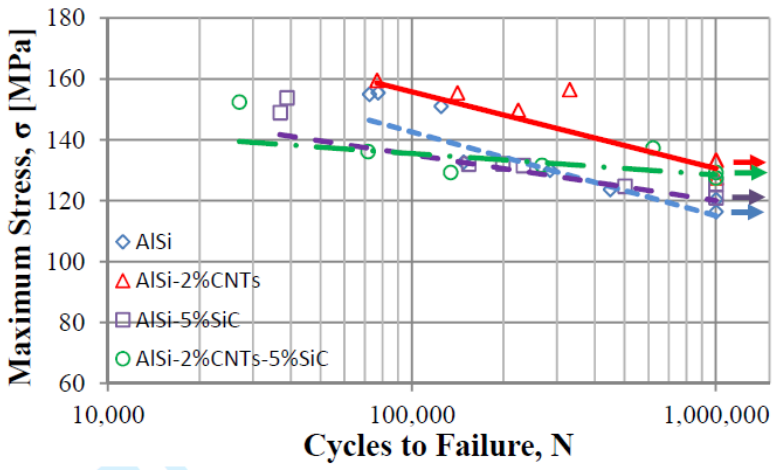

Figure 8. 7 - Maximum stresses (σ_{max}) vs. number of cycles to failure for unreinforced AlSi alloy and for the AlSi composites.

In the case of AlSi-5wt.%SiCp composite at lower stress (purple dashed line – fig. 7), the fatigue life is higher as compared to unreinforced AlSi alloy (red continuous line – fig. 7), while for higher stress levels the fatigue life is lower as compared to unreinforced AlSi alloy. The decrease of fatigue life in the case of AlSi-5wt.%SiCp composite at a higher stress level it can be explained based on large size of SiCp particles. At higher stress levels, according to Masuda et al. [55] the fatigue crack propagates mainly through the AlSi matrix, thus the lower fatigue life can be explained based on the fact that AlSi matrix has a high yield stress (according to [56]) due to hardening effect of SiCp. The hardening is consequence of different CTE between the SiCp and the AlSi matrix (thermal mismatch strengthening mechanism) and due to retention of dislocations (Orowan strengthening mechanism).

At lower stress levels (fatigue limit) the crack tends to orient in the direction of reinforcement particles [55] and thus it is expected a tortuous crack and thus a higher fatigue life. The presence of particles can also contribute to improve in fatigue life due to crack arrest. When the crack reach the particle two thinks can happen: the crack is blocked or the crack tends to be deflected by the particles [57] which contribute to an increase in fatigue like. Another aspect that should be mentioned in the case of AlSi composites is the shape of the SiCp particles which have very sharp edges that contributes to void nucleation due concentration of maximum shear strain near the tip of the of long SiCp particles [58].

Even for lower stress levels, the fatigue life just have a slight increase in fatigue life which can be explained by the presence of SiCp clusters, high yield stress due to hardening effect of the SiCp and the weak interface between the reinforcement and the matrix which contributes to void nucleation.

In case of AlSi-2wt.%CNTs-5wt.%SiCp hybrid composite (green dashed line – Figure 8. 7) the fatigue life is lower than the unreinforced AlSi alloy (red continuous line – Figure 8. 7) until the stress level of about 137 MPa, but after this the value the fatigue life is higher. At lower stress levels (fatigue limit) for all produced composites the fatigue life is higher. This fact is due to the presence of reinforcements (CNTs and SiCp) that have high modulus, high strength, and thus for a given stress, the composite undergoes a lower average strain. It can be seen from Figure 8. 7 that the CNTs have a beneficial effect on the fatigue life at all stress levels (red continuous line – Figure 8. 7). In the case of SiCp particles the fatigue life is lower until the stress level of about 125 MPa, while in the case of the hybrid composite this value is higher 137 MPa. Thus, the fatigue life of the hybrid composite is a consequence of the combined effects of both reinforcements. The improvement in the fatigue life of the hybrid composite life compared to unreinforced AlSi alloy is not linear because of the change on the total volume fraction of the reinforcement.

Figure 8. 8 presents the SEM images of the fracture surface morphologies of unreinforced AlSi alloy and AlSi composites.

It can be clearly seen from Figure 8.8-a that the crack path is very straight in the case of unreinforced AlSi alloy, while in the case of AlSi-2wt.%CNT composite (Figure 8. 8-b) the crack path is very tortuous. More details regarding the fracture morphology of the unreinforced AlSi alloy and of the AlSi-2%wt.CNTs composite are given elsewhere [19].

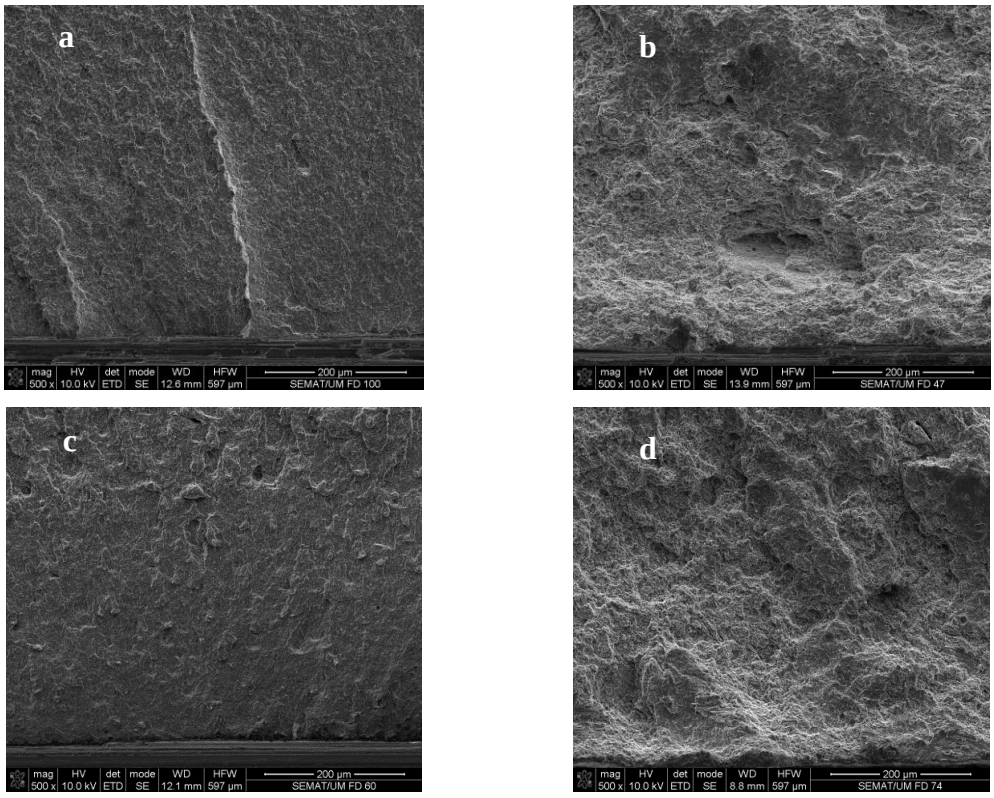

Figure 8. 8 - SEM images of the fracture surface after fatigue test: a. unreinforced AlSi alloy; b. AlSi-2wt. %CNT; c. AlSi-5wt.%SiCp and, d. Al-2wt.%CNT-5wt.%SiCp

From Figure 8. 8-c can be observed that the crack path in the case of AlSi-5wt.%SiCp it similar with the one observed in the case of unreinforced AlSi alloy, but slightly more tortuous. So, the crack travels through the grains of the material (intragranular fracture) and when it reaches a SiCp (as previously mentioned in the case of the tensile tests) if there is not boding between SiCp and AlSi matrix it may travel around the SiCp, but if there is bonding between the SiCp and AlSi matrix the crack may travel through the particle. It can be seen on the fracture surface of the AlSi-5wt.%SiCp composite a very smooth surface of the SiCp particle which can means that the SiCp was fractured. The fracture of the particles may occur when the interface strength is greater than strength of the SiCp and the particle-matrix de-cohesion occurs when the interface strength is less than the strength of the particle [26].

From Figure 8. 8-d can be observed that the crack path in the case of AlSi-2wt.%CNT-5wt.%SiCp hybrid composite is very tortuous. So, the crack propagation is a combined effect between both reinforcements, such as from the SiCp particle-AlSi de-bonding and also from the presence of CNT agglomerates. In well dispersed zones the crack propagates thought matrix

grains/particles (intragranular facture) and when reaches the SiCp, the crack may travels around it and the crack is accelerated due to weak bond between SiCp and AlSi matrix or may travels through it when there is bonding between SiC and AlSi matrix. If the crack reaches a region with CNTs (with good dispersion) the crack propagation is decelerated due to the strengthening effect of CNTs. If the crack reaches a zone with a poor CNT dispersion the crack is accelerated. This happened due to the presence of agglomerates. It is well known that in the case of fine particles, the crack goes around the particles [59], thus it is expected that the crack will not fracture the CNT due to their reduced size. So, CNTs should contribute to an increase in fatigue life due to crack deflection.

The fatigue damage in a metallic material is caused by plastic (irreversible) deformation which is generally produced by the motion of dislocations. The dislocation motion is affected by the precipitates, impurities, grain boundaries [60]. There are different factors that affect the fatigue life of MMCs. Thus, there are several factors related with particles that affect the fatigue resistance of MMCs like particle volume fraction, size, shape and distribution [61-63]. These variables may have a different influence in proposed toughening mechanisms in particulate MMCs, such as crack front bowing (or crack pinning), crack-tip blunting, matrix plastic yielding, particle–matrix interfacial de-bonding, micro-cracking, crack deflection by hard particles etc [64-68].

Higher volume and decreasing in particle size result in higher fatigue strength [62]. Irregular shapes with sharp edges contribute to void nucleation [69, 70]. Thus, the irregular shape of the SiCp particles contributes to the reduction on fatigue life, while due to the nanoscale size of the CNTs, they contribute to an increase on the fatigue life.

A non uniform distribution of the reinforcement and formation of agglomerates can also contribute to void nucleation. Also it well known that the presence of porosity can contribute to crack propagation [71]. In this work is used the powder metallurgy and is used the hot pressing as consolidation processes, thus is not expected porosity. Some porosity can result from the agglomerates of CNTs which does not allow the fill by the matrix. The work hardened of the matrix inhibits strain relaxation to take place by deformation which causes the onset of void nucleation and propagation at a lower far field strain than that observed in the unreinforced material.

8.4.4 Wear properties

The volume loss of the AlSi pins (unreinforced AlSi alloy and AlSi - composites) and also of the mating GCI plate are shown in Figure 8. 9.

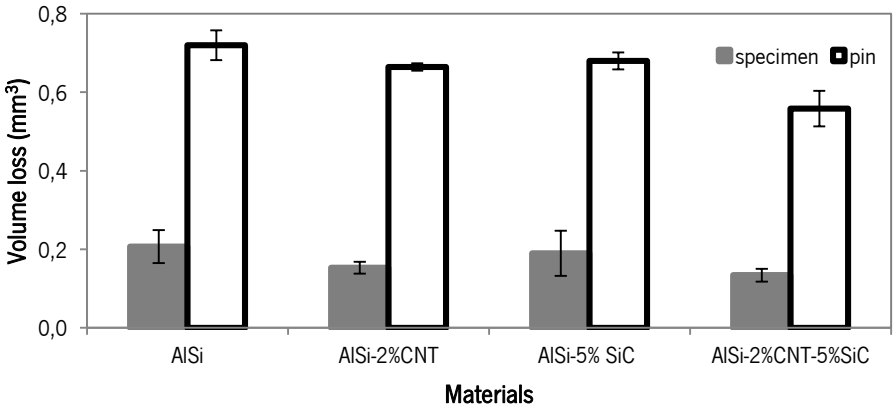

Figure 8. 9 - Variation on volume loss for unreinforced AlSi alloy and AlSi - composites

When comparing all AlSi composites with the unreinforced AlSi alloy it can be clearly seen that the wear of all studied composites is less than that of unreinforced alloy. The wear volume decreased with the addition of CNTs or SiCp, and it is further decreased with the incorporation of both reinforcements.

Figure 8. 10 presents SEM images of the worn surface of unreinforced AlSi alloy and of all AlSi-composites pins.

In the case of unreinforced AlSi pins surface (Figure 8. 10-a) adhesive wear is present, while in the case of AlSi-2wt.%CNTs pins (Figure 8. 10-b) it seems that there is a competition between adhesion and abrasion. More details regarding the wear behaviour of unreinforced AlSi alloy and AlSi-composites are given elsewhere [20, 21].

Regarding the worn surface of AlSi-5wt.%SiCp composite (Figure 8. 10-c) can be observed that it is very similar to the worn surface of unreinforced AlSi alloy (Figure 8. 10-a). It can be observed a large plastic deformation, but it is lower as compared to unreinforced AlSi alloy and much lower than AlSi-2wt.%CNTs composite. It has been demonstrated in a previous work of the same authors that this composites has a lower ductility [72] due to the hardening effect of the SiCp particles.

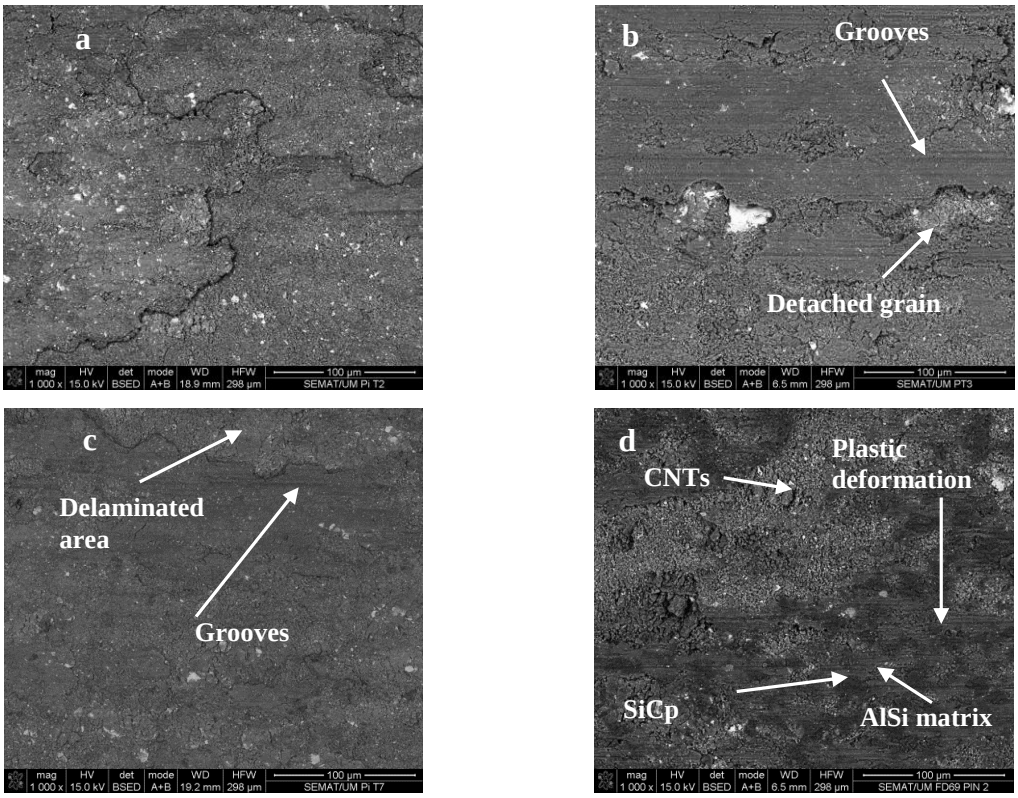

Figure 8. 10 - SEM images of the worn surface of: a unreinforced AlSi alloy; b. AlSi - 2wt.%CNTs; c. AlSi - 5wt.%SiCp and d. Al-2wt.%CNTs-5wt.%SiCp.

Regarding the worn surface of the AlSi-2wt.%CNTs-5wt.%SiCp hybrid composite can be observed (fig. 10d) similar plateaus as the ones observed in the case of unreinforced AlSi alloy: a smooth plateaus (adhesive wear) and the other one with more voids (abrasive wear). The AlSi hybrid composite seems to be controlled essentially by two mechanisms: abrasive wear and adhesive wear that includes a small amount of plastic deformation and material transfer between the mating surfaces. The introduction of both reinforcements (CNTs and SiCp particles) in the AlSi matrix seems to have a beneficial role, once both pin and counterface material exhibited an improvement on wear resistance, as compared to unreinforced AlSi/GCI tribopair.

The main contributions of the reinforcements are: (i) Strengthening effect of CNTs (a stronger bonding between AlSi grain interfaces due to the CNTs); (ii) Self-lubrication effect of CNTs (CNTs and the CNTs agglomerates are released into the contact - that could roll into the sliding contact); (iii) Strengthening effect of SiCp (SiCp increased the hardness of the composite); (iv) Load

bearing elements (during sliding the SiCp particles support the load and prevent the contact between the AlSi matrix and the GCI plate).

It should highlight that the addition of different reinforcement types can contribute in different ways: similar reinforcement mechanisms and/or the same mechanisms by acting at different scales nano-scale or micro-scale) to the final overall mechanical and wear properties of the composites.

It should be mentioned that the beneficial effect of the addition of CNTs and SiCp was mainly observed in the case of the tensile tests. Is was already proved that by increasing the volume fraction of the CNTs until 6wt.%CNTs there was an increase in the tensile strength until a certain reinforcement volume fraction (2%wt of CNTs). The tensile strength increased from σ_r = 170 MPa for unreinforced AlSi alloy to σ_r = 209 MPa for 2%wt of CNTs, followed by a drop on the same mechanical property for a higher content of CNTs. Thus, by adding other reinforcement (5 % wt. SiCp) it was possible to further increase the tensile strength (σ_r = 233 MPa). This was possible only with the simultaneous effect of one mechanism at different scales or with the effect of two different mechanisms.

In the case of fatigue and wear tests this phenomenon may not necessarily occur. As a fact in the case of fatigue behaviour the microstructural characteristics such as pores (ex. CNTs agglomerates, SiC clusters) and defects have a higher detrimental impact than in tensile tests. Thus the fatigue behaviour did not follow the tensile behaviour.

Also in case of wear, the improvement cannot be necessarily attributed to the cumulative effect of both reinforcements. In another study [20] it was already proved the effect of CNT content (from 2wt.% to 6wt.%CNTs) over the wear behaviour of AlSi-CNTs composites. All AlSi-CNT composites experienced a substantial improvement in the wear behaviour when compared to unreinforced AlSi alloy. Although the addition of the 5 % wt. SiCp improved the wear behaviour, it cannot be attributed to the cumulative effect of both reinforcements but to the higher volume fraction of the reinforcement.

So it is important to highlight that by adding the SiCp there is an improvement on mechanical properties such as tensile strength, σ_r and yield strength σ_y but in the same time maintaining the other properties such as wear and fatigue properties. Thus it is concluded that the use of two reinforcements, by using different reinforcement mechanisms or the same mechanism but at different scales, may provide better overall properties than by using one reinforcement.

8.5 Conclusions

From the present investigation on mechanisms governing the tensile, fatigue and wear behaviour of AlSi composites the following conclusions can be drawn:

- AlSi-2wt.%CNT, AiSi-5wt.%SiC_p and AiSi-2wt.%CNT-5wt.%SiCp reinforced composites were successfully produced by hot-pressing technique.

- Compared to unreinforced AlSi alloy the tensile strength, σ_r and yield strength σ_y of AlSi composites was enhanced. The mechanisms responsible for improvement on the mechanical performance are based on the interface reinforcement and also on the matrix hardening. The best result was obtained in the case of hybrid composite.

- Compared to unreinforced AlSi alloy the fatigue life of AlSi–2wt.%CNTs composite was notably increased. This can be attributed to the strengthening of the interfaces and to the crack path deflection due to CNTs that are placed at the interfaces. Compared to unreinforced AlSi alloy the fatigue life of AlSi–5wt.%SiC_p and AlSi-2wt.%CNT-5wt.%SiC_p composites increased only for lower stress levels. The CNTs have a predominant effect on improvement on the improvement on the fatigue properties.

-The addition of both reinforcements (CNTs and SiC_p) in AlSi matrix improved the wear behaviour of the AiSi-2wt.%CNTs-5wt.%SiCp hybrid composite when comparing to AlSi- composites. It is shown that by reinforcing AlSi alloy with both reinforcement the wear behaviour of tribopair (AlSi-hybrid composite/GCI) is improved, when compared with unreinforced AlSi /GCI and AlSi alloy- composites /GCI tribopairs, due to the strengthening effect of CNTs, self-lubrication effect of CNTs and CNTs agglomerates, strengthening effect of SiC_p and load bearing elements of SiC particles.

The introduction of both reinforcements CNTs and SiCp seem to be a good choice for AlSi alloy, as the combination of these reinforcements lead to improvement on overall mechanical and wear behaviours of AlSi hybrid composite.

8.6 Acknowledgements

This work was supported by the Portuguese Foundation of Science and Technology through the project references PTDC/EME-PME/68664/2006, EXCL/EMS-TEC/0460/2012 and through the PhD grant with the reference SFRH/BD/44077/2008.

8.7 References

[1] P.K. Rohatgi, Metal matrix composites. 2013. Defence Sci J. 43: 323-349.
[2] T.S. Srivatsan, I.A. Ibrahim, F.A. Mohamed and E.J. Lavernia. 1991. Processing techniques for particulate-reinforced metal aluminium matrix composites. J Mater Sci. 26: 5965-5978.
[3] H.Y. Chu and J.F. Lin. 2000. Experimental analysis of the tribological behaviour of electroless nickel-coated graphite particles in aluminum matrix composites under reciprocating motion. Wear 239: 126-142.
[4] S.C. Lim, M. Gupta, L. Rena and J.K.M. Kwok. 1999. The tribological properties of Al–Cu/SiCpp metal–matrix composites fabricated using the rheocasting technique. J Mater Process Technol. 89–90: 591-596.
[5] B.G. Park, A.G. Crosky and A.K. Hellier. 2001. Material characterisation and mechanical properties of Al2O3-Al metal matrix composites. J Mater Sci. 36: 2417-2426.
[6] A.T. Alpas and J. Zhang. 1992. Effect of SiCp particulate reinforcement on the dry sliding wear of aluminium-silicon alloys (A356). Wear 155: 83-104.
[7] R. Perez-Bustamante, C.D. Gomez-Esparz, I. Estrada-Guel, M. Miki-Yoshida, L. Licea-Jimenez, S.A. Pérez-García and R. Martínez-Sánchez. 2009. Microstructural and mechanical characterization of Al-MWCNT composites produced by mechanical milling. Mater Sci Eng A-Struct Mater 502: 159-63.
[8] A.M.K. Esawi, K. Morsi, A. Sayed, A.A. Gawad and P. Borah. 2009. Fabrication and properties of dispersed carbon nanotube-aluminum composites. Mater Sci Eng A-Struct Mater 508: 167-173.
[9] I. Sridhar and K.R. Narayanan. 2009. Processing and characterization of MWCNT reinforced aluminum matrix composites. J Mater Sci. 44: 1750-1756.
[10] A.S.M.H. Committee and Klar E. 1984. Metals handbook: Powder metallurgy: 501. American Society for Metals. Powder Metallurgy C.
[11] J-Z. Liao, M-J. Tana and I. Sridhar. 2010. Spark plasma sintered multi-wall carbon nanotube reinforced aluminum matrix composites. Mater Design 31: S96-S100.
[12] C. Suryanarayana. 2004. Mechanical Alloying And Milling. Taylor & Francis: 292-293.
[13] T. Kuzumaki, O. Ujiie, H. Ichinose and K. Ito. 2000. Mechanical characteristics and preparation of carbon nanotube fiber- reinforced Ti composite. Adv Eng Mater 2: 416-418.
[14] S. Mula, K. Mondal, S. Ghosh and S.K. Pabi. 2010. Structure and mechanical properties of Al-Ni-Ti amorphous powder consolidated by pressure-less, pressure-assisted and spark plasma sintering. Mater Sci Eng A-Struct Mater 527: 3757-3763.
[15] Z.A. Munir, U. Anselmi-Tamburini and M. Ohyanagi. 2006. The effect of electric field and pressure on the synthesis and consolidation of materials: A review of the spark plasma sintering method. J Mater Sci 41: 763-777.
[16] C.F. Deng, D.Z. Wang, X.X. Zhang and A.B. Li. 2007. Processing and properties of carbon nanotubes reinforced aluminum composites. Mater Sci Eng A-Struct Mater. 444: 138-145.

[17] R. Perez-Bustamante, I. Estrada-Guel, W. Antunez-Flores, M. Miki-Yoshida, P.J. Ferreira and Martinez-Sanchez R. Novel. 2008. Al-matrix nanocomposites reinforced with multi-walled carbon nanotubes. J Alloys Compd. 450: 323-326.
[18] T.S.M. Babu, M.S.A. Sugin and N. Muthukrishnan. 2012. Investigation on the Characteristics of Surface Quality on Machining of Hybrid Metal Matrix Composite (Al-SiCp-B4C) Procedia Eng. 38: 2617-2624.
[19] O. Carvalho, G. Miranda, M. Buciumeanu, N. Costa, D. Soares and F.S. Silva. September, 2014. Mechanisms Governing the Tensile, Fatigue and Wear Behaviour of Carbon Nanotube reinforced Aluminum Alloy. Submitted to Mech. Adv. Mater. Struc.
[20] O. Carvalho, M. Buciumeanu, D. Soares, J. Gomes and F.S. Silva. 2015. Improvement on sliding wear behaviour of Al/cast iron tribopair by CNTs reinforcement of an Al alloy. Tribol Trans. DOI 10.1080/10402004.2014.1002143.
[21]. O. Carvalho, M. Buciumeanu, S. Madeira, D. Soares, F. S. Silva and G. Miranda. 2015. Dry sliding wear behaviour of AlSi-CNTs-SiCp hybrid composites. DOI 10.1016/j.triboint.2015.04.031.
[22] Q. Zhang. 2012. Carbon nanotubes and their applications. RC Press, Taylor & Francis Group, ed.
[23] G.P. Tandon and G.J. Weng Stress. 1986. Distribution in and Around Spheroidal Inclusions and Voids at Finite Concentration. J Appl Mech. 53: 511-518.
[24] S.F. Corbin and D.S. Wilkinson. 1994. The influence of particle distribution on the mechanical response of a particulate metal matrix composite. Acta Metall Mater. 42: 1311-1318.
[25] F.L. Matthews and R.D. Rawlings. 1999. Composite Materials: Engineering and Science. Taylor & Francis.
[26] K.K. Chawla. 2012. Composite Materials: Science and Engineering. Springer.
[27] V.C. Nardone and K.M. Prewo. 1986. On the strength of discontinuous silicon carbide reinforced aluminum composites. Scrip Metallurgica 20: 43-48.
[28] H.R. Hafizpour and M. Khoeini. 2011. Compaction behavior of aluminum matrix composites reinforced with nano/micro scale SiCp particulates. J. Am. Sci. 7: 753-759.
[29] V.V.B. Prasad, B.V.R. Bhat, Y.R. Mahajan and P. Ramakrishnan. 2002. Structure–property correlation in discontinuously reinforced aluminium matrix composites as a function of relative particle size ratio. Mater Sci Eng A. 337: 179-86.
[30] V.V.B. Prasad, B.V.R. Bhat, P. Ramakrishnan and Y.R. Mahajan. 2000. Clustering probability maps for private metal matrix composites. Scripta Mater 43: 835-840.
[31] A. Slipenyuk, V. Kuprin, Y. Milman, V. Goncharuk and J. Eckert. 2006. Properties of P/M processed particle reinforced metal matrix composites specified by reinforcement concentration and matrix-to-reinforcement particle size ratio. Acta Metall. 54: 157-166.
[32] A. Slipenyuk, V. Kuprin, Y. Milman, J.E. Spowart and D.B. Miracle. 2004. The effect of matrix to reinforcement particle size ratio (PSR) on the microstructure and mechanical properties of a P/M processed AlCuMn/SiCpp MMC. Mater Sci Eng A. 381: 165-170.
[33] H.J. Ryu, S.I. Cha and S.H. Hong. 2003. Generalized shear-lag model for load transfer in SiC/Al metal-matrix composites. J Mater Res. 18: 2851-2858.
[34] E.G. Colgan, M. Mäenpää, M. Finetti and M.A. Nicolet. 1983. Electrical characteristics of thin Ni2Si, NiSi, and NiSi2 layers grown on silicon. J Electron Mater 12: 413-422.
[35] J. Foggiato, W.S. Yoo, M. Ouaknine, T. Murakami and T. Fukada. 2004. Optimizing the formation of nickel silicide. Mater Sci Eng B. 114: 56-60.
[36] F.F. Zhao, J.Z. Zheng, Z.X. Shen, T. Osipowicz, W.Z. Gao and L.H. Chan. 2004. Thermal stability study of NiSi and NiSi 2 thin films. Microelectron Eng.71: 104-111.
[37] D.C. Dunand. 1994. NiAl formation by annealing of infiltrated aluminium-nickel precursors. J Mater Sci. 29: 4056-4060.

[38] H. Okamoto. 1993. Al-Ni (aluminum-nickel). J. Phase Equil. 14: 257-249.
[39] J. Qian, J. Li, J. Xiong, F. Zhang and X. Lin. 2012. In situ synthesizing Al3Ni for fabrication of intermetallic-reinforced aluminum alloy composites by friction stir processing. Mater Sci Eng A. 550: 279-285.
[40] O. Carvalho, M. Buciumeanu, D. Soares, F.S. Silva and G. Miranda. 2015. Evaluation of CNT dispersion methodology effect on mechanical properties of an Al-Si composite. J Mater Eng Perform. DOI: 10.1007/s11665-015.
[41] T. Laha, Y. Chen, D. Lahiri and A. Agarwal. 2009. Tensile properties of carbon nanotube reinforced aluminum nanocomposite fabricated by plasma spray forming. Composites Part A 40: 589-594.
[42] S.R. Bakshi, R.R. Patel and A. Agarwal. 2010. Thermal conductivity of carbon nanotube reinforced aluminum composites: A multi-scale study using object oriented finite element method. Comp Mater Sci. 50: 419-428.
[43] J.N. Coleman, M. Cadek, R. Blake, V. Nicolosi, K. P. Ryan, C. Belton, A. Fonseca, J. B. Nagy, Y. K. Gun'ko and W. J. Blau. 2004. High-performance nanotube-reinforced plastics: Understanding the mechanism of strength increase. Adv Funct Mater. 14(8): 791-798.
[44] S.R. Bakshi, V. Singh, K. Balani, D.G. McCartney, S. Seal and A. Agarwal. 2008. Carbon nanotube reinforced aluminum composite coating via cold spraying. Surf Coat Tech. 202: 5162-5169.
[45] H. Choi, J. Shin, B. Min, J. Park and D. Bae. 2009. Reinforcing effects of carbon nanotubes in structural aluminum matrix nanocomposites. J Mater Res. 24: 2610-2616.
[46] M.Y. Koo, J.S. Park, M.K. Park, K.T. Kim and S.H. Hong. 2012. Effect of aspect ratios of in situ formed TiB whiskers on the mechanical properties of TiBw/Ti–6Al–4V composites. Scripta Mater 66: 487-490.
[47] S. Dong, J. Zhou, D. Hui, Y. Wang and S. Zhang. 2015. Size dependent strengthening mechanisms in carbon nanotube reinforced metal matrix composites. Compos Part A-Appl S. 68: 356–364.
[48] V. Anumandla and R.F. Gibson. 2006. A comprehensive closed form micromechanics model for estimating the elastic modulus of nanotube-reinforced composites. Compos Part A-Appl S. 37: 2178-2185.
[49] R.J. Arsenault and N. Shi. 1986. Dislocation generation due to differences between the coefficients of thermal expansion. Mater Sci Eng. 81: 175-187.
[50] Y-K. Kwon, S. Berbera and D. Tománek. 2004. Thermal contraction of carbon fullerenes and nanotubes. Phys Rev Lett. 92, 015901-1-015901-4.
[51] R.J. Arsenault and N. Shi. 1986. Dislocation generation due to differences between the coefficients of thermal expansion. Mater Sci Eng. 81: 175-187.
[52] Z. Zhang and D.L. Chen. 2006. Consideration of Orowan strengthening effect in particulate-reinforced metal matrix nanocomposites: A model for predicting their yield strength. Scripta Mater 54: 1321–1326.
[53] Z. Zhang and D.L. Chen. 2008. Contribution of Orowan strengthening effect in particulate-reinforced metal matrix nanocomposites. Mater Sci Eng A. 483–484: 148–152.
[54] S-M. Choi and H. Awaji. 2005. Nanocomposites—a new material design concept, Sci Technol Adv Mat. 6: 2-10.
[55] N. Yu, Z.H. Zhang and S.Y. He. 2008. Fracture toughness and fatigue life of MWCNT/epoxy composites. Mater Sci Eng A. 494: 380–384.
[56] C. Masuda and Y. Tanaka. 1992. Fatigue properties and fatigue fracture mechanisms of SiCp whiskers or SiCp particulate-reinforced aluminium composites. J Mater Sci. 27: 413-422.

[57] D. Hull and T.W. Clyne. 1996. An Introduction to Composite Materials. Cambridge University Press.
[58] S. Suresh. 1998. Fatigue of Materials. Cambridge University Press.
[59] R.K. Abu Al-Rub, A.I. Ashour and B.M. Tyson. 2012. On the aspect ratio effect of multi-walled carbon nanotube reinforcements on the mechanical properties of cementitious nanocomposites. Constr. Build. Mater. 35: 647-655.
[60] D. Bikiaris. 2010. Microstructure and Properties of Polypropylene/Carbon Nanotube Nanocomposites. Materials 3: 2884-2946.
[61] F. Ellyin. 1997. Fatigue Damage, Crack Growth and Life Prediction. Springer.
[62] A. Mortensen. 2006. Concise Encyclopedia of Composite Materials. Elsevier Science: 367-371.
[63] N. Chawla, J.W. Jones, C. Andres and J.E. Allison. 1998. Effect of SiCp volume fraction and particle size on the fatigue resistance of a 2080 Al/SiCp p composite. Metall Mater Trans. A29: 2843-54.
[64] A. Kelly, C.H. Zweben. 2000. Comprehensive composite materials. Elsevier.
[65] J. Cho, M.S. Joshi and C.T. Sun. 2006. Effect of inclusion size on mechanical properties of polymeric composites with micro and nano particles. Compos Sci Technol 66: 1941-1952.
[66] T. Adachi, M. Osaki, W. Araki and S-C. Kwon. 2008. Fracture toughness of nano- and micro-spherical silica-particle-filled epoxy composites. Acta Metall. 56: 2101-2109.
[67] S-Y. Fu, X-Q. Feng, B. Lauke and Y-W. Mai. 2008. Effects of particle size, particle/matrix interface adhesion and particle loading on mechanical properties of particulate–polymer composites. Compos Part B-Eng. 39: 933-961.
[68] M. Kotoul and J. Vrbka. 2003. Crack bridging and trapping mechanisms used to toughen brittle matrix composite. Appl Fract Mec. 40: 23-44.
[69] M. Salviato, M. Zappalorto and M. Quaresimin. 2013. Plastic shear bands and fracture toughness improvements of nanoparticle filled polymers: A multiscale analytical model. Compos Part A-Appl S 48: 144-152.
[70] S. Qin, C. Chen, G. Zhang, W. Wang and Z. Wang. 1999. The effect of particle shape on ductility of SiCpp reinforced 6061 Al matrix composites. Mater Sci Eng A. 272: 363-370.
[71] J.E. Spowart and D.B. Miracle. 2003. The influence of reinforcement morphology on the tensile response of 6061/SiCp/25p discontinuously-reinforced aluminum. Mater Sci Eng A. 357: 111-123.
[72] O. Carvalho, G. Miranda, D. Soares and F.S. Silva. 2014. Carbon nanotube dispersion in aluminum matrix composites – quantification and influence on strength. Mech Adv Mat Struct. DOI: 10.1080/15376494.2014.929766.

9 Optimization of AlSi-CNTs functionally graded material composites for engine piston rings

O. Carvalho[1], M. Buciumeanu[2],S. Madeira[1], D. Soares[1], F. S. Silva[1], G. Miranda[1]

[1]CT2M – Centre for Mechanical and Materials Technologies, University of Minho,
Azurém, 4800-058 Guimarães, Portugal
[2]Cross–Border Faculty of Humanities, Economics and Engineering, "Dunarea de Jos" University of Galati,
Domneasca 47, 800008 Galati, Romania

Published in Materials and Design 80 (2015) 163–173

9.1 Abstract

The damage of piston rings is attributed first to wear, then to lubrication and fatigue. Their damage may be substantially mitigated by creating a FGM-Functionally Graded Material composite with optimized mechanical behaviour. The aim of this paper was to produce an AlSi-CNTs functionally graded material (FGM) that can be considered for engine compression piston rings. The AlSi graded composites (reinforced with 0 to 2wt.%CNT FGM approach) was obtained with a new equipment that was designed to produce FGMs by powder metallurgy (PM) processing route. SEM analysis showed that the produced FGMs have a gradual change in %wt. of reinforcement and on mechanical properties. Results of yield strength, ultimate tensile strength, tensile strain, fatigue limit performance and wear loss are presented and discussed. It is expected that the obtained AlSi-CNTs functionally graded composite developed for piston rings may have a global equilibrium of properties and cost.

Keywords: FGMs; CNTs; AlSi; static properties; fatigue life; wear.

9.2 Introduction

In practice the piston rings damage is attributed first to wear (as there are parts in contact and in relative motion), then to lubrication and fatigue [1]. Thus, a compression piston ring should

have some fundamental technical specifications such as: substantially high bulk modulus; high wear resistance on the surface that contacts the cylinder wall; high fatigue resistance; ability to retain oil on its structure during dead periods so that when engine starts there is lubricant on the ring-cylinder wall interface.

There are many manufacturing processes for piston rings. Probably the most conventional production process is casting and subsequent finishing followed by electrodeposition chromium coating in which a process is made that leads to the creation of small surface cracks which serve to retain the oil [2, 3] during dead periods. In order to improve the wear resistance the rings are coated with a hard coating [4]. The main problem here is the interface between the metal and ceramic due to the different thermal expansion coefficients when it is subjected to temperature. The discrete dilatation of the metal and the ceramic leads to the delamination of the coating. Other coatings have an outer surface with a certain degree of porosity in order to retain oil during dead periods. The main problem with these rings is the low mechanical and fatigue resistance, as well as low wear properties [4]. Among the last generation compression piston rings are the physical vapour deposition (PVD) coated steel rings and chromium ceramic coated cast iron rings. PVD have the interface problems (delamination) between steel and coating while the chromium coatings show some problems related with the fatigue resistance due to surface micro-cracks induced during the processing for oil retention [2].

Thus, the solution to overcome the previously mentioned problems would be the creation of a ring with different properties along the section, in accordance with the different local solicitations. In this case, the inner part of the ring should provide the strength and modulus and the outer part should guarantee wear and fatigue resistance along with the ability to retain oil.

The present paper proposes a solution that is able to overcome the previously mentioned problems. This would be achieved by using a Functionally Graded Material (FGMs – creation of a chemical gradient in the component by using a gradation of the reinforcement along the cross section of the piston ring). The processing solution is via a powder metallurgy (PM) route and it will be shown that the process is adequate to produce FGMs.

As reinforcement, CNTs were tested along with an AlSi matrix. CNTs have excellent mechanical properties and high wear resistance while the AlSi alloy is frequently used in engine components such as engine pistons [1] due to low weight.

Among the amazing properties of CNTs, some of them seem to fit very well the design of high performance engine compression piston rings, such as:

(i) The tensile strength of SWNTs can be 20 times that of steel [5] and 6 times more than the most resistant carbon fibre available at the market (T1000 from Torayca). It is about 45 GPa [6] for SWNTs and about 150 GPa for perfect MWNTs from electric arc [7]. It has been already shown that by adding a small volume fraction of CNTs (about 0.5 and 2%, respectively) into an Al alloy, there is an increase of the yield and ultimate strength of about 12% and 23% respectively, as compared to pure Al [8].

(ii) Tensile modulus reaches the highest values ever, 1 TPa for MWNTs [9], and possibly even higher for SWNTs, up to 1.3 TPa [10].

(iii) CNTs are highly wear resistant. CNTs can be used to fabricate composites and coatings with excellent tribological performance [12-16]. The CCVD MWNTs-Cu composites [9, 11] show a high hardness and a low coefficient of friction (COF) and wear loss. The COF was also shown to increase and the wear loss to decrease upon the increase in nano-tube volume fraction in carbon/carbon composites [12].

(iv) CNTs are able to retain oil. The CNTs are able to retain oil inside the tubes. As a fact the inner diameter of CNTs may vary from few nanometers to about 100 nm. These would allow the oil to enter in the CNTs and to be retained there during dead periods. This ability to retain oil along to its liquid adsorption properties make CNTs adequate to be at the contact surface between ring and cylinder wall when engine starts up.

(v) CNTs are light. They have half the mass density of aluminium. Its density may vary from 1,2 g/cm^3 for SWNT to 1,8 g/cm^3 for MWNT [8]. Thus an aluminium matrix composite compression ring reinforced with CNTs will become lighter not only because the matrix is lighter but also due to the reinforcement. This reduces inertia and consequently consumption.

(vi) CNTs have excellent thermal conductivity. Heat transfer from the piston to the cylinder wall is also important on compression piston rings. Thus an AlSi matrix composite compression ring reinforced with CNTs will become a better thermal conductor not only due to the matrix that have a high thermal conductivity, but also due to high thermal conductivity of CNTs.

Some studies show the ability of PM technique to be used with CNTs reinforcement [13-19]. SWNTs are stable up to 750°C in air and up to ≈ 1500–1800°C in inert atmosphere. Thus,

in terms of processing, the CNTs seem to fit the PM technique. In service, (working temperatures of compression piston rings are less then 200°C) the CNTs incorporated in the rings do not suffer degradation. On the other hand on the automotive field, when producing large series, there is a general movement towards sintered parts. There are basically two market drivers that shape the development of automotive components: the drive to reduce costs and the drive to improve vehicle performance. At present, the move to PM parts is being driven by the first of these. Sintered parts can reduce costs dramatically, by up to a half, because of their good precision, suitability for mass production and low material wastage [20].

CNTs are also promising materials as reinforcement in FGMs obtained by PM. PM is also suitable for the production of FGMs. With a proper distribution of the powders and reinforcement is easy to place the materials in the intended locations. In the particular case of the compression rings, powders and CNTs will be placed with the aid of a centrifugal movement in order to change their volume fraction in the radius direction. One of the main advantages of FGMs as compared to coatings is that FGMs present a smooth transition of composition allowing a better distribution of residual stresses. This effect highly enhances the fatigue behaviour of the component as well as its thermal properties.

The aim of this paper was to produce an AlSi-CNTs functionally graded material (FGM) by powder metallurgy (PM) processing route with the aim of being a candidate for engine compression piston rings production. Results of mechanical properties, fatigue limit performance and wear loss of the proposed solution are presented and discussed.

9.3 Experimental procedure

9.3.1 Materials

AlSi alloy powder (size < 325 mesh < 44 μm), with chemical composition as shown in Table 9. 1, was used as matrix material. AlSi powder was purchased from AlfaAesar – Germany. Ni coated MWCNT's with outer diameter > 50 nm, length 0.5-2.0 μm, purity before coating > 95wt% and ash <1.5wt% were used as reinforcement. Ni coated MWCNTs were purchased from CheapTubes.com – USA.

Table 9. 1 - Chemical composition of AlSi alloy (wt.%)

Al	Si	Fe	Others
87.3	11	0.20	1.5

AlSi-2wt.%CNT graded composites were obtained by two steps: gradation and consolidation. The first step, initiates with the mixing of AlSi alloy with MWCNT's inside a closed stainless steel jar with 10 mm diameter steel milling balls at 40 rpm during 6 days (low-energy ball milling) under argon atmosphere. Then, the gradient containing 2wt.% of CNT in AlSi alloy was created using a new equipment as described in section 9.4.2. The bulk consolidation of graded green compact was achieved using powder metallurgy.

9.3.2 Sintering process

The AlSi-matrix composite reinforced by CNTs (AlSi-CNTs) were processed through traditional hot pressing (HP) technique. The specimens were produced under pressure (35 MPa) during 10 minutes at 550°C and under vacuum (10^{-2} mbar), using a high frequency induction furnace. The compaction was made on a graphite cylindrical die with an internal rectangular cavity. The mold was placed inside the chamber where the sample was compressed at 1.3 MPa and heated with a heating rate of 25°C/min. Then, the sample cooled to room temperature under vacuum.

9.3.3 Mechanical characterization

Tensile tests.

Tensile testing was carried out in order to obtain the mechanical properties, such as tensile strength σ_r, yield strength σ_y and tensile strain ε_r. The flat-dog-bone shaped tensile specimens were machined from the produced samples. Tensile tests were carried out using a servo-hydraulic universal testing machine Instron 8874, equipped with a load cell capacity of 25 kN (tension). Tests were performed at room temperature (≈23 °C), with a crosshead speed of 0.05 $mm.s^{-1}$ and 5 specimens were used for each condition.

Fatigue tests.

In order to get the influence of the CNT content on the fatigue life (S-N curve), several fatigue tests were carried out at a stress ratio R=0.1 using a servo-hydraulic universal testing machine Instron 8874. All tests were performed at ambient temperature, in laboratory environment, and at a cyclic frequency of 16 Hz. Tests were performed until final fracture. The flat-dog-bone shaped specimens were machined from the produced samples. A single edge notched configuration was adopted for the fatigue tests.

Wear tests.

Reciprocating pin-on-plate wear tests has been used as a very simplified test for piston ring and cylinder liner materials with the pin representing the ring and the plate representing the cylinder. Figure 9. 1shows schematically the test performed in this work: applied normal load (Fn) on the pin and alternative displacement (d) of the flat specimen. The flat plates (40×18×5 mm) prepared for the wear tests were machined from cast iron. Pins were machined from the AlSi matrix composites reinforced with 2wt.%CNTs, that can be used for engine piston rings. The dimensions of the pin are: radius of curvature 40 mm, thickness 3.5 mm and the arc length 20 mm.

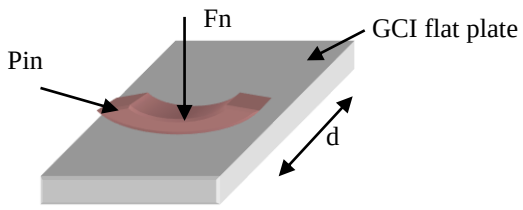

Figure 9. 1 - Schematic test configuration: Fn – Normal applied load; d – alternated displacement amplitude.

Hardness measurements

Hardness measurements were conducted in the unreinforced matrix material, produced MMCs and FGMs. Vickers hardness measurements were obtained as a mean of 16 indentations per sample using a Shimadzu micro hardness tester with a load of 200 gf during 15 s.

The obtained FGM composites were characterized by means of Scanning Electron Microscopy (SEM)/Energy Dispersive Spectrometer (EDS).

9.4 Results and discussion

As the aim of this paper was to develop a FGM that fulfil engine compression piston rings specifications. It well known that stresses are mainly located at inner and outer surfaces. Thus mechanical and fatigue properties are mainly required at these surfaces. Wear resistance is also required mainly at the outer surface due to contact with cylinder wall.

A Functionally graded composite seems to be an adequate solution to achieve these properties by building a linear gradient where the maximum fraction of reinforcement is where the maximum stress and wear properties are required. In order to choose the optimal CNT content that can support the mechanical and wear solicitations of a piston ring first it will be briefly shown the mechanical and wear results of the AlSi-CNT composites with different volume fractions of CNTs and after that the methodology used to develop the proposed FGM and also the mechanical (tensile and fatigue) results of the chosen FGM.

9.4.1 Effect of CNT content over the mechanical behaviour of AlSi-CNT composites

In order to define the best CNTs volume fraction for improved mechanical and fatigue properties, to apply in each zone of the FGMs solution, homogeneous composites were produced. The effect of CNT content (from 0 wt.% to 6 wt.% CNT) over the mechanical behaviour (tensile, fatigue and wear) of AlSi-CNT homogeneous composites was studied.

Mechanical properties (Tensile tests)

Figure 9. 2 shows the mechanical properties (tensile strength, σ_r, yield strength σ_y and tensile strain ε_r) of unreinforced AlSi alloy and of the AlSi composites.

The tensile tests revealed that the AlSi-2wt.%CNT composite is the volume fraction that maximizes tensile strength (improved by about 23%) as well as yield strength (improved about 26%) as compared to unreinforced AlSi alloy and other CNT volume fractions.

This peak was achieved with a reduction in rupture strain. The substantial decrease in rupture strain with addition of the CNTs suggests that there was an embrittlement of the composite. This is due to the difference in the coefficients of thermal expansion between the matrix and the

reinforcement (CNTs is $\approx 10^{-6} K^{-1}$ and for AlSi alloy is $23x10^{-6} K^{-1}$). However although this reduction, a substantial ductility, (about 65% on initial ductility) is still kept in the composite for the AlSi-2wt.%CNT composite.

Figure 9. 3 shows the SEM images of the fracture surface after tensile test (with 1000x magnification) of the unreinforced AlSi alloy and of AlSi - 2wt.%CNT composite.

Figure 9. 3-a shows typical fracture surface morphology of aluminium alloys. The smoother fracture surface observed in the case of the unreinforced AlSi alloy is due the fact that the AlSi grains are very well bonded (control the fracture behaviour). Thus, the crack travels through the AlSi grains of the material (intragranular fracture) and it is accompanied by a large amount of plastic deformation.

Regarding the surface fracture of AlSi-2%wt.CNTs composite (Figure 9. 3-b), there can be well observed smoother regions and a few regions with more pronounced shaped peaks and valleys. This observation may be explained based on the anisotropy of the AlSi-2wt.%CNTs composite pins.

Based on the microstructural images of theAlSi-2%wt.CNTs composite (Figure 9. 4) and on another study of the same authors [21] where was studied the quantification and characterization of CNTs agglomerates and dispersion, it has been demonstrated that there are zones where the CNTs are very well dispersed and zones with a poor dispersion (where the CNTs agglomerations are located). The smoother plateaus correspond to the regions where the CNTs are better dispersed and the rougher regions to the regions where there is a poor distribution of CNTs (where the agglomerates are located). These rougher regions are areas of weakness from which failure was initiated.

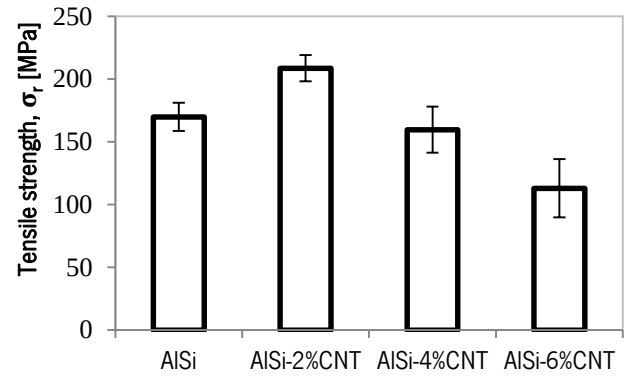

a

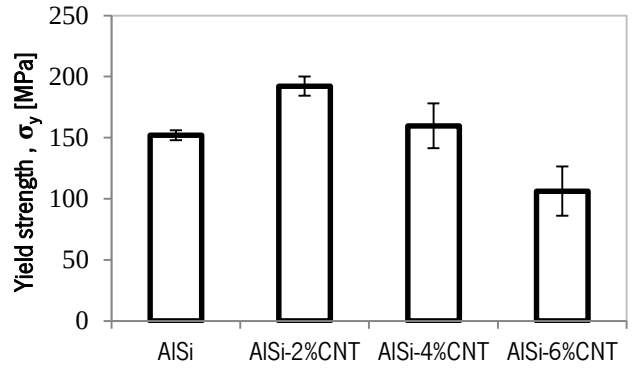

b

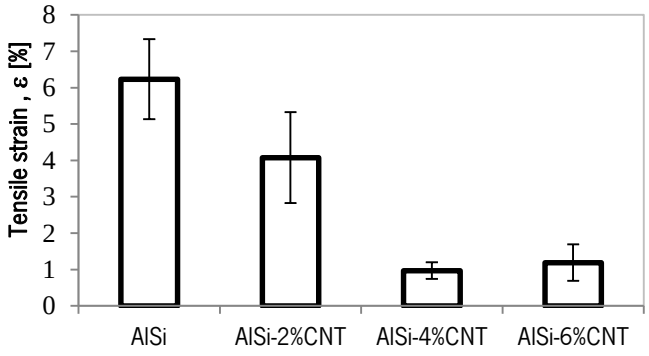

c

Figure 9. 2 - Results of tensile testing of unreinforced AlSi alloy and of the AlSi composites: a. tensile strength, b. yield strength, and c. tensile strain.

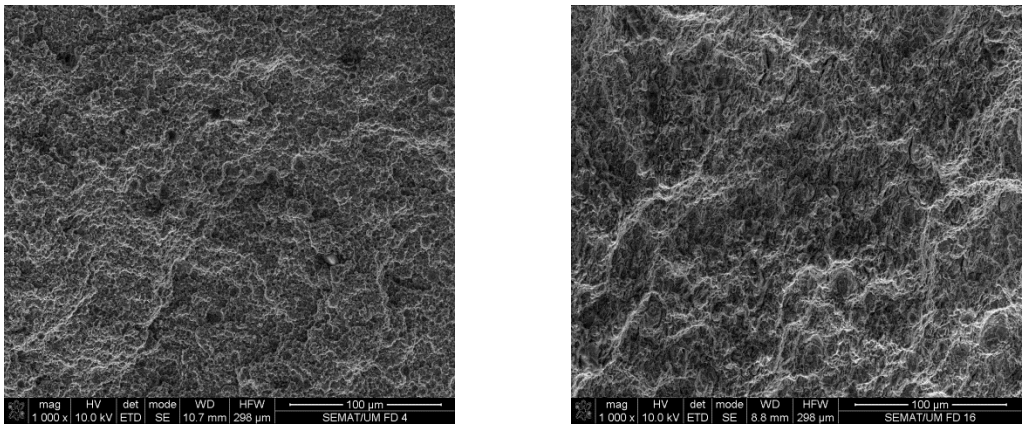

a b

Figure 9. 3 - SEM images of the fracture surface after tensile test (with different magnifications) of: a. unreinforced AlSi alloy; b. AlSi - 2wt.%CNT.

It has been demonstrated in another study of the same authors that the CNT agglomerates have a big influence on the mechanical properties of the composites [22]. The agglomerations of CNTs act like stress concentration zones and thus decrease the mechanical properties. This is in accordance with other studies [24-25]. For example, Jen et al. [25] showed that a high CNT content has an adverse effect on the strength because the stress concentration effects caused by the CNT agglomerates reduce the tensile strength of the nanocomposites.

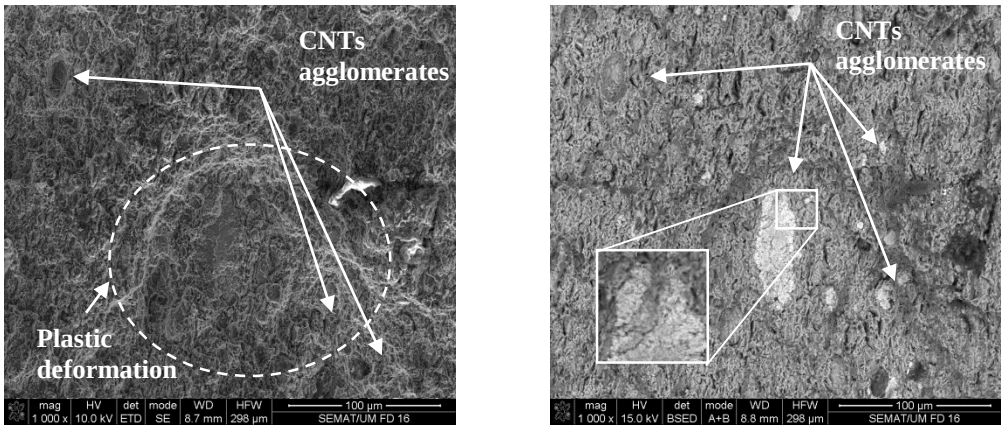

Figure 9. 4 - SEM images of the fracture surface after tensile test showing the presence of CNTs agglomerates (AlSi-2 wt. % CNT composite –with magnification 1000x).

As a result in the case of AlSi composites reinforced by CNTs the fracture (crack) may initiate in the regions of agglomerates (stress concentration). If the crack reaches a region where the CNTs are well dispersed it may travel through the AlSi grain (intragranular fracture), but if the crack reaches zones of weakness (the zones where the agglomerates are located, between the AlSi grains), then the crack follows the grain of the material (intergranular fracture). The consequence of this is a rougher region where the agglomerates are formed and a smoother surface when the crack travels through the AlSi grain.

Even though there are these zones that behaves like stress concentrations (as called weakness zones), the strengthening effect of CNTs in the zones where the CNTs are well dispersed prevails, thus the mechanical properties of the AlSi 2wt.%CNT composite are higher than unreinforced AlSi alloy. Thus, the increase in the tensile strength and yield strength with the addition of the CNTs is related to the fact that the AlSi grains are bonded with an improved strength due to CNTs interface reinforcement effect (Figure 9. 2-b), as stated for example by George et al. [8].

A detailed explanation regarding the tensile behaviour of the unreinforced AlSi alloy and of the AlSi-CNTs composites is given elsewhere [26].

Microstructural characterization

Figure 9. 5 shows the SEM micrographs of the composites with different amounts of CNTs. These images were derived from the images which were obtained by SEM/EDS (x-ray maps). The white areas are CNT agglomerates that were isolated and enhanced by image processing. Doing a qualitative analysis of images represented in Figure 9. 5, it can be seen that CNT agglomerations are increasing as the weight percent of CNTs increases, which contributes to a deterioration of mechanical properties as seen in Figure 9. 2.

Figure 9. 5 shows that the dispersion of CNTs has not been well achieved. As a fact the presence of CNT agglomerates is a major problem in regard to mechanical performance. This phenomenon is difficult to overcome because of the large difference between the size of CNTs and the metal powders and due to their attractive van der Waals interactions [16]. This study is in agreement with other studies which confirm that the amount of CNTs may substantially affect mechanical properties [27-29].

So it is possible that the maximum dispersion rate is achieved with 2 wt% CNTs. When the amount of CNTs increases it is possible that they start functioning as a defect due to agglomerations formations. In fact it was found that some agglomeration of CNTs occurred in samples with 2% wt CNTs (see Figure 9. 4). Therefore, with a quantity higher than 2 wt% it is probable that the number of agglomerates is higher, which is confirmed in Figure 9. 5.

In Figure 9. 6 can be noticed the detrimental effect of CNTs agglomerates on mechanical proprieties. It can be observed the presence of the crack on the agglomerate zone. As already mentioned when the fracture surface was analysed, the agglomerates are considered weak zones that are favourable to crack grow and propagation as can been seen in Figure 9. 6.

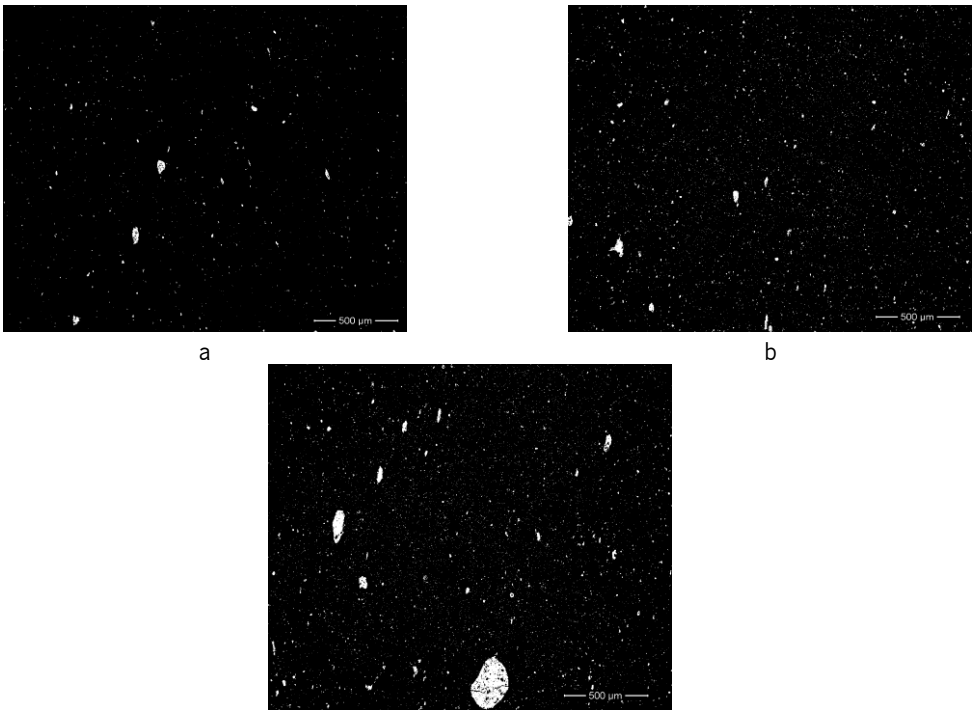

a b c

Figure 9. 5 - SEM micrographs of the composites with different amounts of CNTs to highlight the CNTs agglomerates: a. 2wt.% CNTs; b. 4 wt.% CNTs and c. 6 wt.% CNTs.

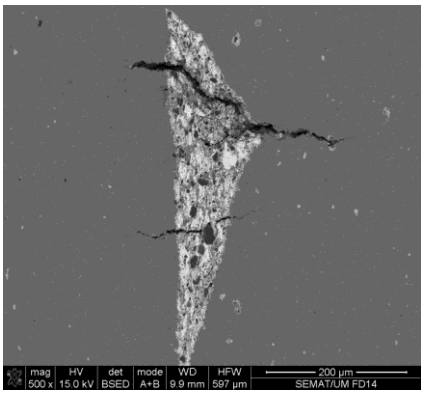

Figure 9. 6 - SEM micrographs of the composites with 2 wt% CNTs showing the crack formation on an CNT agglomerate.

Hardness values as a function of the CNT content

Figure 9. 7 shows the hardness results as a function of CNT content in all AlSi-CNT composites.

As expected, the hardness increases with increasing CNT content. As compared to the unreinforced AlSi alloy (pin), the CNT composites show an increase of about 26% to 41%. This behaviour may eventually be explained based on the fact that the CNTs, placed in the grain interfaces. A deeper explanation regarding the increase of hardness with the CNTs are presented elsewhere [30], and this is in agreement with other studies [31-36].

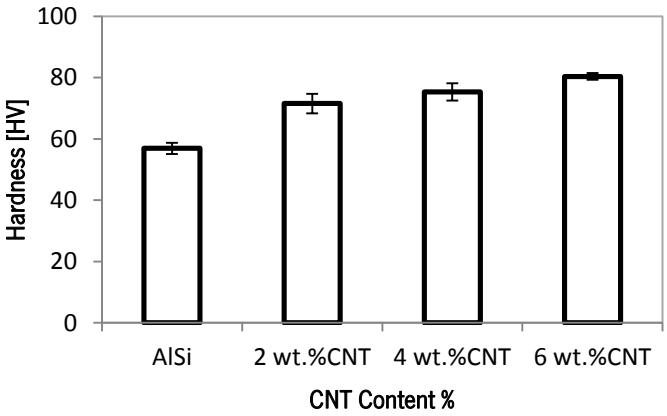

Figure 9. 7 - Hardness as a function of the CNT content.

Wear properties

The wear characteristics (weight loss) according to the CNT content in AlSi alloy matrix composite pins and also for the mating GCI plate are shown in Figure 9. 8.

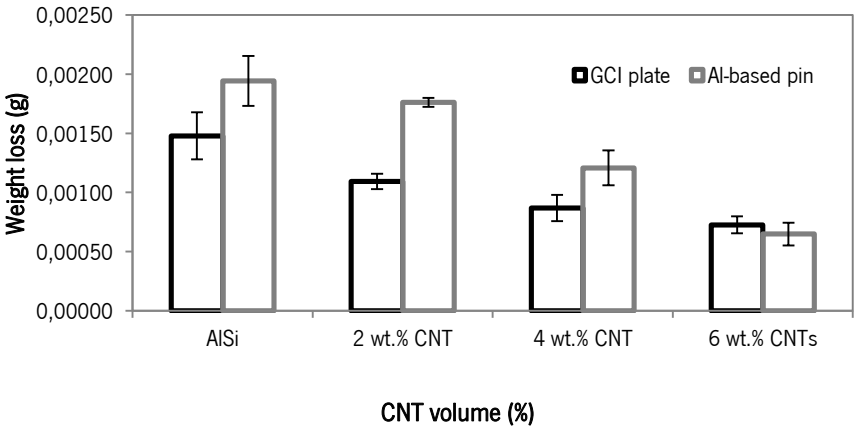

Figure 9. 8 - Wear loss as a function of the CNT content

It can be seen in Figure 9. 8 that the wear loss of both contact surfaces (pin and counterpart) decreases with increasing CNT content. The pin wear loss (AlSi-CNT composites) results are in line with some previous studies [33, 35-38]

Figure 9. 9 shows SEM images of the worn surface unreinforced AlSi pin and AlSi-based pins with different CNT content (left side) and of the GCI plates (130x magnification) (right side).

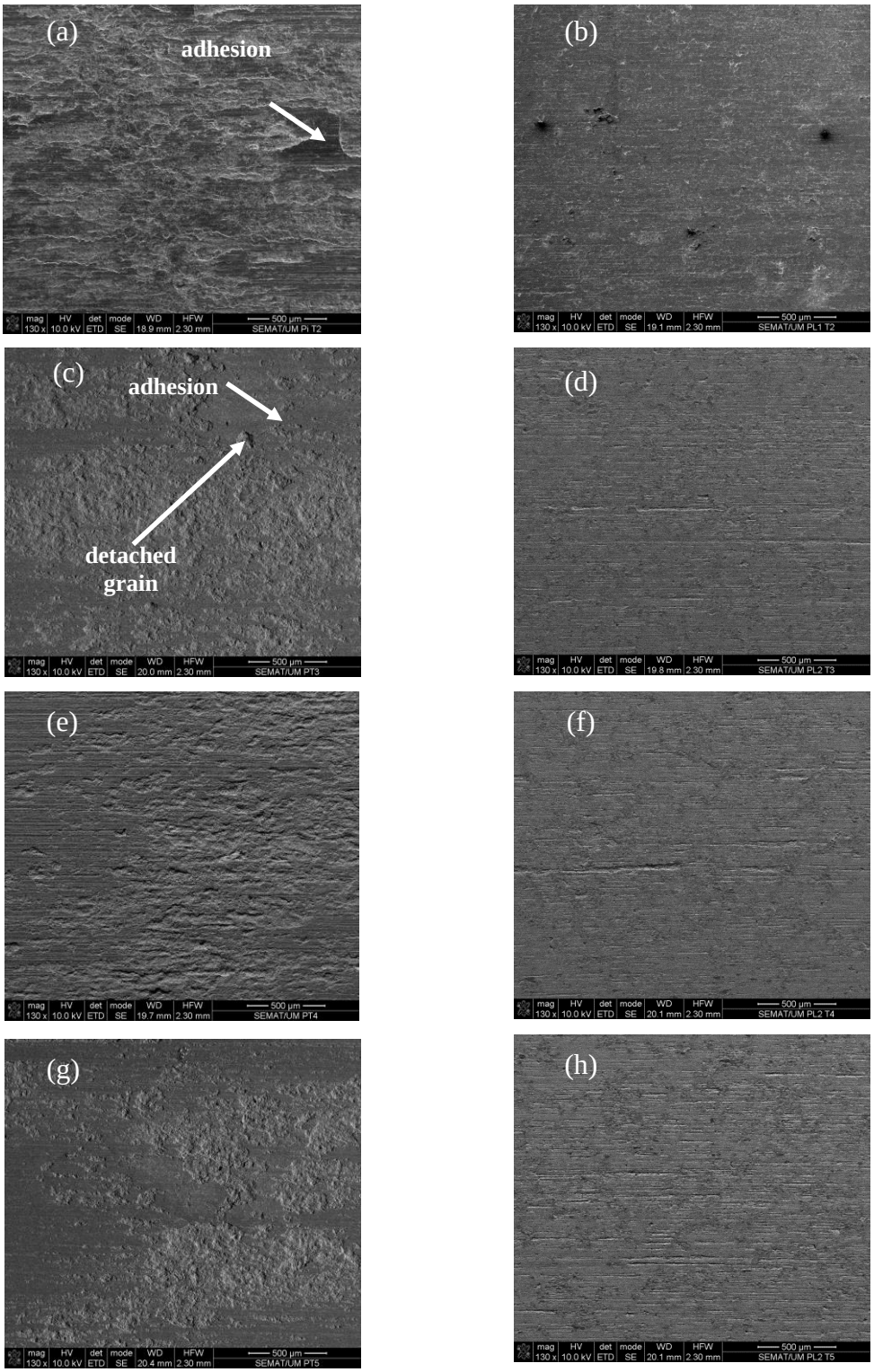

Figure 9. 9 - SEM images of the worn surface of unreinforced AlSi alloy and all AlSi-CNT composites and of the GCI plates: (a/b) unreinforced AlSi alloy/GCI plate; (c/d) AlSi - 2wt.%CNT/GCI plate; (e/f) AlSi – 4 wt. % CNT/GCI plate and (g/h) AlSi – 6 wt. % CNT/GCI plate.

In the case of unreinforced AlSi pins surface (Figure 9. 9-a) adhesive wear is present, due to the fact that the surface is under the influence of applied stresses. In the sliding direction the surface material is removed layer by layer, with deeper craters than the AlSi-CNTs pins.

SEM images of the worn surface of AlSi-CNT pins (see Figure 9. 9- c, e and g) reveal that by increasing the CNT content (from 2 wt.% to 6% wt. CNT) the pin contact surfaces seem to have less voids but deeper. This can indicate a lower material loss in the AlSi-CNTs composites, when comparing to unreinforced AlSi. It can be observed on the contact region after sliding two types of plateaus: a smooth plateaus and others with more peaks and valleys. The smoother plateaus are increasing with the increase of the CNT content. The smoother plateaus correspond to the regions where the CNTs are better dispersed and the rougher regions to the regions where there is a poor distribution of CNTs (where the agglomerates are located). More explications regarding the presence of the agglomerates and their influence on the wear behaviour is given elsewhere [30].These rougher regions are areas of weakness from which failure was initiated to cause wear of the AlSi-composites. It can be observed that the areas of weakness are decreasing with increasing the CNT content. This happens simultaneously with improved diminished wear loss (Figure 9. 9). It is expected that on the zones with good CNT dispersion, the hardness is higher and is responsible for the grooves that can be observed on the plates (Figure 9. 9-c, e and g). It seems that there is a competition between these two zones, so between adhesion and abrasion.

On the SEM image of the wear track of the GCI plate when this is sliding against unreinforced AlSi alloy (Figure 9. 9-b) can be observed the destructive effects of delamination marks. This is the main wear mechanism observed in the case of unreinforced AlSi alloy, but there can also be observed a few tiny grooves. Regarding the worn surface morphology of GCI plates among the different CNT content, it can be seen from Figure 9. 9- d, f and h that all the surfaces presented similar abrasion deeper grooves. However, the degree of GCI surface damage tends to decrease by the presence of CNTs at the mating surface (by increasing the CNTs content), as revealed by the increased extension of smooth plateaus at GCI worn surface from Figure 9. 9-b to g. This observation is in good correlation with the weight loss results presented in Figure 9. 8.

An important aspect to highlight is that previous papers on metallic bulk with CNT as reinforcements [9,11,35,37-39] either with Cu, Mg, Ti, Zn or Al, do not refer to counterparts wear behaviour. Reinforcements introduced in the composite improve its wear behaviour but depending on the counterface material, contact situation, reinforcement type etc. [40] it may reduce the

counterpart wear behaviour. In this study one clearly sees the improvement of the wear response of the tribopair by reinforcing the AlSi alloy with CNTs.

When increasing the CNT content, there is clearly a tendency for improvement in the wear behaviour of the AlSi-CNT composites. Moreover also the wear of counterface material improved. Thus, the wear response of the tribopair by reinforcing AlSi alloy with CNTs is improved, when comparing it with unreinforced AlSi/GCI system. A more detailed explication regarding the improvement in wear behaviour is given elsewhere [26,30].

Fatigue properties

The S-N curve for 2wt% CNT is presented in Figure 9. 13. Fatigue tests were not performed in all homogeneous CNT volume fractions. As a fact fatigue limit usually follows static strength. Thus, based on static results the fatigue limit should have the peak at 2wt% CNT. Moreover, by increasing the CNT volume fraction, as the agglomerates increase and as they act as pores, it is expected that higher volume fractions of CNTs would result in lower values of fatigue limit as compared to the ones obtained for 2wt% CNT.

9.4.2 Developed equipment and the feasibility of the proposed process

Equipment to produce FGMs by powders deposition

The existent techniques used to produce FGM have limitations because they can be only used in cylinder specimens and some of them, such as gravity sedimentation lead interaction between particles during the process and also have limitations in types of gradients that can be produced [41]. For these reasons a new equipment (Figure 9. 10-a) was developed. This equipment allows the creation of a continuous variation of powder distribution along a given axis of the sample. The characteristics of the equipment are represented in Table 9. 2.

The powder mixture (2wt.%CNT with AlSi) inside of equipment was made mechanically through the action of two individual feeders by a stepper motor electronically controlled. In these feeders are introduced the constitutive powders of gradient. The equipment just allows mixtures of two types of powders. However, it is possible, by adding more feeders, to achieve mixtures with more than two types of powders. Then powders pass into a tube where exists a dispersing grid

responsible to spreading the powders, promoting at same time mixing of powders coming from feeders. This grid has a vertical movement due to eccentric, which is connected to the DC motor, and by this way avoids overlap of the powders a single zone. Then, the obtained powder mixture enters in the matrix.

The type of gradient is created by software which was developed by the authors of this work and where the users chose some parameters (e.g. powder mass, final height of specimens, matrix diameter and bulk density). In this work was created linear gradient of AlSi-2wt.%CNT gradient composites.

Afterwards, the AlSi-matrix composite gradually reinforced by CNTs (AlSi-CNTs) were processed through traditional hot pressing (HP) technique previously presented (see 2.2. Sintering process).

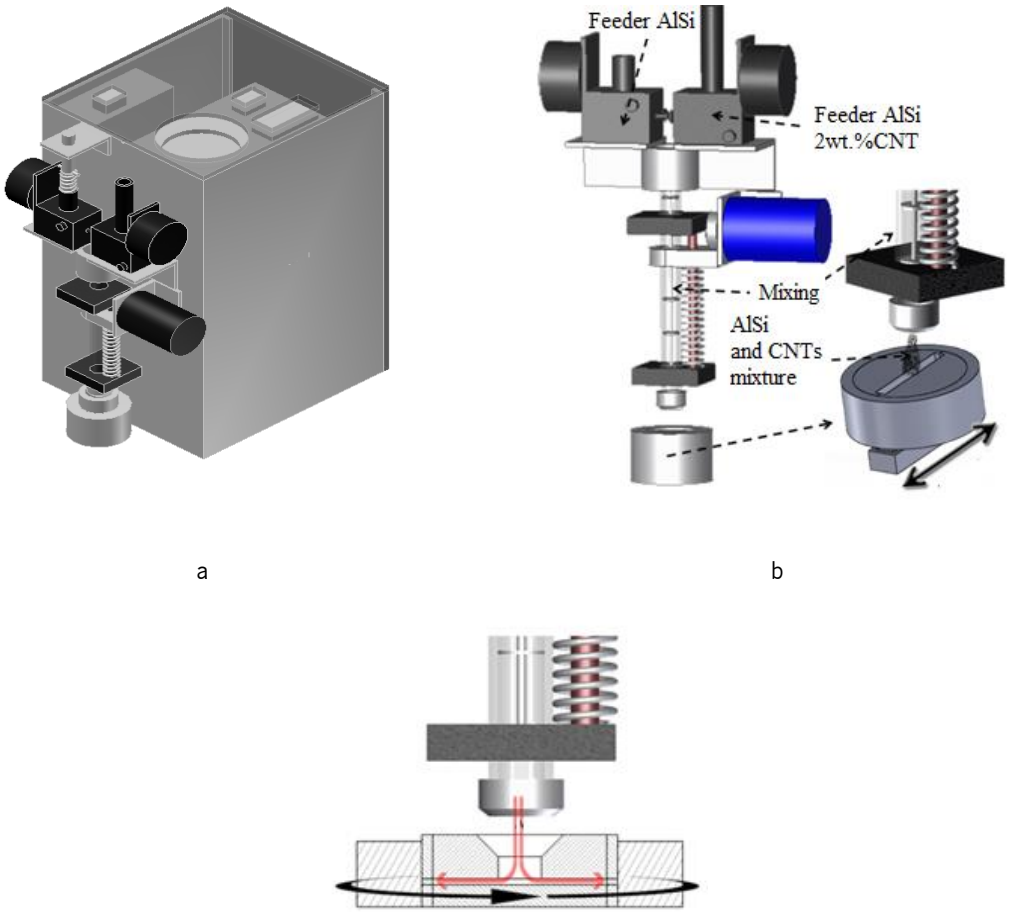

Figure 9. 10 - Schematic representation of the equipment developed to produce FGMs by powders deposition; b. improved device to produce piston rings from FGM: c. centrifugal system

Table 9. 2 - Characteristics of equipment developed to produce FGMs

Capacity of container	3.14×10^{-6} m^3
Operating speed of the stepper motors	Maximum: 0.42 rot/s
Reproducibility	Good reproducibility
Feasible powders	possibility of using different powders (powders flowbility necessary)
Software	LabVIEW + Excel
Dimensions	170 mm*180 mm*300 mm

Validation of the equipment developed to produce FGMs by powders deposition

It should be emphasized that based on previously presented results in the case 2 wt.% CNT content there is an equilibrium among improvement in mechanical properties in the different tests namely tensile and wear. As a fact the tensile strength with CNTs as reinforcement, presented its peak with 2% of CNTs. Regarding the wear results, increasing the reinforcement content would allow to increase the wear resistance but it would substantially decrease the tensile strength (see Figure 9. 8).

Based on the obtained results, and according to the application (piston ring), and based on the fact that different properties are required in specific areas of the piston rings, a functionally graded composite will be produced with a linear gradient where the maximum fraction of reinforcement is 2wt%CNTs at the surfaces (where the maximum tensile and wear are required). The inner part of the ring does not have CNTs due to the cost of them.

With the controlled deposition equipment (Figure 9. 10-a) will be produced a powders gradient with a linear variation from 2wt.% in the periphery and 0wt.% in the middle again increasing up to a maximum of 2 wt% in another periphery.

In order to verify the distribution of the CNTs along the axis of the sample the following procedure it was followed: (i) Micro-photographs were taken for each polished sample by using an optical microscope (Leica DM 2500M, Leica Microsystems, Germany) connected to a computer for image processing, using Leica Application Suite software (Leica Microsystems, Germany); (ii) The software Adobe Photoshop (Adobe Systems Software, Ireland) was used to produce black and white images, with the black representing the AlSi matrix and the white the CNTs. (iii) Image J software (National Institutes of Health, USA) were used to quantify the amount of CNTs in percentage.

It can be seen from Figure 9. 11 that the real curve is similar to theoretical curve which proves the reliability of the produced equipment (Figure 9. 10-a).

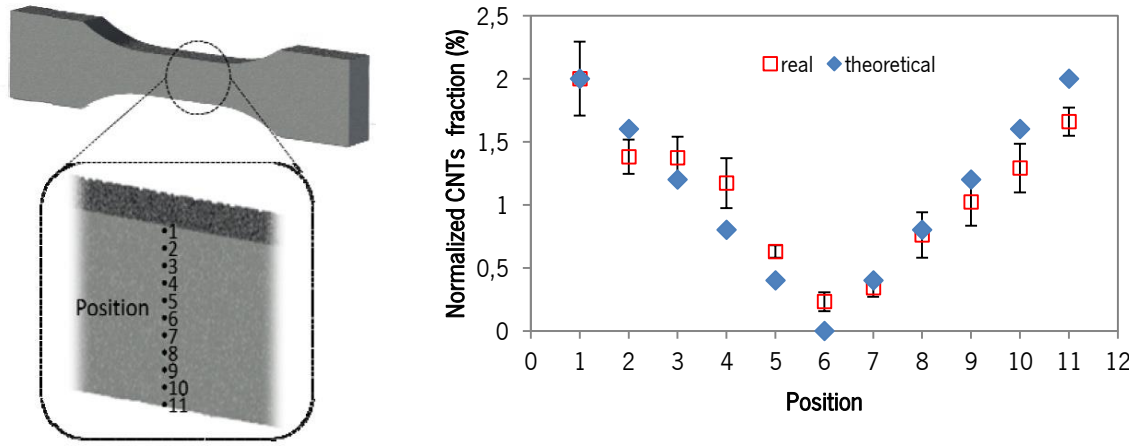

a b

Figure 9. 11 - The variation of chemical composition of AlSi-2 wt. % CNTs FGM composite. a. Cross section of sample where the chemical composition was evaluated; b. Variation of the CNTs (wt.%) vs. position

Proposed device to obtain an engine piston ring by powder metallurgy

Figure 9. 10-b shows the proposed design for building a piston ring from the AlSi-CNT FGM.

In order to optimize the relationship between the mechanical and wear properties, and the final cost of the piston ring has been proposed a new FGM for piston ring.

The CNTs are placed only on the outer surfaces of the piston ring since it is the area which is subject to more wear and higher stresses. The inner surface of piston ring is subject to compressive stresses so that they do not contribute to the appearance of fatigue cracks.

Figure 9. 10-b schematically shows the changes made to the device in order to produce the piston rings. This device allows to make a radial distribution of the powders. This device consists of a matrix and some punches. Once distributed powders of the desired punches are driven gradient powders pressed into its final shape. The action of the punch may also be responsible for creating a porosity gradient if desired. Subsequently, the consolidated powders are sintered.

The equipment as well as the analysis developed in this work can be applied to other pairs of materials, depending on the local requirements of defined component.

9.4.3 Mechanical properties of the AlSi -CNT functionally graded composite

Tensile tests of AlSi –CNT functionally graded composite

Figure 9. 12 presents the representative tensile stress–strain curves of unreinforced AlSi alloy, AlSi-2% wt. CNT and AlSi - CNT FGM composites. The mechanical properties (tensile strength, σ_r, yield strength σ_y and tensile strain ε_r) are listed in Table 9. 3.

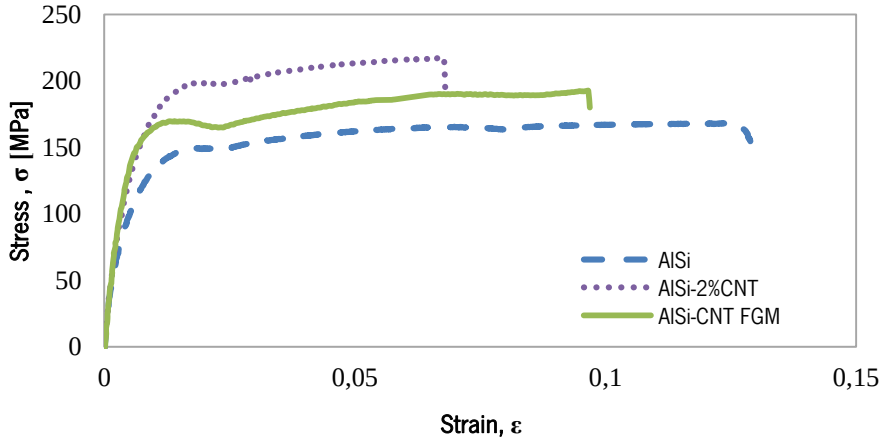

Figure 9. 12- Stress–strain curves from tensile testing of unreinforced AlSi alloy and AlSi – 2 wt.% CNT's composite

Table 9. 3 - Results of tensile testing of unreinforced AlSi alloy and AlSi-2 wt. % CNT's composite

Material	σr [MPa]	σy [MPa]	εr [%]
AlSi	170	152	13
AlSi-2 wt. % CNT's	209	192	7
AlSi - CNT FGM	192	172	9

It is observed that the tensile strength, σ_r, of AlSi-2% wt. CNT composite improved by about 23% as compared to unreinforced AlSi alloy. The yield strength σ_y of AlSi-2% wt. CNT composite improved by 26% as compared to unreinforced AlSi alloy. The AlSi - CNT FGM composite have, as expected, an average behaviour between unreinforced AlSi alloy and AlSi-2 wt. % CNT.

Fatigue properties of AlSi –CNT functionally graded composite

Figure 9. 13 shows the fatigue results obtained as S-N curves for the unreinforced AlSi alloy and also for all the produced composites.

It can be seen from Figure 9. 13 that under identical loading conditions the AlSi-2 wt. % CNTs composite has longer fatigue lives (continuous line – Figure 9. 13) and a higher fatigue life than the unreinforced AlSi alloy (dashed line – Figure 9. 13). It can be seen that at a stress level of about 140 MPa the fatigue life of AlSi-2% wt. CNTs composite increased by 270% compared to unreinforced AlSi alloy.

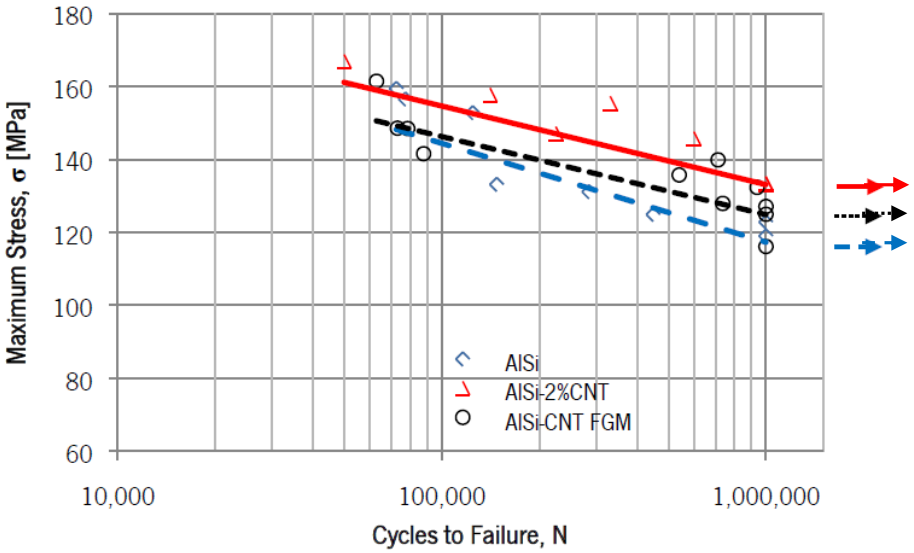

Figure 9. 13 - Maximum alternating stresses (σ_{max}) vs. number of cycles to failure for unreinforced AlSi alloy , AlSi-2 wt. % CNTs and AlSi-2 wt. % CNTs FGM composite

Figure 9. 14 presents the SEM images of the fracture surface morphologies of both unreinforced AlSi alloy and AlSi-2% wt. CNTs composite.

It can be clearly seen from Figure 9. 14-a that the crack path is very straight in the case of unreinforced AlSi alloy (smoother surface), while in the case of AlSi-2% wt. CNTs composite (Figure 9. 14-b) the crack path is very tortuous (slightly rougher surface). This observation indicates that in the case of the unreinforced AlSi alloy the crack travels through the grains/powders of the material (intra Al-Si matrix particles fracture), due to the fact that the AlSi grains/powders are very well bonded. In the case of AlSi-2% wt. CNTs composite the fatigue crack may initiate in the region with agglomerations (fatigue cracks frequently initiates from the stress concentrated regions). If the

crack reaches a region where the CNTs are well dispersed, the crack is deflected due to the stronger interface between matrix and CNT, and then may travel through the AlSi grain (intra Al-Si matrix particles fracture). Crack deflection is a common effect in metal matrix composites [42]. If the crack reaches a region with agglomerates (zones of weakness) the propagation of the crack is accelerated. So, in the case of composite there is a mixture/competition between intra and inter Al-Si matrix particles fracture. Thus, even though in the case of AlSi-2% wt. CNTs composite there are these weak regions (CNTs agglomerates) that may accelerate the crack propagation, CNTs act as interface barriers to crack propagation [25, 43], increasing the fatigue life of the AlSi-2% wt. CNTs composite. More explanation regarding the fatigue behaviour of the unreinforced AlSi alloy and of the AlSi-2%wt. CNTs is given elsewhere [26].

The crack propagation in the case of FGM composite has an average behaviour between unreinforced AlSi alloy and AlSi-2 wt. % CNTs.

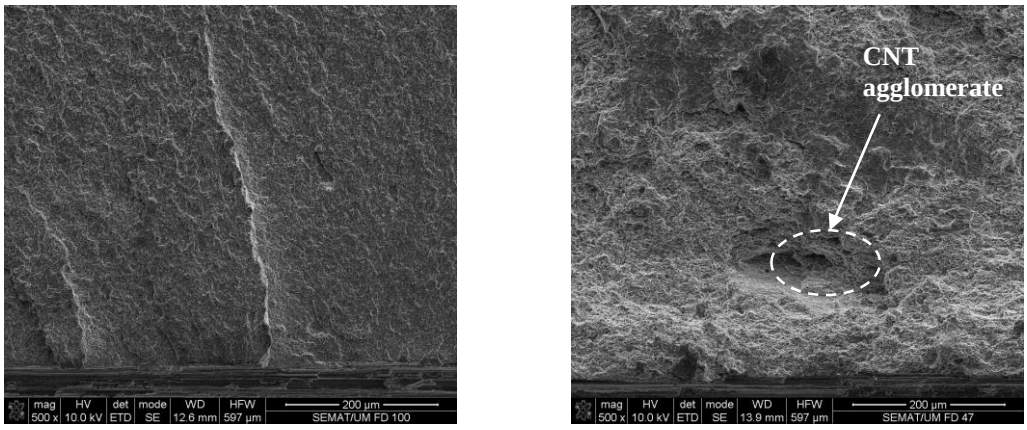

a b

Figure 9. 14 - SEM images of the fracture surface after fatigue test of:
a. unreinforced AlSi alloy and b. AlSi-2 wt. % CNT's composite

Hardness values as a function of the CNT content

Figure 9. 15 shows the hardness results as a function of the position of the CNT variation.

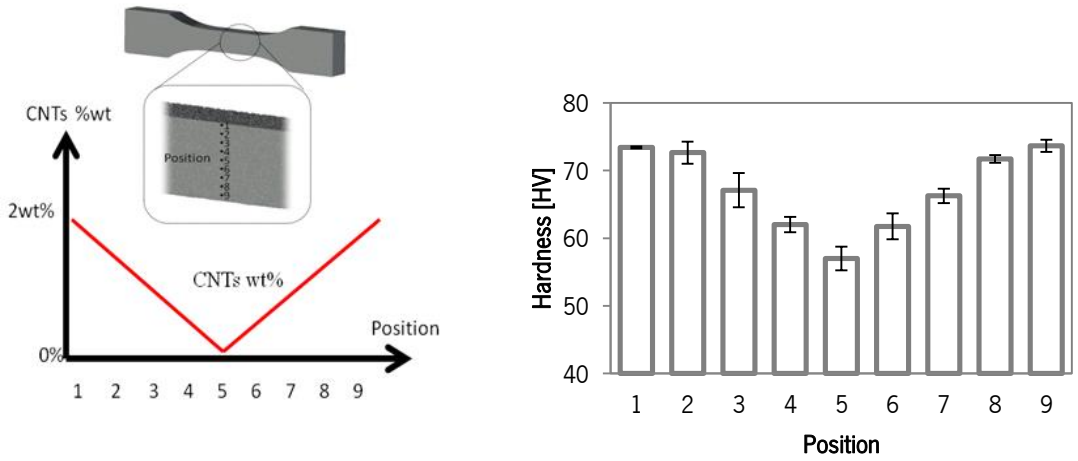

a b

Figure 9. 15 - Hardness values of the AlSi-2 wt. % CNT's FGM composite: a. Position on the sample where the hardness was measured and CNTs wt% as a function of the position; c. Hardness as a function of the position.

As expected, the hardness decreases with decreasing CNT content. Comparing the values obtained in the FGM in positions where the CNTs content is 0 wt% (position 5, in the middle of the sample, and 2wt% (position 1 and 9 in the top and bottom of the sample) it can be seen that the values are very similar with the values obtained in the case of unreinforced AlSi alloy and AlSi-2 wt. % composite respectively (Figure 9. 7).

Thus, it can be seen that the FGM, with the gradient defined in this study, allows for the improvement in mechanical properties, fatigue resistance, and wear behaviour. This is achieved with the introduction of a small quantity of CNT's having thus a small additional cost due to the reinforcement. These properties may not be achieved with a coating solution. Further to this it is expected and already demonstrated in other studies [44] that the introduction of CNT's enhance the thermal conductivity of the matrix. Another benefit from this approach is the retention of oil in the CNTs which is important for lubrication in dead periods. The CNTs have more than one effect on the tribological behaviour of the composite: self lubrication effect and strengthening effect (increase the bonding between the grains on the Al matrix), so it is more difficult to remove them as the mechanical properties have confirmed [21]. Due to their shape and size, mainly the CNTs that come from the disaggregation of agglomerates could roll between the mating surfaces [45,46].

9.5 Conclusions

From the present investigation on an AlSi alloy reinforced by CNTs that aimed to develop a strategy to produce an FGM that that can fulfil all the requirements of a piston ring, the following conclusions can be drawn:

- AlSi-CNT composites were successfully produced by hot-pressing technique in order to evaluate the different fractions of CNTs;

- The best mechanical properties for homogeneous specimens were obtained in the case of 2wt% CNTs, while the best wear results were obtained in the case of 6wt% CNTs. Thus, the 2wt% of CNTs composite was chosen to produce the FGM since it was the composition that has the best compromise between mechanical and wear properties;

- The AlSi-CNT FGM composite was successfully produced by controlled deposition equipment. The linear gradient consists of variation from 2wt% of CNTs on inner surface to a 0wt% of CNTs in middle and 2wt% of CNTs on the outer surface of piston ring. This gradient was chosen taking in account the mechanical and wear solicitations of a piston ring;

- The evaluation of mechanical properties of AlSi-CNT FGM composites shows that it improves the properties as compared to the unreinforced alloy and that it has an intermediate behaviour between unreinforced alloy and 2wt% CNTs composite;

- The evaluation of fatigue limit of AlSi-CNT FGM composites shows that it improves the properties as compared to the unreinforced alloy and that it has an intermediate behaviour between unreinforced alloy and 2wt% CNTs composite;

Finally it was proposed a FGM piston ring were CNTs are placed on the outer surfaces of the ring as these are the regions that are subjected to higher mechanical stresses and increased wear. It should be also highlighted that the choice of a 2wt.% gradient only on the outer surfaces is related with the best cost benefit ratio. The better compromise between mechanical properties and wear arise at composition of 2wt.%. CNTs larger fractions contribute to improved wear resistance but in return we are witnessing a reduction in mechanical properties.

9.6 Acknowledgements

This work was supported by the Portuguese Foundation of Science and Technology through the project references PTDC/EME-PME/68664/2006, EXCL/EMS-TEC/0460/2012 and through the PhD grant with the reference SFRH/BD/44077/2008.

9.7 References

[1] F.S. Silva. 2006. Fatigue on engine pistons – A compendium of case studies. Eng. Fail. Anal. 13: 480–492.
[2] N. Costa. 2009. Analysis of the influence of processing parameters on the fatigue life of engine piston rings. PhD Thesis.
[3] N. M. Costa, F.S. Silva.2006. Influence of Process Stages over Fatigue Crack Behaviour of Electroplated Chromium Coatings. 5th International Surface Engineering Congress, 15-18 May, Seattle (USA).
[4] U. Dworak, Baltmannsweiler, H. Olapinski, Aichwald, Dieter Fingerle, Hochdorf, Ulrich Krohn, Leoberg, 17 de Janeiro de 1984, Piston ring for an internal combustion engine, 4522415, 11 de Junho de 1985.
[5] M.-F. Yu, O. Lourie, M. J. Dyer, K. Moloni, T. F. Kelley, R. S. Ruoff. 2000. Strength and breaking mechanism of multiwalled carbon under tensile load. Science 287:637–640.
[6] D. A. Walters, L. M. Ericson, M. J. Casavant, J. Liu, D. T. Colbert, K. A. Smith, R. E. Smalley. 1999. Elastic strain of freely suspended single-wall carbon nanotube ropes. Applied Physic Letters 74: 3803–3805.
[7] B. G. Demczyk, Y.M. Wang, J. Cumingd, M. Hetamn, W. Han, A. Zettl, R. O. Ritchie. 2002. Direct mechanical measurement of the tensile strength and elastic modulus of multiwalled carbon nanotubes. Materials Science and Engineering A 334: 173–178.
[8] R. George, K.T. Kashyap, R. Rahul, S. Yamdagni. 2005. Strengthening in carbon nanotube/aluminium (CNT/Al) composites. Scripta Materialia 53: 1159–1163.
[9] M. M. J. Treacy, T. W. Ebbesen, J. M. Gibson. 1996. Exceptionally high Young's modulus observed for individual carbon nanotubes. Nature 381: 678–680.
[10] Yao, V. Lordie. 1998. Young's modulus of single-wall carbon nanotubes.Journal of Applied Physics 84: 1939–1943.
[11] S.R. Dong, J.P. Tu, X.B. Zhang. 2001. An investigation of the sliding wear behavior of Cu-matrix composite reinforced by carbon nanotubes. Materials Science and Engineering A 313: 83–87.
[12] D. S. Lim, J. W. An, H. J. Lee. 2002. Effect of carbon nanotube addition on the tribological behavior of carbon–carbon composites. Wear 252: 512–517.
[13] T. Kuzumaki, K. Miyazawa, H. Ichinose, K. Ito. 1998. Processing of carbon nanotube reinforced aluminum composite. Journal of Materials Research 13: 2445–2449.
[14] R. Zhong, H. Cong, Hou, P. 2003. Fabrication of nano-Al based composites reinforced by single-walled carbon nanotubes. Carbon 41: 848–851.
[15] A.M. Esawi, M.A. El Borady. 2008. Carbon-nanotube-reinforced aluminum strips. Composites Science and Technology 68: 486–492.
[16] A. Esawi, K. Morsi. 2007. Dispersion of carbon nanotubes (CNTs) in aluminum powder. Composites A 38: 646–650.

[17] K. Morsi, A. Esawi. 2007. Effect of mechanical alloying time and carbon nanaotube (CNT) content on the evolution of aluminum (Al)-CNT composite powders. Journal of Materials Science 42: 4954–4959.
[18] Perez-Bustamante, R., Estrada-Guel, I., Antunez-Flores, W., Miki-Yoshida, M., Ferreira, P.J. and Martinez-Sanchez, R. Novel. 2008. Al-matrix nanocomposites reinforced with multi-walled carbon nanotubes. Journal of Alloys and Compounds 450: 323–326.
[19] He, C., Zhao, N., Shi, C., Du, X., Li, J., Li, H. and Cui, Q. 2007. An approach to obtaining homogeneously dispersed carbon nanotubes in Al powders for preparing reinforced Al-matrix composites. Advanced Materials 19: 1128–1132.
[20] Minnet, S. 2000. The Sinter Revolution, Metal Powder Report, Nov. 1-3.
[21] O. Carvalho, G. Miranda, D. Soares, F.S. Silva. 2014. Carbon nanotube dispersion in aluminum matrix composites – quantification and influence on strength. Mechanics of advanced materials and structures. DOI: 10.1080/15376494.2014.929766.
[22] O. Carvalho, G. Miranda, D. Soares and F.S. Silva. 2013. CNT-reinforced aluminium composites: processing and mechanical properties. Conference of Sociedade portuguesa de Materiais, 25-27 March, Coimbra, Portugal.
[23] T. Laha, Y. Chen, D. Lahiri, A. Agarwal. 2009. Tensile properties of carbon nanotube reinforced aluminum nanocomposite fabricated by plasma spray forming. Composites Part A-Applied Science and Manufacturing 40: 589-594.
[24] G.S. Goh, J. Wei, L.C. Lee, M. Gupta. 2008. Ductility improvement and fatigue studies in Mg-CNT nanocomposites. Composites Science Technology 68: 1432–1439.
[25] Y.M. Jen, Y.C. Wang. 2012. Stress concentration effect on the fatigue properties of carbon nanotube/epoxy composites. Composites: Part B. 43: 1687–1694.
[26] O.Carvalho, M. Buciumeanu, G. Miranda, N. Costa, D. Soares, F.S. Silva. 2015. Mechanisms Governing the Tensile, Fatigue and Wear Behavior of Carbon Nanotube reinforced Aluminum Alloy. Accepted to Mechanics of advanced materials and structures.
[27] T. Premkumar, R. Mezzenga, K.E. Geckeler. 2012. Carbon nanotubes in the liquid phase: addressing the issue of dispersion. Small, 8: 1299-1313.
[28] J.S. Oh, K.H. Ahn, J.S. Hong. 2010. Dispersion of entangled carbon nanotube by melt extrusion. Korea-Australia Rheology Journal 22: 89-94.
[29] W. Salas, N.G. Alba-Baena, L.E. Murr. 2007. Explosive shock-wave consolidation of aluminum powder/carbon nanotube aggregate mixtures: optical and electron metallography. Metallurgical and Materials Transactions A 38: 2928-2935.
[30] O. Carvalho, M. Buciumeanu, D. Soares, J. Gomes, F. S. Silva. 2014. Improvement on sliding wear behaviour of Al/cast iron tribopair by CNT's reinforcement of an Al alloy. Accepted to Tribology Transactions. DOI 10.1080/10402004.2014.1002143.
[31] S.R. Bakshi, A.K. Keshri, A. Agarwal. 2011. A comparison of mechanical and wear properties of plasma sprayed carbon nanotube reinforced aluminum composites at nano and macro scale. Materials Science and Engineering A 52: 83375–3384.
[32] S.R. Dong, J.P. Tu, X.B. Zhang. 2001. An investigation of the sliding wear behavior of Cu-matrix composite reinforced by carbon nanotubes. Materials Science and Engineering A 313: 83–87.
[33] S.R. Bakshi, D. Lahiri, A. Agarwal. 2010. Carbon nanotube reinforced metal matrix composites – a review. International Materials Reviews 55: 41-64.
[34] T. Threrujirapapong, K. Kondoh, J. Umeda, H. Imai. 2008. Friction and wear behavior of titanium matrix composite reinforced with carbon nanotubes under dry conditions. Transactions of JWRI 379: 51-56.

[35] H.J. Choi, S.M. Lee, D.H. Bae. 2010. Wear characteristic of aluminium-based composites containing multi-walled carbon nanotubes. Wear 270: 12–18.
[36] A.M.Al-Qutub, A.Khalil, N.Saheb, A.S. Hakeem. 2013. Wear and friction behavior of Al6061 alloy reinforced with carbon nanotubes. Wear 297: 752–761.
[37] I.Y Kim, J.H. Lee, G.S. Lee, S.H. Baik, Y.J. Kim, Y.Z. Lee. 2009. Friction and wear characteristics of the carbon nanotube–aluminium composites with different manufacturing conditions. Wear 267: 593–598.
[38] S. Zhou, X. Zhang, Z. Ding, C. Min, G. Xu, W.Zhu. 2007. Fabrication and tribological properties of carbon nanotubes reinforced Al composites prepared by pressureless infiltration technique. Composites Part A: Applied Science and Manufacturing S 38: 301–306.
[39] J. Umeda, K. Kondoh, H. Imai. 2009. Friction and wear behavior of sintered magnesium composite reinforced with CNT-Mg2Si/MgO. Mat. Sci. Eng. A 504: 157–162.
[40] V. Kumar, G.B., Rao, C.S.P., N. Selvaraj. 2011. Mechanical and Tribological Behavior of particles reinforced aluminium metal matrix composites – a review. Journal of Minerals and Materials Characterization and Engineering 10: 59-91.
[41] Kieback B, Neubrand A, Riedel H. 2003. Processing techniques for functionally graded materials. Materials Science and Engineering A 362:81-106.
[42] Shang JK, Yu W, Ritchie RO. 1988. Role of silicon carbide particles in fatigue crack growth in SiC-particulate-reinforced aluminum alloy composites.Materials Science and Engineering A 102:181–192.
[43] Loos MR, Yang J, Feke DL, Manas-Zloczower I, Unal S, Younes U. 2013. Enhancement of fatigue life of polyurethane composites containing carbon nanotubes. Composites: Part B 44:740–744.
[44] A. Bhat, Vamsi K. Balla, S. Bysakh, D. Basu, S. Bose, A. Bandyopadhyay. 2011. Carbon nanotube reinforced Cu–10Sn alloy composites: Mechanical and thermal properties. Materials Science and Engineering A 52: 6727–6732.
[45] M. R. Falvo, R.M. Taylor II, A. Helser, V.Chi, F.P. Brooks Jr, S. Washburn, R. 1999. Superfine, Nanometre-scale rolling and sliding of carbon nanotubes. Nature 397: 236-238.
[46] F. Dassenoy, L. Joly-Pottuz, J.M. Martin, T. Mieno, Carbon nanotubes as advanced lubricant additives, V.N. Popov and P. Lambin (eds.), Carbon Nanotubes, 2006237–238, Springer, Netherlands.

10 Interface analysis on an eutectic AlSi alloy reinforced with Ni coated MWCNT

O. Carvalho[1], M. Buciumeanu[2],S. Madeira[1], D. Soares[1], F. S. Silva[1], G. Miranda[1]

[1]CT2M – Centre for Mechanical and Materials Technologies, University of Minho,
Azurém, 4800-058 Guimarães, Portugal;
[2]Cross–Border Faculty of Humanities, Economics and Engineering, "Dunarea de Jos" University of Galati,
Domneasca 47, 800008 Galati, Romania

Submitted to composites part B

10.1 Abstract

This aim of this paper was to study the interface reaction between an AlSi alloy reinforced with Ni coated Multi-Wall Carbon Nanotubes (MWCNTs). A powder metallurgy processing route was used to produce AlSi composites. SEM, DSC, XRD and TEM analysis showed the formation of Al3Ni due to the presence of Al from AlSi matrix and Ni from CNT coating. This contributes to stress transfer from matrix to CNT reinforcement and consequently to enhancement of mechanical properties of the composites. Also it was observed some dissolution of Ni to AlSi and that the CNTs are very stable as they maintain their integrity. The coating of CNTs seems to be a good solution for application of this reinforcement in commercial alloys.

Keywords: Carbon nanotube (CNT), powder metallurgy, AlSi eutectic alloy.

10.2 Introduction

Due to CNTs excellent properties, these have been used as reinforcement in different kinds of composites, whether metal, ceramic or polymeric matrix composites [1].With the introduction of CNTs it is expected to overcome some of the shortcomings presented by some materials, such as electrical conductivity of polymers and toughness of ceramics. The major challenge in the manufacture CNT-reinforced metal matrix composites is the CNTs dispersion on the matrix. The second major challenge is to establish a favourable bonding at metal matrix/CNT interface.

Regarding aluminium matrices, some studies use CNTs as reinforcement for commercial alloys by means of powder metallurgy. However, most of the studies use pure aluminium, once it allows a higher control over the reactivity between CNTs and the matrix.

It has been reported that CNTs are very stable when regarding chemical reactions, nevertheless some of the defects on CNTs (open tips in CNTs [2])might lead to reaction with aluminium[3]. According to the majority of the studies, the reaction product between aluminium and CNTs is aluminium carbide (Al_4C_3) [3-5]. In this reaction it is assumed that the free surface of CNT remains intact, due to the reduced processing time and temperature. Otherwise, CNTs would be fully transformed into Al_4C_3 [6]. Al_4C_3 was identified mainly in liquid phase process (plasma sintering processes [3]) but also in solid sate process (hot pressing [7]).

According to Kwon et. al. [4, 8] the formation of Al_4C_3 has a beneficial effect on enhancing mechanical strength. Additionally, this compound is responsible for an efficient stress transfer effect from matrix to reinforcement [9]. For aluminium alloys, the formation of Al_4C_3 was also observed due to the presence of carbon, as in aluminium silicon matrix composites reinforced with carbon fibres, produced by metal liquid infiltration [10]. Vidal-Setif et. al. [11] showed that in this case there was a strength reduction due to Al_4C_3 formation. Therefore, Al_4C_3 formation and extent should be attentively controlled because of its brittleness [12, 13].

Furthermore, in CNT-reinforced aluminium silicon composites, besides Al_4C_3, also SiC was formed [14, 15]. Different carbides (formed in interfacial zones) differently influence these composites mechanical properties. The carbides strength determines the stress transfer ability from matrix to reinforcement.

The reinforcement/matrix interface should guarantee the chemical stability of CNTs, by avoiding its complete reaction and simultaneously provide that the reaction products ensure an effective stress transfer from matrix to interface.

A possible approach to control reactivity between a reinforcement and matrix is the use of coatings on reinforcements [16, 17]. Similar to carbon fibres coating [16, 17], CNTs coating could be a solution towards reactivity control. No studies were found concerning nickel coated CNTs as reinforcement for commercial aluminium alloys.

Nickel is the most widely used metal for coating particles and ceramic fibres for use on aluminium composites [18-22]. The majority of the coatings are made by electroless plating,

process also used for coating CNTs [23-25]. Coating the reinforcement influences the physical, mechanical and chemical properties of the composites.

Most of the existing studies use pure aluminium and uncoated CNTs, where the formation the formation of Al_4C_3 is found beneficial to improve the stress transfer ability (Kwon et. al. [4, 8]. This work presents a different approach, by using Ni coated MWCNT to reinforce a commercial aluminium-silicon alloy. This work addresses the reinforcement/matrix interface, once this should guarantee the chemical stability of CNTs, by avoiding its complete reaction and simultaneously provide that the reaction products ensure an effective stress transfer from matrix to interface.

10.3 Experimental procedure

10.3.1 Fabrication of CNT-reinforced Al-Si composites

Aluminum Silicon powder (Al-Si 88-12 wt. %, 99% pure - 325 mesh) purchased from AlfaAesar - Germany, and Multi-Wall Carbon Nanotubes (MWCNTs) Nickel coated, grown by CVD, from *CheapTubes.com* - USA, were used to produce Al-Si based nanocomposites. Al-Si powder had a measured average particle diameter of 8 μm, while the MWCNT had a length between 0.5 and 2.0 μm and a diameter higher than 50 nm (information given by the supplier).

The Al-matrix composite reinforced by CNTs was processed through traditional hot pressing technique. The pressure was 35 MPa, applied for 10 minutes at a temperature of 550°C under vacuum (10^{-2} mbar). The mixing of the Al powders was performed inside a closed stainless steel jar with the powders mixture and steel milling balls (10 mm diameter). The ball/powder ratio was 10:1 and the atmosphere was argon. The jar was placed in a rotation machine and the mixing was made with a constant rotation speed of 40 rpm during 6 days (low-energy ball milling).

Afterwards the Al-Si/MWCNT mixture was introduced in a graphite die (Figure 10. 1) and slightly compacted. The die was then placed in a vacuum chamber (Figure 10. 1), where it was heated until 550°C.

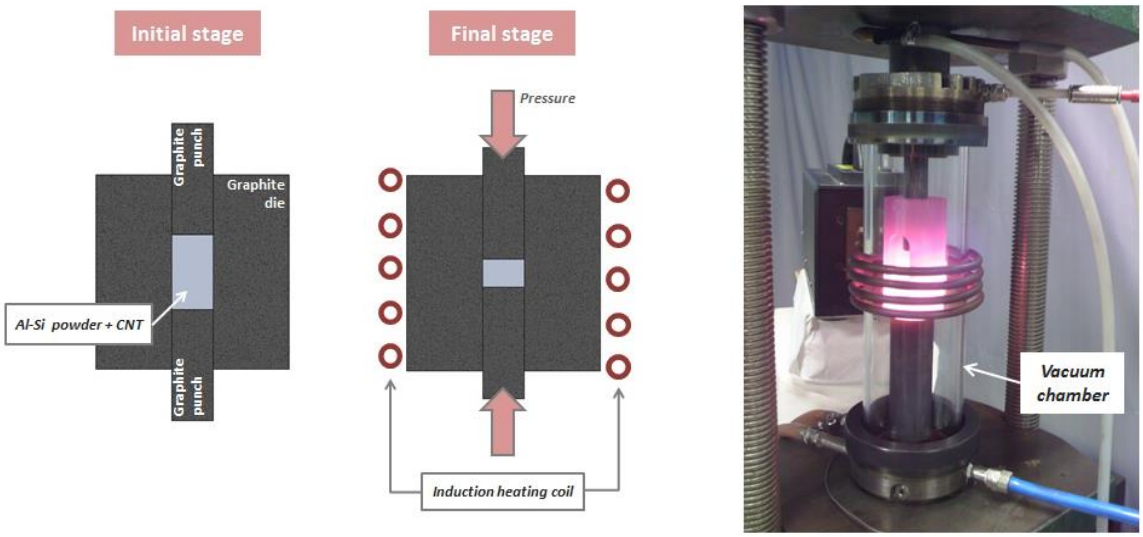

(a) (b)

Figure 10. 1 - Hot pressing (a) schematic representation and (b) vacuum chamber detail.

The samples were produced applying uniaxial load pressure of 35 MPa and a temperature of 550 °C during 10 minutes (hot pressing).

10.3.2 Metallurgical evaluation

Scanning Electron Microscopy with Energy dispersive spectroscopy (EDS) analysis was used to examine the dispersion of CNTs within the AlSi matrix. Differential Scanning Calorimetry (DSC) tests were carried out to evaluate the reactivity between CNTs and AlSi matrix. DSC heating rate of 10°C/min and a constant flow of argon was used.X-ray diffraction analysis was performed using a Bruker AXS D8 Discover diffractometer, in mode 929 with steps of 0.04° and an integration time of 1s. XRD was used for phase identification. Transmission electron microscopy (TEM) was performed in order to analyse the formed interface and potential reactions.

10.4 Results and discussion

10.4.1 SEM with EDS analysis

Figure 10. 2-a shows a SEM image of CNTs, where can be noticed the presence of agglomerates. In Figure 10. 2-b, c amplified images of a CNT agglomerate are presented. Figure 10. 2-d shows an amplified SEM image of a singular CNT, where the CNT and the Ni coating can be observed.

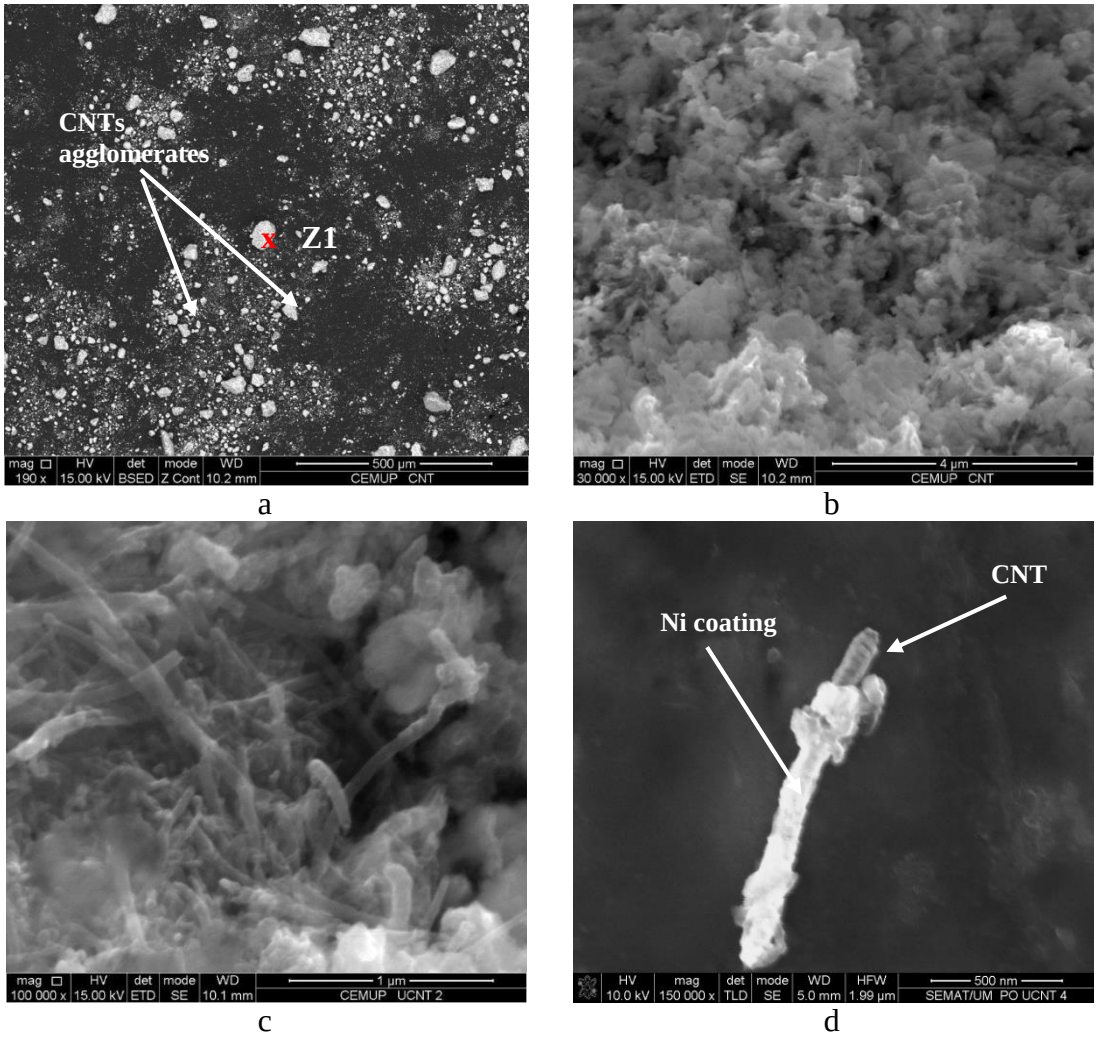

Figure 10. 2 - SEM images showing: (a) CNTs (magnification 190x);
(b) CNT agglomerate (magnification 30000x); (c) CNT agglomerate (magnification 100000x and (d) singular CNT (magnification 150000x).

Figure 10. 3 shows the chemical composition performed on a CNT agglomerate (powder sample), where mainly C and Ni were found, together with some residual elements (resulting from CNT production process).

Figure 10. 4 shows, for a CNT-reinforced composite, the presence of agglomerates. Once CNTs are Ni coated these are easily observed in backscattered view (CNTs white colour comes from the nickel coating). Table 10. 1 presents the chemical composition of the white areas, observed in Figure 10. 4, confirming that the white areas are CNTs.

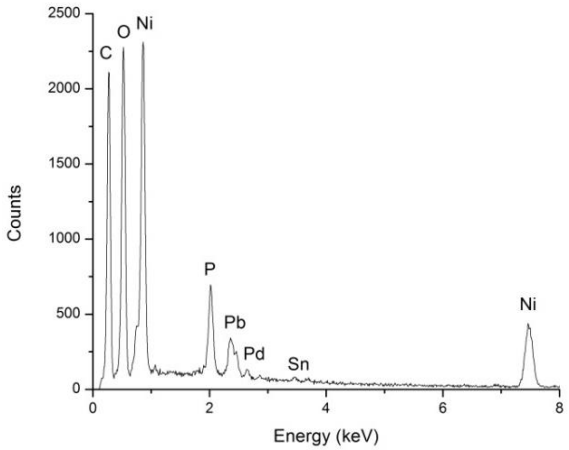

Figure 10. 3- EDS spectrum of a CNT agglomerate, corresponding to zone Z1 (white zone) identified in Figure 10. 2 a).

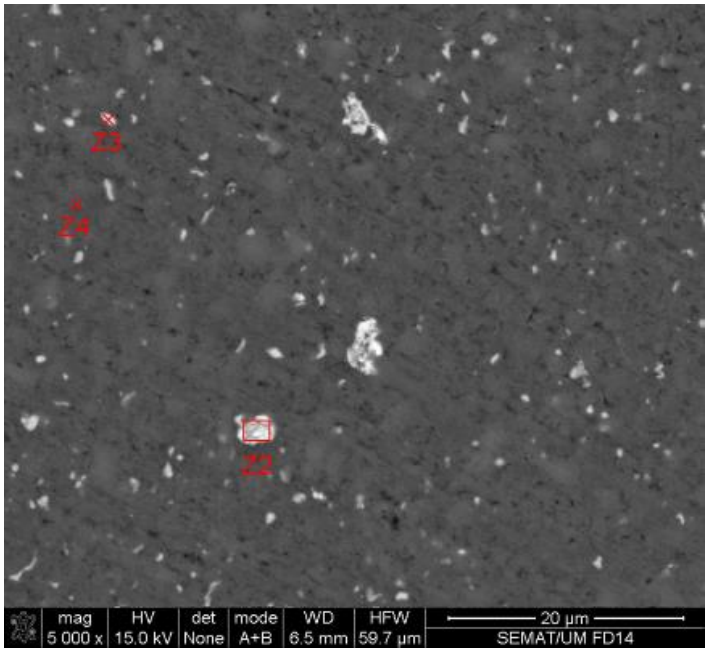

Figure 10. 4 - SEM image in backscattered view of an Al-Si/2%CNT composite sample.

Table 10. 1 - Chemical composition of Z2 and Z4 zones, presented in Figure 10. 4.

Element	Concentration (wt. %)	
	Z2	Z4
Al	60.8	89
Si	3.6	11
Ni	30	-
C	5.6	-

10.4.2 Differential Scanning Calorimetry analysis

Figure 10. 5 presents DSC curves for unreinforced AlSi alloy powders and for AlSi-CNT composite powders. From this figure it can be seen that only endothermic peaks, attributable to the powder melting were detected. These results indicate that no reactions between Ni coated MWCNTs and the AlSi alloy were detected during the sintering stage (until a temperature of 550 ± 2 °C). It can also be seen on Figure 10. 5 that above the working sintering temperature the thermal analysis curves present some differences between the unreinforced AlSi alloy and AlSi-CNT composites. CNTs seem to reduce the melting temperature, possibly due to some Ni diffusion through the AlSi matrix, once Ni lowers the melting temperature of Al. Thus, it means that some Ni coating can be dissolved in AlSi matrix, preserving the CNT integrity (no C diffusion).

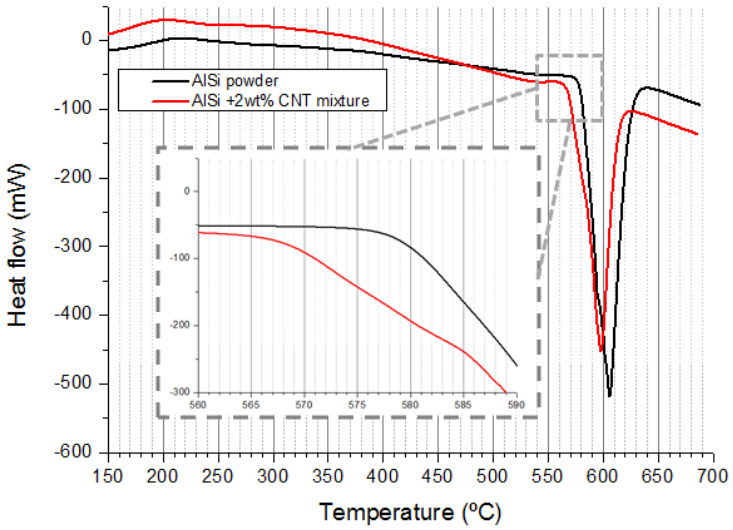

Figure 10. 5 - DSC curves obtained for AlSi alloy andAlSi-CNT composite powders.

10.4.3 X-ray diffraction analysis

X-ray diffraction analysis was performed with analytical software EVA. The crystalline phases were indexed with the ICDD database. The determination of each phase amount was performed with TOPAS software.

By analyzing XRD pattern (Figure 10. 6) it is possible to detect peaks corresponding to AlSi alloy. These CNTs peaks were not detected.

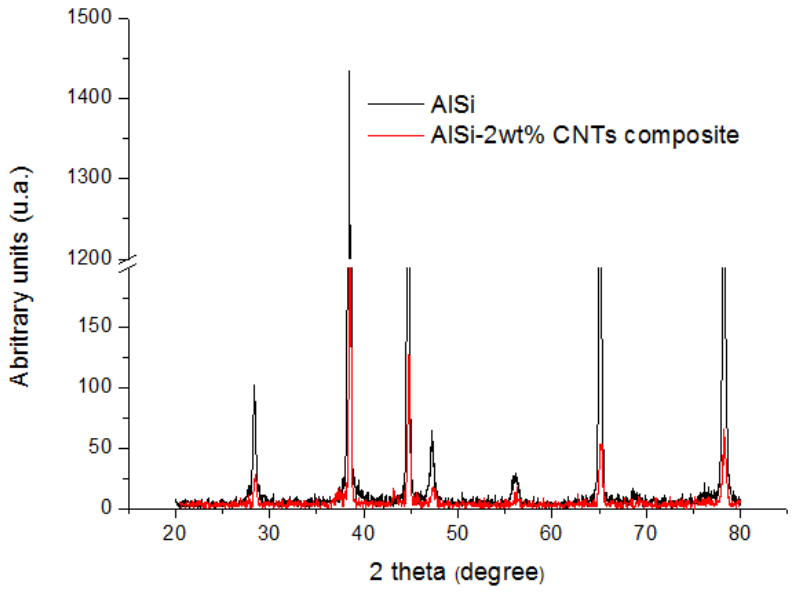

Figure 10. 6 - XRD analysesfor AlSi alloy andAlSi-CNT composite powders andAl-Si/2%CNT composite.

10.4.4 Transmission electron microscopy

By using SEM/EDS, DSC and XRD no reaction between CNTs and AlSi matrix was detected. In order to complement this study, TEM analysis was performed, and it was possible to verify that a Nickel-aluminide was formed on the interface, namely $NiAl_3$.

Figure 10.7 shows the chemical analysis of different regions (performed by TEM). This analysis was performed in an area where an agglomerate is present to more easily identify CNTs.

Figure 10.7-b (z1 zone) corresponds to a Si particle. Figure 10.7-c (z2 zone) corresponds to a reaction product between Al and Ni, with 74.72 at.% Al and 25.28 at.% Ni. The atomic ratio between Al and Ni indicates that Al_3Ni is formed in this region, due to CNTs Ni coating reaction with Al as expected.

Figure 10.7-d (z3 zone) evidences the presence of Ni, P and Pb, corresponding to a particle derived from CNT production process. Figure 10.7-e (z4 zone) corresponds to a CNT, once mainly Ni and C were detected. Figure 10.7-f (z5 zone) corresponds to the Al matrix, once only Al was detected.

Figure 10.8 shows different regions of a CNT-AlSi composite. In Figure 10.8a) an isolated CNT is found next to an agglomerate, while in Figure 10.8b)-d) well dispersed CNT are found. In Figure 10.8-c the catalyst Ni particle (form where the CNT growed during the CVD production) is shown. These TEM images showed that the Ni coating guaranteed the CNT integrity.

From this analysis it is possible to conclude that Al reacts with Ni (coming from CNTs coating) leading to the formation of Al_3Ni. This reaction is more extensive in regions where Al is in contact with Ni coated CNTs. When CNTs are in contact with Si (z4 zone on Figure 10.7-e), apparently there is no reaction between CNT and Si, once CNT is not bonded to Si. These sites can be void nucleation points when subjected to mechanical stress.

According to Kwon et. al. [4,8] the formation of Al_4C_3 can be beneficial to improve the stress transfer ability. Related with Ni coated MWCNT reinforcing commercial AlSi alloy, no studies were found regarding Ni-Al intermetallic formation (particularly Al_3Ni). However, Miranda et. al. [26] produced Ni particle reinforced AlSi composites where the formation of Al_3Ni has detected. It was noticed that this intermetallic led to a stress transfer enhancement (from matrix to reinforcement (Ni)).

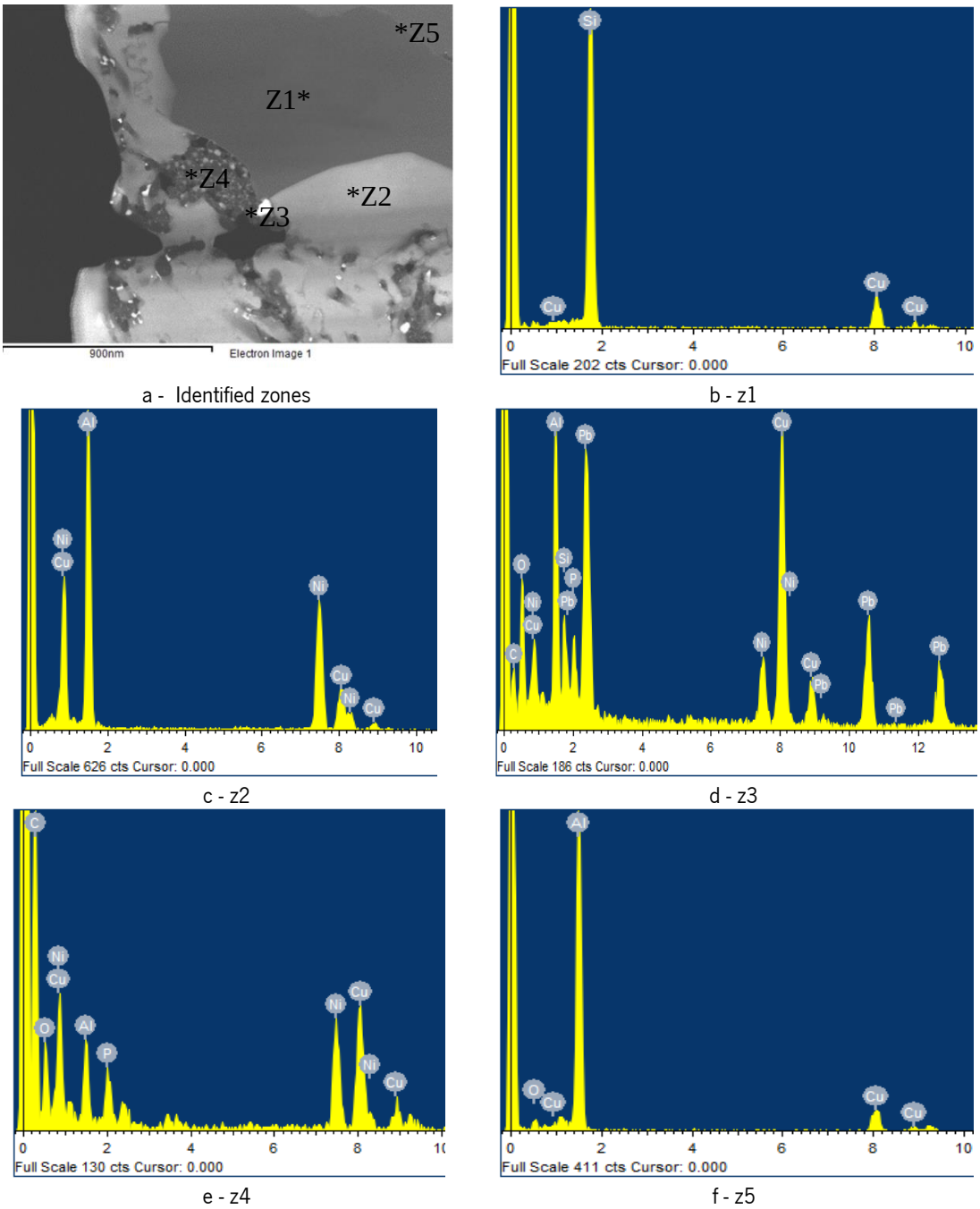

Figure 10.7 - EDS spectrum of several identified zones.

Therefore, it is expected the same stress transfer effect to these Ni coated MWCNT. The formation of Al_3Ni intermetallic not only contributes to the stress transfer but also guarantying the CNT integrity. By coating CNTs, it seems possible to introduce these reinforcements on commercial alloys, an advance to current CNT-reinforced metal matrix composites.

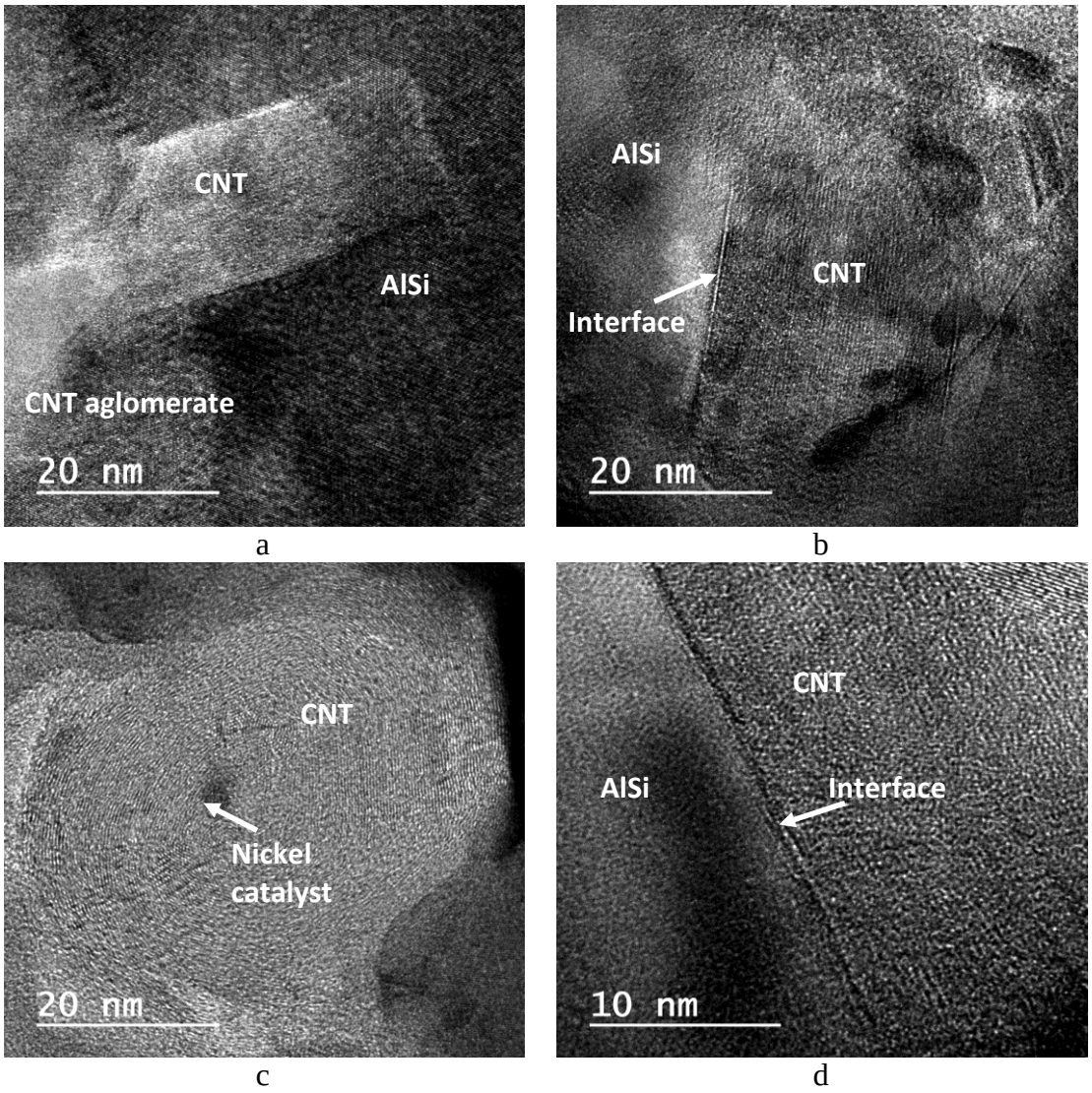

Figure 10.8 - TEM images of CNT-AlSi composite regions, showing a) CNTnext to agglomerate; b)-d) well dispersed CNT.

10.5 Conclusions

This study allowed to conclude that Al_3Ni is formed due to Al reaction with Ni, coming from the coating of the MWCNTs. Additionally, some Ni dissolution was found in the AlSi matrix. This Ni coating was proven to be effective for maintaining CNT integrity.

The formation of Al_3Ni was considered beneficial to stress transfer from matrix to CNT reinforcement, thus contributing to enhance the composites mechanical properties.

This approach, the coating of CNTs for use as reinforcement in a metal matrix, seems to be an effective solution to incorporate this reinforcement in commercial alloys.

10.6 Acknowledgements

This work was supported by the Portuguese Foundation of Science and Technology through the project references PTDC/EME-PME/68664/2006, EXCL/EMS-TEC/0460/2012 and through the PhD grant with the reference SFRH/BD/44077/2008.

10.7 References

[1] Khare R, Bose S. 2005. Carbon nanotube based composites-a review. Journal of Minerals & Materials Characterization & Engineering 4:31-46.
[2] Kwon H, Cho S, Leparoux M, Kawasaki A. 2012. Dual-nanoparticulate-reinforced aluminum matrix composite materials. Nanotechnology 23:225704.
[3] Ci L, Ryu Z, Jin-Phillipp NY, Ruehle M. 2006. Investigation of the interfacial reaction between multi-walled carbon nanotubes and aluminum. Acta Materialia 54:5367-75.
[4] Kwon H, Estili M, Takagi K, Miyazaki T, Kawasaki A. 2009. Combination of hot extrusion and spark plasma sintering for producing carbon nanotube reinforced aluminum matrix composites. Carbon 47:570-7.
[5] Laha T, Chen Y, Lahiri D, Agarwal A. 2009. Tensile properties of carbon nanotube reinforced aluminum nanocomposite fabricated by plasma spray forming. Composites Part a-Applied Science and Manufacturing 40:589-94.
[6] Kwon H, Leparoux M. 2012. Hot extruded carbon nanotube reinforced aluminum matrix composite materials. Nanotechnology 23:415701.
[7] Xu CL, Wei BQ, Ma RZ, Liang J, Ma XK, Wu DH. 1999. Fabrication of aluminum–carbon nanotube composites and their electrical properties. Carbon 37:855-8.
[8] Kwon H, Park DH, Silvain JF, Kawasaki A. 2010. Investigation of carbon nanotube reinforced aluminum matrix composite materials. Composites Science and Technology 70:546-50.
[9] Cho S, Kikuchi K, Kawasaki A, Kwon H, Kim Y. 2012. Effective load transfer by a chromium carbide nanostructure in a multi-walled carbon nanotube/copper matrix composite. Nanotechnology 23:315705.
[10] Sanctis M, Pelletier S, Bienvenu Y, Guigon M. 1994. On the formation of interfacial carbides in a carbon fibre-reinforced aluminium composite. Carbon 32:925-30.
[11] Vidal-Sétif MH, Lancin M, Marhic C, Valle R, Raviart JL, et al. 1999. On the role of brittle interfacial phases on the mechanical properties of carbon fibre reinforced Al-based matrix composites. Materials Science and Engineering: A 272:321-33.
[12] Besterci M. 2006. Preparation, microstructure and properties of Al–Al4C3 system produced by mechanical alloying. Materials & Design 27:416-21.
[13] Lancin M, Marhic C. 2000. TEM study of carbon fibre reinforced aluminium matrix composites: influence of brittle phases and interface on mechanical properties. Journal of the European Ceramic Society 20:1493-503.
[14] Laha T, Kuchibhatla S, Seal S, Li W, Agarwal A. 2007. Interfacial phenomena in thermally sprayed multiwalled carbon nanotube reinforced aluminum nanocomposite. Acta Materialia 55:1059-66.
[15] Bakshi SR, Singh V, Seal S, Agarwal A. 2009. Aluminum composite reinforced with multiwalled carbon nanotubes from plasma spraying of spray dried powders. Surface and Coatings Technology 203:1544-54.

[16] Aggour L, Fitzer E, Heym M, Ignatowitz E. 1977. Thin coatings on carbon fibers as diffusion barriers and wetting agents in Al composites. Thin Solid Films 40:97-105.
[17] Himbeault DD, Varin RA, Piekarski K. 1989. Tensile properties of titanium carbide coated carbon fibre — aluminum alloy composites. Composites 20:471-7.
[18] Gopa Kumar K, Pavithran C, Rohatgi PK. 1980. Preparation of copper-coated titania particles for composites. Journal of Materials Science 15:1588-92.
[19] Beigi Khosroshahi N, Azari Khosroshahi R, Taherzadeh Mousavian R, Brabazon D. 2014. Effect of electroless coating parameters and ceramic particle size on fabrication of a uniform Ni–P coating on SiC particles. Ceramics International 40:12149-59.
[20] He P, Huang S, Wang H, Huang Z, Hu J, et al. 2014. Electroless nickel–phosphorus plating on silicon carbide particles for metal matrix composites. Ceramics International 40:16653-64.
[21] Mohammadpour M, Azari Khosroshahi R, Taherzadeh Mousavian R, Brabazon D. 2014. Effect of interfacial-active elements addition on the incorporation of micron-sized SiC particles in molten pure aluminum. Ceramics International 40:8323-32.
[22] Chen Y, Cao M, Xu Q, Zhu J. 2003. Electroless nickel plating on silicon carbide nanoparticles. Surface and Coatings Technology 172:90-4.
[23] Kong FZ, Zhang XB, Xiong WQ, Liu F, Huang WZ, et al. 2002. Continuous Ni-layer on multiwall carbon nanotubes by an electroless plating method. Surface and Coatings Technology 155:33-6.
[24] Ang LM, Hor TSA, Xu GQ, Tung CH, Zhao SP, Wang JLS. 2000. Decoration of activated carbon nanotubes with copper and nickel. Carbon 38:363-72.
[25] Yang Z, Xu H, Li M-K, Shi Y-L, Huang Y, Li H-L. 2004. Preparation and properties of Ni/P/single-walled carbon nanotubes composite coatings by means of electroless plating. Thin Solid Films 466:86-91.
[26] Miranda G, Buciumeanu M, Carvalho O, Soares D, Silva FS. 2015. Interface analysis and wear behavior of Ni particulate reinforced aluminum–silicon composites produced by PM. Composites Part B: Engineering 69:101-10.

11 General discussion

The aim of this work is the development and characterization of new and improved functionally graded materials, based on aluminum-silicon alloys reinforced by nickel coated carbon nanotubes and obtained by a powder metallurgy technique.

This development was based on a demonstrative component: an AlSi-CNTs functionally graded material engine compression piston ring, designed to fulfil its specifications such as high wear resistance on the contact surface (with cylinder wall) and high fatigue resistance for instance.

As referred in Chapter 1, the theoretical and experimental work towards the development of AlSi-CNT FGM piston ring, followed the below mentioned steps:

- Review (Include chapter 2);

- Assessment of several mixing processes for mixing aluminium powders and the reinforcement (Include chapter 3 and 10);

- Assessment of the optimum reinforcement fraction for these composites (Include chapter 4);

- Study and explanation of the effective reinforcing mechanisms on these composites (tensile, fatigue and wear) (Includes chapter 5, 6, 7, 8);

- Development of an equipment to obtain components with selected graded composition and design of a graded composition (reinforcement distribution) for piston rings production (Include chapter 9).

This work starts with optimization of the processing parameters for the aluminium-silicon matrix alloy was performed, in order to obtain the better mechanical properties. Although not been presented in any chapter of this thesis, this assessment focuses on the following processing parameters: temperature, time and sintering process.

Two consolidation processes were evaluated: cold pressing and sintering and also hot pressing. In the cold pressing and sintering process, a green compaction pressure of 750 MPa and

a sintering temperature of 550 °C during one hour, under vacuum (≈10^{-5} mBar) were used. In the hot pressing process, two different sintering temperatures were tested (500 and 550°C) and three sintering times (10, 30 and 60 minutes), with compaction pressure of 35 MPa.

Sintering by hot pressing process (temperature of 550°C during 10 minutes), lead to the better mechanical properties. Furthermore, this evaluation allowed to show that with hot pressing it is possible to achieve higher densification with less time. A reduction of the sintering time is an advantageous aspect once it allows a better control over the reactivity between reinforcement and matrix.

In Chapter 3, designated by Evaluation of CNT dispersion methodology effect on mechanical properties of an Al-Si composite, it was made the assessment and optimization of the dispersion methodologies of the reinforcement (multi-wall CNT functionalized with Ni) on the aluminium-silicon matrix. This assessment was mainly based on the mechanical properties of the obtained composites (processed by hot pressing).

Different procedures for mixing CNTs with the AlSi matrix were tested, using for all of them 2wt.% CNTs. The mechanical behaviour of the specimens was assessed by shear tests. Scanning electron microscopy (SEM) and differential scanning calorimetry (DSC) were used to investigate the microstructure of the composites and interface reactions. This work evidenced the influence of the CNTs dispersion methodology in the enhancement of the composites mechanical properties.

Mechanical alloying process was used for all the tested mixing methodologies. However, different procedures were tested: effect of the milling time, the existence or not of a mixture pre-treatment (preliminary ultrasonic mixing in ethanol), the energy involved in the milling process (high/low energy milling) and the milling environment (wet or dry).

This work allowed to conclude that the mechanical properties of the composites are dependent on the mixing process and the pre-treatment of the mixture, once they have influence on the reinforcement distribution. The addition of a preliminary ultrasonic mixing in ethanol, to the high energy mixing process, does not seem to bring relevant advantages to overcome the costs associated with the process.

Regarding the mechanical mixing environment, a wet environment was tested in order to evaluate the influence of liquid viscosity and turbulence on CNTs dispersion. It was shown that a wet environment (ethanol) during the mixing slightly improved the CNTs dispersion, when comparing with dry conditions.

Regarding the mechanical mixing energy, the high energy process (one minute test duration) does not seem to bring advantages when compared to low energy processes (at least for one minute test duration). For high energy mechanical alloying, further increases on the mixing time, would improve CNTs dispersion, although their deterioration could happen along with a powder size increase (by a powder welding mechanism leading to worst sinterability).

The low energy mixing process provided better mechanical properties, together with the advantage of its simplicity and low cost. However, the mechanical properties improvement is still far from what is expected, based on excellent mechanical properties and cost of CNTs. CNT agglomerates were found in all the composites, after all the tested mixing procedures. These were found responsible for the under expected mechanical properties.

The main conclusion regarding dispersion processes is that a combination of different mixing processes lead to the highest improvement on CNTs dispersion.

Therefore the selected process to mix AlSi powders and CNTs consisted in introducing AlSi powders and CNTs in a closed stainless steel jar, together with steel milling balls, with a ball-to-powder weight ratio of 10:1 (ball diameter of 10 mm). Mechanical mixing with a constant rotation speed of 40 rpm, during 6 days (low-energy ball milling).

At the end of this chapter a study on the reactivity between the Ni coated MWCNT and the AlSi matrix is presented. A more detailed study was performed and is presented on Chapter 10 (Interface analysis on an eutectic AlSi alloy reinforced with Ni coated MWCNT). These studies allowed to conclude that Al_3Ni is formed due to Al reaction with Ni coming from the coating of the MWCNTs. The formation of Al_3Ni was considered beneficial to the stress transfer from matrix to CNTs, thus contributing to enhance these composites mechanical properties.

In Chapter 4 designated as Carbon nanotube dispersion in aluminium matrix composites – quantification and influence on strength it was made optimization of the reinforcement fraction for AlSi-CNT composites.

This chapter presents a study on the influence of different CNT volume fraction on the metallurgical and mechanical properties of the composites. This study also assessed the influence of CNTs agglomerates content on the mechanical properties of these composites.

Three types of composites were produced, with different CNT fractions: 2, 4 and 6 wt. %. For comparison purposes unreinforced AlSi samples were also produced by the previously selected mixing process (step three).

These composites were characterized regarding CNT distribution on the matrix, especially concerning the presence of agglomerates, by means of Scanning Electron Microscopy. The obtained images were then processed, applying a threshold filter in order to further highlight CNTs for posterior quantification.

Two types of agglomerates measurements were performed. The first, regarding agglomerates with areas up to 50 μm^2, representing well dispersed CNTs, as well as agglomerates of one to few CNTs (pictures with magnification of 5000 times were used). The second, concerns measurements of agglomerates with areas up to 1950 μm^2 (pictures with amplifications of 123 times were used).

In all the composites (with 2, 4 and 6 wt. % CNTs) it was verified that more than 93% of the agglomerates are less than 1 μm^2 in area (Figure 4. 8). Considering the representativeness of these small agglomerates ([0, 1] μm^2) they were named Type A agglomerates. Similarly, it was verified that more than 93% of the agglomerates have area above 50 μm^2 and less than or equal to 550 μm^2 (Figure 4. 10).Considering their representativeness (area within the range]50, 550] μm^2) these agglomerates were named Type B.

This works shows that by increasing CNTs fraction in the composites (from 2 to 6 wt. %) the ability to disperse the CNTs is decreased, once well dispersed CNTs number are reduced, as well as "small" (Type A - [0, 1] μm^2) agglomerates (with agglomerates area increase tendency). Additionally, with CNT fraction increase, the so called "bigger" agglomerates (Type B -]50, 550] μm^2) increase their number and also their area.

Regarding mechanical properties, this study showed that 2 wt.% CNT-reinforced composite revealed the higher tensile strength. This result indicated that the detrimental effect of the agglomerates is higher that the beneficial effect of well dispersed CNTs.

In the end of this chapter, an empirical correlation of tensile strength as a function of CNT content in the matrix was established. This analysis considered the beneficial effect of CNTs and the detrimental effect of agglomerates on CNTs reinforced aluminium mechanical properties. The proposed model should now be tested under other different processing conditions, in order to evaluate its validity.

In Chapter 5, named as Improvement on sliding wear behaviour of Al/cast iron tribopair by CNTs reinforcement of an Al alloy, and Chapter 6, designated as Mechanisms Governing the Tensile, Fatigue and Wear Behaviour of Carbon Nanotube reinforced Aluminum Alloy, it was made the explanation of the effective reinforcing mechanisms on these composites (tensile, fatigue and wear) was performed on the fifth step.

Chapter 5 concerns the influence of different CNT fractions in the tribological behaviour of these AlSi-CNT composites. These tests were performed under dry reciprocating sliding conditions, against a grey cast iron (GCI) from a cylinder engine. The wear resistance was investigated as a function of CNT content, that varied from 2 to 6 wt.%. In order to understand the mechanisms responsible for the reported wear behaviour, SEM and EDS analysis were performed on the surfaces of the unreinforced AlSi alloy and on the produced AlSi-CNTs composites.

This chapter clearly shows that by reinforcing AlSi alloy with CNTs, the wear behaviour of tribopair (AlSi-CNT/GCI) is improved, when compared with unreinforced AlSi alloy/GCI tribopair.

The wear damage of AlSi-CNT composites seemed to be controlled essentially by two mechanisms: adhesive wear and pull-out of grains/particles or agglomerates. Regarding the pull-out mechanism, correlation with CNT content was found, once by increasing CNT content an increase in pull-out of grains/particles or agglomerates occurred.

With CNT content increase there is an increase in the number of observed cracks that could be associated with the higher number of macro-agglomerates (as seen in Chapter 4). The lower mechanical properties obtained for the composites with higher CNT contents (4 and 6 wt.%), as presented on Chapter 4, are related with this fact.

In spite of the reduction on mechanical properties with CNT content increase, there is an improvement in the wear response. This can be explained based on two different phenomenon: the strengthening effect and the self lubrication effect of CNTs. Therefore although agglomerates have a detrimental effect on void nucleation, they may have a beneficial effect on wear behaviour, due to their release during sliding (CNTs self lubrication effect).

The strengthening effect of CNTs is explained by a stronger bonding between AlSi interfaces (between AlSi powders) due to CNTs presence. Additionally, CNTs exert an effect on the matrix by restricting dislocations movement. On the other hand, CNT agglomerates have a detrimental effect, being responsible for voids nucleation.

The disintegration of agglomerates due to shear forces, on the wear tests, lead to the appearance of individual CNTs that roll into the sliding contact. These CNTs and CNT agglomerates released during sliding contribute to the self-lubrication effect.

Chapter 5 demonstrated that the CNT content plays a relevant role on wear behaviour, by substantially reducing the wear loss of AlSi-CNT composites and additionally of the grey cast iron counterface. AlSi-CNT composites exhibited a substantial improvement in the wear behaviour when compared to unreinforced AlSi alloy. AlSi composites reinforced with 6 wt.% CNTs presented the highest wear behaviour improvement.

In Chapter6, named as Mechanisms Governing the Tensile, Fatigue and Wear Behaviour of Carbon Nanotube reinforced Aluminium Alloy, It was studied the influence of reinforcing mechanisms of CNTs on mechanical, wear, and fatigue of CNT-reinforced AlSi composites are presented. This study is based on fracture morphology analysis and comparison between AlSi matrix alloy and 2wt.% CNT-reinforced AlSi composite.

Chapter 5 and 6 showed that 2wt.% CNT-reinforced AlSi composite exhibited the highest mechanical properties and 6 wt.% CNT-reinforced AlSi composite exhibited the highest wear resistance. CNTs agglomerates were found in all the composites. The agglomerates detrimental effect on the mechanical properties was proven, however some beneficial effects on the wear behaviour due to its presence was found (self-lubricating effect). Thus, 2wt.% CNTs was found to be the composition in which is possible to obtain a better compromise between mechanical properties and wear resistance. In this context, chapter 6 aims to clarify the role of CNTs and CNTs agglomerates on these composites mechanical and wear behaviour.

Fracture tests showed that in 2 wt.% CNTs-reinforced composite the fracture (crack) may initiate in agglomerates regions (areas of stress concentration). If the crack reaches a region where CNTs are well dispersed it may travel through the AlSi grain/particle (intragranular fracture), but if the crack reaches zones of weakness (lower bond strength region, where agglomerates are located, between AlSi grains/particles), then the crack follows the grain/particle border(intergranular fracture). The consequence of this phenomenon is a rougher region (where agglomerates are formed) and a smoother surface (when the crack travels through the AlSi grain/particle).

CNTs strengthening effect is effective on zones where they are well dispersed. Thus, the tensile and yield strength increase with CNTs addition is related to the fact that AlSi grains/particles are bonded with an improved strength due to CNTs interface reinforcement effect. Despite the

existence of agglomerates, the well dispersed CNTs strengthening effect on mechanical properties was found to prevail over the detrimental effect of CNTs agglomerates (as shown in chapter 4).

This chapter also showed that it is possible to increase fatigue behaviour with CNTs addition. For 2 wt.% CNTs-reinforced composites, fatigue cracks may initiate in agglomerates regions (fatigue cracks frequently initiate at stress concentration sites).The presence of CNT agglomerates, that can be regarded as inclusions, have when concerning fatigue, a much more expressive detrimental effect than in tensile tests.

During crack propagation, if a crack reaches a region where CNTs are well dispersed, the crack is deflected due to a stronger interface between matrix and CNT, and then may travel through the AlSi grain/particle (intragranular fracture). If the crack reaches a region with agglomerates (weaker zones) the crack propagation is accelerated. Therefore, for composites there is a mixture/competition between intragranular and intergranular fracture. Thus, even though there are weak zones (CNTs agglomerates) that may accelerate the crack propagation, well dispersed CNTs act as interface barriers to crack propagation, increasing the length of the crack (due to its deflection) and therefore the fatigue life of AlSi-2 wt.% CNT composites.

Wear testes showed (as mentioned in Chapter 6) that CNTs improve the wear behaviour of AlSi-CNT composites by means of strengthening effect and self-lubrication effect.

The strengthening effect of CNTs is revealed in both tensile and fatigue tests i.e. CNTs strengthens the bonding between AlSi grain interfaces by direct strengthening (shear lag) and by indirect strengthening through the Orowan and thermal mismatch mechanisms. In wear tests the CNT agglomerates (poor dispersion zones) have a detrimental effect because it is easier to detach the grains but they have also a beneficial effect due to Self-lubrication effect (the explanation was previously done in chapter 5). Chapter 6 shows that CNTs area good choice for reinforcing AlSi alloys in order to improve mechanical, wear, and fatigue behaviour.

Chapter 4, 5 and 6showed that composites with 2wt.%CNT revealed the highest mechanical properties and that 6wt.% CNT composites presented the highest wear resistance. CNTs agglomerates, found in all the produced composites, were found to have a detrimental effect on mechanical properties, although having some beneficial effect on wear performance due to their self-lubricating effect. AlSi-2wt.%CNT composites were found to have the best compromise between mechanical properties and wear resistance.

Hybrid composites present, as strategic advantage, the ability to take benefit of different reinforcement's, that have different properties, towards a composite with improved overall performance (regarding mechanical and wear).

Chapter 7 named Dry sliding wear behaviour of AlSi-CNTs-SiCp hybrid composites and Chapter 8 designated as Mechanical, wear and fatigue behaviour of an AlSi-CNTs-SiCp hybrid composite focus on a new hybrid composite: AlSi-2wt.%CNT-5wt.%SiCp.These two chapters are concerned with the understanding of the reinforcing effects of Multi-Wall Carbon Nanotubes and Silicon Carbide particles on mechanical, wear and fatigue performance.

By introducing two different reinforcements it was expected that different contributions would arise from these reinforcements that can differ in properties, shape and size. In order to explain the role of each reinforcement on the hybrid composite performance, tensile, fatigue and wear tests were performed, for unreinforced AlSi alloy and AlSi-2wt.%CNT, AlSi-5wt.%SiCp and AlSi-2wt.%CNT-5wt%.SiCp composites.

Chapters 4, 5 and 6 proved that 2wt.%CNT-reinforced composite revealed the highest tensile strength, with subsequent decay for higher CNT content (4 and 6 wt.%). Regarding wear, when increasing the CNT content from 2 to 6 wt.% an increase in wear resistance occurred, with all AlSi-CNT composites exhibiting higher wear resistance when compared to unreinforced AlSi alloy.

In this sense, chapter 7 and 8 aims to to determine the combined effects of combined reinforcing constituents (CNT and SiC) on mechanical properties (tensile and fatigue) and also on wear behaviour. The purpose of this study was to clarify if, when a certain reinforcement reaches its optimal fraction (with highest beneficial effect on a given property), a second reinforcement could further increase a certain composite property, without compromising other relevant properties.

The obtained results confirmed this expectation. The 5wt.% SiCp addition to the 2 wt.% CNT-reinforced composite (thus obtaining AlSi-2wt.%CNT-5wt.%SiCp hydride composite) leads to an increase in tensile strength without losing wear resistance. In fact, further increases in CNT content above 2 wt.% did not lead to tensile strength improvement, however when adding a different reinforcement (SiCp) to 2 wt.% CNT-reinforced composites, further improvement was possible.

Wear tests performed on hybrid composites revealed that AlSi alloy, AlSi-2wt.%CNT and AlSi-5wt.%SiCp composites seemed to be controlled essentially by abrasive and adhesive wear

(including plastic deformation and material transfer between the mating surfaces). AlSi-2wt.%CNT-5wt.%SiCp hybrid composites seemed to be controlled by the same mechanisms, although presenting a lower level of plastic deformation and material transfer between the mating surfaces.

The introduction of CNTs and SiCp in the AlSi matrix seemed to have a beneficial effect, both on pin and counterface material, once they exhibited an improvement on wear resistance, as compared to unreinforced AlSi/GCI tribopair.

This improvement resulted from: (i) strengthening effect of well dispersed CNTs; (ii) CNTs self-lubrication; (iii) strengthening effect of SiCp; (iv) SiC load bearing effect. The strengthening effect of well dispersed CNTs and also CNTs self-lubrication effect were detailed addressed in previous chapters. The strengthening effect of SiCp is related with matrix strengthening mainly by shear lag and thermal mismatch (SiCp increases the composite hardness). The SiC load bearing effect results when, during sliding, SiC particles support the load and prevent the contact between AlSi matrix and the GCI plate.

Chapter 8 brings, along with a wear performance analysis, a mechanical properties assessment, characterizing AlSi-2wt.%CNT-5wt%.SiCp composite. Unreinforced AlSi alloy; AlSi-2wt.%CNT and AlSi-5wt.%SiCp were also studied in order for comparison with the hybrid composite.

AlSi-2wt.%CNT-5wt%.SiCp hybrid composite presented the higher tensile strength, and regarding the fracture morphology, this seem to result from de-bonding and fracture of SiCp and from the presence of CNT agglomerates.

In these hybrid composites, CNTs agglomerates and interfaces between the SiCp and AlSi matrix act as stress concentration points where most commonly voids nucleate acting as crack initiating sites. In CNT well dispersed zones the crack propagates thought AlSi matrix grains and when finding SiCp two scenarios can occur: crack surrounds the SiCp (for weakly bonded particles) and crack travel through the particle (for well bonded particles). In CNT agglomerates zones, when the crack finds an agglomerate, the crack travels through the agglomerates (offering lower resistance to the crack progression).

Shear lag effect, thermal mismatch and Orowan strengthening were found to be acting in AlSi-2 wt. %CNT-5 wt. % SiCp hybrid composite. Regarding the shear lag effect, this study showed that both SiCp and CNT contribute to strengthen the hybrid composite. Reactivity between reinforcement and matrix influences the load transfer (shear lag effect). Thermal mismatch strengthening contribution obtained by adding CNTs is larger than that obtained by adding SiCp,

due to a higher differential in coefficient of thermal expansion, reduced size and higher aspect ratio for CNTs. By Orowan strengthening, CNTs act as impenetrable obstacles, increasing the yield strength. Once SiC particles have a larger size when compared to CNTs, this mechanism should be less expressive for SiCp.

Fatigue tests revealed that for identical loading conditions AlSi-2wt.%CNT composite showed higher fatigue life than unreinforced AlSi alloy and also AlSi-5wt.%SiCp and AlSi-2wt.%CNTs-5wt.%SiCp composites.

Regarding AlSi-2wt.%CNTs-5wt.%SiCp hybrid composite, for higher stress levels, the fatigue life was found lower than that of unreinforced AlSi alloy and AlSi-5wt.%SiCp. For lower stress levels, hybrid composite fatigue life although inferior to AlSi-2wt.%CNTs, was found to be higher than unreinforced AlSi alloy and AlSi-5wt.%SiCp. This behaviour can be explained by the reduction of ductility in hybrid composites that combined with a higher plastic deformation when under higher stress levels, leads to a lower opposition to crack propagation.

Regarding wear, both AlSi-2wt.%CNT and AiSi-5wt.%SiCp composites exhibited an improvement in wear behaviour when compared to unreinforced AlSi alloy, AlSi- 2wt.%CNT and AiSi-5wt.%SiCp. These results, as referred in previous chapters, are consequence of the strengthening effect of well dispersed CNTs, CNTs self-lubrication effect and CNTs agglomerates, besides the strengthening effect of SiCp and SiCp load bearing effect.

Summarizing, CNT-reinforced composites were found to achieve the higher tensile strength for 2 wt.% of CNTs, as shown in Chapter 4 and 6. Therefore, by increasing the CNT content above this value, the tensile strength was not improved, however this increase resulted in a wear resistance improvement (as shown in Chapter 5). This study has proven that the peak of tensile strength (when achieved with one reinforcement (CNT)) is possible to be further increased by adding another type of reinforcement (SiCp) (Chapter 8). The reason for this behaviour seems to lie on the simultaneous effect of two different reinforcement mechanisms or on the same mechanism but acting at different scales. AlSi–2wt.%CNTs composite fatigue life was notably the best among all the composites produced (Chapter 8).

Finally in Chapter 9 named as Optimization of AlSi-CNTs functionally graded material composites for engine piston rings, it was made the development of a device to obtain components with a graded chemical composition and also the optimization of graded chemical composition (reinforcement distribution) applied to piston rings.

Piston rings damage is attributed first to wear, then to lubrication and fatigue. Their damage may be substantially mitigated by creating a FGM composite with optimized mechanical properties. This chapter aims to produce an AlSi-CNT functionally graded material that can fulfil the engine compression piston rings specifications. Once fatigue is an important specification for piston rings, the best composite composition, when regarding fatigue - AlSi - 2wt.%CNT composite, was set as the starting point for the production of the FGM piston ring.

AlSi graded composites (from 0 to 2wt.%CNT) were produced by a new equipment that was developed/designed to produce FGMs by powder metallurgy processing route. This equipment was found highly efficient for the production of these graded composites.

A first productive approach used a linear gradient through the cross section of the piston ring (2wt% CNTs at inner region, 0wt% in the middle and 2wt% at the outer region) was tested. This gradient was chosen by taking in account the mechanical and wear requirements of a piston ring. Results regarding tensile strength and fatigue life showed that this composite has an intermediate behaviour between unreinforced AlSi alloy and 2wt% CNT-reinforced composite.

A second approach was proposed, being considered the most effective. According to this solution, CNTs are placed on the outer region of the piston ring, once this is the region under greater mechanical stresses and higher wear. Once the better compromise between mechanical properties and wear is found for a composition of 2 wt.% CNT, this was chosen for the outer regions.

This study is very appealing for components design once it allows the development of controlled materials gradients suited for particular requirements. This work developed a possible solution for a piston ring, but a similar analysis/process can be applied to other components, where there is differential mechanical and wear requirements along a component.

As general remarks it can be concluded that:

- The use of commercial aluminium alloys (at least Al-Si alloys) reinforced with Ni coated CNTs seems to be adequate for industrial applications;

- The use of the reinforcement distribution process seems to e adequate for some industrial applications such as the one in this thesis, with radial gradation, or even other components;

- The reinforcement dispersion along the matrix was not fully optimized and the expected contribution of the reinforcement on the overall composite behaviour was not fully achieved.

11.1 Suggestions for future works

The findings of the research presented in this thesis opens future perspectives. The first future work concerns the development of an integrated process for dispersion CNTs and production of CNTs reinforced composites. Ideally, CNT incorporation/dispersion should be performed during the metal powders production and/or by CNTs growth on the metal powder. For this work, the matrix powder and the reinforcement (CNT) should be in the same size range.

Another future work relates with CNTs functionalization that should be done with particular features tailored for particular metals. This functionalization has two functions: eliminate Van der Walls forces and promote an optimized bonding between CNTs and the matrix, in order to enhance stress transfer to CNTs.

These two future works should also include an integrated approach by converging different knowledge areas, like materials science, chemistry, physics and mechanical engineering.

A third future work is the appliance of some results obtained in the scope of this thesis (AlSi - 2wt% CNT composite agglomerates quantification) to develop a predictive fatigue model. This model, inspired by Murakami model, will take in account inclusions (here including agglomerates) influence in the fatigue life of these composites.

A final proposal is the development of a strengthening model for CNT-reinforced composites that takes in consideration the following main mechanisms/variables: shear lag, CTE and elastic mismatch, Orowan and also matrix microstructure characteristics (grain shape and size, inclusions, defects, porosity). The influence of each mechanism/variable over the other should be considered. This model should also consider CNT fraction, orientation, distribution/dispersion, curvature, number of walls and formed interface. This development will use different validation methodologies: micro mechanics analysis; finite element modeling and experimental data.